On the Prevalence and Role of Addition Reactions in Lipid Peroxidation

By: Anas Mamdouh Abou-Zaid

A thesis submitted to the Department of Chemistry and Biomolecular Sciences in conformity with the requirements for the degree of Master of Science in Chemistry

Supervisor: Dr. Derek A. Pratt

Department of Chemistry and Biomolecular Sciences
University of Ottawa
Ottawa, Canada

Abstract

Plasmalogens have been reported to possess antioxidant activity; a paradoxical finding given that plasmalogens often comprise highly oxidizable polyunsaturated fatty acids esterified to the central position of the glycerol backbone. However a reasonable mechanism accounting for plasmenyl lipid activity has yet to be advanced, despite the fact that other monounsaturated lipids including cholesterol and oleate have been extensively studied. Plasmenylcholine was synthesized *de novo* to resolve its antioxidant activity as well as to carry out mechanistic studies to understand its basis. Autoxidation of a vinyl ether model substrate yielded a k_p of 6 M^{-1} s^{-1}, which affirmed it was as slower than cholesterol. However, corresponding experiments with a deuterated substrate yielded a value of 89 M^{-1} s^{-1}, questioning the reliability of these studies.

Our studies of plasmenyl lipid peroxidation inspired us to look into the mechanism of autoxidation of the monounsaturated lipid, oleate (using LC-MS/MS with APCI+), which was reported to proceed exclusively via H-atom transfer (HAT). Herein we have shown for the first time that oleate epoxides are formed in the autoxidation of the monounsaturated lipid.

Statement of Originality

I hereby certify that all of the work described in this thesis is the original work of the author, with exceptions for work performed by collaborators noted in the preface to each chapter. The basis of this research originates from a significant amount of published articles in peer-reviewed journals. Any published (or unpublished) ideas and/or results from the work of others are fully acknowledged in accordance with the references.

Anas M. Abou-Zaid

Acknowledgements

Firstly, I would like to thank Dr. Derek Pratt for providing me with the opportunity to join his research group and for being a stimulating mentor who motivated me to continually question and learn from my observations. The assigned project aligned very well with my research interests as it allowed me to apply and expand upon my organic chemistry knowledge while working towards solving a biologically relevant problem. The project was extremely challenging, and we encountered many hurdles throughout the optimization processes for both the synthesis and instrumental methods, but it was very rewarding when we overcame those hurdles.

I would also like to especially thank Dr. Pierre Faudot dit Bel for his supervision, guidance throughout the completion of this project. I cannot thank you enough for your time and patience in teaching me each new laboratory techniques and familiarizing me with the facilities.

Additionally, I would like to acknowledge every member of this research group for their contributions to the development of my laboratory skills and troubleshooting tips. Emily Shaefer, you were like a second mentor, you provided much needed guidance many times when I was working independently. Markus, thank you for assisting with technical issues. Ron and JP, thank you for your guidance and daily suggestions for synthetic modifications. I would like to thank Evan Haidez, Zosia Zielinski, JP Chauvin, Kareem Harrison, Omkar Zilka, Luke Farmer, Katie Shirley, Mark Raycroft, Demar Pitter, Jia-Fei Poon, Neill Penner, Spencer Short, and Dmitry Saraev, for providing advice whenever I reached an impasse in my project.

List of Abbreviations

AA	arachidonic acid
ACAT	acyl-CoA:cholesterol acyltransferase
AIBN	azobisisobutyronitrile
AO	antioxidant
APCI	atmospheric-pressure chemical ionization
α-TOH	α-tocopherol
BDE	bond dissociation enthalpy
BHT	butylated hydroxytoluene (2,6-di-t-butyl-4-methoxyphenol)
BODIPY	boron dipyrromethene
b.p.	boiling point
$CDCl_3$	chloroform-d_3
C_6D_6	benzene-d_3
COSY	^{1}H-^{1}H Correlated Spectroscopy
DCM	dichloromethane/methylene chloride
DEPT	distortionless enhancement by polarization transfer
DPPH	2,2-diphenyl-1-picryl-hydrazyl-hydrate
DTBN	di-tert-butyl-hyponitrite
DTUN	di-tert-undecyl-hyponitrite
EtOAc	ethyl acetate
ESI	electrospray ionization
GPX	glutathione peroxidase
GSH	glutathione
HAT	hydrogen atom transfer
HEK 293	human embryonic kidney cell line
HEX	hexanes
HMBC	heteronuclear multiple bond correlation
HOCl	hypochlorous acid
HPLC	high performance liquid chromatography
HSQC	heteronuclear single quantum correlation
IPA	isopropanol

KIE	kinetic isotope effect
Lyso-PC	1-lysophosphatidylcholine
MeO-AMVN	2,2'-azobis(4-methoxy-2,4-dimethylvaleronitrile) [V70]
MPO	myeloperoxidase
MS	mass spectrometry
MS/MS	tandem mass spectrometry
m/z	mass-to-charge ratio
NMR	nuclear magnetic resonance spectroscopy
NOESY	nuclear Overhauser effect spectroscopy
PBS	phosphate-buffered saline
PC	plamenycholine
PDA	photodiode array
PDI	polydispersity index
PE	plasmenylethanolamine
PL	plasmenyl lipid
PLPC	1-palmitoyl-2-linoleoylphosphatidylcholine
PPh_3	triphenylphosphine
PUFA	polyunsaturated fatty acid
ROS	reactive oxygen species
RTA	radical-trapping antioxidant
r.t.	room temperature
SM	starting material
SOD	superoxide dismutase
^tBuOOH	tert-butyl hydroperoxide
TCE	trichloroethylene
THF	tetrahydrofuran
TIC	total ion chromatogram
UPLC	ultra-performance liquid chromatography
UV-Vis	ultra-violet visualization
TEMPO	(2,2,6,6-tetramethylpiperidin-1yl)oxyl
TTBP	2,4,6-Tri-tert-butylpyrimidine

Table of Contents

List of Tables

List of Figures

List of Schemes

Statement of Contribution

The research projects contained herein were primarily designed and directed by the principal investigator, Dr. Derek Pratt. Dr. Pierre Faudot dit Bel provided invaluable conceptual and technical advice during the early stages of the study of the plasmalogen autoxidation. Emily Shaefer provided a great deal of guidance with respect to all HPLC and UPLC-UV/MS-MS experimentation and method optimization. Melodie Mallais tested the synthesized vinyl ether model substrates, partially deuterated vinyl ether model substrates, plasmenylcholine intermediates, and the final plasmalogen products in liposomes and cells in order to determine their effects on the lipid membrane models and in biological systems. Ron Shah, and JP Chauvin regularly provided tips in the lab to optimize or modify my synthetic procedures or instrumental methods. Dr. Markus Griesser provided valuable LFP and computational data for the vinyl ether model substrate tests. Dr. Zosia Zielinski provided the foundations for the Oleate autoxidation study including the proposed synthesis of the partially deuterated methyl oleate(-8,8,11,11-d_4), LC method optimization, computational modeling, and the natural and d_4-hexadec-8-ene autoxidation results which were compared with the autoxidation results of methyl oleate and methyl oleate-8,8,11,11-d_4.

CHAPTER 1: Background and Significance

Nearly everything around us is comprised of hydrocarbons which are constantly exposed to oxygen in the air which slowly degrades those organic compounds via the process of autoxidation. Autoxidation is a spontaneous radical chain reaction that oxidizes a substrate in the presence of molecular oxygen present in the air. This is demonstrated by the yellowing/discolouration of plastics over time, and deterioration of physical properties. The autocatalytic process primarily results in the formation of peroxides and/or hydroperoxides which eventually decompose to carbonyl compounds, sometimes with cleavage of the C-C bonds of the substrate. This facilitates the radical propagation throughout the material leading to a potential compromise of structural integrity and function. The general mechanism of hydrocarbon autoxidation was initially proposed by Charles E. Frank in 1950 [1] and was further developed later on by Dr. Keith Ingold [2]. The general mechanism involved 3 major steps, initiation, propagation, and termination, which will be elaborated on in the subsequent sections where lipids are the hydrocarbons substrate under consideration.

1.1 Lipid Peroxidation

Lipid peroxidation involves the autoxidation of membrane lipids where these free radical events have traditionally been associated with the propagation of neurodegenerative diseases. Biological membranes are susceptible to lipid peroxidation due to the presence of polyunsaturated fatty acids (PUFAs). These are the substrates on which radical chain propagation occurs between the lipophilic fatty acid tails on glycerophospholipids [3].

1.1.1 General Lipid Peroxidation Mechanism

The widely accepted general lipid peroxidation mechanism similarly follows that of the autoxidation of hydrocarbons as shown in **Scheme 1.1**. Lipid autoxidation differs in that the transfer step involving the H-atom abstraction by the radical initiator occurs on a lipid substrate.

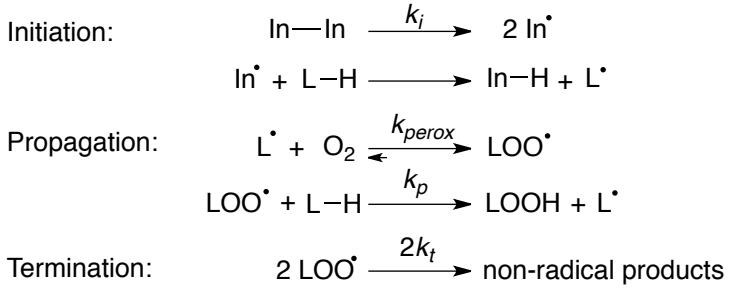

Scheme 1.1 Lipid peroxidation general mechanism. In = Initiator L = Lipid [3] [4].

Initiation of lipid peroxidation in cell membranes may occur as a result of exogenous factors such as exposure to sub 2.5μm particulate matter ($PM_{2.5}$) in environmental pollution and smoking, or UV-light [5] [6]. Reactive species such as hydroxyl radicals, superoxide, and peroxyl radicals present in biological systems have the capacity to initiate lipid peroxidation events. The electron transport chain (ETC) may 'leak' electrons, which reduce molecular oxygen to a superoxide, which can subsequently dismutate to hydrogen peroxide spontaneously or via catalysis by superoxide dismutase (SOD). This hydrogen peroxide can follow one of two major pathways, either the Haber-Weiss process utilizing Fenton-like chemistry to achieve a highly reactive hydroxyl radical and a hydroxide ion, or the hydrogen peroxide may be detoxified by glutathione peroxidase (GP_x) into water and molecular oxygen (**Scheme 1.2**) [5] [7]. If the hydrogen peroxide does not follow either of the aforementioned pathways, then it may be converted into hypochlorous acid (HOCl) by myeloperoxidase (MPO) for antimicrobial (lysosomal) action. HOCl undergoes an electron

transfer followed by a homolytic cleavage thereby forming a highly reactive hydroxyl radical and a chloride ion as the by-products [3] [8] [9].

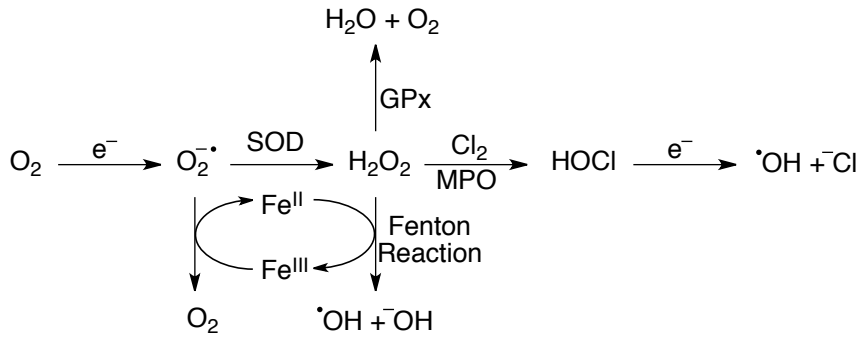

Scheme 1.2 Initiation of lipid peroxidation: *in vivo* ROS (hydrogen peroxide and hypochlorous acid) formation via superoxide (molecular oxygen) degradation [3] [8].

The autocatalytic process results in the decomposition of a hydroperoxide group (ROOH) to RO• and •OH. The radical intermediates can both perform H-atom abstractions from a substrate (RH) which yields a carbon centered radical (R•). Propagation follows, where the carbon centered radical reactions proceed near diffusion-controlled rates (10^9 M^{-1} s^{-1}) with molecular oxygen [3]. These can undergo peroxyl radical addition or H-atom abstraction. These competing pathways are dependent on the nature of the substrate. Sterols including the monounsaturated lipid, cholesterol have been reported to undergo both HAT and peroxyl radical addition, but oleate, a long chain monounsaturated lipid has only been reported to undergo HAT exclusively [4] [10]. Peroxyl and hydroperoxyl radicals are capable of oxidizing the bis-allylic positions found in PUFAs since the bis-allylic C-H bonds are known to have a BDE of approximately 76 kcal/mol, making them some of the weakest reported C-H bonds [3] [11] [12]. The rate of the H-atom abstraction is related to the bond dissociation energy (BDE) of the C-H bond. The HAT is rate limiting step (RLS) in the

propagation step and defined by the second-order rate constant k_p (**Scheme 1.3**). The rate of propagation must be greater than the rate of termination in a proper radical chain reaction.

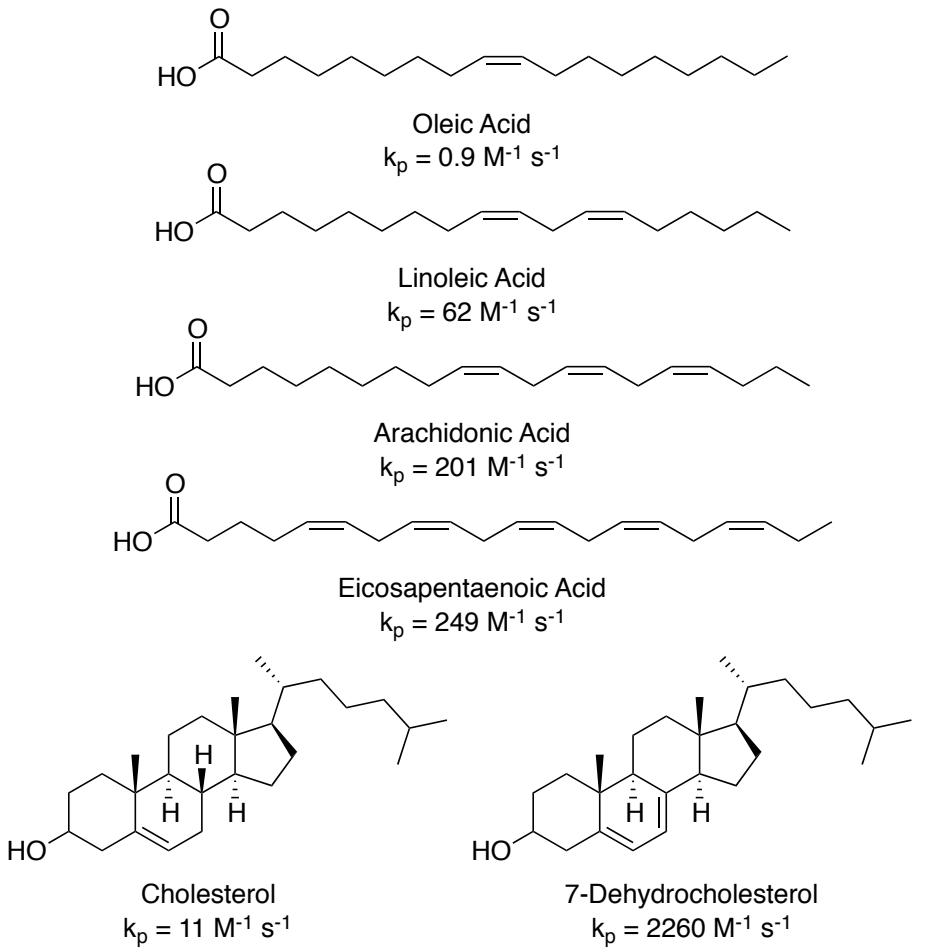

Scheme 1.3 Representative PUFAs and sterols and their corresponding rate constants for propagation. Adapted from Pratt & Zielinski (2017) [4] [5].

Radical chain termination occurs when two peroxyl radicals react head-to-head to produce a non-radical product. This predominates over other radical-radical reactions due to how quickly addition of O_2 to R• occurs, as well as the fact that it is a highly exergonic reaction [11] [12]. Although the rate constant of termination is very high (k_t = 6 x 10^8 M^{-1} s^{-1}), the low steady state concentration of peroxyl radicals relative to substrate means that propagation can compete. A single initiating radical may yield elevated concentrations of ROOH which demonstrates the exponential damage potential imparted by autoxidation.

1.1.2 Fates of Lipid Hydroperoxides in Biological Systems

Once lipid peroxides have formed in a biological system they can undergo a number of different pathways, such as dehydration (detoxification of peroxides by glutathione peroxidase-4 – GPX-4) to generate carbonyls, or acid catalyzed Hock fragmentation to produce two carbonyl by-products [3]. Lipid derived carbonyls have been associated in the regulated cell death pathway by the caspase-dependent apoptotic process and recent advancements have directly implicated lipid hydroperoxides in the auto-initiation of Ferroptosis [3]. Cells may be sensitized to Ferroptosis by accelerated rates of lipid metabolism leading to increases in oxidized polyunsaturated phospholipid concentrations which disrupt the iron (glutathione – GSH) equilibrium [13] [14]. This cell death pathway is controlled by the GPX4-GSH-cysteine axis [14]. Ferroptosis has been reported to link the observed accumulation of lipid peroxidation products with the various phenotypic dysfunctions detected in organ systems. This still requires further research to relate ferroptosis to specific disease pathologies [3] [13].

Correlations between lipid peroxidation and cell death have been reported as early as the 1960s [15] [3]. PUFAs have been widely reported to have large KIE (k_H/k_D) values which define their protective effects in cells supplemented with deuterated-PUFAs [10] [16]. This protective role was demonstrated by Shchepinov *et al.* with 20% supplementation of 11,11-d_2-linoleate to cells reducing the lipid autoxidation-induced cell death [17] [10]. This result was corroborated in a study using mouse models for Parkinson's disease where the protective RTA effect was reported upon administration of the deuterated-PUFAs to reduce rates of death [18] [10].

1.2 Plasmalogens

Plasmalogens are a class of phospholipids that are biosynthesized and widely distributed throughout cell membranes of mammalian tissues and, particular anaerobic microorganisms [19]. They comprise one fifth of all phospholipids in the body, yet plasmalogens remain the least studied of all common phospholipids. Plasmenylcholine comprises a subclass of plasmalogen phospholipids which are characterized by the presence of a distinctive O-(Z)-alkenyl (vinyl) ether at the *sn*-1 position of the glycerol backbone. This class of phospholipids is believed to be involved in a wide range of biological processes including signalling between cells, membrane adhesion, membrane dynamics, and lipid peroxidation [19]. Plasmalogens are a biomolecule of particular interest since they seem like radical trapping antioxidants (RTAs) yet they are lipids.

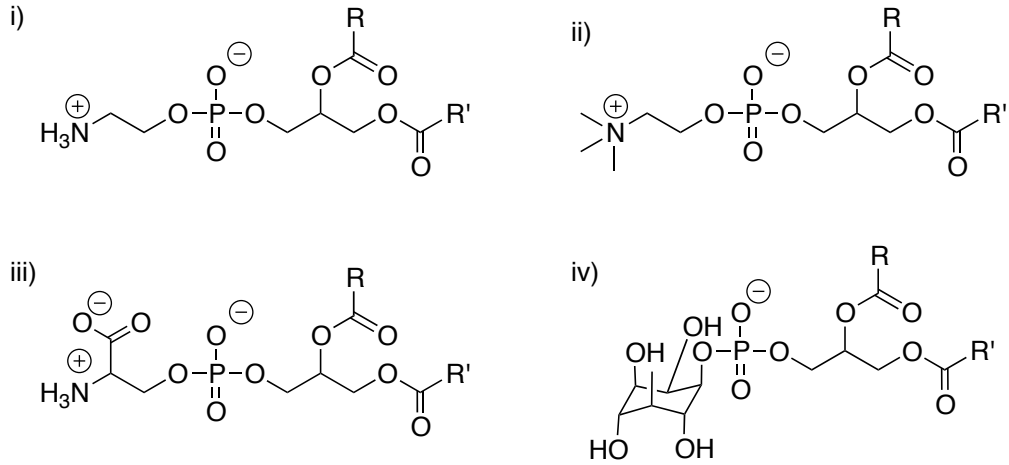

Scheme 1.4 Common types of polar head groups found at the *sn-3* position of glycerophospholipids. i) Ethanolamine ii) Choline iii) Serine iv) Inositol [19].

Glycerophospholipids are a class of membrane protein typically comprised of a glycerol backbone attached to long fatty acid chains at the *sn*-1 and *sn*-2 positions. They are defined by the class of polar head group bound by a phosphodiester linkage at *sn*-3 position. The most common hydrophilic head groups include choline, ethanolamine, serine, and

inositol as shown in **Scheme 1.4**. The most common fatty acids bound to glycerophospholipids include arachidic acid, stearic acid, palmitic acid, linoleic acid, oleic acid, linolenic acid, arachidonic acid and uric acid. The first three of the aforementioned fatty acids are the most commonly observed in phospholipids [20].

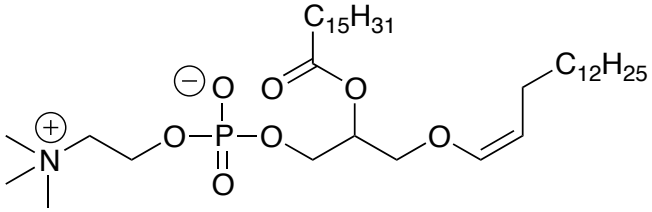

Scheme 1.5 Plasmenylcholine structure.

These particular plasmalogens can include differing polar head groups at the sn-3 position and contain an ester linkage to a highly unsaturated fatty acid at the sn-2 position **Scheme 1.5** [19] [21] [22]. The type of head group bound does not define this subclass. Plasmalogens were serendipitously discovered by German biochemists, Feulgen and Voit, in 1924 [23]. They coined the term plasmalogen to describe the unknown compound that generated a plasma aldehyde when it was treated with acid. The general structure of a plasmalogen was characterized in 1957 and stereochemistry of the O-(Z)-alkenyl ether was determined in 1962 via infrared spectroscopy by Rapport *et al*., Debuch *et al.* and, reconfirmed by Marinetti and Erbland [24] [25] [26] [27]. They had determined that the parent compound was a glycerophospholipid coupled to an acid labile vinyl ether group at the *sn-1* position, but they had not yet deduced the stereochemistry of the vinyl ether component at the *sn-1* position [28]. Plasmalogen research plateaued in the 1970's and 1980's when the main focus was on ascertaining the correct biosynthetic pathway [29].

The biosynthetic pathway generating plasmenylethanolamine has been well studied, and characterized by Nagan and Zoeller [20]. Plasmenylcholine biosynthesis is not well understood. Plasmenylethanolamine is suspected as being a precursor but this has yet to be confirmed. The key step was believed to occur later in the biosynthesis within the endoplasmic reticulum where alkyl ether phosphatidylethanolamine/plasmanylethanolamine was converted to the characteristic vinyl ether phosphatidylethanolamine through an O_2 dependent oxidation [30]. The difficulty with justifying and accepting this biosynthetic pathway arose from the absence of a specific identifiable plasmanylethanolamine desaturase; the enzyme responsible for catalyzing this reaction. This unknown desaturase was coined the 'Orphan enzyme' [31] [32] . The most reasonable pathway proposed involves the use of choline-diacylglycerol ethanolaminephosphotransferase to convert alkenylglycerol from plasmenylethanolamine to plasmenylcholine. The formation of alkenylglycerol is not fully understood yet the accumulation of alkenylglycerols in the myocardial membranes of rabbits provides strong evidence in support of this [20].

In recent years there have been significant leaps in our understanding of plasmalogen biosynthesis. Firstly, *Myxococcus xanthus* (obligate aerobe, which biosynthesized plasmalogens) was thought to require the multifunctional catalytic enzyme ElBD, or alternatively MXAN_1676 to be directly involved in the alkenyl ether bond formation [33] [34]. This was disproven shortly after when the bacterial enzyme CarF (homologous to the human enzyme TMEM189) was found in *Myxococcus xanthus* (obligate aerobe) and was determined to act as a membrane associated indirect sensor of oxidative damage in cells. CarF activation initiates signaling following a similar pathway to that of protoporphyrin IX when it's photoactivated it released singlet oxygen, which inactivated CarR, then triggered

the release of CarQ (cognate σ-factor) [35]. This activated the transcription of genes coding for the proteins required for carotenoid biosynthesis which present RTA activity thereby quenching singlet oxygen and other reactive oxygen species present. This is can be detected empirically using spectrophotometry to monitor the rate of change in color from yellow to red which corresponds to the conversion to the Car^+ phenotype. This suggest that CarF plays a protective role against ROS in the biological system. Furthermore, CarF homologs are highly conserved amongst both animals and plants and share a number of notable similarities which indicates that it plays a vital role in their well-being [36].

Finally, it was revealed that TMEM189 was in fact the highly sought 'orphan desaturase' that was responsible for performing the key biosynthetic step [36]. It was also discovered that it was only present in animals since animal CarF homologs shared 11 of the 12 conserved histidine residues, while the plant CarF homologs only shared 8 histidine residues. This may have affected protein binding through decreased coordinated bonding with the substrate and prevented the correct orientation from being achieved to allow for the conversion to the target [36].

The reliance on TMEM189 to produce plasmalogens was demonstrated when the ether lipid content was measured and compared between HAP1 human cell lines and CRISPER/Cas9 *TMEM189* knockout (KO) cells. The control HAP1 samples presented chromatographic peaks consistent with plasmalogen lipids while the peaks were absent for the KO samples. The discovery of this animal plasmanylethanolamine desaturase is a significant step forward as it allows us to 'feed' substrate (plasmalogen precursor) to the enzyme and exploit its catalytic activity to generate more plasmalogen material for additional studies. This would be a more economical approach and avoids the challenges of

synthesizing the target with the highly sought after cis-vinyl ether functionality the target *de novo* [35] [36].

1.2.1 Role of Plasmalogens in Pathophysiology

Plasmalogen phospholipids have been implicated in a proliferation of a multitude of degenerative diseases including Alzheimer's disease [37], Parkinson's disease [38], and Neonatal Progeroid Syndrome (NPS); progressively debilitating diseases such as atherosclerosis and asthma [39] [40]; and a variety of other plasmalogen-deficiency disorders [41] [42] [43]. Plasmalogen phospholipids have demonstrated a crucial role in Neonatal Progeroid Syndrome (NPS) pathology, but the precise mechanism of action has yet to be elucidated as there has not been a detailed study investigating plasmenyl-bound phospholipid species.

Preliminary research supports the hypothesis that plasmalogens play a protective role in the cell membranes through the antioxidant activity (termination of lipid peroxidation chain reaction) imparted by the distinct cis-vinyl ether functionality present at the *sn*-1 position on the glycerol head. This was expanded to imply that plasmalogen-deficient cells are more susceptible to oxidative stress than cells with a natural plasmalogen distribution which acted as a sacrificial antioxidant. Cell membrane fidelity maybe compromised in patients with plasmalogen-deficiency disorders due to the lack of radical trapping, which leads to an exponential increase in the rate of degradation/cleavage of the lipophilic fatty acid tails as proposed by Murphy [44]. Moreover, the introduction of peroxidic by-products within the lipid bilayer would disrupt the tight packing and increase polarity leading to increased water permeation due to the change in structural integrity which may eventually lead to micellization [3]. The propagation mechanism is attenuated due to the proximal requirements for reactivity of a bis-allylic methylene group. The hydroperoxide bound

moiety at the *sn-1* position is fairly unstable and will readily oxidize to generate lyso-PC and an armed glycerol head. As the oxidative stresses accumulate, the morphology of the cell membrane begins to change and there is increased leakage of ions in the cells which increases susceptibility to cell death (**Scheme 1.6**) [19] [45]. Additionally, their free-radical scavenging activity is enhanced due to the higher oxidizability in comparison to natural polyunsaturated fatty acids (PUFAs), and the presence of the vinyl-ether moiety oriented very close to the surface of the lipid bilayer. Alternatively, researchers contend that plasmenyl lipid peroxidation would lead to the generation of highly-reactive products which may have damaging effects on cell membrane structural integrity and biological systems as a whole [46].

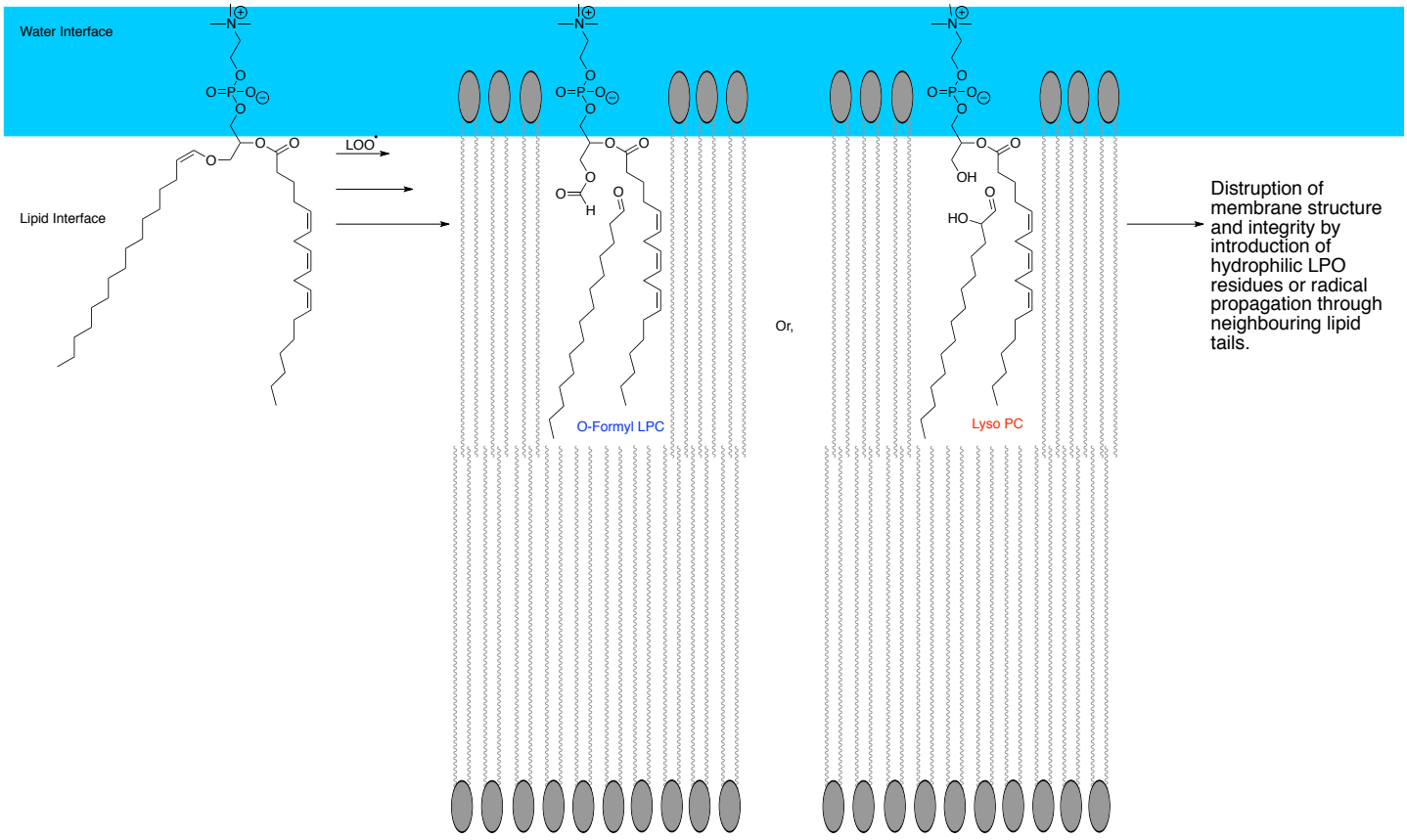

Scheme 1.6 Effects of LPO on phospholipid membrane integrity adapted from Thompson (2017) [47].

Autoxidation of plasmalogen was reported to cleave the vinyl either to yield long-chain aldehydes which are of interest based on their perplexing activity. Certain lipid-derived aldehydes have been reported to have protective antioxidant effects observed *in vivo* while other long-chain aldehydes (ex. 9-hydroxynonenal) were implicated with the pathogenic effects of lipid peroxidation [48] [49]. Lipid hydroperoxides formed as a by-product of lipid peroxidation are suspected of having detrimental effects upon the membrane bilayers in biological systems since they may shift the newly polarized portion to the surface of the membrane [50]. This may lead to reduced thickness which would adversely impact the structural integrity and permeability of the membrane [51]. Additionally, by-products of lipid autoxidation may be highly electrophilic, such as aldehydes, which would wreak havoc by covalently binding proteins through augmenting protein folding and function. Free electrophiles in the body may also bind with the negatively charged DNA bases and silence gene expression [52].

In vivo, newly generated ROS can initiate a lipid peroxidation reaction which may affect the fidelity of the cell membrane. The plasmenylcholine molecule's hydrophobic-hydrophilic interface includes two sp^2-hybridized carbon atoms (vinyl carbons), which are further activated by electron-donating nature of the neighbouring oxygen atom. Moreover, the hydrogen atoms neighbouring the vinyl ether bond are prone to abstraction as a result of their low dissociation energies [44]. Plasmalogens are preferentially oxidized over the natural diacyl-glycerophosphates in the presence of free radicals and singlet oxygen as demonstrated by their consumption in the reaction and formation of stable lyso-lipid by-products [53].

This demonstrates the radical trapping antioxidant abilities and possible protective antioxidant properties of plasmenylcholine, which are facilitated by radical propagation throughout the side-chains of the neighbouring plasmalogens. Currently there is very little known about autoxidation of O-(Z)-vinyl ethers on plasmenylcholine.

1.2.2 Plasmalogen Synthesis and Challenges

Isolation of these plasmalogen phospholipids from natural sources is extremely challenging due to the difficulty in chromatographic separation of the ester and ether glycerolipids bound to polar head groups. The O-(Z)-alkenyl ether is especially reactive to photo- and thermally-catalyzed oxidation under acidic conditions which presents a significant synthetic challenge, that drastically limited the reagents and separation conditions that may be applied. Conventional lipid extraction methods employed acidic conditions to ensure protonation and extraction of acidic lipids, but in this case the acidic conditions degrade plasmalogens through hydrolysis of the vinyl ether [20]. Moreover, under basic or mildly acidic conditions, the acyl group at the *sn-2* position is susceptible to quick migrations (rearrangements) to the *sn-1* or *sn-3* positions [23]. These constraints imply that plasmalogens must be synthesized de novo in order to study O-(Z)-alkenyl ether functionality at the *sn-1* position.

Difficulties in obtaining sufficient quantities of plasmalogens from natural sources, and lack of authentic standards for analytical comparison led Thompson and colleagues to develop various synthetic pathways to plasmenylcholine in the early 1990s. Thompson furthermore had a vested interest obtaining plasmenylcholine synthetically in order to study the photo-triggered morphological changes in plasmalogen liposomes using visible light, which may be exploited for targeted photo-induced liposomal drug delivery. In the early

2000s, the Thompson research group pioneered a multitude of syntheses from a wide variety of starting materials, but only achieved a racemic product. Thompson and his colleagues finally discovered an enantioselective synthesis of plasmenylcholine in 2007 (**Scheme 1.7**) [19].

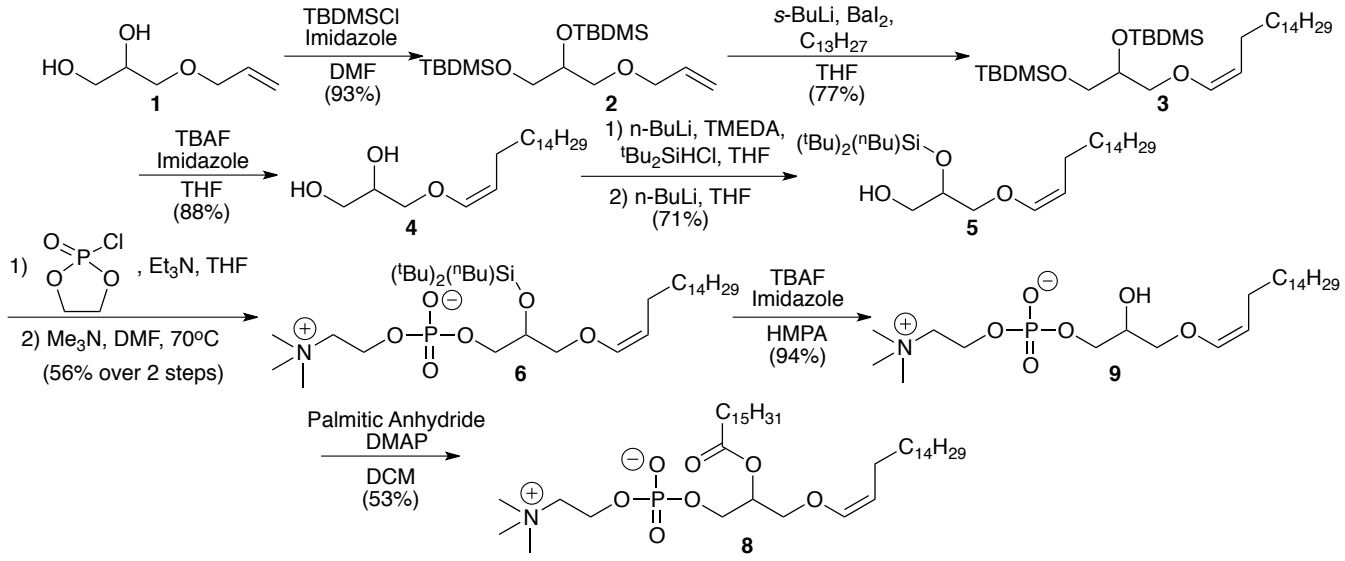

Scheme 1.7 Regioselective plasmenylcholine synthesis by Thompson **[21]**

1.2.3 A Proposal for the Antioxidant Activity of Plasmalogens

Dr. Zosia Zielinski performed a number of computations using MeO-Butene as a cis-vinyl ether model substrate for the plasmenyl lipids. The initial HAT rate constant was calculated as $k_{calc} = 0.6\ M^{-1}\ s^{-1}$ while the rate constant accounting for the proton tunneling was $k_{calc,\ tunneling} = 60$. The subsequent epoxidation was shown to have an overall rate constant of $k_{calc} = 16\ M^{-1}\ s^{-1}$. The first epoxidation step had a second order rate constant of $16.4\ M^{-1}\ s^{-1}$ (reverse of this step was $252\ s^{-1}$). The second epoxidation step had a first order rate constant of $9.5\times10^{5}\ s^{-1}$. These results indicated that addition may play a more significant role, but this requires future work to ascertain.

Based on the reported HAT and peroxyl radical addition pathways by which lipids are known to autoxidize, two possibilities can be considered for plasmalogens (**Scheme 1.7**). Either a fragmentation yielding an peroxyl radical that is capable of initiating a subsequent chain reaction will form in the case of the peroxyl addition; or the superoxide will be lost in order to expel the radical character from the lipid in the case of the H-atom abstraction. The HAT pathway was anticipated based on the close proximity of the cis-vinyl ether moiety to the water-lipid interface allowing for phase transfer of the propagating radical as observed in the peroxide mediated peroxidation by coenzyme Q10 [3]. Both of the intermediates are capable of generating lyso-PC but a direct mechanism accounting for the production of the O-formyl lyso-PC has not been established. The lyso-PC product generated is stable and would not initiate another chain reaction [44].

Based on the autoxidation product distribution between lyso-PC and O-formyl lyso-PC, one may deduce which of the plasmalogen autoxidation mechanistic pathways is favored. If the O-formyl LPC is detected as the major product of plasmalogen autoxidation, then it supports the peroxyl addition mechanism. If the Lyso-PC is detected as the major product of the peroxidation, then it supports the alternative H-atom abstraction pathway.

O-formyl-LPC may not have been anticipated as a product of plasmalogen autoxidation previously and therefore was not sought or detected in previous studies. The challenges in autoxidation monitoring through product monitoring could be circumvented by measuring the rate of superoxide formation, plasmenylcholine consumption as alternative indirect monitoring techniques. By probing the mechanism using contemporary analytical chemistry techniques and instruments, it would allow us to view the results from a modern lens. Understanding the fundamental underpinnings of the plasmalogen mechanism of

oxidation would shed a light on how it may be inhibited if it is found to be detrimental or accelerated if it is found to be beneficial.

1.2.4 Methyl Linoleate Clocking

This clocking technique operates based on the competition between unimolecular peroxyl radical rearrangement (k_R) and bimolecular H-atom transfer (k_H) [55]. The methyl linoleate autoxidation mechanism was extensively studied and had a reported rate constant for the reaction with peroxyl radicals of $k_{H\text{-linoleate}} = 62\ M^{-1}\ s^{-1}$. The product distribution of methyl linoleate autoxidation products is extremely dependent on the hydrogen atom donor (H-donor) rate constant which regulates the competing processes (**Scheme 1.8**) [55].

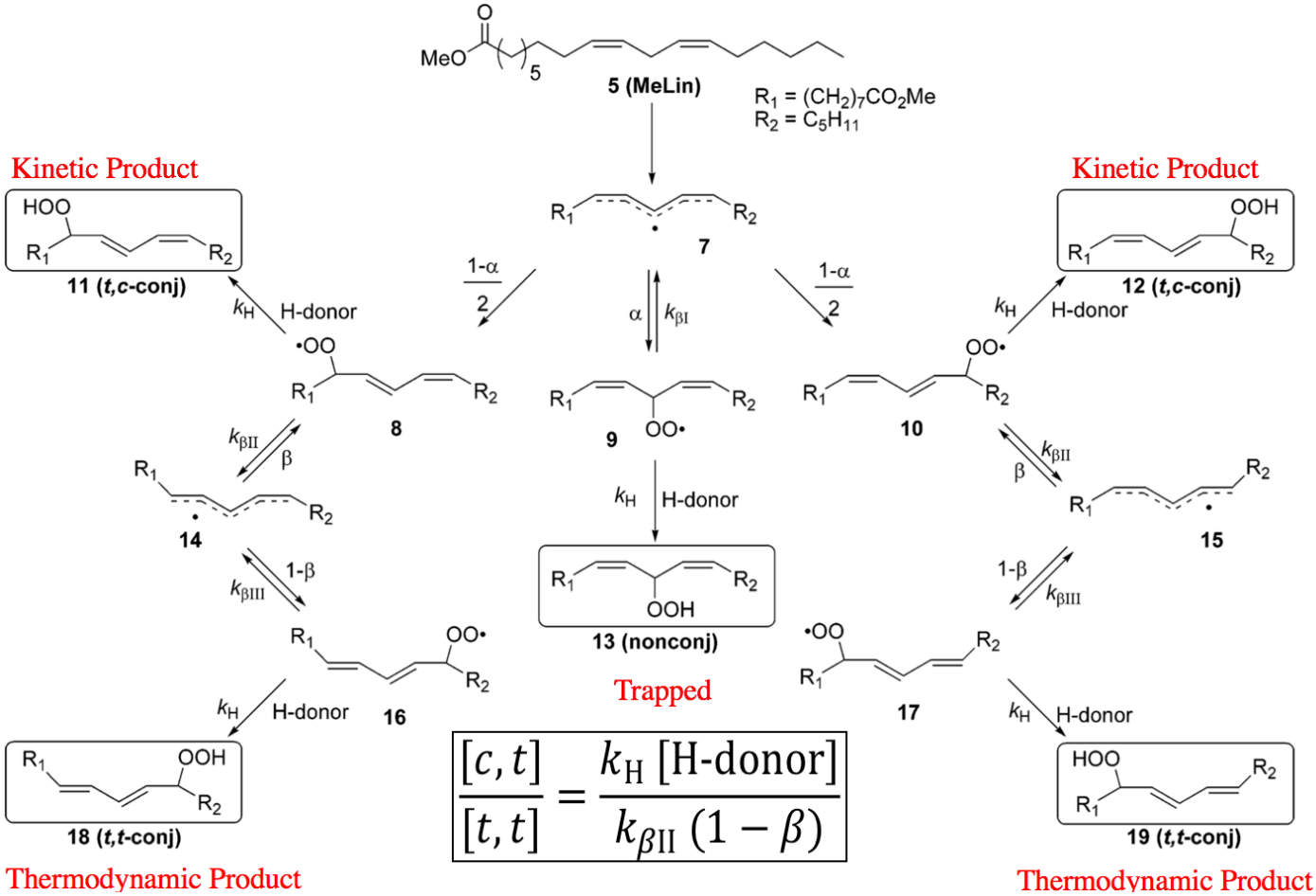

Scheme 1.8 Methyl linoleate autoxidation mechanism adapted from Porter *et al.* (2006) [55].

Methyl linoleate autoxidation initiated with a H-atom abstraction from the bis-allylic position, forming the pentadienyl radical (**Scheme 1.8: 7**). Molecular oxygen then added at positions of radical electron delocalization and increased spin density (C9, C11, and C13). Following the O_2 partitioning across the 3 potential positions the alkyl peroxides could then be trapped by an H-donor, antioxidant, or lipid molecule to form conjugated (**Scheme 1.8: 8, 10**) or nonconjugated (**Scheme 1.8: 9**) peroxyl radicals. The partitioning coefficient for the conjugated peroxyl radicals was 1-α and the partitioning coefficient for the nonconjugated peroxyl radicals was α [55].

In the presence of a good H-donor, only the kinetically controlled oxidation products would be observed (**Scheme 1.8: 11, 12, 13**). Due to the fact that the β-fragmentation of the conjugated peroxyl radicals wouldn't compete with the trapping, then only the *cis,trans*-hydroperoxides (**Scheme 1.8: 11, 12**) would be observed. The nonconjugated peroxyl radical is capable of performing a fast β-fragmentation ($k_{\beta I}$) to reform the pentadienyl radical. This fragmentation is in completion with the HAT (k_H) to the peroxyl radical leading to the generation of the nonconjugated hydroperoxide (**Scheme 1.8: 13**) [55].

In the presence of a poor H-donor, only the thermodynamic conjugated hydroperoxides (**Scheme 1.8: 11, 12, 18, 19**) were observed due to the increased strength of the C-OO bond and the minor rate of β-fragmentation. This was a result of the lack of competition between the H-donors and β-fragmentation ($k_{\beta I}$). $k_{\beta I}$ comprised the major pathway and as such there were insignificant amounts of the nonconjugated peroxyl radical formed (**Scheme 1.8: 9**) therefore, only the conjugated peroxyl radicals (**Scheme 1.8: 8, 10**) were of importance with respect to thermodynamically controlled autoxidations. Once they had formed they could undergo a bond rotation then a β-fragmentation ($k_{\beta II}$) thereby

generating a new pentadienyl radical (**Scheme 1.8: 14, 15**) with a *trans-cis*-conformation. Oxygen then adds at one of the two ends (cisoid or transoid) to form *trans,cis*- (**Scheme 1.8: 8, 10**) or *trans,trans*-conjugated peroxyl radicals (**Scheme 1.8: 16, 17**). The partitioning coefficient of β corresponded to the *trans,cis*-conjugated peroxyl radicals while the *trans,trans*-conjugated peroxyl radicals maintained a O_2 partitioning coefficient of 1-β. The conjugated peroxyl radicals can convert to the original pentadienyl radical through a β-fragmentation ($k_{\beta II}$, $k_{\beta III}$). This fragmentation is in completion with the HAT (k_H) to the peroxyl radical leading to the generation of the *trans,cis*-conjugated hydroperoxides (**Scheme 1.8: 11, 12**), and the *trans,trans*-conjugated hydroperoxides (**Scheme 1.8: 18, 19**) The rate constants of the β-fragmentation clock reactions were reported in the 10^6 to 10^2 s^{-1} regions and as such the rate constant for the antioxidant could then be calculated based on the formula shown in **Scheme 1.8** [55].

1.2.5 Research Objectives

The purpose of this research project was to synthesize plasmenyl lipids, their alkyl glycerol precursors and, cis-vinyl ether model substrates to compare their impact on the rate of phospholipid peroxidation. Moreover, we sought to synthesize deuterated analogues to provide insight as to whether HAT or peroxyl radical addition was the mechanism responsible for any observed antioxidant activity. We aimed to autoxidize the natural and selectively deuterated plasmalogen substrates while monitoring their rates of consumption over time then comparing to establish if a kinetic isotope effect (KIE) was involved in this mechanism. If there is no change in the substrate consumption (autoxidation) rates between the natural and partially deuterated plasmalogen then it would indicate there is no KIE. This would imply that the H-atom abstraction pathway is not possible and that a peroxyl addition

mechanism was favored, conversely if a KIE was present then the HAT mechanism would predominate (**Scheme 1.9**) [56].

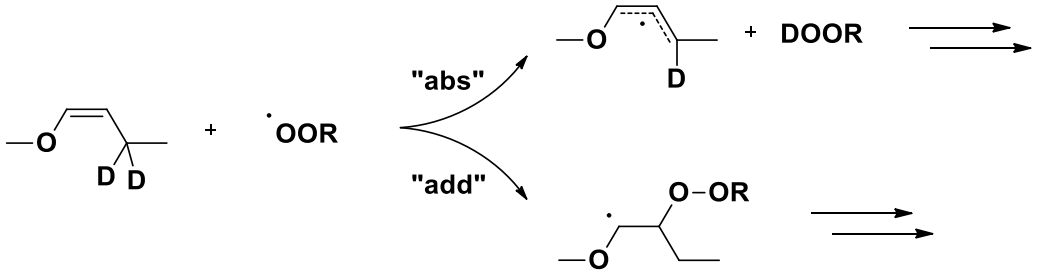

Scheme 1.9 Generalized hypothesis illustrating 2 potential fates for the mechanism of autoxidation of the cis-vinyl ether.

1.3 On the Relevance of Addition to Unsaturated Fatty Acid Oxidation

As mentioned above, unsaturated fatty acids are believed to propagate solely by HAT. However, given how relatively unactivated monounsaturated fatty acids are to HAT, they may be expected to undergo addition reactions, too, like cholesterol and its derivatives as well as plasmalogens [57] [10]. Indeed, epoxides of oleate sidechains of phospholipids have purportedly been observed [58]; however, as far as we are aware, there is no evidence that monounsaturated fatty acids propagate by addition.

Methyl oleate autoxidation was initially investigated by Farmer and Sutton in 1943 when they proposed that the autoxidation product mixture would contain a mixture of C8- and C11- oleate hydroperoxides [59] [60]. They continued to develop their hypothesis when they determined that C9- and C10- oleate hydroperoxides may also be present in the methyl oleate autoxidation product mixture [59] [60]. Their overall hypothesis was summarized by Frankel et al. in 1977 where a symmetric mechanism was presented (**Scheme 1.10**) [61]. The products were expected to have an equal distribution since the hydroperoxyl would be able to attack any position (8, 9, 10, and 11) with equal probability and partition the oleate

radical between those positions; as such the resulting unsaturation would be similarly present at the original $\Delta^{9,10}$ position or neighbouring $\Delta^{8,9}$, or $\Delta^{10,11}$ positions [61] [62] [57].

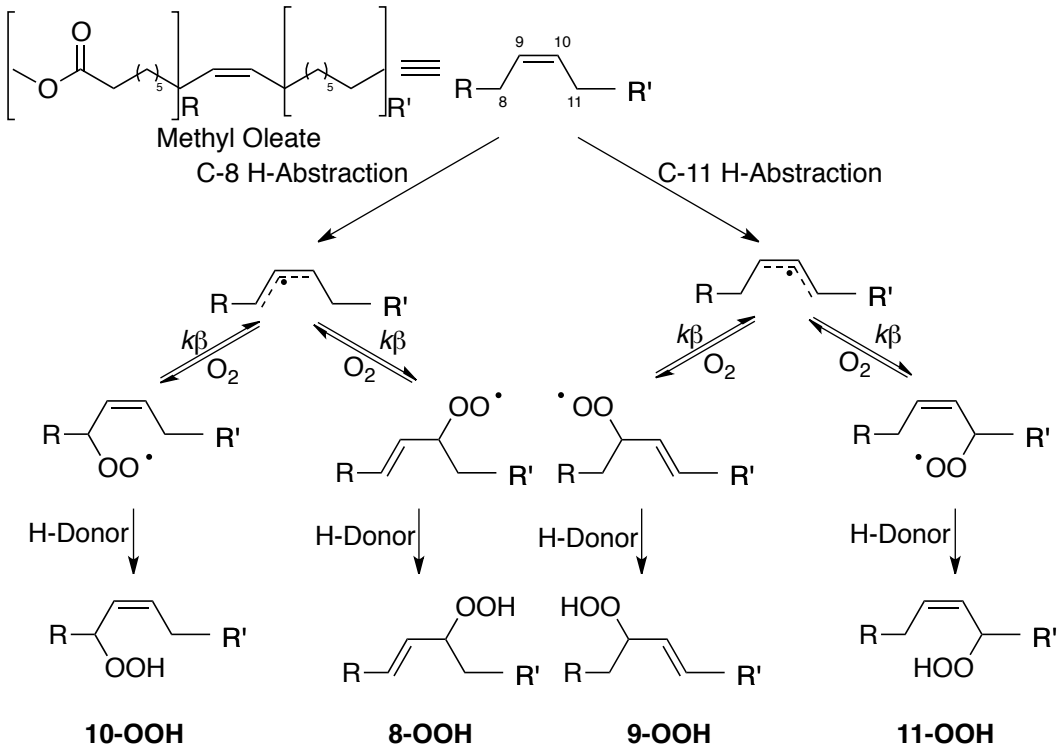

Scheme 1.10 First proposed methyl oleate autoxidation mechanism [61] [62] [57].

Later on, Porter *et al.* (1994) demonstrated that the aforementioned mechanism was incorrect and that the product distribution was skewed based on the fact that it was more kinetically favorable for singlet oxygen to attack the higher spin density allyl terminus position. This was supported by the discovery of the oleate autoxidation product distribution ratio 11-*cis*:9-*trans* of 1:1.2. It was noted that this arose from the unequal addition where 55% of the oxygen added to the 9-position to form 9-*trans* allylperoxyl, and 45 % of the oxygen added to the 11-position leading to 11-*cis* allylperoxyl. The presence of methyl oleate derived allyl radicals has been studied and confirmed via EPR spectroscopy. Porter *et al.* also suggested that the rearrangement of the allylperoxyl radical that led to the formation of the thermodynamic products 11-*trans* and 8-*trans* as well as 9-*trans* and 10-*trans* oleate

hydroperoxides from the kinetic products that were rapidly formed initially. These were formed when the intermediate peroxyl radicals undergo a bond rotation followed by a β-fragmentation, and subsequent O_2 addition, then a HAT (**Scheme 1.11**) [62] [57].

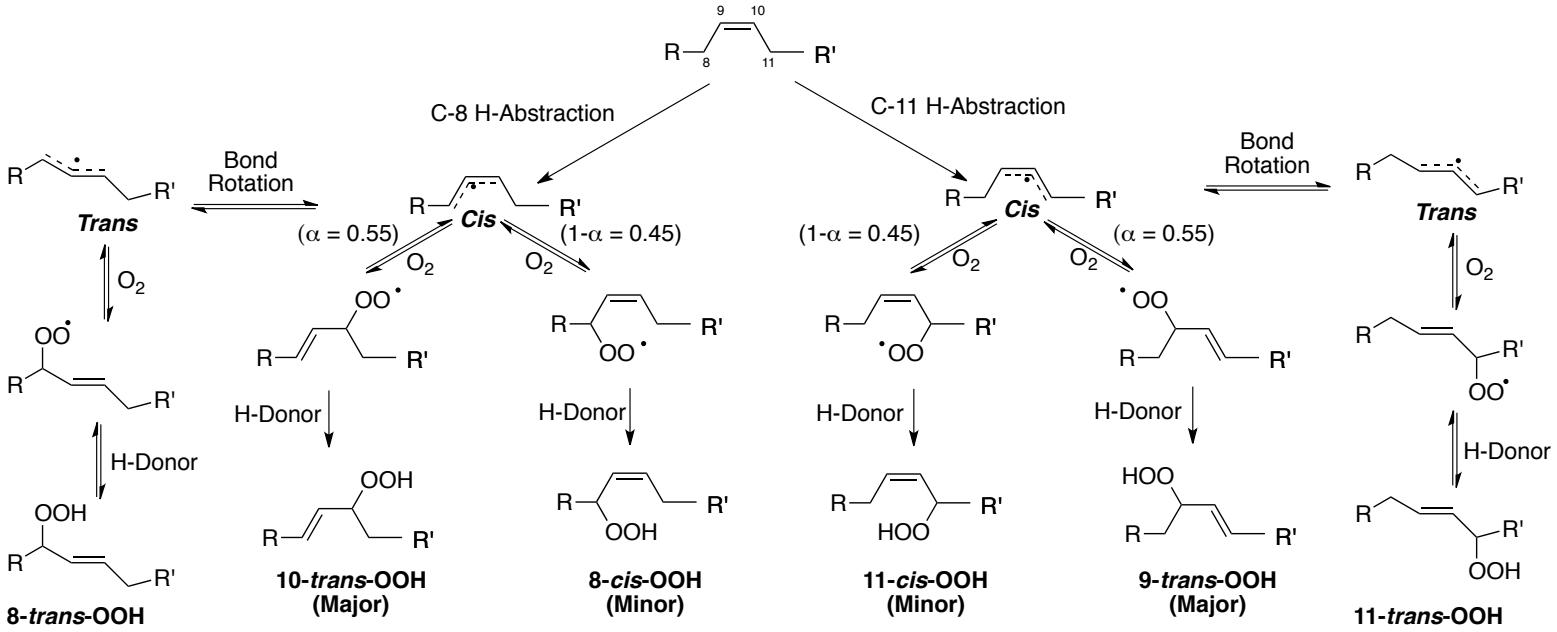

Scheme 1.11 Updated methyl oleate autoxidation mechanism illustrating the formation of the 6 possible products of methyl oleate autoxidation [57].

Neither Farmer and Sutton (1943), Frankel (1977), nor Porter (1994) mention detection of epoxides derived from oleate autoxidation. Given the role of peroxyl radical addition in the mechanism of autoxidation of cholesterol (also a monounsaturated lipid), Dr. Zosia Zielinski recently investigated the possible role of peroxyl radical addition to monounsaturated lipids using both computational and experimental methods. To provide experimental insight, Dr. Zielinski looked at the autoxidation of hexadec-8-ene. This substrate was chosen as a model for monounsaturated fatty acids such as oleate, since its symmetry would simplify the product distribution, and the product distribution arising from autoxidation would be amenable to analysis by gas chromatography. The computational rate (k_{calc}) of HAT with hexadec-8-ene was 1.0 M^{-1} s^{-1} which is notably slower than other PUFAs;

the calculated rate of peroxyl addition was 1.04 M^{-1} s^{-1} (reverse was 18.9 s^{-1}) and the subsequent epoxidation was calculated to proceed at 6.4 x 10^4 s^{-1}. Both rates are slower than with cholesterol, but the epoxidation was ten-fold slower. Hexadec-8-ene and hexadec-8-ene-7,7,10,10-d_4 were synthesized and autoxidized, revealing that epoxides were formed and to a greater extent in the deuterated substrate. These results imply the formation of epoxides in the autoxidation of oleate and other monounsaturated fatty acids – and suggest that they may have been previously overlooked due to the resolution afforded by the analytical techniques in use at the time (**Scheme 1.12**).

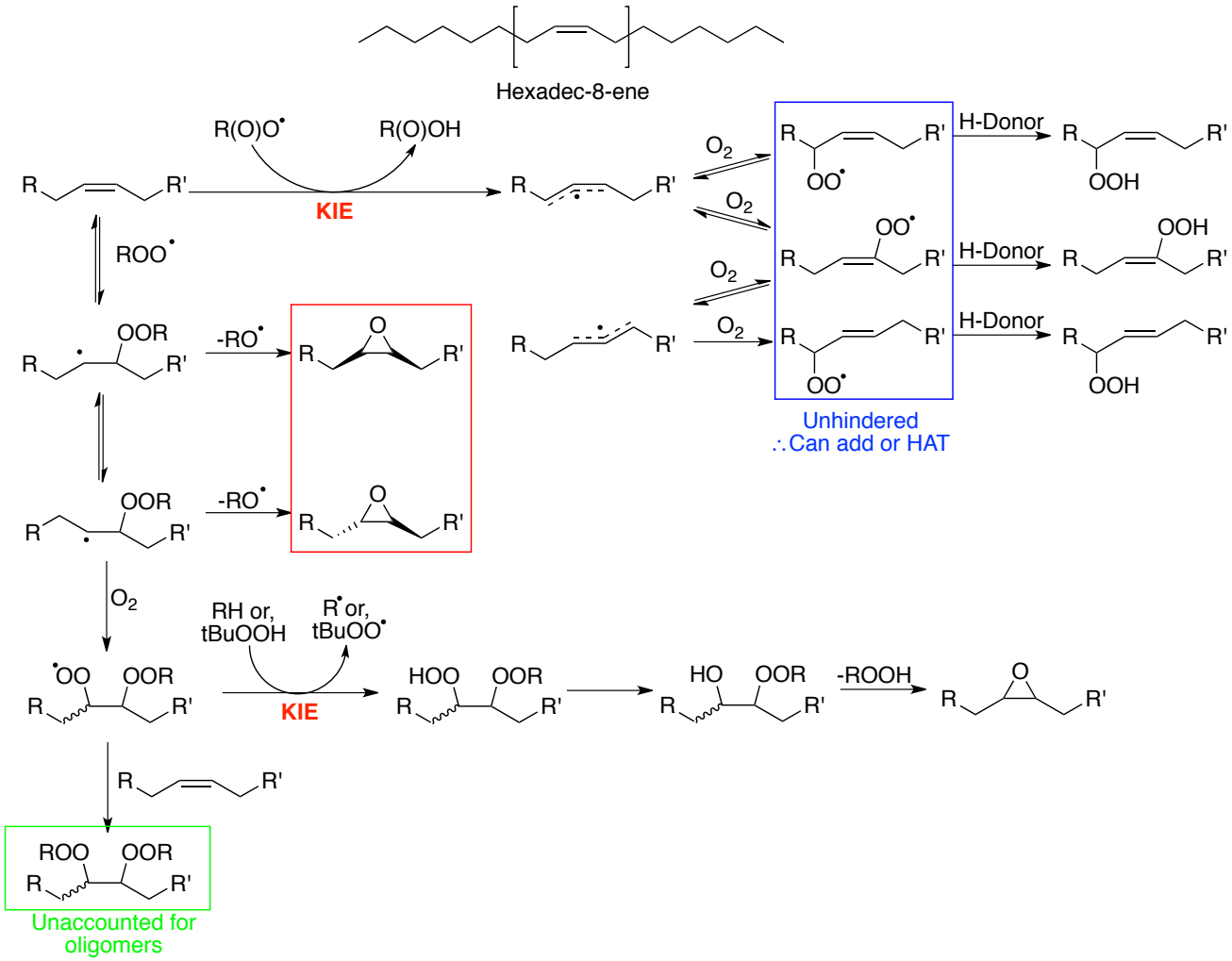

Scheme 1.12 Current hypothesis for the mechanism of hexadec-8-ene. (Proposed by Dr. Zosia Zielinski)

1.3.1 Research Objectives

The purpose of this project was to autoxidize methyl oleate along with its partially deuterated analog (methyl oleate-8,8,11,11-d_4), then analyze the mixtures using an analytical method capable of resolving the epoxide(s) products that are believed to form. Thus, we sought to synthesize a methyl oleate-8,8,11,11-d_4, and the epoxide standards (methyl oleate-9,10-*cis*-epoxide, methyl oleate-9,10-*trans*-epoxide, and methyl oleate-9,10-*cis*-epoxide-8,8,11,11-d_4), determine the appropriate autoxidation conditions, and develop an analytical detection method. We sought to rationalize the observation of the epoxide products in cholesterol autoxidation (formed through the peroxyl radical addition), with the aforementioned lack of reports of methyl oleate epoxide products propagating autoxidation. If there is a higher rate of conversion to epoxides, then it would support the presence of the peroxyl radical addition mechanism. If there is a higher conversion rate to hydroperoxides, then it would support the H-atom abstraction mechanism.

CHAPTER 2: Plasmalogen Synthesis and Attempts to Evaluate its Autoxidizability

2.1 Introduction

Previous investigations into plasmalogen autoxidation were not adequate as such we aim to establish a robust synthetic approach to generate plasmalogen for the study of its autoxidizability.

We developed a synthesis based on the modifications reported by Shin and Thompson (2002 [24], 2003 [63] [65], and 2007 [21]) by combining the beneficial features from each synthesis. The first approach proposed by Shin and Thompson involved the selective protection of the *sn*-2 alcohol to generate a racemic mixture of plasmenylcholine, but this achieved poor yields (**Scheme 2.1**) [22].

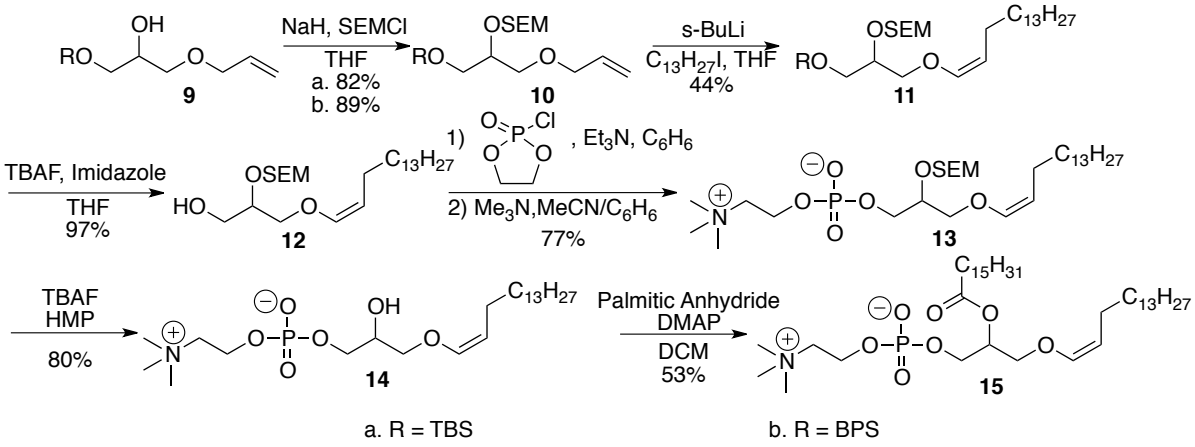

Scheme 2.1 Racemic plasmenylcholine synthesis from Shin & Thompson (2002) [24].

The second approach proposed by Shin and Thompson [24] (**Scheme 2.2)** was intended to generate a chiral plasmenylcholine and mitigate acyl migration in the last TBAF-mediated desilylation (**14**) through installation of the phosphatidylcholine group to the *sn*-3 position prior to deprotection and acylation of the *sn*-2 position. This posed late stage purification challenges following the addition of the charged phosphate groups, as separation of an amphiphilic target is tedious.

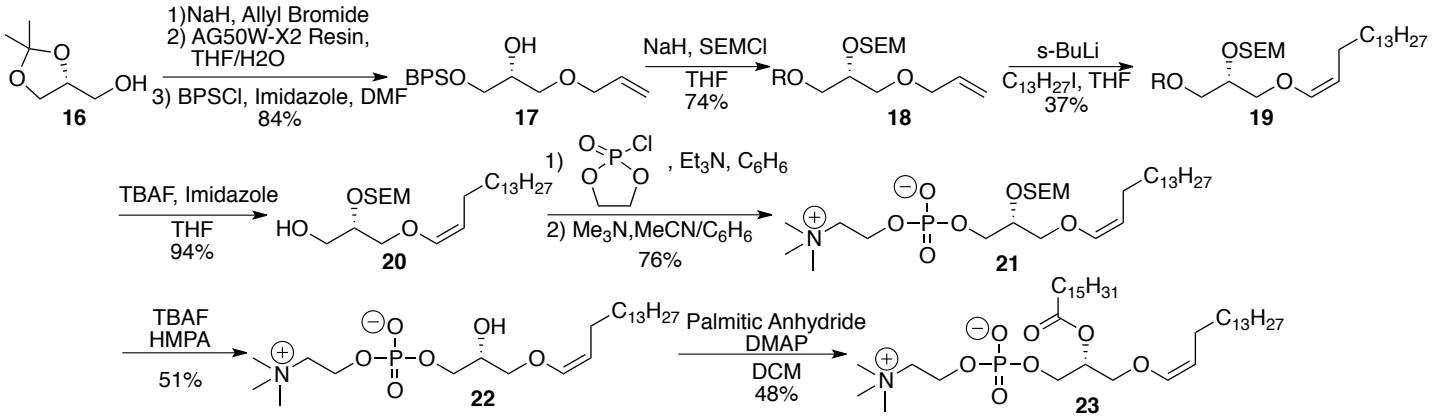

Scheme 2.2 Chiral-(R)-plasmenylcholine synthesis from Shin & Thompson (2002) [24].

A later approach by Thompson in 2007 aimed to optimized yield of the alkylation through the use of organobarium intermediates (**Scheme 2.3**) [21]. This was intended as an optimization of the former approach but failed to address the challenges of isolating amphiphilic intermediates.

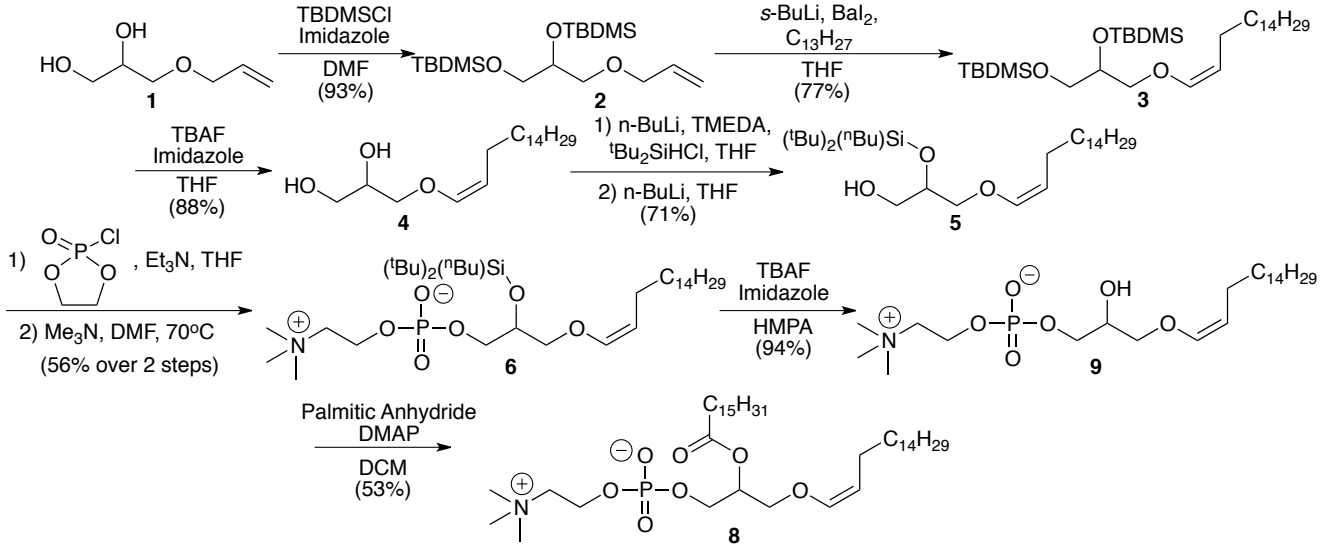

Scheme 2.3 Plasmenylcholine synthesis adapted from Thompson (2007) [21].

We proposed the following retrosynthesis **(Scheme 2.4**) which employed the first di-protection, alkylation, and deprotection from (**Scheme 2.3**), then the first protection from (**Scheme 2.3**) was repeated with 1 equivalent of tert-butyl dimethyl silyl chloride to

selectively protect the *sn*-2 alcohol. The next step was the acylation from **Scheme 2.3** followed by the TBAF desilylation presented in **Scheme 2.1**. Finally, the choline addition from **Scheme 2.3** was applied.

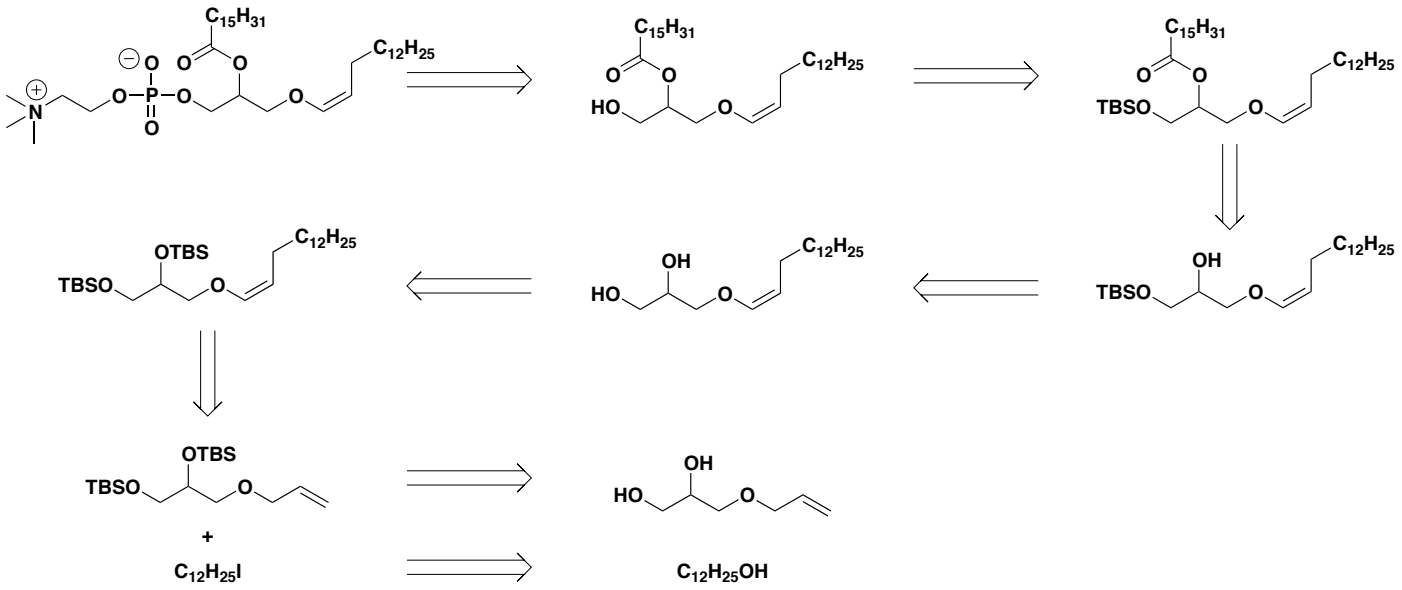

Scheme 2.4 Plasmenylcholine retrosynthesis.

The new approach couples the polar choline head group to the *sn-3* of the glycerol backbone in the last step, which circumvents the chromatographic challenges in isolating an amphiphilic compound. Moreover, the acylation (addition of fatty acid) was performed after the alkylation to reduce the likelihood of unwanted side reactions with the relatively reactive acyl group under the harsh alkylation conditions.

Research into the oxidizability of plasmenylcholine and plasmalogens as a whole is lacking and very few research groups have pursued it due to the challenges in synthesis and/or in isolation of pure samples from natural sources. The inaccessibility of the plasmalogen target greatly limited our understanding of this notable phospholipid. Previous

attempts at quantification of the oxidation products were not sufficiently thorough as they used a GC-ECD or LC-UV-detector as the principle methods of detection and internal standards were not obtained for the anticipated product [66] [64]. Photooxidation of plasmalogens has been reported to cleave the O-(Z)-vinyl ether moiety to form long chain aldehydes or α-hydroxy aldehydes [47] [66]. Allylic H-atom abstraction yielding a hydroperoxide from plasmalogen has not been reported previously [67]. We sought a consistent, reproducible analytical method that would allow for the accurate monitoring of the rate of consumption of plasmalogens over time to enable determination of any kinetic isotope effect. The analogues used for these experiments included the cis-vinyl ether model substrate, and d_3-cis-vinyl ether model.

2.2 Results

Our optimized, robust, and reproducible synthetic approach is shown in **Scheme 2.5** which incorporated synthetic changes gathered from the issues outlined by the Thompson group [21]. Detailed descriptions of the synthetic methods used can be found in the experimental section and supporting spectral data can be found in appendix A.

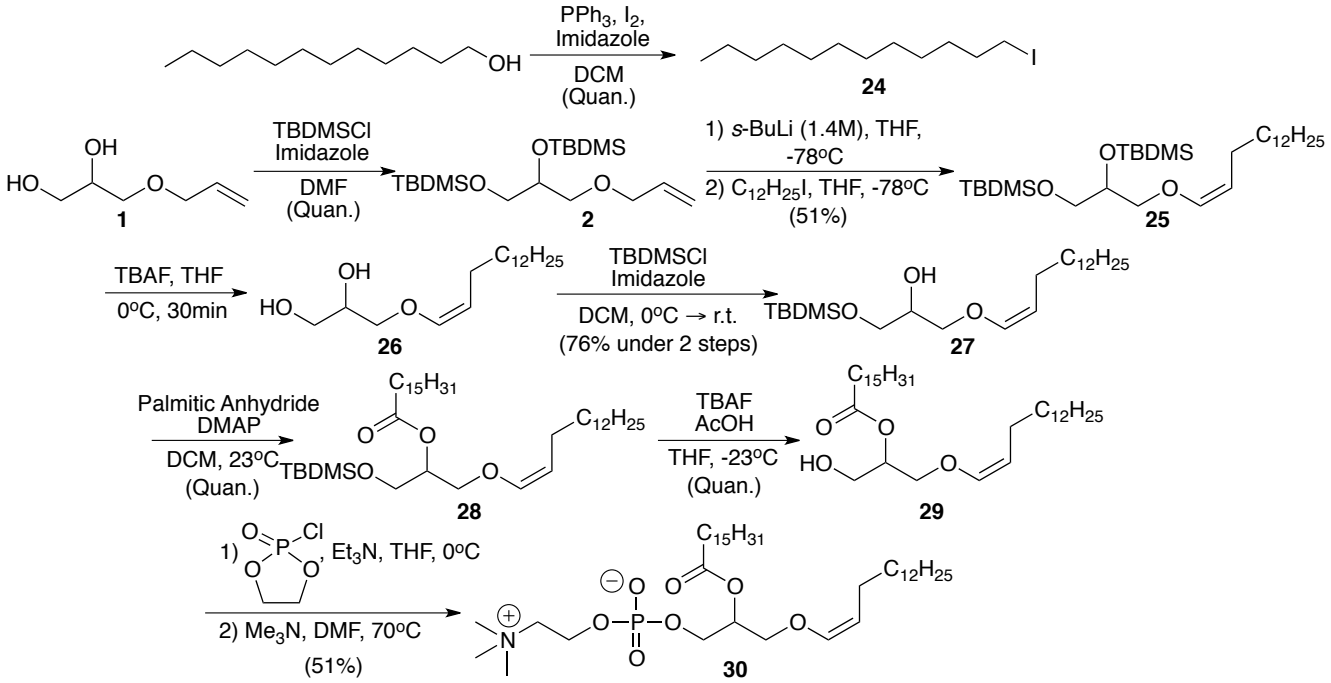

Scheme 2.5 Optimized plasmalogen preparation.

2.2.1 Observations Gleaned from working with Vinyl Ether Intermediates

The synthesis was inspired by Thompson (2003) [63] and efforts were made to replicate experimental conditions, but the pursuit was fruitless. A number of incremental optimizations were applied to develop a robust and reproducible approach that could accommodate larger scale (~5.0 g) synthesis.

It was evident that the plasmalogen and the intermediates containing the cis-vinyl ether functionality were highly susceptible to oxidation by oxygen in the atmosphere or hydrolysis by moisture in the air. This necessitated the application of very stringent inert and anhydrous conditions. Following the installation of the vinyl ether functionality the

intermediates formed were very time and temperature sensitive and were stored at -80 ^{o}C to mitigate decomposition. It was noted that the plasmalogen would hydrolyze and generate a number of artifacts when it was prepared for NMR analysis with deuterated chloroform ($CDCl_3$) compared with deuterated benzene (C_6D_6). This affirmed that freshly obtained anhydrous NMR solvents were required to acquire the cleanest spectra.

The plasmalogen synthesis was initially attempted using 1-iododododecanol to generate a shorter alkyl chain at the *sn*-1 position of the glycerol head due to the lower cost of the evenly numbered 1-dodecanol (in comparison with a primary alcohol and an odd numbered alkyl chain such as 1-tridecanol or 1-pentadecanol). This was done throughout the synthetic optimization process in order to reduce costs.

2.2.2 Appel Reaction (Iodination of 1^{o} Alcohol)

The first transformation in the sequence was the iodination of 1-dodecanol with an Appel Reaction under standard reported conditions (**Scheme 2.6**).

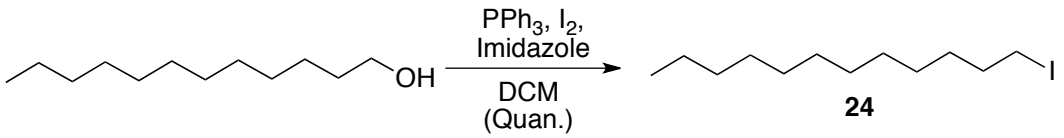

Scheme 2.6 Iodination of 1-dodecanol to generate 1-iododododecane.

This reaction consistently proceeded following literature [21] when conducted on small scale (<5 g SM), but it couldn't easily be replicated on 20 g scale without splitting the crude into multiple aliquots for workup and purification due to the volume of material and glassware limitations. After the synthetic optimizations, a quantitative yield of pure product was obtained in accordance with reported yields and spectral shifts [21].

2.2.3 Silyl Ether Protection of sn-2 and sn-3 Alcohols

The second reaction was a silyl protection of two alcohols to produce a di-protected glycerol (**Scheme 2.7**). This was synthesized following Thompson's report and the product was isolated as reported in literature [21].

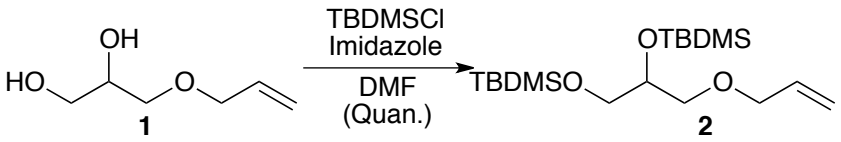

Scheme 2.7 Di-protection of alcohols at the *sn-2* and *sn-3* positions by the TBDMSCl protecting groups.

Three equivalents of tert-butyldimethylsilyl chloride were used to ensure complete protection of the alcohols. The only challenge presented was the removal of excess unquenched TBDMSCl when repeating this experiment on large scale (> 5 g). The excess TBDMSCl posed a significant issue as it interacted with the intermediate in the next synthetic step leading to decomposition. Removal of excess unquenched TBDMSCl was performed by distillation or silica gel column chromatography. A quantitative yield of pure product was obtained, consistent with reported characterization but Thompson reported a slightly lower yield of 93 % [21].

2.2.4 Optimization of Alkylation to Yield the Key Vinyl Ether

The key synthetic step (**Scheme 2.8**) involves alkylation of **1** to **2** while simultaneously locking the stereochemistry in the formation of O-(Z)-vinyl ether. The reaction conditions initially proposed by Thompson were tested but never yielded a pure product in reasonable yields [21].

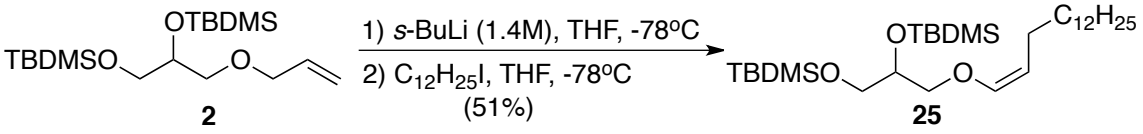

Scheme 2.8 Alkylation scheme depicting the optimized reaction conditions scheme for the alkylation of compound 2.

Thompson proposed that the barium iodide may increase the rate of product formation [21]. This procedure was repeated in an attempt to replicate the experiment only to yield starting material, the product of α-alkylation, and the product of trans-isomerization (**Scheme 2.9**). The first time the reaction was performed BaI_2 was left to dry under high vacuum for 2 days at 170°C as described in literature. The reaction was then performed without BaI_2 to determine if it may have not been dry enough, but the result was the same. Water content and purity of the THF solvent appeared to play a significant role in the yield of this reaction. This was discovered later on when THF from the solvent still, or dried over molecular sieves, was used and resulted in no product formation. Diethyl ether was eliminated from the synthesis as it was deemed not sufficiently dry. Triplicates of the experiment were then performed without any barium iodide and they only generated the product of isomerization. Compared to when the THF used after being freshly distilled, where the rate of conversion to the product of interest was noticeably higher in addition to the reduction in decomposition products in the corresponding NMR spectrum.

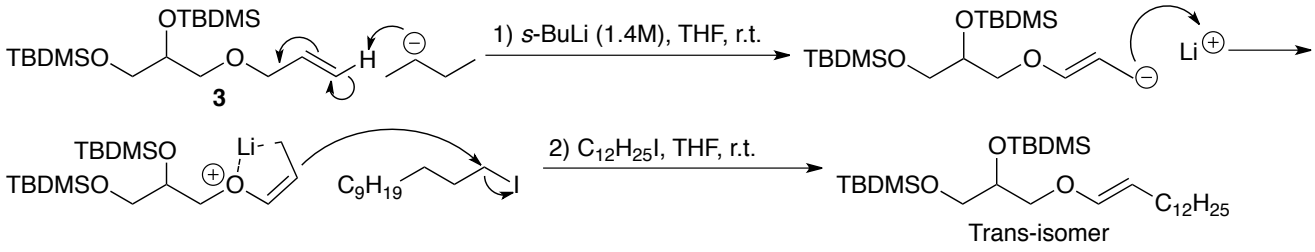

Scheme 2.9 Undesired alkylation product from lithiated intermediates.

Freshly distilled THF was used in the synthesis along with BaI_2 but yet again no product formed in the test reactions. This led us to question if the BaI_2 may just be a confounding factor that does not contribute to the formation of the product. As a result, BaI_2 was eliminated from the synthesis, and the experiment was repeated using benzaldehyde as an excellent electrophile to establish if the nucleophilic attack was even possible. The product of this reaction was the product of isomerization indicating that the addition was possible. Finally, when freshly distilled THF was used directly in the reaction (without BaI_2), the product of interest had formed.

In the next experiment the equivalence of *s*-BuLi was increased to determine if there was an insufficient concentration before, but no product had formed. We suspected that the *s*-BuLi used may not have been as concentrated as indicated on the bottle (1.4M in THF– Sigma Aldrich) and during the initial phases of troubleshooting I had performed titrations to determine the exact concentration of the nucleophilic solution in the bottle before use. The newly calculated concentration was then used to account for the amount of s-BuLi solution to be added to reaction based on the required number of moles. This did not significantly affect the yield (only reduced by 2-3 % in test reactions) but it indicated that a slight greater excess was required. Using newer *s*-BuLi reagent from sure-sealed bottles yielded the cleanest conversion and highest yields.

Later on, after our solvent still system was refreshed with new adsorbent material, a Karl-Fischer titration was performed to determine the level of dryness of the solvent eluting from the drying column. This indicated that the THF was sufficiently anhydrous (below detection limits of Karl Fischer Titration affirming sub-5 ppm water content) which emboldened us to attempt the experiment again with this solvent. The results of this

experiment were reassuring as they were similar to those obtained when using freshly distilled THF. As such, we opted to use the THF from the solvent still instead as it was easier to dispense and didn't require the upkeep which allowed me to spend more time on synthetic efforts. THF dryness and grade was shown to have a significant influence on the results of the experiments, as outlined in **Table 2.1**.

SM	RI	*s*-BuLi	BaI_2	Solvent	Product
1 eq.	$C_{13}H_{27}I$ (1.1 eq.)	1.1 eq.	1.1 eq.	THF (Solvent Still)	SM + Isomerization
1 eq.	$C_{12}H_{25}I$ (1.1 eq.)	1.1 eq.	1.1 eq.	THF (Freshly Distilled)	SM Only
1 eq.	$C_{12}H_{25}I$ (1.1 eq.)	1.1 eq.	1.1 eq.	THF (Freshly Distilled)	SM + α-addition
1 eq.	$C_{12}H_{25}I$ (1.1 eq.)	1.1 eq.	1.1 eq.	THF (Freshly Distilled)	SM + α-addition
1 eq.	$C_6H_{13}I$ (1.1 eq.)	1.1 eq.	1.1 eq.	THF (Freshly Distilled)	SM Only
1 eq.	$C_{13}H_{27}I$ (1.1 eq.)	1.1 eq.	0 eq.	THF (Solvent Still), Et_2O	SM Only
1 eq.	Benzaldehyde (1.1 eq.)	1.1 eq.	0 eq.	THF (Dried on MS), Et_2O	SM + Isomerization
1 eq.	Benzaldehyde (1.1 eq.)	1.1 eq.	0 eq.	THF (Solvent Still), Et_2O	Isomerization
1 eq.	$C_6H_{13}I$ (1.1 eq.)	1.1 eq.	0 eq.	THF (Dried on MS), Et_2O	SM + Isomerization
1 eq.	$C_6H_{13}I$ (1.1 eq.)	1.3 eq	0 eq.	THF (Dried on MS), Et_2O	SM Only
1 eq.	$C_6H_{13}I$ (1.1 eq.)	1.1 eq.	0 eq.	THF (Dried on MS), Et_2O	Isomerization
1 eq.	$C_6H_{13}I$ (1.1 eq.)	1.1 eq.	0 eq.	THF (Dried on MS), Et_2O	Isomerization
1 eq.	$C_6H_{13}I$ (1.1 eq.)	1.1 eq.	0 eq.	THF (Dried on MS), Et_2O	Isomerization
1 eq.	$C_6H_{13}I$ (1.1 eq.)	1.1 eq.	0 eq.	THF (Freshly Distilled)	SM Only
1 eq.	$C_6H_{13}I$ (1.1 eq.)	1.1 eq.	0 eq.	THF (Freshly Distilled)	8% Product
1 eq.	$C_6H_{13}I$ (1.1 eq.)	1.1 eq.	0 eq.	THF (Freshly Distilled)	10% Product
1 eq.	$C_6H_{13}I$ (1.1 eq.)	1.1 eq.	0 eq.	THF (Freshly Distilled)	16% Product
1 eq.	$C_6H_{13}I$ (1.1 eq.)	1.1 eq.	0 eq.	THF (Freshly Distilled)	23% Product
1 eq.	$C_{12}H_{25}I$ (1.1 eq.)	1.1 eq.	0 eq.	THF (Freshly Distilled)	SM Only
1 eq.	$C_{12}H_{25}I$ (1.1 eq.)	1.1 eq.	0 eq.	THF (Freshly Distilled)	SM + 3% Product
1 eq.	$C_{12}H_{25}I$ (1.1 eq.)	1.1 eq.	0 eq.	THF (Freshly Distilled)	α-addition + 4% Product
1 eq.	$C_{12}H_{25}I$ (1.1 eq.)	1.1 eq.	0 eq.	THF (Freshly Distilled)	16% Product
1 eq.	$C_{12}H_{25}I$ (1.1 eq.)	1.1 eq.	0 eq.	THF (Freshly Distilled)	15% Product
1 eq.	$C_{12}H_{25}I$ (1.1 eq.)	1.1 eq.	0 eq.	THF (Freshly Distilled)	21% Product
1 eq.	$C_{12}H_{25}I$ (1.1 eq.)	1.1 eq.	0 eq.	THF (Freshly Distilled)	43% Product
1 eq.	$C_{12}H_{25}I$ (1.1 eq.)	1.1 eq.	0 eq.	THF (Freshly Distilled)	50% Product
1 eq.	$C_{12}H_{25}I$ (1.1 eq.)	1.1 eq.	0 eq.	THF (Freshly Distilled)	49% Product
1 eq.	$C_{12}H_{25}I$ (1.1 eq.)	1.1 eq.	0 eq.	THF (Still System)	30% Product
1 eq.	$C_{12}H_{25}I$ (1.1 eq.)	1.1 eq.	0 eq.	THF (Still System)	48% Product
1 eq.	$C_{12}H_{25}I$ (1.1 eq.)	1.1 eq.	0 eq.	THF (Still System)	49% Product
1 eq.	$C_{15}H_{31}I$ (1.1 eq.)	1.1 eq.	0 eq.	THF (Still System)	48% Product
1 eq.	$C_{15}H_{31}I$ (1.1 eq.)	1.1 eq.	0 eq.	THF (Still System)	51% Product

Table 2.1 Summary of synthetic conditions tested for while optimizing the alkylation reaction of compound 3.

Changes in alkyl-iodide chain length were not significant. 1-Iodotridecane and 1-iodopentadecane are relatively expensive so a cheaper alternative, 1-iodododecane, was used instead. 1-Iodohexane was used during repetition of experiments to save the more valuable 1-iodododecane while the optimal conditions were established. Synthesis of the final plasmalogen was conducted with 1-iodopentadecane.

The reaction was extremely temperature sensitive, which was demonstrated when the product of isomerization would form as the favored product at elevated temperatures (-40 ^{o}C). Based on this discovery, the reaction was performed in an acetone-dry ice cooling bath saturated with dry ice to ensure that the reaction maintained -78 ^{o}C throughout the 2-hour reaction time. The reaction was also very time sensitive, when the reaction was left to run with the intention to push for a higher conversion rate to the target, but the product would decompose quite quickly in the first 1-hour after the reported reaction time .

The purification via silica gel column chromatography of this intermediate posed significant challenges at the beginning of the research investigation since all the isomers and side products would elute with the product of interest since they'd have roughly the same R_f values. Additionally, the products of decomposition would also co-elute as they are similarly lipophilic to the intermediate of interest. It was then suggested that the acidic silanols present in the silica may interact with the intermediate and may catalyze the hydrolysis of the cis-vinyl ether leading to overall decomposition. The column was deactivated with 1% triethylamine (NEt_3) in hexanes then the triethylamine was flushed off the column with hexanes. Trimethylamine had to be flushed as it would constantly elute as fractions were collected and when analyzed using TLC would obscure the spots of interest since it had a R_f value of about 0.2 and this would complicate the process of aggregating and concentrating

samples. The column was flushed with 2 column volumes of 100 % hexanes to allow for a separation between the product of interest and the contaminants. The solvent system was ramped up in polarity to 10% DCM:Hex which allowed the plasmalogen intermediate to readily elute.

After all of the modifications have been applied it was possible to replicate the synthesis on large scale and still obtain an extremely clean product in reasonable yields. The very clean product was isolated with 51 % yield, and the corresponding NMR spectrum was consistent with reported characterization [21].

2.2.5 Deprotection (Desilylation) of Alcohol

The fourth transformation involving the cleavage of the silyl ethers to yield the corresponding diol with TBAF (**Scheme 2.10**) was initially carried out as described by Thompson but the reported results were not reproducible [21].

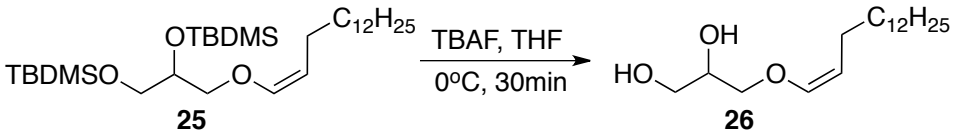

25 **26**

Scheme 2.10 TBAF deprotection of *sn-2* and *sn-3* positions.

Thompson proposed the use of imidazole for this deprotection step, but we eliminated it from our synthetic scheme to simplify the reaction and avoid potential side reactions. Additionally, imidazole does not appear to serve a purpose in this step as the deprotection was nearly quantitative without it.

The workup was modified to entirely remove the contaminants by incorporating a second round of washes with diethyl ether to precipitate the TBA-salts and push the residues into the aqueous phase after the first wash with EtOAc. Remarkably, after concentration, this

approach yielded a pure intermediate that was consistent with reported spectra [21] and was carried forward without further purification. This intermediate was not stable and underwent rapid decomposition, even when stored under nitrogen and reduced temperatures. As a result, the material must be pushed forward to the next step on the same day.

2.2.6 Selective Mono-Protection of Terminal (sn-3) Alcohol

The selective mono-protection of the sn-3 alcohol was performed following the reported protocol by Thompson and Shin (**Scheme 2.11**) [21]. This was not reproducible as they used DMF as a solvent which was difficult to remove via a simple workup and removal required high heat which resulted in decomposition of the vinyl ether (VE) moiety and diminished yields. DCM was then used as it can be removed under milder conditions.

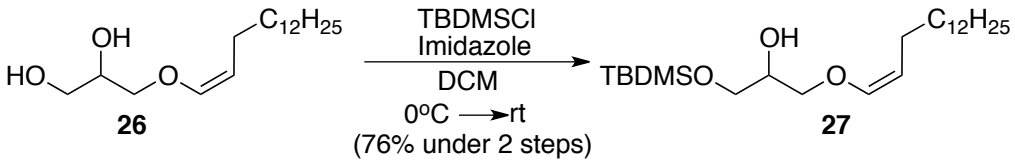

Scheme 2.11 Mono-protection of the alcohol at the *sn-3* position.

Selective tert-butyl-dimethyl-silyl (TBDMS) protection of the alcohol at the *sn-3* position exploited the steric hindrance, which disfavoured reaction with the *sn*-2 alcohol. The quality of the TBDMSCl significantly impacted the results of this reaction. Silica gel column chromatography was again applied in a similar fashion as the alkylation step presented in **Section 2.2.3**.

After many iterations of this reaction, each with an incremental modification, it was possible to isolate a pure oil. This intermediate was more stable and able to be stored for up to 1-2 months under nitrogen and at -78 °C without decomposition or unwanted changes. When stored for longer periods of time (4-6 months) NMR spectra of the samples would

suggest that there may have been isomerization leading to the formation of a mixture of *sn*-2 protected, and *sn*-2 and *sn*-3 protected products along with the product of interest. The product characterization was consistent with that which was reported by Thompson [21].

2.2.7 Acylation of sn-2 Alcohols

When the synthesis was first attempted, we followed a reported Steglich esterification protocol method reported initially by Neises and Steglich [68] and modified by Thompson [21] but were unable to reproduce the result. In this reaction palmitic acid was coupled to the *sn*-2 position via a Steglich esterification mechanism facilitated by the coupling agent dicyclohexylcarbodiimide (DCC) and 4-dimethylaminopyridine (DMAP).

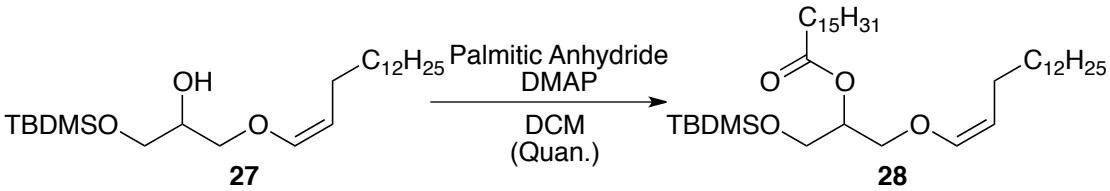

Scheme 2.12 Reaction scheme depicting the Steglich esterification reaction conditions required for the acylation of the sn-2 position.

The coupling agents proved difficult to separate from the target compound, and it was determined that the excess DCC/DCU was negatively impacting the subsequent synthetic steps. An alternative protocol was then employed to circumvent the use of DCC. The updated protocol was reported by Thompson in 2007 (**Scheme 2.12**) [21]. The use of palmitic anhydride greatly simplified the workup since the DMAP was removed with relative ease and there was no carbodiimide to contaminate the crude product. The product was isolated, and the characterization was in accordance with that which was reported by Thompson. The quantitative yield obtained was significantly higher than reported yield of 53 % by Thompson [21].

2.2.8 Desilylation of Protected sn-3 Alcohol

Cleavage of the silyl ethers to yield the corresponding alcohol (**Scheme 2.13**) was initially carried out as described by Thompson [21] but the reported results were not reproducible.

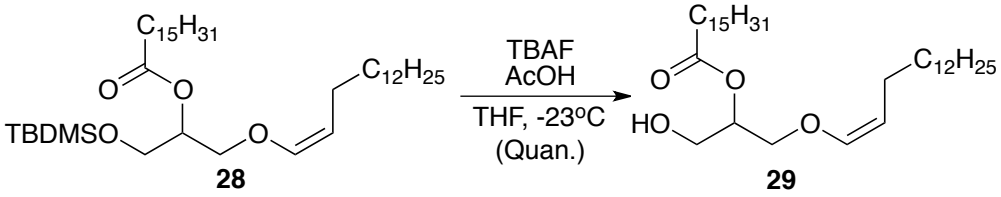

Scheme 2.13 TBAF deprotection of *sn-3* alcohol under acidic conditions.

This TBAF mediated deprotection step is similar to that performed earlier on in the synthesis with the exception of the acetic acid and the tight temperature control with a cold probe. A large excess of acetic acid (10 equivalents) was necessary to avoid displacing the palmitic acid moiety at *sn-2* position. The product of this updated method was extremely clean based on the NMR spectrum acquired when compared with characterization data reported by Thompson and we were confident in carrying it forward in the next synthetic step. The quantitative yield was obtained while Thompson reported a yield of 94% [21].

2.2.9 Choline Addition at the sn-3 Position

The final step of this synthesis involved a phosphorylation of a primary alcohol followed by a ring opening mediated by trimethylamine and was carried out as described by Thompson [21]. Initially this was not reproducible but after some experimental optimization the result was replicated.

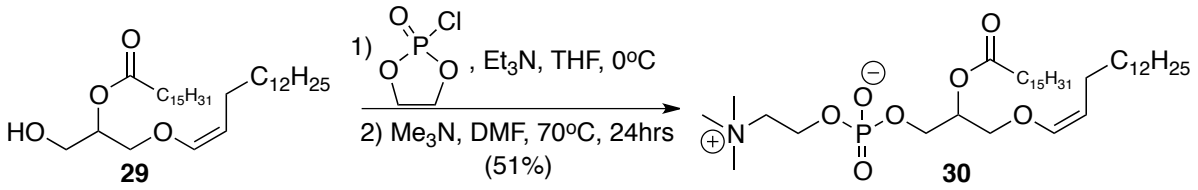

Scheme 2.14 Addition of choline head group to form plasmenylcholine.

This step involved a phosphorylation at 0°C under basic conditions (**Scheme 2.14**). We suspect that the triethylamine was used as a base in order to deprotonate the *sn-3* alcohol to facilitate a nucleophilic attack on ethylene chlorophosphate, displacing chlorine alternatively triethylamine may be reacting directly with ethylene chlorophosphate prior to the addition. The next step involved the use of trimethylamine, which was used as a hydrochloride salt and required addition through the gas phase. A cannula was used along with a cold finger to condense and collect liquid NMe_3. The trimethylamine was added to the high pressure vessel at low temperature (-78°C) which was then sealed and left to stir for 1 day at high temperature (70°C).

Two different workup approaches were tested to establish if it was required and if it resulted in a cleaner product. The first method involved directly concentrating the reaction mixture then purifying. The second approach involved an extraction with DCM. Each sample was purified via column chromatography using a relatively polar solvent system comprised of 63:32:5 CH_2Cl_2:MeOH:H_2O. This was the most successful solvent system for separation but resulted in some difficulties with evaporation due to the presence of water. After completion of purification it was evident that the workup involving extraction with DCM generated the cleanest product with the greatest yield. The product obtained was yellow oil.

When the product was solubilized in a minimum volume of deuterated chloroform a white precipitate was observed on the walls of the vial. This was consistent with the product

described by Thompson [21], and affirmed by NMR analysis and high-resolution mass spectrometry. Although the product was originally synthesized successfully, the NMR spectrum was unsatisfactory as it still contained a number of contaminants. This was likely due to residual traces of tert-butyl ammonium (TBA)-salts and DCC/DCU that were present in the SM due to the previously mentioned challenges in separations prior to the extensive optimization allowing for the synthesis of much cleaner SM.

When this step was repeated with the cleanest SM synthesized it generated a fairly clean product in acceptable yields, and consistent characterization with what is reported Thompson [21], and purification was straight forward since the all the reagents used in this step were volatile.

2.2.10 Vinyl Ether Model Substrate

A vinyl ether model was sought as a short-term alternative to the plasmalogen for the optimization of the key plasmalogen synthetic step (alkylation). Additionally, it was used to investigate the analytical methods available for monitoring substrate when autoxidized. Finally, it would guide the synthetic efforts with respect to producing a partially deuterated model VE substrate. The synthetic approach proposed is shown in **Scheme 2.15**.

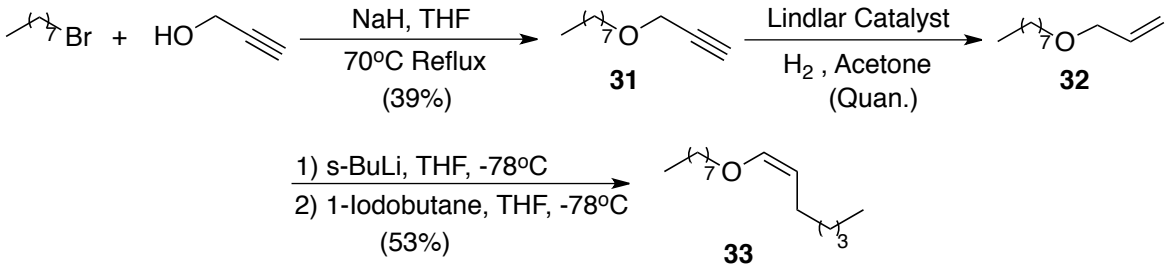

Scheme 2.15 Preparation of O-(Z)-vinyl ether model substrate.

The first step involved a Williamson ether synthesis to form 1-(prop-2-yn-1-yloxy)octane (**31**). The product formed in reasonable quantities and was purified without much difficulty. The reduced yield may be attributed to potentially partially quenched sodium hydride (60 % NaH dispersed in mineral oil). Care was taken when evaporating this product as it was relatively volatile and lost to the high-vacuum during the first attempt at this synthesis. The product of interest had formed in accordance with literature data [69].

The second step of this reaction involved a Lindlar reduction of the terminal alkyne with hydrogen gas. This was based on widely reported and commonly used reduction procedures [70]. After experimental optimization the target (**32**) was isolated quantitatively and in consensus with reported characterization data [70].

The final step, involving the alkylation of the VE model substrate, of proceeded as previously described in **Section 2.2.5**; this also comprised some of the optimization of the step since this was used to test a variety of modifications to the experimental conditions and reagents used. Purification of this product was easier as there was significantly less decomposition than observed when working with the plasmalogen intermediate. The product generated was extremely clean and used in the autoxidation experiments [71].

This material decomposed fairly readily and had to be purified via prep-HPLC prior to use to remove oxidation products. The product was eluted under normal phase column conditions with 100 % hexanes at a flow rate of 2 mL/min through a dedicated preparatory HPLC column. Multiple wavelengths were monitored simultaneously to determine when the target eluted but the significant regions were about 227 and 247 nm and the product would elute cleanly between 4-7 min before contaminants begin co-eluting. This allowed for the rapid purification of the analyte prior to use.

2.2.11 Preparation of d_3-Vinyl Ether Model Substrate

The partially deuterated vinyl ether model substrate was synthesized to probe VE autoxidation mechanism. This was synthesized in a similar fashion to the natural vinyl ether model substrate (**Section 2.2.5**). The differences include the initial deuteration of the terminal alkynyl position of the propargyl alcohol; and the Lindlar reduction conducted under deuterium gas to selectively deuterate the allylic positions (**Scheme 2.16**). The NMR spectra obtained while synthesizing the previous natural model substrate were used to compare with the product of this reaction since characteristic vinylic signals (doublet at 5.89 ppm) were supressed by the presence of deuterium. This was invaluable as it aided in determining reaction progress and gauging quality of the product since it should be as clean as the previous model to ensure consistency in the analytical results between them.

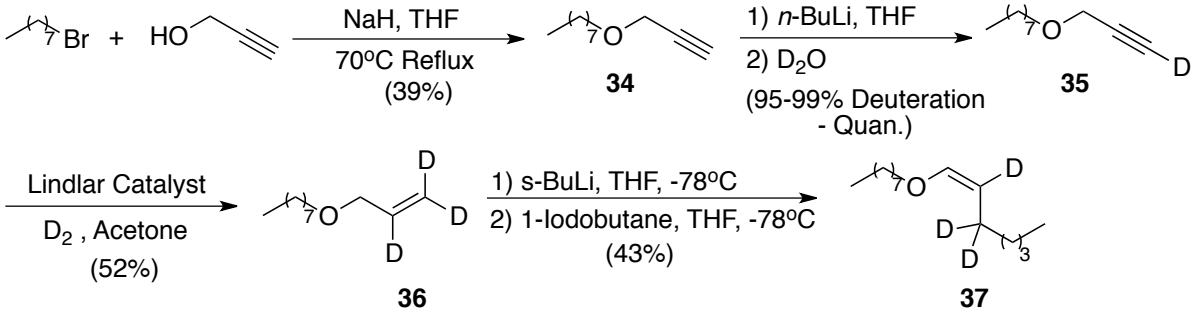

Scheme 2.16 Preparation of partially deuterated d_3-vinyl ether model substrate.

The second step, which comprised the deuteration of the terminal alkyne, involved the facile deprotonation by *n*-BuLi which was added dropwise at -78 ºC. After 30 minutes, the reaction mixture was quenched with an excess amount of deuterium oxide before being left to stir for another 30 min. The reaction was worked up and extracted with diethyl ether before being carefully evaporated to avoid losing the volatile product to the vacuum. A quantitative deuteration was achieved based on the loss of the singlet peak at 2.41 ppm (^{1}H

NMR in $CDCl_3$) which indicated that the SM had been deprotonated and the carbanion quenched with a deuterium ion provided by deuterium oxide (D_2O) [72].

The third step in this synthesis was similar to the reduction shown in **Scheme 2.15** except $D_{2(g)}$ was used instead. After stringent anhydrous protocols were adhered to a 95 % deuteration rate was achieved. Any water (residual or otherwise) present in the reaction vessel would quench the catalyst rendering it useless and reducing the intended concentration in the reaction. Anhydrous acetone was used for this step. The reaction progress was monitored via crude NMR and evaluation of the increase in integration of the peak at 3.98 ppm (^{1}H NMR in $CDCl_3$) which corresponded to the CH_2 protons located α to the ether and the deuterated allyl. Additionally, disappearance of the peak at 2.41 ppm (^{1}H NMR in $CDCl_3$) indicated consumption of the SM and conversion to product [70].

The final alkylation step proceeded as previously described but slightly lower yield was obtained in comparison to the previously reported yield. The reaction progress was assessed by evaluating the integration of the characteristic cis-vinyl ether peak commonly found about 5.88ppm (^{1}H NMR in $CDCl_3$) [71]. The product was still produced very cleanly based on NMR spectra obtained for characterization.

This synthesis was used as the basis for the synthesis of a partially deuterated plasmalogen analogue.

2.2.12 Consumption of Vinyl Ether Monitored by ^1H NMR

The analytical efforts began with the use of NMR to determine the rate at which vinyl ether was consumed in an autoxidation. Initially this involved an autoxidation conducted in the NMR tube with deuterated benzene (C_6D_6), 100 mM of the model substrate, and 92 mM of 1,2,4-trichlorobenzene and 5 mM V70 then heated to 37 ºC. The internal standard, 1,2,4-trichlorobenzene, was selected as it was not anticipated to interact with the other substrates and since the corresponding signals appeared around the aromatic region in the proton NMR spectra and therefore would overlap with the downfield vinylic proton of the substrate (dt at 5.88 ppm) (**Figure 2.1 and 2.2**). The integration of the 3 internal standard peaks were averaged in order to calculate the relative concentration of vinyl ether present.

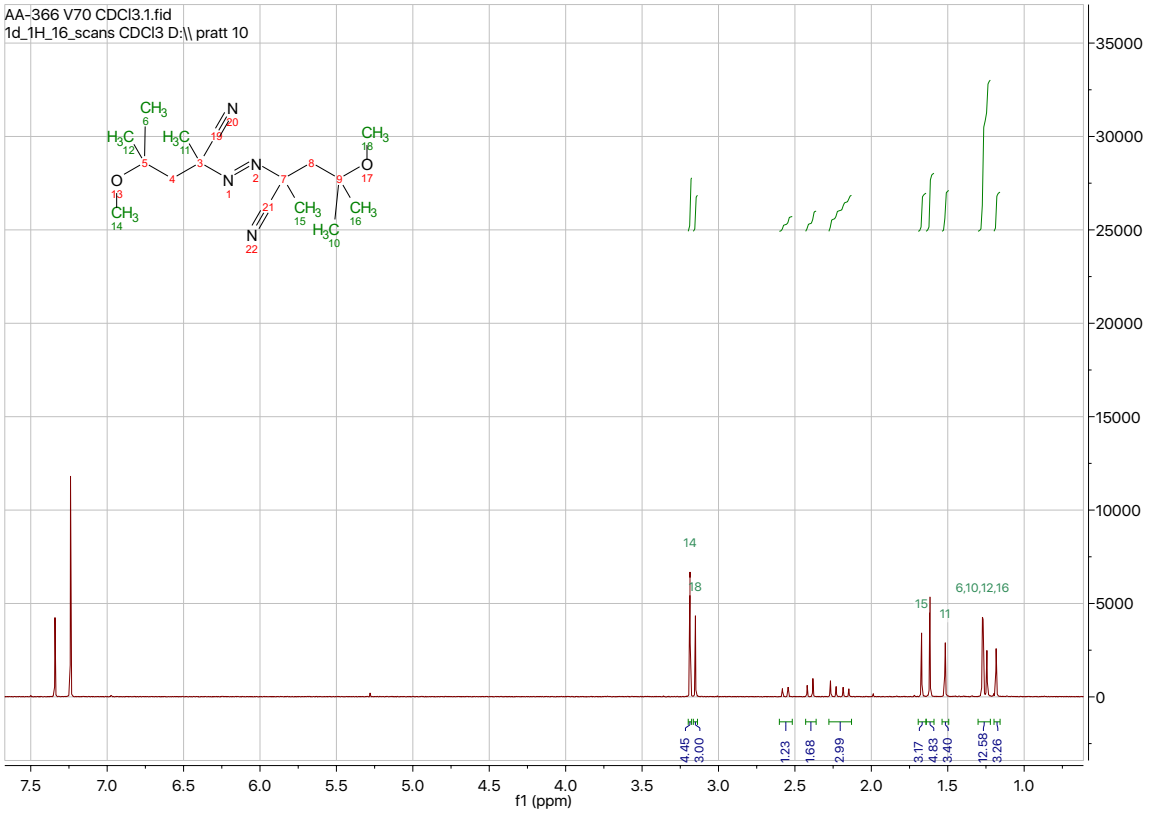

Figure 2.1 Annotated ^{1}H-NMR (300 MHz) spectrum of V70 in *d*-chloroform.

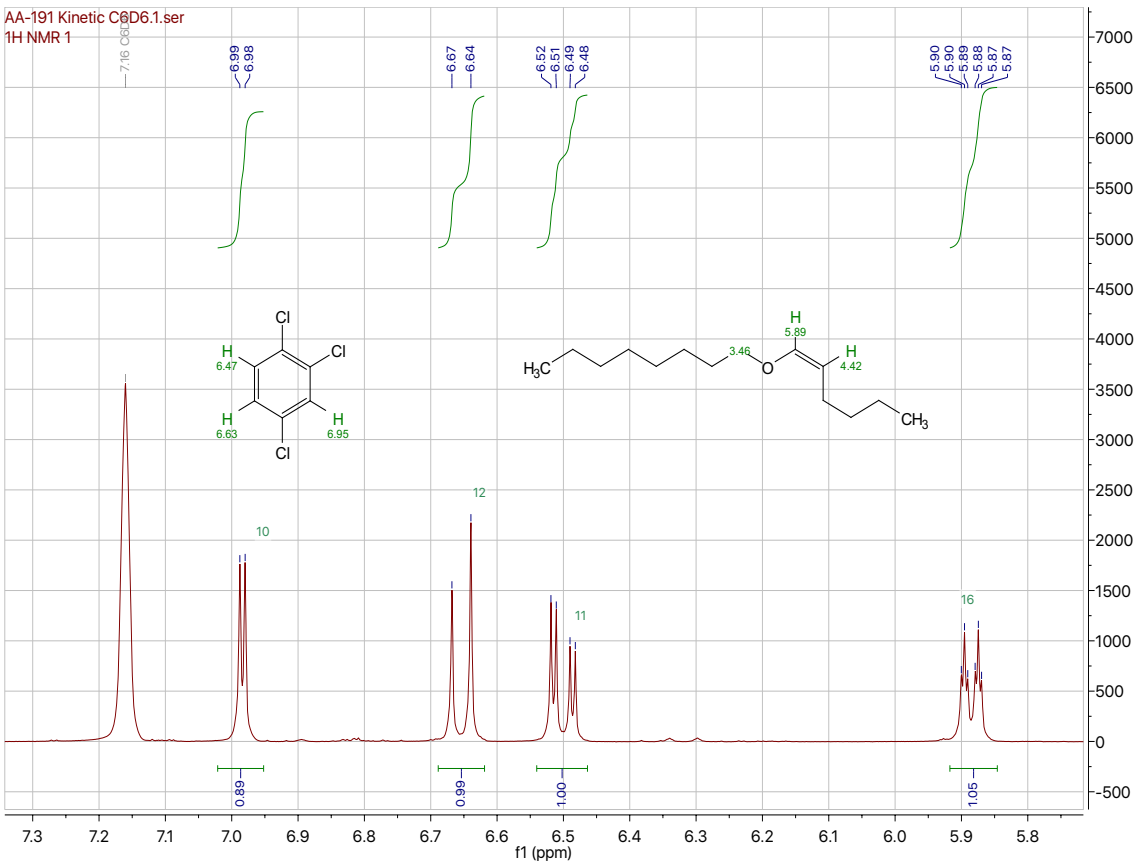

Figure 2.2 ^{1}H-NMR (300 MHz) Spectrum of the key cis-vinyl ether model substrate peak along with the internal standard (1,2,4-trichlorobenzene) peaks.

The 3-hour vinyl ether model substrate (100 mM) autoxidation was conducted using V70 in benzene-d_6. 92 mM 1,2,4-trichlorobenzene was added and used as the internal standard. Unexpected results were repeatedly obtained, where the VE concentration would increase rapidly and inexplicably at the start of the experiment before the expected decay in concentration was observed (**Figure 2.3**). This was observed under many different concentrations of initiator (3,5,10, and 40 mM V70 tested); even when tested with a newer batch of V70 in case there may have been a contaminant or issue with the initiator used in the previous assays.

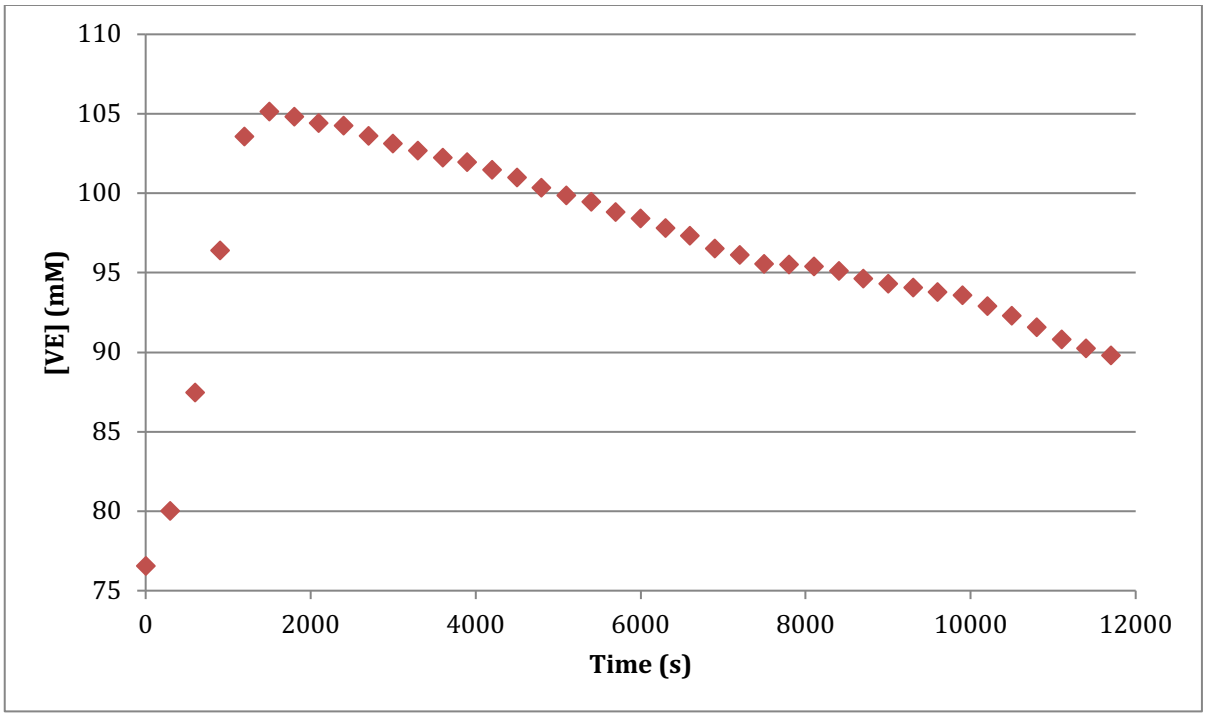

Figure 2.3 Representative plot depicting the inexplicable increase in VE concentration over the course of the autoxidation conducted in the NMR tube with benzene-d_6, 100 mM of the VE model substrate, and 92 mM of 1,2,4-trichlorobenzene, and 5 mM V70 then heated to 37 ^{o}C for 3.25 hours. Rate of VE consumption (following initial increase) was 1.50 x 10^{-6} M s^{-1} while the reported rate constant for unimolecular decomposition of V70 was 3.18 x 10^{-5} s^{-1} at 37 ^{o}C ($R_{i,exp}$ = 1.4 x 10^{-7} M s^{-1}) [73] [74].

2.2.13 Consumption of Vinyl Ether Monitored by GC-FID

The results of this autoxidation were disappointing since both data sets presented no distinct trend (**Figure 2.4**). It did not appear that there was any significant difference in VE concentration in the presence of V70 compared to the control trial and the VE inhibited autoxidation presented the same increase in VE concentration during what can be presumed to be the initiation period.

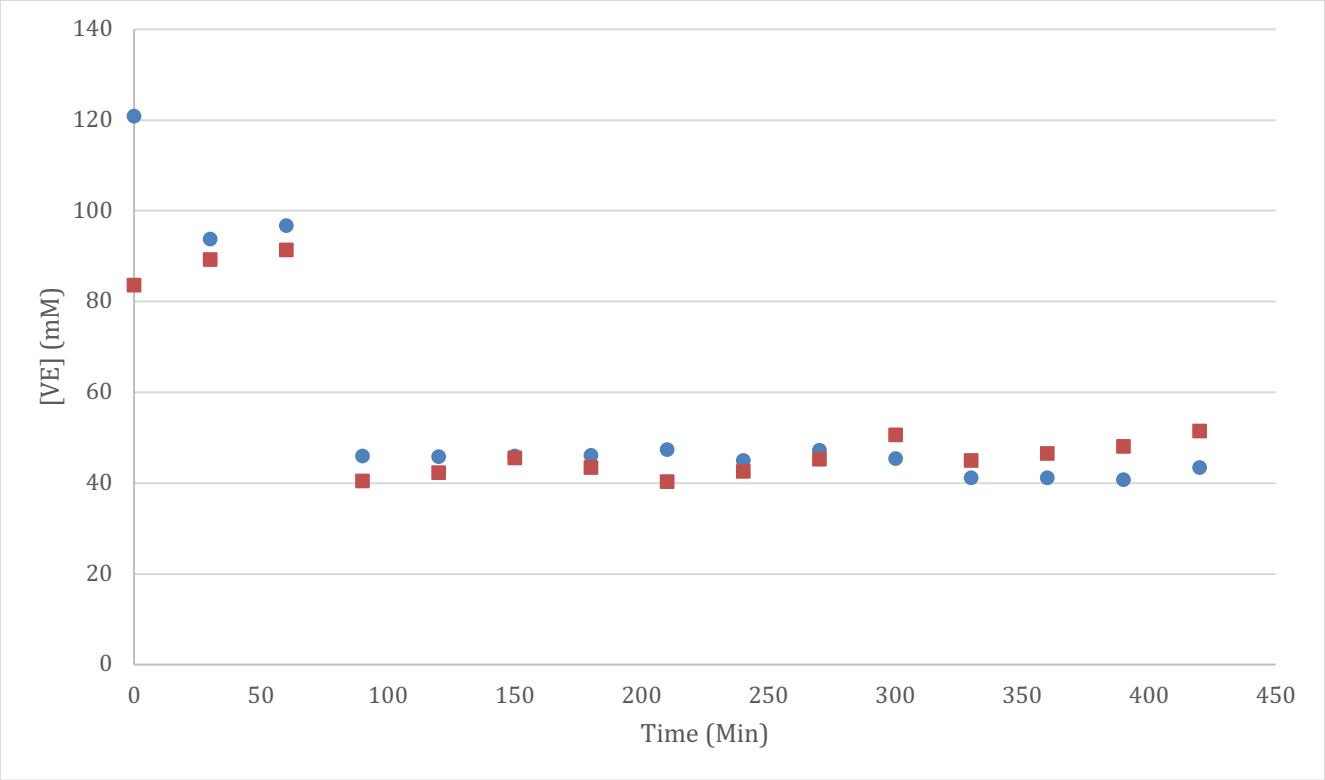

Figure 2.4 Graph illustrating the results of the cis-VE model substrate (●) and autoxidation and a control experiment (■) whose results were analyzed via GC-FID. 100 mM VE model substrate and, 97.3 mM V70 were combined in benzene (V_f = 3 mL; Ri = 2.7 x 10^{-6} M s^{-1}) and heated at 37 ºC with time points taken every 30 minutes. Aliquots were diluted 20-fold with benzene and 1 mM hexadecane was added as an internal standard before injection on GC-FID.

Another discernable difference was the change in y-intercept indicating that there may have been some variability in the reaction mixtures at the start of the experiment. This was initially attributed to systemic error in terms of performance of the experiment but were ruled out after repeating the experiment using the same stock VE solution and achieving a similarly scattered result with an overall flat trend. The plotted data points were erratically scattered, and further analysis of the chromatograms indicated that the integration of the IS peak was fluctuating between runs on the instrument. This was validated by running the same sample twice from the same autosampler vial and attaining different results. This was

similar to what was previously observed when NMR analysis was used to indirectly evaluate the rate the autoxidation. This insinuates that the VE may be undergoing unanticipated chemistry and that the internal standard may also be involved in some way.

The same experiment was repeated with 500 mM VE model substrate, and 50 mM AIBN in benzene (R_i = 1.1 x 10^{-7} M s^{-1}) (**Figure 2.5).** Aliquots taken at the given time points were diluted and prepared as described above. AIBN was used as the azo-initiator since it decomposed at a considerably slower rate than the previously used V70 (V70). Previously, V70 may have decomposed too quickly to react with the VE in the autoxidation reaction mixtures which may justify the lack of change in the VE concentration.

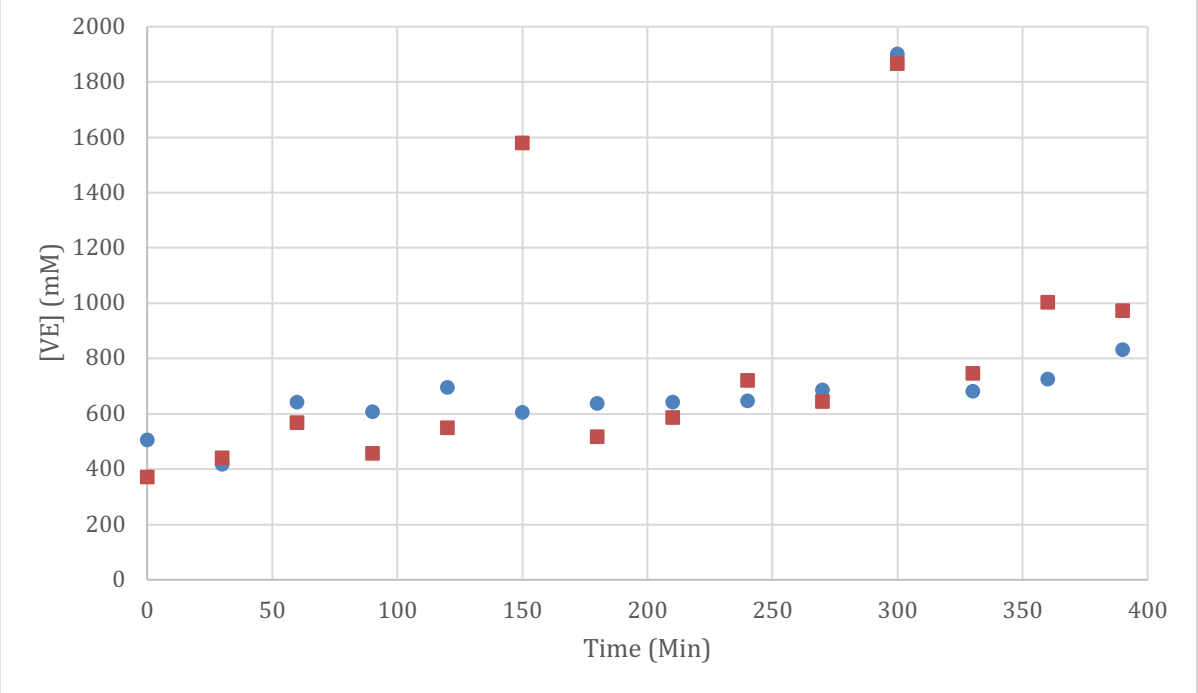

Figure 2.5 Graph illustrating the results of the cis-VE model substrate autoxidation (●) and control with no initiator (■) experiments whose results were analyzed via GC-FID. 500 mM VE model substrate and, 50 mM AIBN (**R_i** = 1.1 x 10^{-7} M s^{-1}**)** were combined in benzene (V_f = 3mL) and heated at 37 °C with time points taken every 30 minutes for 6.5 hours. Aliquots were diluted 20-fold with benzene and 1 mM hexadecane was added as an internal standard before injection on GC-FID. Outliers were not excluded.

The attuned approach using the slower radical initiator yielded similarly poor and inexplicable results (**Figure 2.5**). The increasing trend may be attributed to evaporation over the course of the reaction; although this was minimized as much as possible by only uncapping the vials to withdraw quickly. Autosampler vials with septa were also tested to no avail.

Alternative oxidative conditions were sought to allow us to conduct the autoxidation of VE. The autoxidation conditions were partially derived from the reported co-autoxidation conditions for methyl oleate by Ned Porter *et al*. [57] since it was suspected that these conditions may enable the autoxidation of the alkenyl ether functionality commonly present in plasmenyl lipids, based on the challenges experienced with oxidizing the monounsaturated lipid methyl oleate substrate and the subsequent success with this experimental approach. The established co-autoxidation conditions involved 331 mM of the cis-VE model substrate with 3.6M tert-butyl hydroperoxide (^{t}BuOOH) and 5.53mM V70 ($R_i = 1.51 \times 10^{-7}$ M s^{-1} in benzene-d_6) to be combined in a sealed vial and heated to 37^{o}C with regular aliquots taken at time points throughout the duration of the experiment. The V70 stock was made in benzene-d_6 to mitigate peak overlap and interference in internal standard integration by benzenes aromatic proton signals in the NMR spectra. Time points were taken hourly for the first 5 hours, then the autoxidation was allowed to run for 24 hours at 37^{o}C to evaluate the extent of the VE model substrate consumption over the lifetime of the azo-initiator (approximately 16 hours at 37^{o}C). Aliquots (10 μL) were taken for the GC-FID analysis and diluted with 890 μL benzene, then 100 μL of 10mM hexadecane was added for an 1 mM internal standard concentration and to complete the 100-fold dilution.

Astonishingly, the alkenyl ether model substrate persisted over 24-hours at which point GC-FID chromatograms indicated consumption of ~74 mM VE model substrate. The consistency in the VE loss over time observed between two independent instrumental approaches (NMR and GC)was encouraging since it affirmed that the vinyl ether may not be oxidatively labile as we anticipated and that the infinitesimal slopes previously obtained may in fact have accurately conveyed the reaction progress. The plotted results illustrated a small yet observable decrease in vinyl ether concentration over time (**Figure 2.6**). This was within the range observed when tested using the NMR approach. Additionally, it would be consistent with a chain reaction as the rate is greater than R_i.

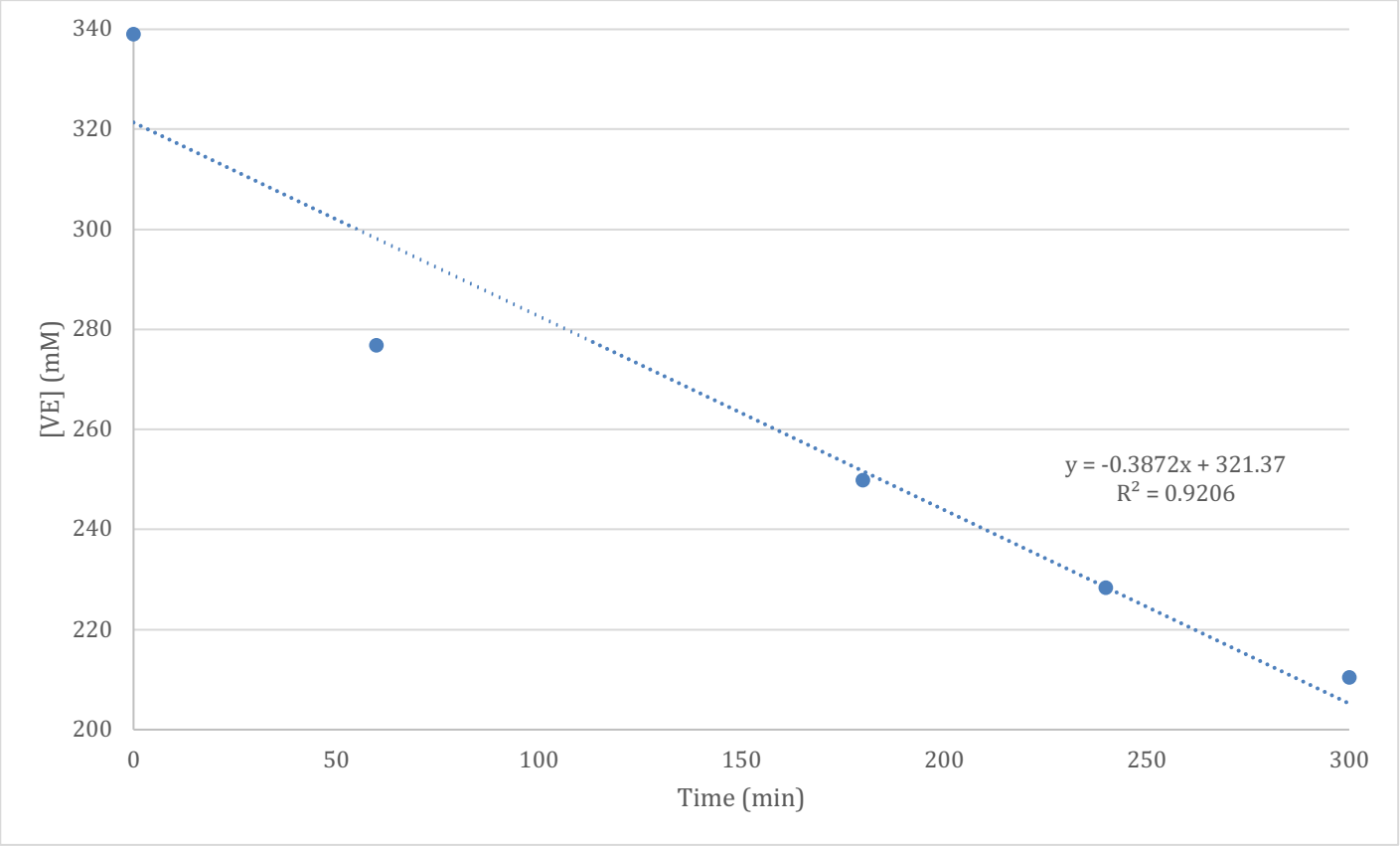

Figure 2.6 Plotted GC-FID results extrapolated from the co-autoxidation of 331 mM cis-vinyl ether (VE) model substrate with 3.6 M ^{t}BuOOH and 5.5 mM V70; performed at 37^{o}C. The first 6-hour period was shown while the last 18-hour period was excluded.

The GC-FID investigation into the mechanism of autoxidation of the cis-vinyl ether yielded successful oxidative conditions that may be applied to the plasmenylcholine and the deuterated equivalent. The results obtained via GC-FID were consistent with previously reported NMR spectral results.

2.2.14 Co-autoxidations of Methyl Linoleate and Vinyl Ether Monitored by HPLC-UV

Given the challenges with the NMR and GC approaches in determining reaction progress, the extent to which the vinyl ether could participate in autoxidation was probed using the peroxyl radical clock approach using methyl linoleate as the autoxidizable substrate. The methyl linoleate clocking experiments were performed under the standard conditions established and reported by Porter *et al.* [55]. A representative chromatogram of a methyl linoleate autoxidation depicting the product distribution of thermodynamic (major) and kinetic (minor) products with no added vinyl ether is shown in **Figure 2.7.**

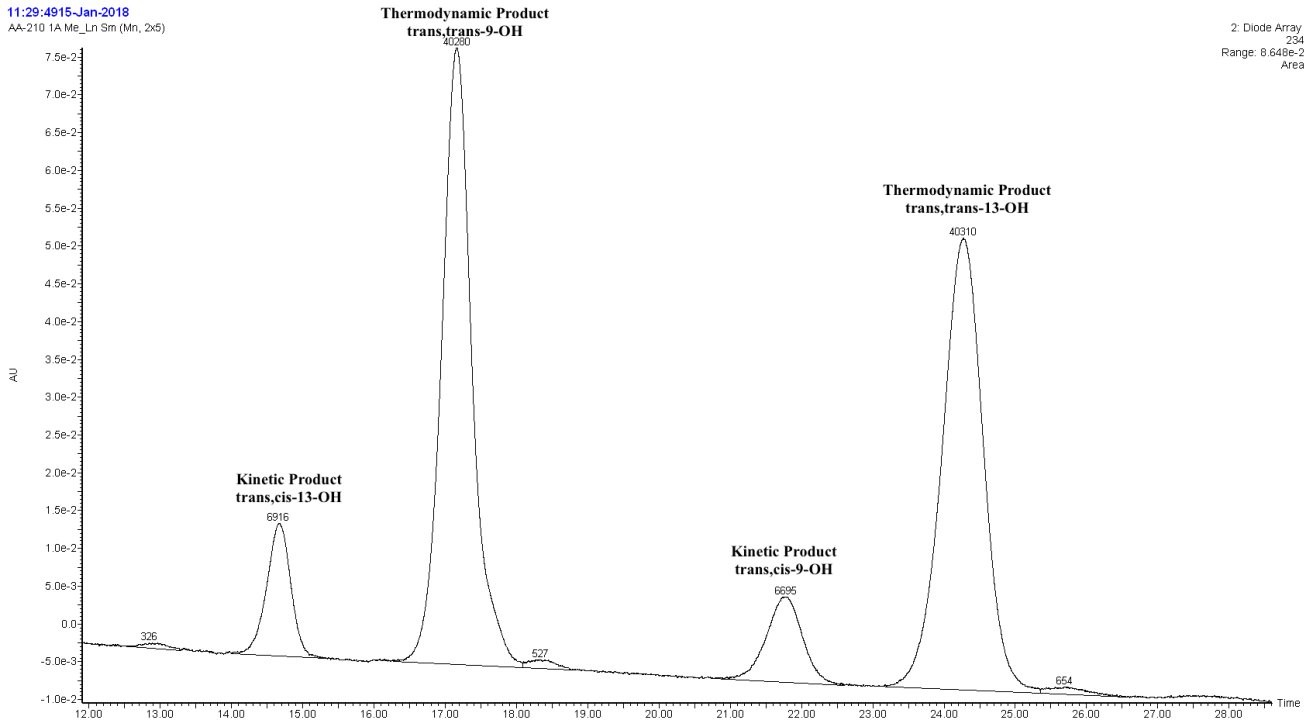

Figure 2.7 Sample chromatogram depicting the expected relative distributions of each peak corresponding to the characteristic products of methyl linoleate autoxidation. Obtained from sample run under conditions described by Porter *et al.* **[55]**. Autoxidation conditions: 100 mM AO (VE model substrate or deuterated-VE model substrate), 100 mM methyl linoleate, 10 mM V70 heated to 37 ºC.

The integrals of the peaks corresponding to the kinetic (*cis,trans*-conj.) and thermodynamic (*trans,trans*-conj.) products were used to calculate the rate constants for the VE model substrate and the deuterated-VE model substrate following the formula presented in **Figure 1.10**. The product ratios obtained for each clock were plotted as a function of the H-Donor (vinyl ether) concentration as shown in **Figure 2.8 and 2.9**. The constants used for these calculations were $k_{\beta II}$= 690 s^{-1} and $\beta = 0.686$ [55].

Methyl linoleate clocking experiments were conducted in triplicate with the vinyl ether model substrate to ensure accuracy in results. The plotted averaged data is presented in **Figure 2.8** including the corresponding error bars. The slope of the line of best fit appeared presented a positive correlation (0.03 mM^{-1}). The $k_{p,H}$ was calculated as being 6 M^{-1} s^{-1}.

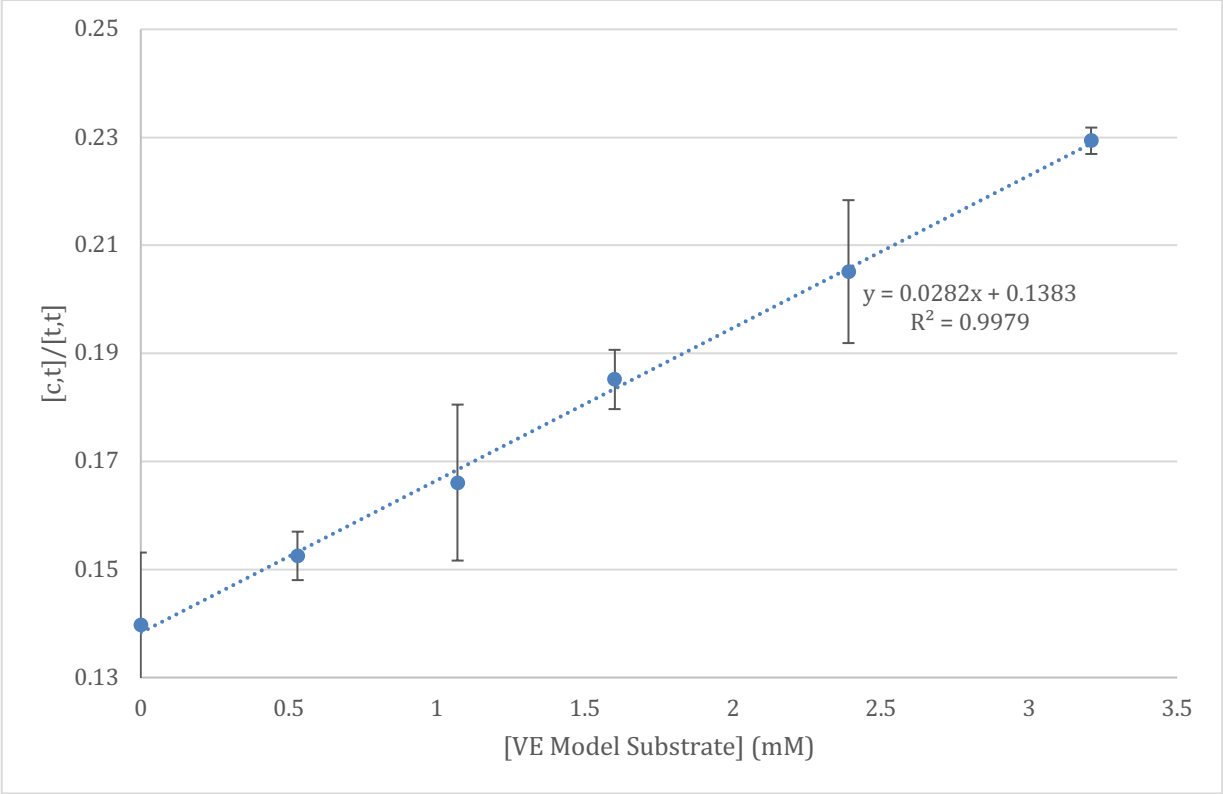

Figure 2.8 Plotted experimental results of methyl linoleate clocking experiments conducted with the model substrate and performed in triplicates in order to attain an average and determine the error range. The experiment was performed as previously described by Porter *et al.* **[55]** following the volumes used in Table 2.3. Autoxidation conditions: 100 mM AO (VE model substrate), 100 mM methyl linoleate, 10 mM V70 heated to 37 ºC.

Methyl linoleate clocking experiments were conducted with the deuterated vinyl ether model substrate to determine if there was a KIE. The plotted averaged data is presented in **Figure 2.9**. Due to limited quantities of the deuterated vinyl ether model substrate triplicates could not be performed. The slope of the line of best fit appeared to be 0.41 mM^{-1} but the y-intercept was too high (expected 0.15-0.2 as it corresponds to the rate of trapping of the peroxyls with methyl linoleate itself without any added H-atom donor) indicating there was an issue with the experiment. The $k_{p,D}$ was calculated as being 89 M^{-1} s^{-1} affirming that this was likely an erroneous experiment.

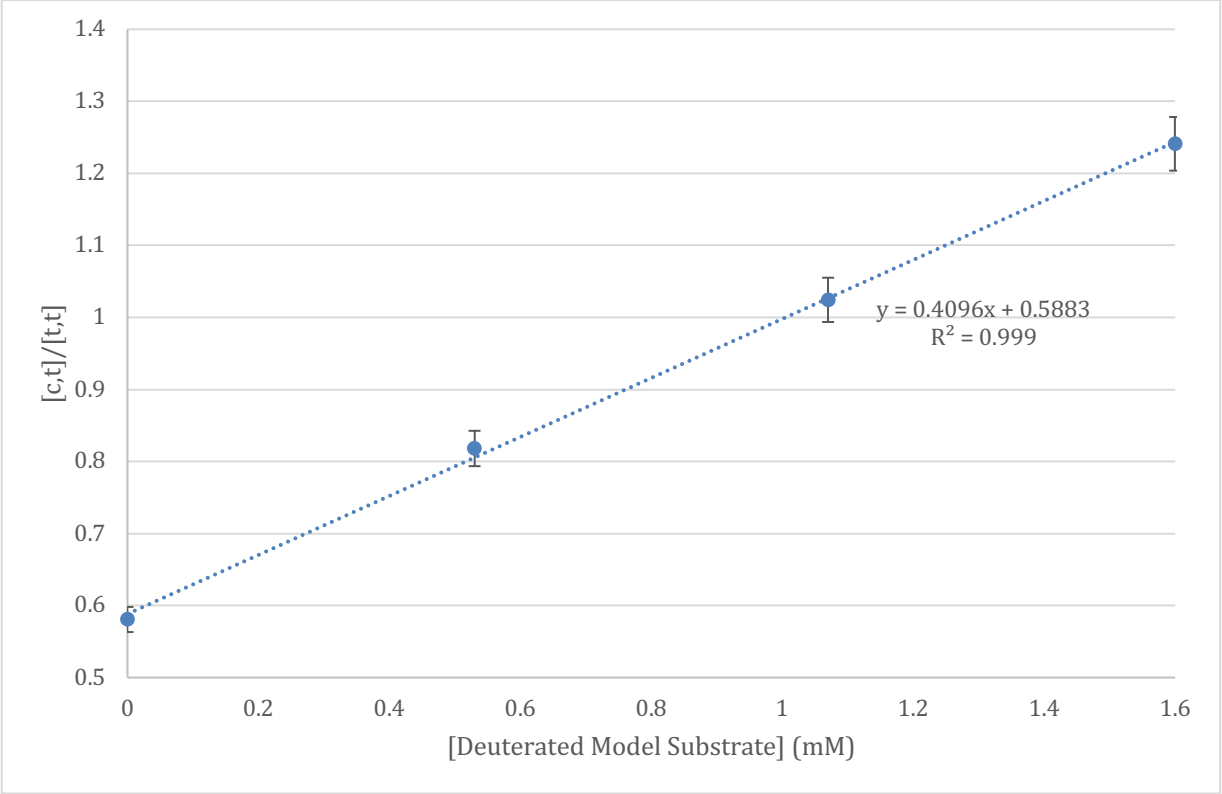

Figure 2.9 Plotted experimental results of methyl linoleate clocking experiments conducted with the newly purified d_3-VE model substrate. The experiment was performed as previously described by Porter *et al.* **[55]** (Table 2.3). Autoxidation conditions: 100 mM AO, 100 mM methyl linoleate, 10 mM V70 heated to 37 °C.

2.3 Discussion

The purpose of this project was to synthesize plasmenylcholine and simple vinyl ether models thereof and the study of their rates of consumption to shed light on the dominant autoxidation pathway to better understand their (patho)physiological role in degenerative disease. This would provide insight on the pro-oxidant or anti-oxidant roles of plasmalogens in living systems [48]. Despite the fact that propagation rates (k_p) were well studied and reported for other monounsaturated lipids including cholesterol and oleate, they remain unknown in plasmenyl lipids. Furthermore, sterols such as cholesterol have been revealed to proceed via a mix of both HAT and peroxyl radical addition while oleate previously was only reported to undergo HAT [57] [75].

Dr. Zielinski carried out computational experiments with MeO-butene as a model for plasmenyl lipids which yielded a rate constant (k_{calc}) of HAT of 0.6 M^{-1} s^{-1} (enhanced 10-fold by tunneling corrections; $k_{calc,\ tunneling}$ = 60 M^{-1} s^{-1}) which is notably slower than other PUFAs; the calculated rate constant of peroxyl addition was 16.4 M^{-1} s^{-1} and the subsequent intramolecular homolytic substitution to yield the epoxide was calculated to proceed at 9.5 x 10^5 s^{-1} suggesting that the addition pathway should be competitive, and that it should be the major pathway by far upon introduction of deuterium atoms at the methylene groups flanking the vinyl ether. Thompson characterized and reported some of the products of plasmalogen photooxidation as well as hydrolysis, but this was not adequate as they used GC-ECD (electron capture detector) and LC-UV, they failed to characterize all of the products formed, and they did not monitor the rate of plasmenyl lipid oxidation [66].

The synthetic approach demonstrated by Thompson **(Scheme 2.1**) was quite problematic as it involved a high temperature reflux of *n*-BuLi in THF and as well as a series

of tedious purifications of the intermediates due to addition of the choline head group early on in the synthesis. This led to significant modifications in our own efforts, which were implemented based on a patent published in 2014 [45]. It was evident that certain synthetic steps (alkylation, deprotection, and acylation) proceeded more efficiently without the addition of some of the proposed reagents as they would interfere with the reaction and result in lower rates of product formation as well as increased decomposition or rearrangement to unwanted side products.

Reproducing much of Thompson's reported plasmalogen syntheses was not possible and extensive optimization was necessary. Thompson proposed that barium iodide may coordinate the reactants in the alkylation step in order to kinetically favour the formation of the Z-vinyl ether over the E-vinyl ether [19]. The first issue that was faced involved the use of BaI_2 by Thompson. Although the prescribed protocol was diligently replicated for drying barium iodide under high heat and vacuum for 2 days, it did not appear to impact the selectivity of the reaction. Elimination of the BaI_2 achieved significantly cleaner product with greater yield.

The acylation of the plasmalogen intermediate posed a long-standing challenge in terms of isolation based on the difficulty in removal of excess DCC/DCU. It was clear that new material had to be generated using a different approach and the DMAP mediated esterification using palmitic anhydride was pursued instead. When it was conducted the results were remarkable, the isolated product was very clean and entirely recovered.

When the second deprotection in the synthesis involving the primary alcohol at the *sn*-3 position on the glycerol head was performed above -23 ^{o}C the product of interest would undergo a desilylation followed by a rapid intramolecular acyl migration from the *sn*-2

position to the *sn*-3 position to form the thermodynamically stable product. This was also observed in deprotections performed under moderately basic conditions; as was the case when excess DCC was present in the SM. The reaction progressed as reported in literature once the cold manipulations of the material were perfected.

The final step, involving the installation of the phosphatidylcholine group at the sn-3 position of the glycerol backbone was performed following reported protocols [21]. The number of equivalents of trimethylamine was increased to ensure there was a gross excess present in order to push the reaction forward and favor ring opening. The amphiphilic nature of the plasmalogen product led some difficulties in separation as it would readily form emulsions when extracting using aqueous workup conditions. This was remedied by careful mixing the separatory funnel and avoiding aggressive shaking.

Synthesis of the model substrate commenced when significant impediments were observed in the plasmalogen synthesis and a general O-(Z)-vinyl ether substrate was sought. The opening coupling of 1-bromooctane with propargyl alcohol proceeded with a lower yield than expected but this may have been attributed to partially quenched sodium hydride (60 % dispersion in mineral oil). The product was easily purified and carried forward in the subsequent hydrogenation. Lindlar Catalyst (5 wt %) was employed in the reduction of the terminal alkyne to the alkene. This product was carried forward cleanly following a quick filtration. This step was of interest as it would be applied in the partially deuterated model substrate synthesis using deuterium gas for the reduction in place of hydrogen gas. The final alkylation required stringent control over the temperature, reaction time, and conditions. This was performed using newly acquired *s*-BuLi (1.4 M in THF) and freshly distilled THF. It was evident that extremely clean SM was necessary to conduct the alkylation step with

maximal yield (53 %). After about 9-months the sample required silica gel column chromatography to purify the target from the oxidation products that had formed.

Synthesis of the deuterated model substrate was initiated following the successful synthesis of the natural VE model substrate. This synthetic pathway was similar to the route used to generate the natural VE model substrate, but it involved 2 additional steps to selectively install the 3 deuterium atoms about the unsaturation. Reaction progress was monitored by comparing the reaction NMR spectra with the NMR spectra obtained for the natural VE model substrate. The second step (not present in the original synthesis of the VE model substrate) involved the deprotonation of the terminal alkynyl proton and addition of deuterium. This partially deuterated intermediate was reduced using Lindlar Catalyst along with deuterium gas to selectively deuterate the unsaturation. The yield was noticeably attenuated in this deuteration in comparison to the hydrogenation that was conducted with quantitative returns. This may have been ascribed to oxidative lability or susceptibility to hydrolysis facilitated by water present in the atmosphere of the deuterated substrate. The final alkylation, which results in the formation of the O-(Z)-alkenyl ether functional group, proceeded with slightly diminished returns in comparison to the natural VE model substrate. The presence of a small amount of residual acetone from the previous step may have resulted in the poor conversion rates in this synthesis. The final product was isolated quite cleanly and stored in a round bottom flask at -78 ^{o}C to protect the VE from oxidative degradation.

A synthesis of the deuterated plasmalogen equivalent was necessary to generate material to perform the autoxidation experiments necessary to determine if KIE was present in the reaction. We proposed a synthesis (**Scheme 2.17**) based on the modifications that we had made in the original plasmalogen synthesis in addition to incorporating some of the steps

that were optimized in the synthesis of the partially deuterated model substrate. Characterization was expected to be challenging as some of the most defining characteristic peaks (VE doublet of triplets at 5.89 ppm, and peaks corresponding to protons present on glycerol head between 3.3-4.5 ppm in C_6D_6 on 400MHz NMR) would be suppressed by the presence of deuterium. The spectra acquired during the synthesis of the natural plasmalogen may be used as a standard for a comparison with the deuterated synthetic intermediates to monitor the reaction progress over time.

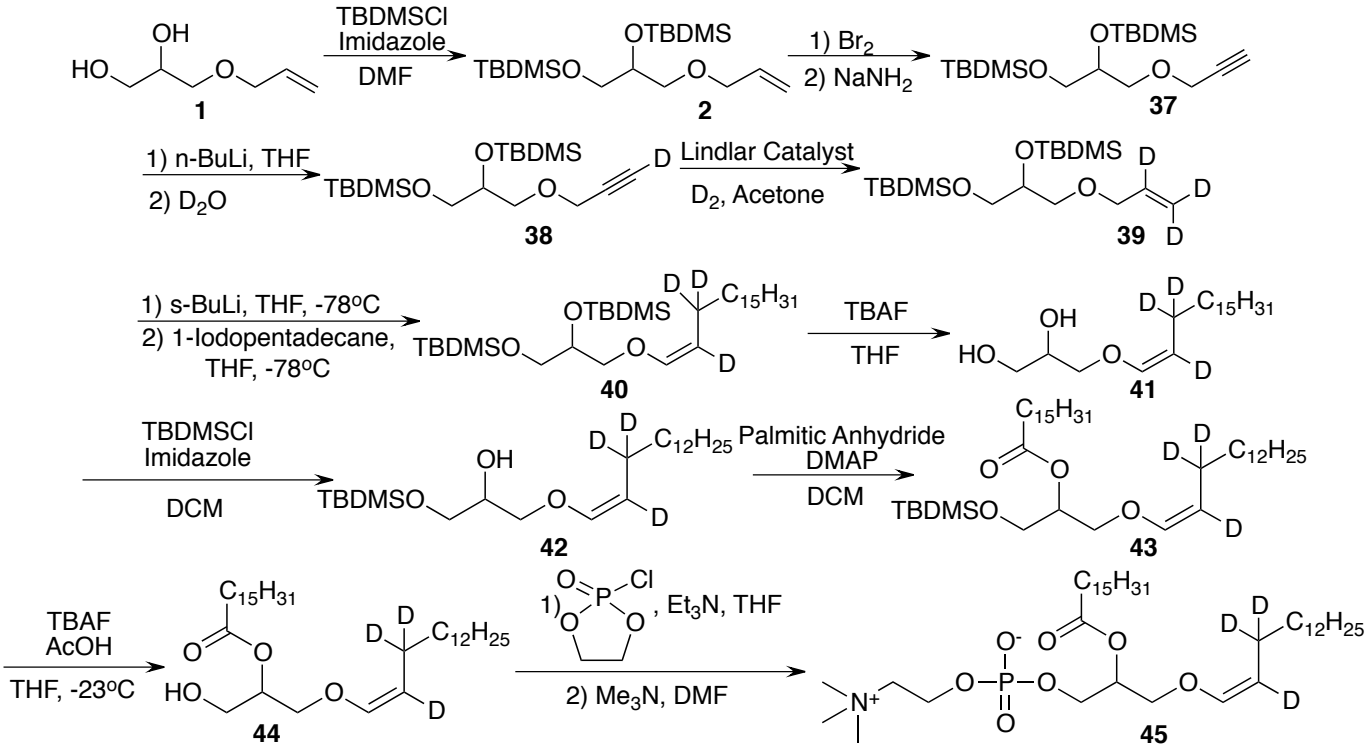

Scheme 2.17 Proposed synthesis of d_3-plasmalogen, based on modifications from lessons learned during the synthesis of the natural plasmalogen and deuterated vinyl ether model substrate.

This synthesis was the result of combining features of the plasmalogen synthesis and the key deuteration steps from the d_3-VE model substrate synthesis. This approach allowed the use of the same di-protected (TBDMS) 3-allyloxy-1,2-propanediol which was synthesized in large quantities for the natural plasmalogen synthesis. The second step in this

synthetic route involved the bromination and terminal alkene followed by a base catalyzed double elimination to form the desired terminal alkyne. This step was untested on the plasmalogen intermediate, but the experimental conditions were commonly used and reported. Additionally, the SM and the product of the second step are both considered to be quite stable and may not be as susceptible to side reactivity as the intermediates after the addition of the cis-vinyl ether. The subsequent steps are expected to proceed as reported in the aforementioned plasmalogen and the d_3-vinyl ether model substrate syntheses.

The analysis of the mechanism of autoxidation of the cis-vinyl ether moiety present in plasmenyl lipids was initially anticipated to be straight forward based on the fact that the methods were previously used to evaluate other lipid models with great success and consistency [55] [56]. Additionally, the instrumental methods that were optimized for other lipid models were predicted to function without significant modifications thereby expediting the process. The synthesized VE model substrate and d_3-VE model substrate were used in these experiments.

We attempted to determine the rates of substrate consumption, in anticipation of using the deuterated substrate to establish the extent of the kinetic isotope effect, by NMR or GC. The first approach involved the use of NMR spectroscopy to monitor the rate of autoxidation directly by examining the reduction in integration of the peak (5.89 ppm in C_6D_6 at 400MHz) corresponding consumption of the cis-vinyl ether with respect to an unreactive internal standard. This approach posed unprecedented challenges based on the inexplicable increase in substrate concentrations when tested under a variety of experimental conditions. The rate of VE model substrate consumption was calculated as 1.50×10^{-6} M s^{-1} and was an order of magnitude faster than the reported rate for the unimolecular

decomposition of V70 at 37 °C ($R_{i,exp}$ = 1.51 x 10^{-7} M s^{-1}) demonstrating that it did proceed via a chain reaction. GC yielded similar results as the NMR approach.

Methyl linoleate clocking experiments were performed using HPLC-UV (normal phase) in order to determine the ratio of thermodynamic to kinetic products formed; thereby allowing for the determination of the KIE based on the difference in the propagation rate constants (k_p) of the VE model substrate and the d_3-VE model substrate. The ratio of thermodynamic to kinetic products formed depends on the nature of the substrate tested. The KIE value obtained would shed a light on the favored mechanism of autoxidation (**Figure 1.11:** H-atom abstraction vs. peroxyl addition). The constants used in the calculations of the propagation rate constants were $k_{\beta II}$= 690 M^{-1} s^{-1} and β = 0.686 [55]. The k_H was calculated as being 6 M^{-1} s^{-1}, while the k_D could not be calculated.

Given the difficulties encountered in attempting the experimentally determine k_p for a vinyl ether and DKIE thereupon via indirect methods, direct kinetic measurements using LFP were conducted by Dr. Markus Griesser. This required the use of alkoxyl radicals generated by benzophenone triplet which revealed a k_H value of 6.4 ± 0.3 x 10^8 M^{-1} s^{-1} for the natural VE model, a k_D value of 4.2 ± 0.3 x 10^8 M^{-1} s^{-1} for the d_3-VE model, and a KIE of 1.5 (1.4-1.7). The k_H was significantly higher than the previously obtained value of 6 M^{-1} s^{-1}. The KIE was smaller than the values reported for similar lipids like cholesterol (11 ± 2 M^{-1} s^{-1}), linoleic acid (13 ± 1) [75] [10] and this indicates that peroxyl radical addition may in fact take place along with H-atom abstraction to a smaller extent. Overall, the results of the LFP tests were in agreement regarding the k_H value determined for the VE model substrate as being bigger than the k_H value of both oleate and cholesterol which is inconsistent with previous expectations of uniformity with the k_H of cholesterol.

2.4 Conclusion

In summation, this investigation of the autoxidation of cis-vinyl ethers present in plasmenylcholine yielded valuable insight regarding the dominance of the peroxyl radical addition autoxidation pathway over the H-atom abstraction. In conducting this study, the total synthesis of plasmalogens was optimized, an efficient synthesis of cis-vinyl ether functional groups was established, synthesis of selectively deuterated O-(Z)-vinyl ethers, and finally a synthesis of a partially deuterated plasmenylcholine analogue were proposed.

The plasmalogen model substrates were autoxidized and rates of consumption were monitored yielding a rate constant for the HAT of k_H of 6 M^{-1} s^{-1} for the VE-model substrate which was obtained via methyl linoleate radical clocking, and affirmed it was as slower than cholesterol. However, LFP studies revealed a KIE of 1.5 which indicates that the peroxyl radical addition is dominant over the H-atom abstraction pathway for the autoxidation of plasmalogen in comparison other structural similar monounsaturated lipids.

The material synthesized was adequate for a small number of liposome oxidation studies conducted in cells as model biological systems performed by Ms. Melodie Mallais. The results required additional experimentation to resolve. The autoxidations should be repeated with the deuterated plasmalogen analogue to determine if a KIE is truly present when compared with plasmenylcholine. The results of this investigation may be expanded upon by studying the effects of peroxidation/epoxidation on the propagation of the free radical throughout the lipid membrane as well as the effects on the membrane fluidity and integrity. A variety of different lipids (anhydrides) can be installed at the *sn*-2 position following the synthesis that was developed and enhanced to accommodate the use of alternatives to palmitic anhydride. These can be tested and compared with plasmenylcholine results.

2.5 Experimental Methods

NMR Spectroscopy:

^{1}H NMR and ^{13}C NMR spectra obtained at 298K were recorded using a Bruker AVANCE 300 MHz, or Bruker AVANCE 400 MHz as indicated. Residual monoprotic solvent peaks were used as an internal reference for ^{1}H NMR ($CDCl_3$: δ = 7.26 ppm; C_6D_6: δ = 7.16 ppm) and ^{13}C NMR spectra ($CDCl_3$: δ = 77.16 ppm; C_6D_6: δ = 128.1 ppm). Coupling constants (*J*) are quoted to the nearest 0.1 Hz. The following abbreviations (or combinations thereof) were used to describe ^{1}H NMR multiplicities: s = singlet, d = doublet, t = triplet, q = quartet, m = multiplet.

Mass Spectrometry:

High-resolution ESI+ (m/z) spectra were measured on a Thermo-Fisher Scientific LTQ XL Orbitrap. High-resolution EI+ (m/z) spectra were measured on a Kratos Concept Magnetic Sector MS System. MassLynx 4.0 of Water-Micromass was used for data analysis.

Experimental Procedures, reagents and glassware:

All starting materials and reagents and solvents were purchased from commercial suppliers (Sigma-Aldrich, or Alfa) and used without further purification unless otherwise indicated. Reactions were performed under the positive pressure of anhydrous nitrogen gas in base-bath washed and oven-dried glassware. All reactions were monitored using silica gel TLC and visualized using potassium permanganate. Intermediates were stored at -80 ^{o}C to mitigate oxidative degradation. Column chromatography was carried out using flash silica gel (60 Å, 40-63 μ, 500 m^2/g).

Corresponding spectral raw data and characterization is provided in Appendix A.

2.5.1 Synthetic Procedures

Iodination of Primary Alcohol (Appel Reaction)

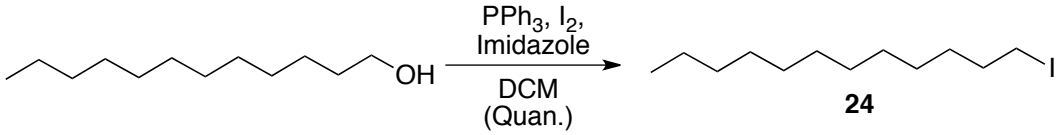

1-Iodododecane (24) A solution of DCM (400 mL) and 1-dodecanol (15.0 g, 80.5 mmol, 1.0 eq.) was stirred together for 10 min. The following reagents were added in order, imidazole (10.96 g, 161.0 mmol, 2.0 eq.), triphenylphosphine (42.23 g, 161.0 mmol, 2.0 eq.), and iodine (40.25 g, 158.6 mmol, 1.97 eq.). The golden yellow reaction mixture was left to stir for 1 hour. Reaction progress was monitored via TLC (100 % P.E.). Excess iodine is quenched using sodium thiosulfate before being extracted with DCM (3x100 mL), brine (1x100 mL) and, water. The combined organic phases were concentrated, and petroleum ether was added facilitate the precipitation of triphenylphosphine oxide (white crystals). The solution was dried over magnesium sulfate, vacuum filtered and concentrated. The crude colorless oil was purified using silica gel column chromatography (100 % Hexanes). Yield: 23.4 g; Quantitative yield. R_f = 0.7 (100 % P.E.); clear oil with yellow crystal precipitant. ^{1}H NMR ($CDCl_3$, 400MHz) δ 3.19 (t, *J* = 7.1 Hz, 2H), 1.82 (p, *J* = 7.1 Hz, 2H), 1.38 (t, *J* = 7.3 Hz, 2H), 1.26 (s, 22H), 0.87 (t, 3H). ^{13}C NMR (400 MHz Chloroform-*d*) δ 33.8, 32.1, 30.7, 29.8, 29.7, 29.6, 29.5, 28.7, 22.8, 14.3, 7.4. HRMS (+EI) (M^+) calculated [$C_{12}H_{25}I$] 296.1001, found 255.8219 (lost terminal C_3H_7 group). In accordance with the literature ^{1}H and ^{13}C shifts, and MS data [76] [21].

Silyl Protection of *sn*-2 and *sn*-3 Alcohols:

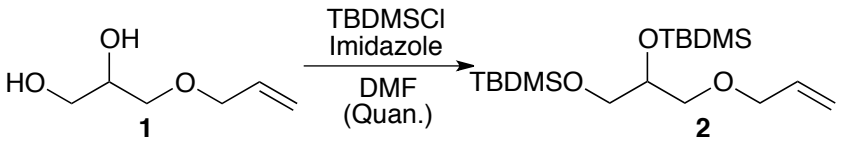

5-((allyloxy)methyl)-2,2,3,3,8,8,9,9-octamethyl-4,7-dioxa-3,8-disiladecane (2) Imidazole (15.5 g, 227.0 mmol, 1.5 eq.) was added to a solution of 3-allyloxy-1,2-propanediol (**1**) (20.0 g, 151.3 mmol, 1.0 eq.) in DMF (300 mL). In a separate flask TBDMSCl (68.4 g, 454.0 mmol, 3.0 eq.) was combined with DMF (300 mL). The TBDMSCl solution in DMF was added dropwise to the reaction mixture at 0ºC. Solution was left to stir overnight. TLC (5 % EtOAc:P.E.) was used to assess the progress of the reaction. The aqueous phase was extracted with EtOAc (3x100 mL), brine (1x100 mL), and water. The combined organic phases were dried over magnesium sulfate, filtered and, concentrated. The crude colorless oil was purified using silica gel column chromatography (10 % EtOAc:P.E.). Yield: 54.6 g; Quantitative yield. R_f = 0.4 (10 % EtOAc:P.E.); clear colorless oil. ^{1}H NMR ($CDCl_3$, 400MHz) δ 5.88 (d, J = 17.2, 10.4, 5.5 Hz, 1H), 5.24 (dd, J = 17.3, 1.7 Hz, 1H), 5.18 – 5.07 (m, 1H), 3.97 (dt, J = 5.5, 1.5 Hz, 2H), 3.81 (dd, J = 5.8, 4.6 Hz, 1H), 3.61 – 3.45 (m, 3H), 3.34 (dd, J = 9.9, 5.7 Hz, 1H), 0.12 – -0.08 (m, 17H). ^{13}C NMR (400 MHz Chloroform-*d*) 135.0, 116.5, 72.7, 72.2, 65.1, 26.0, 25.9, 18.4, -4.6. HRMS (+EI) (M^+) calculated 360.2516, found 303.2175. In accordance with the literature ^{1}H and ^{13}C shifts, and MS data [21].

Alkylation for the Preparation of the Key O-(Z)-Vinyl Ether

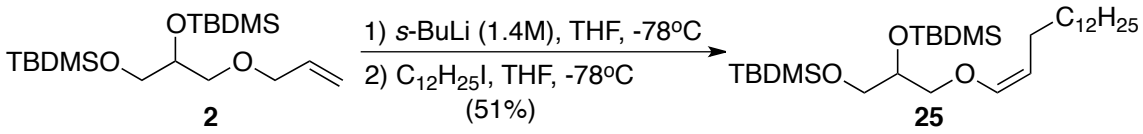

(Z)-2,2,3,3,8,8,9,9-octamethyl-5-((pentadec-1-en-1-yloxy)methyl)-4,7-dioxa-3,8-disiladecane (25) All glassware was flame-dried under high-vacuum prior to use and all manipulations were performed under inert N_2 atmosphere and in accordance with air-sensitive techniques. THF was freshly distilled immediately before use. A solution of **2** (7.0 g, 19.4 mmol, 1.0 eq.) in dry THF (300 mL) was prepared and left to stir for 30 min at -78 ^{o}C. 1.4 M s-BuLi (15.2 mL, 21.4 mmol, 1.1 eq.) was added dropwise to the reaction mixture before being left to stir for 1 hour at -78 ^{o}C. In a separate dry flask, 1-iododododecane (**1**) (6.3 g, 21.4 mmol, 1.1 eq.) was combined with dry THF (150 mL). The initial reaction mixture was kept in the -78 ^{o}C cooling bath as the solution of **1** in THF was slowly added in a dropwise fashion. The reaction was left to stir for 1 hour at -78 ^{o}C. Progress of the reaction was monitored via ^{1}H NMR (C_6D_6). Reagents were quenched, and the crude product was extracted with EtOAc (3x100 mL) and brine (1x100 mL) quickly. The combined organic phases were dried over magnesium sulfate, filtered and, concentrated. The crude pale-yellow oil was purified using silica gel column chromatography deactivated with 1 % NEt_3:Hexanes, then flushed with 100 % Hexanes before loading the crude material and eluting with 5 % DCM:Hexanes. Yield: 5.3 g; 51 %. R_f = 0.2 (5 % DCM:Hexanes); clear colorless oil. ^{1}H NMR (C_6D_6, 400MHz) δ 6.03 (d, J = 6.2 Hz, 1H), 4.50 (q, J = 7.3, 6.3 Hz, 1H), 4.02 (dd, J = 5.8, 4.2 Hz, 1H), 3.87 (dd, J = 10.6, 4.2 Hz, 1H), 3.75 (dd, J = 23.5, 5.9 Hz, 3H), 2.42 (qd, J = 7.3, 1.4 Hz, 2H), 1.65 – 1.26 (m, 23H), 1.05 (d, J = 20.9 Hz, 20H), 0.28 – 0.09 (m, 13H). ^{13}C NMR (C_6D_6, 400MHz) δ 145.7, 106.3, 74.1, 72.8, 64.8, 32.0, 30.1, 29.8, 29.7, 29.7, 29.6, 29.5, 25.8, 25.7, 24.4, 22.8, 18.2, 18.0, 14.0, -4.8, -4.8, -5.6, -5.7. HRMS (+EI) (M^+) calculated 529.4472, found 472.3645 (lost tert-butyl). In accordance with the literature ^{1}H and ^{13}C shifts, and MS data [21].

Desilylation of *sn*-2 and *sn*-3 Alcohols

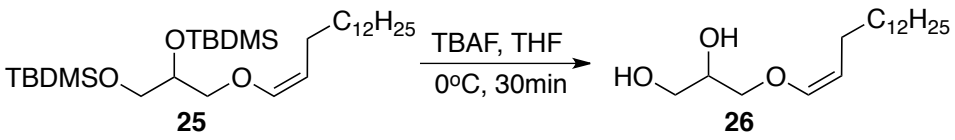

25 **26**

(Z)-3-(pentadec-1-en-1-yloxy)propane-1,2-diol (26) A solution of **25** (5.0 g, 9.4 mmol, 1.0 eq.) in dry THF (150 mL) was left to stir for 10min at 0°C. 1.0M TBAF (18.9 mL, 18.9 mmol, 2.0 eq.) added dropwise and the solution was left to stir for 30 min. Reaction progress was monitored via TLC (20% EtOAc:Hexanes). The organic product was extracted from the aqueous phase with Et_2O (1x100 mL), EtOAc (2x100 mL), brine (1x100 mL), and water (1x100 mL). The combined organic phases were dried over magnesium sulfate, filtered and, concentrated. The crude colorless oil was carried forward to the next synthetic step without further purification. ^{1}H NMR of the crude product was only used to ascertain that the product of interest was still present and to confirm that the deprotection proceeded to completion. Yield: 5.51 g. R_f = 0.1 (5 % DCM:Hexanes). ^{1}H NMR (C_6D_6, 400MHz) δ 6.15 (d, J = 6.2, 1.5 Hz, 1H), 4.42 (q, J = 7.2, 6.2 Hz, 1H), 4.32 – 4.09 (m, 2H), 4.09 – 3.98 (m, 3H), 3.90 (q, J = 7.1 Hz, 7H), 3.64 – 3.55 (m, 1H), 3.41 – 3.23 (m, 38H), 2.61 (s, 11H), 0.98 – 0.89 (m, 18H), 0.11 (d, J = 41.2 Hz, 12H). ^{13}C NMR (400 MHz Chloroform-*d*) 144.7, 108.6, 73.5, 70.1, 63.9, 32.2, 29.9, 29.8, 29.6, 24.2, 23.0, 14.4. HRMS (+EI) (M^+) calculated 300.2664, not found. In accordance with the literature ^{1}H and ^{13}C shifts [21].

Selective Silyl Protection of *sn*-3 Alcohol

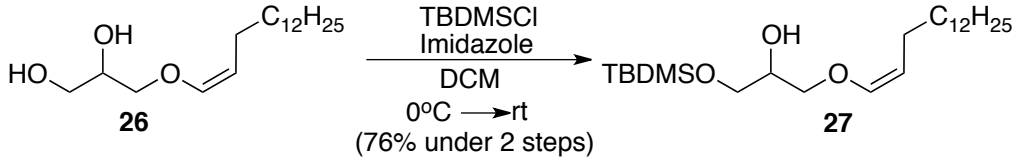

26 **27**

(Z)-1-((tert-butyldimethylsilyl)oxy)-3-(pentadec-1-en-1-yloxy)propan-2-ol (27) A solution of **26** (5.5 g, 19.4 mmol, 1.0 eq.) in DCM (180 mL) was left to stir for 10 min. The reaction flask was placed in a 0 °C ice bath. Imidazole (1.5 g, 21.3 mmol, 1.1 eq.) was added followed by TBDMSCl (2.9 g, 19.4 mmol, 1.0 eq.). The reaction was left to stir overnight (18 hours). TLC (20 % EtOAc:Hexanes) was used to determine progress of reaction. Reaction was quenched with ice and the aqueous phase was extracted with DCM (3x100 mL), brine (1x100 mL), and water. The combined phases were dried over magnesium sulfate, filtered and, concentrated. The crude pale-yellow oil was purified using silica gel column chromatography (100 % P.E. →10 % DCM:P.E.). Yield: 6.1 g; 76 % over 2 steps. R_f = 0.2 (10 % DCM:P.E.); clear colorless oil. ^{1}H NMR (C_6D_6, 400MHz) δ 5.96 (d, J = 6.2, 1.5 Hz, 1H), 4.49 (q, J = 7.3, 6.2 Hz, 1H), 3.85 (q, J = 5.3 Hz, 1H), 3.71 (d, J = 5.5 Hz, 2H), 3.65 (d, J = 5.1 Hz, 2H), 2.36 (dd, J = 7.2, 1.5 Hz, 1H), 2.19 (d, J = 5.5 Hz, 1H), 0.98 (d, J = 8.2 Hz, 2H), 0.97 (s, 9H), 0.08 (d, J = 6.0 Hz, 0H), 0.08 (s, 5H). ^{13}C NMR (C_6D_6, 400MHz) δ 145.4, 107.1, 72.6, 70.7, 64.0, 32.1, 30.1, 29.9, 29.9, 29.8, 29.6, 29.6, 25.8, 24.3, 22.9, 18.2, 14.1, -5.6. HRMS (+EI) (M^+) calculated 414.3529, found not found. In accordance with the literature ^{1}H and ^{13}C shifts and MS data [21].

Acylation of *sn*-2 Alcohol

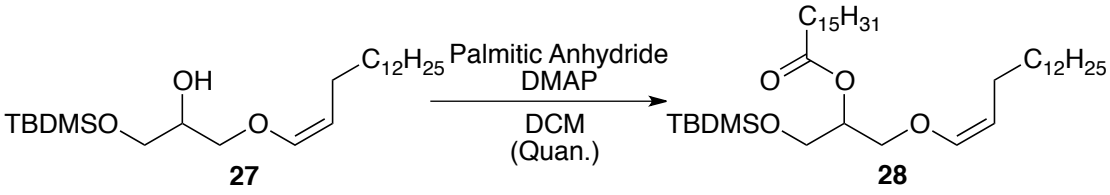

(Z)-1-((tert-butyldimethylsilyl)oxy)-3-(pentadec-1-en-1-yloxy)propan-2-yl palmitate (28) A 0 °C ice bath was applied to a solution of **27** (1.9 g, 4.1 mmol, 1.0 eq.) in dry DCM (210 mL). The following reagents were then added in order, palmitic anhydride (3.6 g, 7.4

mmol, 1.77 eq.), and DMAP (1.0 g, 8.1 mmol, 1.95 eq.). Let stir for 20 hours at r.t. TLC (5 % DCM:Hex) was used to determine progress of reaction. The aqueous phase was extracted with water (1x100 mL), DCM (2x100 mL), and brine (1x100 mL). The combined organic phases were dried over magnesium sulfate, filtered and, concentrated. The crude clear colorless oil was purified using silica gel column chromatography (deactivated and flushed before eluting with 5 % DCM:Hex). Yield: 3.0 g; Quantitative recovery. R_f = 0.2 (5 % DCM:Hex); clear colorless oil. ^{1}H NMR (Chloroform-*d*, 400 MHz,) δ 5.90 (dt, *J* = 6.2, 1.5 Hz, 1H), 5.00 (p, *J* = 5.2 Hz, 1H), 4.34 (td, *J* = 7.3, 6.2 Hz, 1H), 3.92 – 3.80 (m, 2H), 3.80 – 3.69 (m, 2H), 2.31 (dd, *J* = 8.0, 7.1 Hz, 2H), 2.03 (tt, *J* = 7.2, 3.6 Hz, 2H), 1.38 – 1.20 (m, 69H), 0.94 – 0.82 (m, 27H), 0.05 (s, 6H).^{1}H NMR (C_6D_6, 400MHz) δ 5.98 (d, J = 6.2 Hz, 0H), 5.31 (t, J = 5.0 Hz, 0H), 4.52 (q, J = 7.3, 6.1 Hz, 0H), 3.92 – 3.75 (m, 1H), 2.45 – 2.27 (m, 1H), 1.01 (d, J = 11.8 Hz, 3H), 0.13 (d, J = 4.7 Hz, 1H). ^{13}C NMR (C_6D_6, 400MHz). δ 145.3, 107.2, 72.8, 70.0, 61.4, 34.2, 32.0, 30.0, 29.9, 29.8, 29.7, 29.6, 29.5, 29.2, 25.7, 25.0, 24.2, 22.8, 14.0. HRMS (+EI) (M^+) calculated 652.5826, found 595.5080 (lost tert-butyl). In accordance with the literature ^{1}H and ^{13}C shifts and MS data [21].

Desilylation of *sn*-3 Alcohol

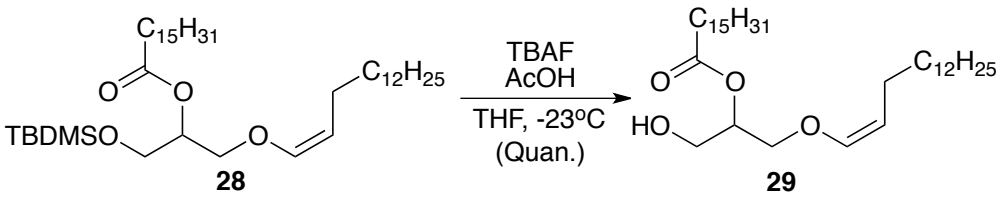

(Z)-1-hydroxy-3-(pentadec-1-en-1-yloxy)propan-2-yl palmitate (29) A 0° C ice bath was applied to a solution of **28** (1.5 g, 2.2 mmol, 1.0 eq.) in THF (25 mL). 1.0M TBAF (21.6 mL, 21.6 mmol, 10.0 eq.) was added dropwise followed by acetic acid (1.3 g, 21.6 mmol, 10.0

eq.). Let stir for 1 hour at -23 °C (cooled with cold probe). TLC (20 % EtOAc:Hexanes) was used to determine progress of reaction. THF and acetic acid were removed at 0°C, using rotary evaporation with a high-vacuum. A silica gel column was deactivated and flushed with cold solvent (-40 °C) then the crude material was directly loaded on the column. Cold eluent (30 % Et_2O:Hex) was then used to flush the product off the column quickly into a cooled flask. Concentrate again at 0°C, using rotary evaporation with a high-vacuum. Yield: 1.43 g; Quantitative yield. R_f = 0.1 (30 % Et_2O:Hex); pale yellow oil. ^1H NMR (C_6D_6, 400MHz) δ 5.82 (dt, J = 6.2, 1.4 Hz, 1H), 5.05 (p, J = 5.1 Hz, 1H), 4.44 (td, J = 7.4, 6.2 Hz, 1H), 3.90 (q, J = 7.1 Hz, 1H), 3.65 (dd, J = 5.1, 1.2 Hz, 2H), 3.51 (d, J = 5.1 Hz, 2H), 2.29 (qd, J = 7.3, 1.5 Hz, 2H), 2.17 (td, J = 7.3, 1.1 Hz, 2H), 0.99 – 0.83 (m, 14H). ^{13}C NMR (C_6D_6, 400MHz) δ 122.3, 94.8, 77.6, 57.2, 22.8, 20.0, 11.2, -16.2, -18.3, -18.7, -20.3, -20.4, -20.5, -20.5, -20.6, -20.7, -20.8, -20.9, -21.2, -25.3, -26.1, -27.5, -27.6, -30.1, -36.3, -36.3. HRMS (+EI) (M^+) calculated 538.8854, found 531.2512. In accordance with the literature ^1H and ^{13}C shifts, and MS data [21].

Choline Addition to *sn*-3 Alcohol

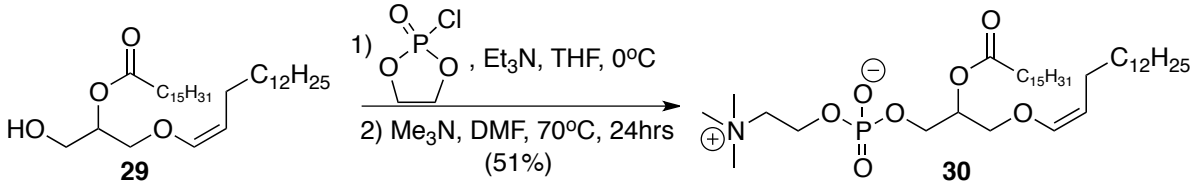

Plasmenylcholine (30) All glassware was flame-dried under high-vacuum prior to use and all manipulations were performed under inert N_2 atmosphere and in accordance with air-sensitive techniques. In a dry pressure vessel charged with a stir bar, a solution of **29** (1.4 g, 2.5 mmol, 1.0 eq.) in dry THF (40 mL) was prepared. The following were then added in

order, triethylamine (4.2 g, 41.8 mmol, 17.0 eq.) and ethylene chlorophosphate (1.4 g, 9.9 mmol, 4.0 eq.). An inert atmosphere was established, and a positive pressure was induced using a balloon filled with N_2. The reaction mixture was left to stir for 3 hours at 0 ^oC before concentration. The oil was solubilized in a minimum amount of anhydrous DMF (70 mL). In a separate flask, trimethylamine-hydrochloride salt (5.0 g, excess) was added, and a cannula was applied in headspace between a collection vessel (in a -78 ^oC cooling bath) and the flask containing NMe_3•HCl. A saturated aqueous NaOH solution was quickly added to the trimethylamine-hydrochloride salt to liberate trimethylamine gas, which was condensed using a cold finger with -78 ^oC acetone-dry ice cooling solution. The positive pressure induced by the balloon forces the NMe_3 gas into the pressure vessel. NaOH was added until no more NMe_3 gas evolved. The condensed trimethylamine solution was kept in a dry ice box until ready for use. The reaction mixture was cooled to -78 ^oC before trimethylamine solution was added (in solution to mitigate losses to evaporation) then sealed very tightly. The pressure vessel was then left to warm to r.t. before placing it in a 70 ^oC oil bath to heat it for the subsequent 24 hours while stirring. The reaction vessel was cooled quickly using a 0^oC ice bath before carefully opening. The aqueous phase was extracted with DCM (3x10 mL), and brine (1x10 mL). The combined organic phases were concentrated. The crude yellow oil was purified using silica gel column chromatography (deactivated with 1 % NEt_3:Hex before eluting with the following gradient 100 % CHCl3 → 20 % MeOH:$CHCl_3$ → 70:26:4 $CHCl_3$:MeOH:H_2O). Yield: 1.0 g (51 %), white powder. R_f = 0.3 (70:26:4 $CHCl_3$:MeOH:H_2O). ^{1}H NMR ($CDCl_3$, 400MHz) δ 5.92 (d, J = 6.1 Hz, 1H), 5.15 (s, 1H), 4.44 – 4.22 (m, 2H), 3.93 (s, 6H), 3.34 (s, 7H), 2.54 (s, 5H), 2.31 (t, J = 7.6 Hz, 2H), 2.14 – 1.91 (m, 2H), 1.58 (t, J = 7.3 Hz, 2H), 1.25 (s, 50H), 0.88 (t, J = 6.8 Hz, 8H). ^{13}C NMR

($CDCl_3$, 400MHz) δ 173.2, 144.7, 107.5, 70.4, 54.5, 34.3, 31.8, 29.7, 29.7, 29.6, 29.6, 29.5, 29.3, 29.3, 29.1, 24.9, 23.8, 22.6, 14.0. HRMS (EI+) $(M+)^+$ calculated 703.5516, found 704.5411 ($M+H^+$). In accordance with the literature ^1H and ^{13}C shifts [21].

Alkylation of Propargyl Alcohol with 1-Bromohexane

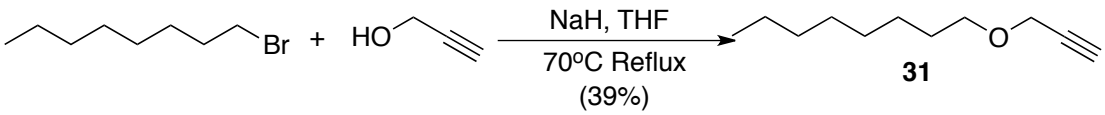

1-(prop-2-yn-1-yloxy)octane (31) A solution propargyl alcohol (5.0 g, 5.2 mL, 89.2 mmol, 1.0 eq.) was prepared in dry THF (200 mL). Sodium hydride (60 % dispersion in mineral oil; 3.8 g, 98.1 mmol, 1.1 eq.) was then added carefully while stirring. The reaction mixture was left to stir at r.t. for 30minutes. 1-Bromooctane (17.2 g, 15.4 mL, 89.2 mmol, 1.0 eq.) was added, then a water-cooled condenser was applied. The reaction mixture was left to reflux and stir a 70 ºC overnight. TLC (5 % Et_2O:Hexanes) was used to assess the progress of the reaction. The aqueous phase was extracted with Et_2O (3x150 mL), brine (1x150 mL), and water (1x150 mL). The combined organic phases were dried over magnesium sulfate, filtered and, concentrated. The crude colorless oil was purified using silica gel column chromatography (100 % Hexanes → 2 % Et_2O:Hexanes). Yield: 5.8 g; 39 % yield. R_f = 0.3 (2 % Et_2O:Hexanes); clear colorless oil. ^1H NMR (400 MHz, Chloroform-*d*) δ 4.13 (d, *J* = 2.4 Hz, 2H), 3.51 (t, *J* = 6.7 Hz, 2H), 2.41 (t, *J* = 2.4 Hz, 1H), 1.58 (dt, *J* = 8.1, 6.6 Hz, 2H), 1.39 – 1.19 (m, 11H), 0.92 – 0.80 (m, 4H). ^{13}C NMR (400 MHz Chloroform-*d*) 79.4, 75.6, 71.6, 59.3, 31.8, 29.7, 29.4, 29.3, 26.2, 22.7, 14.1. HRMS (ESI+) $(M+)^+$ calculated 168.1514, found 83.0854 [$C_5H_7O^•$] and 85.1015 [$C_6H_{13}^•$]. In accordance with the literature ^1H and ^{13}C shifts, and MS data [69].

Lindlar Reduction of Terminal Alkyne

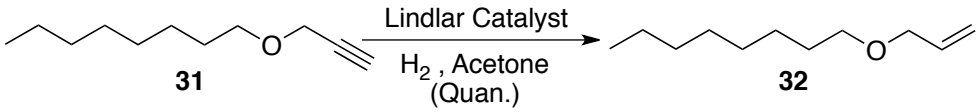

1-(allyloxy)octane (32) A solution of 1-(prop-2-yn-1-yloxy)octane (9.2 g, 54.9 mmol, 1.0 eq.) was prepared in dry acetone (92 mL). Lindlar Catalyst (2 wt%, 184.6 mg, Excess) was then added before flushing the reaction vessel with nitrogen gas and vacuum then flushing with hydrogen gas before applying a triple walled balloon filled with $H_{2(g)}$. The reaction progress was monitored via TLC (2 % Et_2O:Hexanes). After exactly 25 minutes the mixture was filtered and concentrated directly to generate a crude pale-yellow oil with complete reduction. Yield: 8.4 g; Quantitative. R_f = 0.3 (2 % Et_2O:Hexanes). ^1H NMR (400 MHz, Chloroform-*d*) δ 5.92 (ddt, *J* = 17.2, 10.4, 5.7 Hz, 1H), 5.27 (dq, *J* = 17.2, 1.7 Hz, 1H), 5.17 (dq, *J* = 10.4, 1.4 Hz, 1H), 3.96 (dt, *J* = 5.6, 1.5 Hz, 2H), 3.46 – 3.37 (m, 3H), 1.67 – 1.51 (m, 3H), 1.41 – 1.17 (m, 13H), 0.95 – 0.79 (m, 4H). ^{13}C NMR (400 MHz Chloroform-*d*) 134.0, 117.4, 72.0, 70.3, 31.79, 29.7, 29.4, 29.3, 26.2, 22.7, 14.1. In accordance with the literature ^1H and ^{13}C shifts [70].

Alkylation of Terminal Alkene

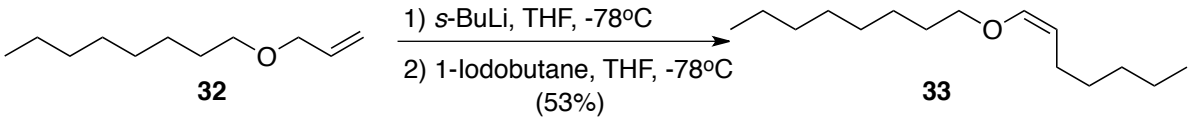

(*Z*)-1-(hept-1-en-1-yloxy)octane (33) All glassware was flame-dried under high-vacuum prior to use and all manipulations were performed under inert N_2 atmosphere and in accordance with air-sensitive techniques. THF was freshly distilled immediately before use. A solution of 1-(allyloxy)octane (4.2 g, 24.7 mmol, 1.0 eq.) in dry THF (60 mL) was

prepared and left to stir for 30 min at -78 °C. 1.4 M s-BuLi (19.4 mL, 27.1 mmol, 1.1 eq.) was added dropwise to the reaction mixture before being left to stir for 1 hour at -78 °C. In a separate dry flask, 1-iododobutane (5.0 g, 27.1 mmol, 1.1 eq.) was combined with dry THF (60 mL). The initial reaction mixture was kept in the -78 °C cooling bath as the solution of 1-iododobutane in THF was slowly added in a dropwise fashion. The reaction was left to stir for 1 hour at -78 °C. Progress of the reaction was monitored via ^{1}H NMR (C_6D_6). Reagents were quenched, and the crude product was extracted with EtOAc (3x100 mL) and brine (1x100 mL) quickly. The combined organic phases were dried over magnesium sulfate, filtered and, concentrated. The crude pale-yellow oil was purified using silica gel column chromatography deactivated with 1 % NEt_3:Hexanes, then flushed with 100 % Hexanes before loading the crude material and eluting with 100 % Hexanes. Yield: 5.7 g; 53 %. R_f = 0.2 (100 % P.E.); clear colorless oil. ^{1}H NMR (400 MHz, Benzene-d_6) δ 5.89 (dt, J = 6.3, 1.4 Hz, 1H), 4.45 (td, J = 7.3, 6.2 Hz, 1H), 3.48 (t, J = 6.5 Hz, 2H), 2.36 (qd, J = 7.3, 1.5 Hz, 2H), 1.56 – 1.39 (m, 5H), 1.37 – 1.12 (m, 18H), 1.02 – 0.74 (m, 10H). ^{13}C NMR (400 MHz, Benzene-d_6) 144.0, 143.6, 128.0, 127.8, 126.1, 106.6, 83.8, 50.5, 33.6, 32.8, 31.4, 29.3, 25.9, 24.9, 23.8, 22.5, 14.1. HRMS (EI+) $(M+)^+$ calculated [$C_{15}H_{30}O^{\bullet}$] 226.2297, found 226.2301 [$C_{15}H_{30}O^{\bullet}$]. In accordance with the literature ^{1}H and ^{13}C shifts, and MS data [71].

Deuteration of Terminal Alkyne

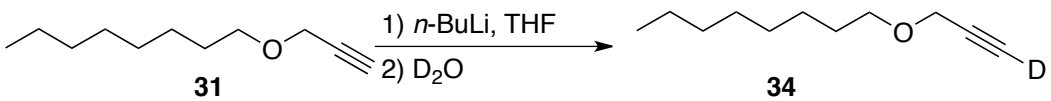

31 **34**

d_1-1-(prop-2-yn-1-yloxy)octane (34) A solution of 1-(prop-2-yn-1-yloxy)octane (7.2 g, 43.1 mmol, 1.0 eq.) was prepared in dry THF (350 mL) then cooled to -78 °C using an

acetone-dry ice cooling bath. 2.3 M *n*-BuLi (20.7 mL, 47.4 mmol, 1.1 eq.) was then added dropwise to the cooled solution. The reaction mixture was left to stir for 30 minutes at -78 ^{o}C before D_2O (3.9 g, 3.5 mL, 193.8 mmol, 4.5 eq.) was added to deuterate the terminal position while quenching excess n-BuLi. Solution was left to stir for 30 minutes. The organic phase was extracted with Et_2O (3x150 mL), brine (1x150 mL), and water (1x150 mL). The combined organic phases were dried over magnesium sulfate, filtered and, concentrated very carefully to avoid volatilization of the target. Yield: 6.8 g; Quantitative; 95 % Deuteration. R_f = 0.3 (2 % Et_2O:Hexanes). ^{1}H NMR (400 MHz, Chloroform-*d*) δ 4.13 (s, 2H), 3.57 – 3.46 (m, 3H), 1.65 – 1.52 (m, 2H), 1.42 – 1.24 (m, 10H), 0.92 – 0.81 (m, 3H). ^{13}C NMR (400 MHz, Chloroform-*d*) 75.2, 73.7, 70.3, 58.0, 31.8, 29.5, 25.8, 22.6, 14.0. In accordance with the literature ^{1}H and ^{13}C shifts [72].

Lindlar Reduction of Deuterated Terminal Alkyne with $D_{2(g)}$

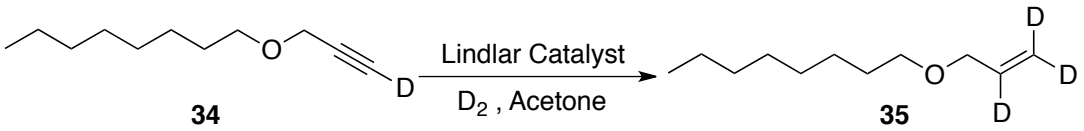

34 **35**

d_3-1-(allyloxy)octane (35) A solution of d_1-1-(prop-2-yn-1-yloxy)octane (6.8 g, 40.4 mmol, 1.0 eq.) was prepared in dry acetone (85 mL). Lindlar Catalyst (2 wt%, 136.8 mg, Excess) was then added before flushing the reaction vessel with nitrogen gas and vacuum then flushing with deuterium gas before applying a triple walled balloon filled with $D_{2(g)}$. The reaction progress was monitored via TLC (2 % Et_2O:Hexanes). After exactly 25 minutes the mixture was filtered and concentrated directly to generate a crude pale-yellow oil with complete reduction. The crude product was carried forward without further purification. Yield: 5.5 g; 52 %. R_f = 0.2 (2 % Et_2O:Hexanes). ^{1}H NMR (400 MHz, Chloroform-*d*) δ 4.13

(s, 2H), 3.51 (t, *J* = 6.7 Hz, 2H), 1.65 – 1.51 (m, 4H), 1.26 (dd, *J* = 14.3, 10.2 Hz, 18H), 0.94 – 0.81 (m, 5H). ^{13}C NMR (400 MHz, Chloroform-*d*) 135.2, 121.6, 71.2, 69.6, 31.8, 29.5, 29.3, 26.2, 22.7, 14.1. In accordance with the reported ^{1}H and ^{13}C shifts [70].

Alkylation of Selectively Deuterated Terminal Alkene

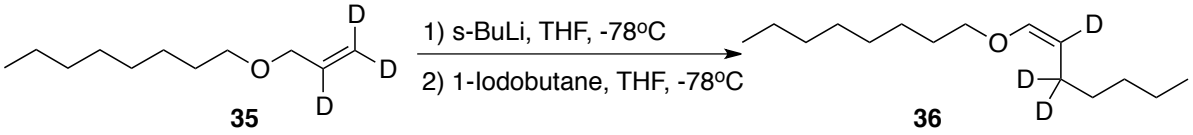

35 **36**

d_3-(*Z*)-1-(hept-1-en-1-yloxy)octane (36) All glassware was flame-dried under high-vacuum prior to use and all manipulations were performed under inert N_2 atmosphere and in accordance with air-sensitive techniques. THF was freshly distilled immediately before use. A solution of d_3-1-(allyloxy)octane (2.8 g, 16.0 mmol, 1.0 eq.) in dry THF (40 mL) was prepared and left to stir for 30 min at -78 ºC. 1.4 M *s*-BuLi (12.3 mL, 17.7 mmol, 1.1 eq.) was added dropwise to the reaction mixture before being left to stir for 1 hour at -78 ºC. In a separate dry flask, 1-iododobutane (2.9 g, 1.8 mL, 16.0 mmol, 1.0 eq.) was combined with dry THF (40 mL). The initial reaction mixture was kept in the -78 ºC cooling bath as the solution of 1-iododobutane in THF was slowly added in a dropwise fashion. The reaction was left to stir for 1 hour at -78 ºC. Progress of the reaction was monitored via ^{1}H NMR (C_6D_6). Reagents were quenched, and the crude product was extracted with EtOAc (3x100 mL) and brine (1x100 mL) quickly. The combined organic phases were dried over magnesium sulfate, filtered and, concentrated under reduced pressure. The crude pale yellow oil was purified using silica gel column chromatography deactivated with 1 % NEt_3:Hexanes, then flushed with 100 % Hexanes before loading the crude material and eluting with 100 % P.E. Yield: 2.8 g; 43 %. R_f = 0.2 (100% P.E.); clear colorless oil. ^{1}H NMR (400 MHz,

Chloroform-*d*) δ 5.91 (s, 1H), 3.69 (t, J = 6.6 Hz, 2H), 1.65 – 1.57 (m, 2H), 1.41 – 1.20 (m, 22H), 0.94 – 0.79 (m, 16H). ^{13}C NMR (400 MHz, Chloroform-*d*) 140.0, 117.4, 71.4, 39.0, 21.8, 29.6, 29.4, 28.9, 27.0, 26.3, 22.7, 22.1, 14.1, 14.0. HRMS (EI+) $(M+)^+$ calculated for $[C_{15}H_{27}D_3O^+]$ m/z 229.2485 found $[C_{15}H_{27}D_3OH^+]$ m/z 230.2563 m/z . In accordance with the literature ^{1}H and ^{13}C shifts, and MS data for the proteiated equivalent [71].

2.5.2 NMR Clocking Experimental Conditions

A NMR method was developed with the following parameters:

The autoxidation mixture was incubated at 37^{o}C in a pre-heated heating block for 20 minutes prior to commencing the NMR experiment. The NMR heating chamber was pre-heated for approximately 20 minutes (display indicates when temperature has equilibrated). The instrumental method involved obtaining 16 scans for 1 minute without spinning the sample, then spinning the sample for 4 minutes in the 37 ^{o}C heated chamber; additionally, a 4 second pulse delay was applied for the acquisition of the scans.

2.5.3 Methyl Linoleate Clocking Experimental Conditions

The clocking experiments were conducted as reported by Porter *et al.* [55].

Methyl linoleate was purified via silica gel column chromatography eluted with 5% EtOAc:Hex immediately before use. Purified methyl linoleate was stored under nitrogen in a flask covered in aluminum foil to block light which may photo-oxidize the sample. The integrity of the methyl linoleate was evaluated using NMR prior to each use.

The following were added in a 1mL HPLC autosampler vial charged with a stir bar in the given order (Following the volumes outlined in **Table 2.2)**: solvent (chlorobenzene), AO

(VE model substrate or deuterated-VE model substrate), 100 mM Methyl Linoleate (5 μL of 2 M methyl linoleate in PhCl), 10 mM V70 (5μL of solution comprised of 30.8 mg V70 in 0.5 mL PhCl). The vials were capped with a clean but used (provided a partially opened injection port in the septum) autosampler caps to ensure adequate exchange with atmospheric O_2. 100 mM AO, and 10mM of the radical azo-initiator V70 (V70) were then added to each sample and placed in a heating block that was preheated and equilibrated at 37°C before being left to stir for 90 minutes.

PhCl (μL)	VE Substrate (M)	VE Substrate (μL)	2 M ML (μL) in PhCl	0.2 M V70 (μL) in PhCl
90	0	0	5	5
85	0.16	5	5	5
80	0.32	10	5	5
75	0.53	15	5	5
70	0.64	20	5	5
65	0.85	25	5	5
60	1.07	30	5	5
55	1.17	35	5	5
50	1.28	40	5	5
45	1.6	45	5	5

Table 2.2 Concentrations and volumes of AO (VE model substrate and deuterated-VE model substrate), initiator (10 mM V70/V70), and clocking substrate (100 mM Methyl Linoleate [ML]) used in methyl linoleate clocking experiments [V_f = 100 μL].

Reaction conditions were selected in order to ensure that less than 5 % of the H-donor was consumed. A blank was run at the beginning of each experiment to ensure that the clock substrate (methyl linoleate) was uncontaminated. Commercially obtained methyl linoleate contained measurable quantities of oxidation products varying from 1-2 % contamination on average. Methyl linoleate was freshly purified via column chromatography and eluted with a 5 % ethyl acetate in hexanes prior to each set of experiments to ensure consistency in results.

At the conclusion of the experiment, the products of the methyl linoleate autoxidation were quenched with 50 mM BHT (50 μL of 1 M BHT in chlorobenzene), then 50 mM triphenylphosphine (50 μL of 1 M PPh_3 in chlorobenzene) was added to reduce the hydroperoxides to their corresponding alcohols. This was done to improve the chromatography and generate a greater separation between the peaks of interest. The samples were subsequently diluted to 700 μL by the addition of 500 μL of hexanes and left to stir at r.t. for 30 minutes before UPLC-UV analysis had commenced. The samples were diluted in order to obtain an appropriate range for LC analysis and avoid flooding the detector and column.

The HPLC-UV column was rinsed with solvent, primed, and equilibrated prior to the start of the experiment. HPLC analysis was performed on normal phase using a 100 mm Waters SunFire C_{18} column eluted with 0.5 % IPA:Hex run at a flow rate of 1mL/min. Samples were evaluated to ensure no turbidity was present prior to LC injection and any sample with opacity was processed through a 0.2 μm Teflon syringe filter to ensure the mixture would not obstruct the instrument. The samples in the autosampler vials were then placed in a random order on the sample tray. Standards of all reagents and solvents used were run along with the autoxidation samples. The HPLC-UV queue was prepared such that every 4 sample injections, a 2 % IPA:Hex wash was run for 60 minutes to remove traces of methyl linoleate left on the column. A 25 μL injection volume was used, and each sample was run for 60 minutes followed by a 15min wash to remove triphenylphosphine oxide left on the column from each sample. An equilibration period was incorporated into this to ensure the subsequent injection and chromatographic separation was performed under the

identical solvent polarity). Maximal absorption at 234 nm was observed using a photodiode array detector and the integration of the peaks of interest was conducted at this wavelength.

2.5.4 GC-FID Experimental Conditions

The use of Gas Chromatography (Agilent GC7890A System) coupled with a Flame Ionization Detector (FID) was sought as an alternative analytical approach for monitoring clocking experiments instead of the NMR. This was also done to corroborate the experimental results obtained through the methyl linoleate clocking investigation via liquid chromatographic techniques. Instrumental conditions were initially derived from Dr. Zosia Zielinski's Hexadec-9-ene GC-FID method that was previously developed on the instrument. This was used due to the structural similarity in the substrates which led us to speculate that it may elute similarly. Sample runs presented carryover when using the method and therefore the instrumental method was tailored for the chromatography of the VE model substrate. The VE model substrate was freshly purified before being used in the autoxidation trials.

A 50:1 split injection method was used to allow for small sample injections to avoid retaining artifacts on column or flooding the detector if larger injection volumes were used. A sample injection volume of 3 μL was used. A glass 10 μL autosampler syringe was used by the instrument to draw the sample/solvent at a rate of 300 μL/minute and dispense the sample/solvent at a rate of 6 mL/minute. Acetonitrile washes (8 μL) of the syringe were performed before and after each injection to ensure no residual contaminants were carried through to subsequent injections. The inlet was equilibrated at 250^{o}C to ensure adequate volatilization of the samples. Additionally, the inlet had a helium gas flow rate of 94.8 mL/minute.

The gas chromatography column used was an Agilent HP-5 GC Column (19091J-413) packed with low-polarity fused silica. This column had a total length of 30 m, an internal diameter of 0.32 mm, and a film thickness of 0.25 μm. A column flow rate of 1.58 mL/minute was used (~10.6 psi). A temperature gradient was applied to the column oven to improve the chromatographic separation and to ensure any contaminants were washed off the column after each sample was run. The maximum oven temperature was set to 300 ^{o}C to avoid overheating. The temperature gradient method encompassed an initial set point temperature of 130 ^{o}C. As soon as the sample was injected the temperature would slowly ramp up from 130 ^{o}C to 160 ^{o}C at a rate of 3 ^{o}C/minute (total 10 minutes). The temperature was then rapidly increased from 160 ^{o}C to 300 ^{o}C at a rate of 35 ^{o}C/minute (total 4 minutes). This was followed by a temperature hold at 300 ^{o}C for 1 minute to remove traces of contaminants from the column, before to being allowed to cool back to 130 ^{o}C at a rate of 40 ^{o}C/minute. The oven temperature was held at the 130 ^{o}C set point until the following sample was injected. The overall run time was 15 min (not including the 1-2 minutes for the wash cycle and injection between each run). The flame ionization detector was set to 300 ^{o}C, with a hydrogen gas flow rate of 50 mL/min, air flow rate of 400 mL/min, and makeup flow rate of 25 mL/min.

Preliminary trials were performed to determine the elution time of the product of interest (VE model substrate), an internal standard, and the initiator. This allowed us to monitor the decrease in peak integration and therefore concentration over the course of an autoxidation. As such we could establish a rate of consumption and determine the duration of the inhibition period. This was done using a 1 mM VE model substrate in HPLC grade hexanes (100 μL of 10 mM stock + 900 μL hexanes).

After the preliminary instrumental method optimization; the VE model substrate appeared to elute from the column at 7.5 minutes (increasing concentrations were tested in a random order to confirm) (**Figure 2.14**). The internal standard chosen for the assay was hexadecane as it was considerably heavier than the target analyte and was not anticipated to participate in the autoxidation reaction. A 1 mM standard in hexanes to ascertain its elution time and confirm that it did not co-elute with the VE model substrate. Hexadecane eluted at 8.6 minutes under the standard conditions established and used to test the VE model substrate (**Figure 2.14**). The azo- initiator V-70 (V70) was found to elute noticeably later at approximately 12.1 minutes. An injection of 100 % benzene was also tested to ensure that there were no contaminants in the solvent.

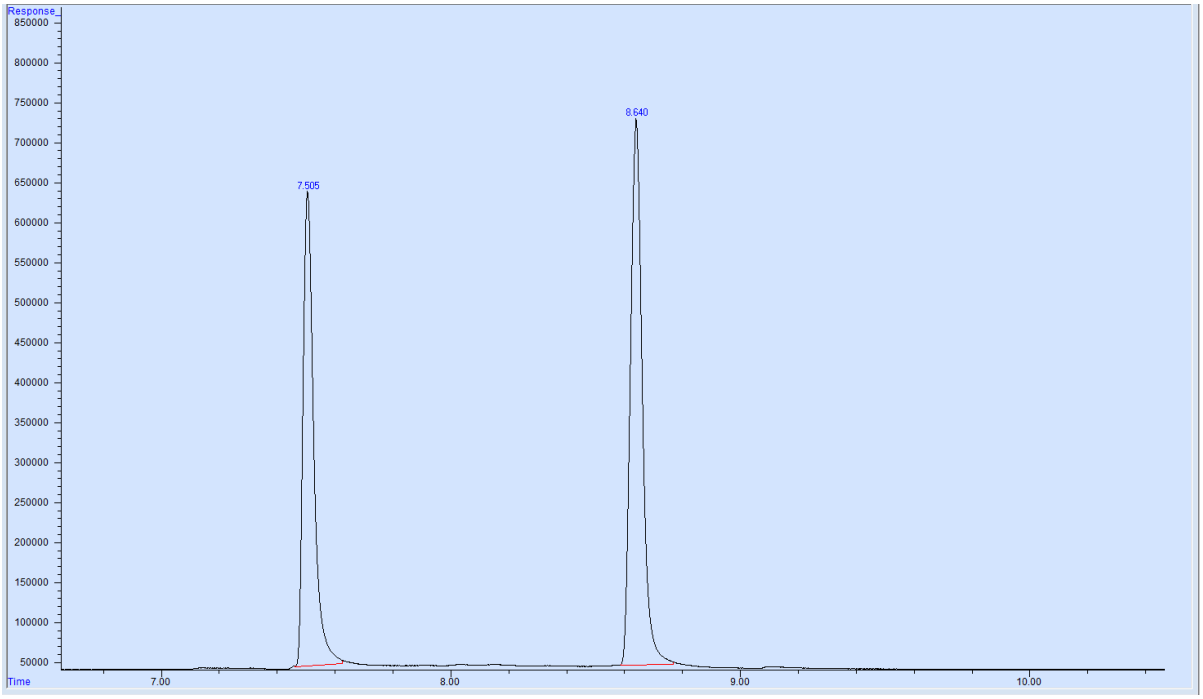

Figure 2.14 Sample chromatogram from a VE model substrate standard curve trial depicting the peak corresponding to the *cis*-vinyl ether model substrate at 7.505 minutes and the peak corresponding to the internal standard 1 mM hexadecane (in benzene) at 8.640 minutes.

A concentration curve was generated for the cis-vinyl ether model substrate in benzene to determine the response factor, using 1 mM hexadecane as an internal standard. This was conducted to optimize chromatography conditions required to generate standard curve to be used to establish linear region of concentrations to be used in subsequent autoxidation. Benzene was used instead of hexanes since it was drier and consequently, mitigated minor cis-vinyl ether oxidative decomposition that initially resulted in unexpected chromatograms depicting many artifacts about the baseline. The volumes of the stock solutions and the target concentration for each standard was calculated and shown in **Table 2.3**.

[VE Model Substrate] (mM)	Vol 20 mM VE Model Substrate in Benzene (μL)	Vol 10 mM Hexadecane (μL) (IS)	Vol Benzene (μL) (Solvent)	Total Vol (μL)
0	0	100	900	1000
0.05	2.5	100	897.5	1000
0.1	5	100	895	1000
0.25	12.5	100	887.5	1000
0.5	25	100	875	1000
0.75	37.5	100	862.5	1000
1.0	50	100	850	1000
2.0	100	100	800	1000
3.0	150	100	750	1000
4.0	200	100	700	1000
5.0	250	100	650	1000
6.0	300	100	600	1000
7.0	350	100	550	1000
8.0	400	100	500	1000
9.0	450	100	450	1000
10.0	500	100	400	1000

Table 2.3 Concentrations and volumes tested for the vinyl ether model substrate (VE) response factor curve generated on GC-FID.

A standard curve was developed with a vinyl ether model substrate stock solution and an internal standard stock solution to establish a response factor and demonstrated linearity

over the range that was expected to be measured, with linearity being tightly maintained in the 0-2.5 mM region (**Figure 2.15**). Deviation from linearity was observed above 9 mM (as such the 10 mM data point was not included in the standard curve presented in **Figure 2.15**).

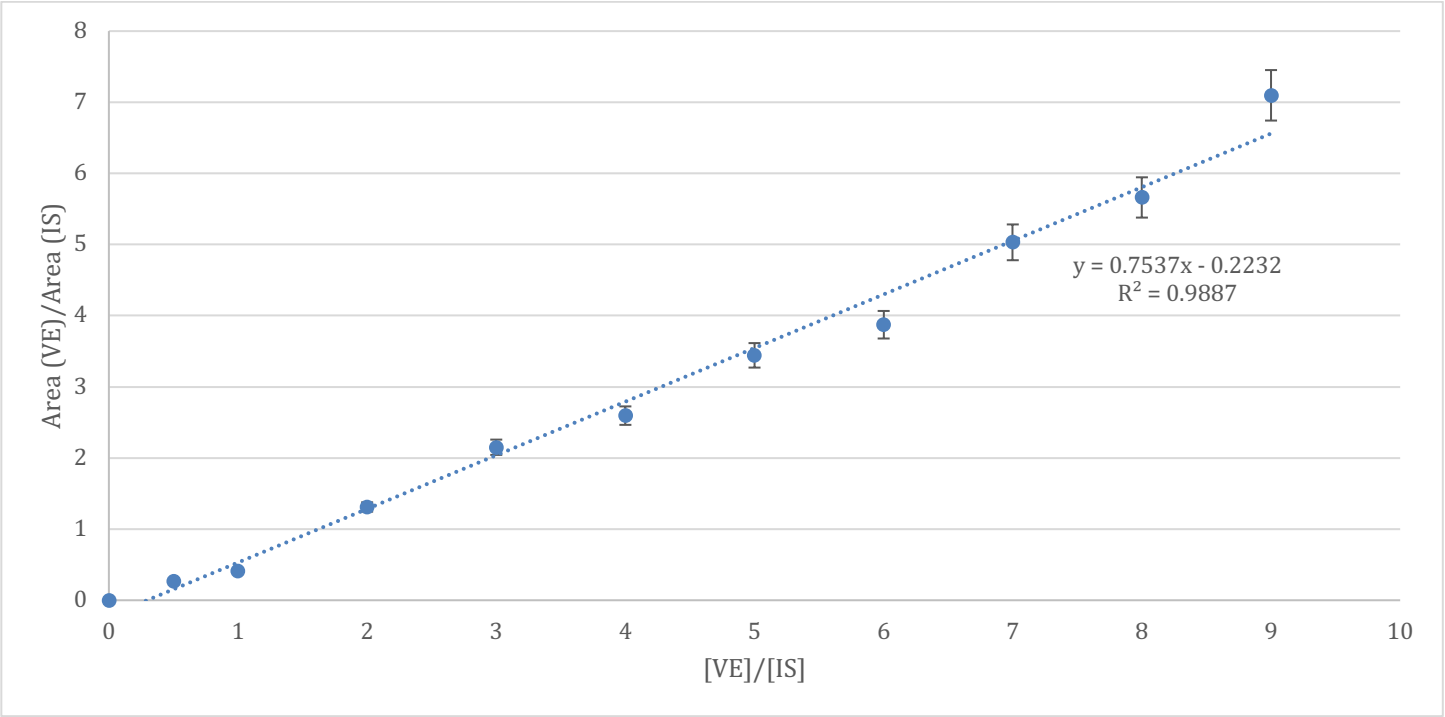

Figure 2.15 A standard curve of increasing VE model substrate concentrations where 1 mM hexadecane was used as the IS. Triplicate trials were conducted and the average relative response of 3 experiments was plotted against the concentration of the VE model substrate, with the corresponding error bars.

A vinyl ether model substrate autoxidation experiment was designed and conducted alongside a control experiment in which only vinyl ether model substrate and the solvent were present in the mixture. The established instrumental method that was validated through the generation of the calibration curve was used to run all of the samples. The control experiment was conducted to determine if the internal standard peak integration fluctuated during the course of the experiment and establish the rate of thermally catalyzed decomposition/oxidation of the VE model substrate without any radical initiators present.

The samples were run in a random order to ensure there is no cross over of contaminants between runs; this may not be evident if the samples were run sequentially.

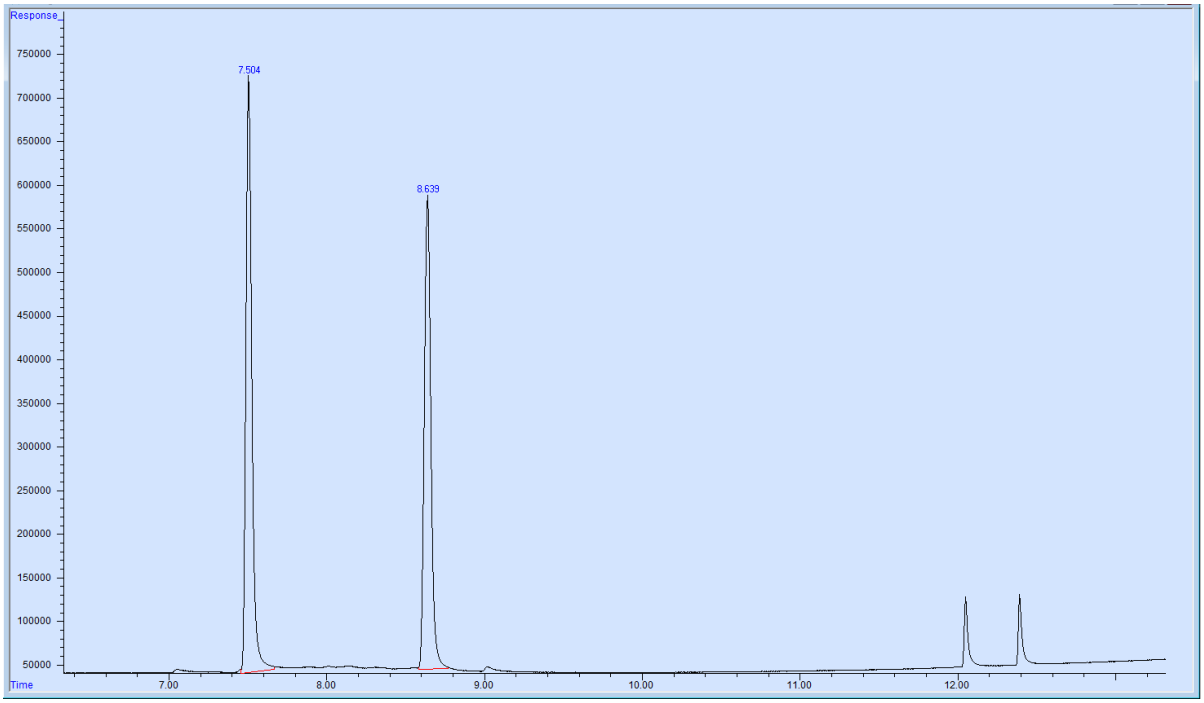

Figure 2.16 Sample chromatogram from an autoxidation trial depicting the VE (7.504 min) and IS (8.639 min) (1 mM hexadecane) peaks as illustrated and described in Figure 2.44 in addition to the V70 peak at 12.1 min and a presumed decomposition product peak at 12.4 minutes. Solvent front was excluded (standard was run to confirm).

The autoxidation (3 mL final volume) was performed in a 4 mL vial charged with a stir bar and placed in a heating block that was warmed and equilibrated at 37 ºC. The autoxidation required 100 mM VE model substrate (110.5 mg VE in 2.9 mL dry HPLC grade benzene), 97.3 mM V70 (3 mg V70 in 100 µL dry HPLC grade benzene) (**Figure 2.16**). Immediately after the initiator was added the vial was placed in the heating block and the first time point was taken. 50 µL aliquots were taken at 30 minutes time points for 6 hours using glass micro syringes that were cleaned with benzene, hexanes, acetone, and water in that order then repeated in reverse to ensure dryness. The 50 µL aliquots were diluted with

850 μL of benzene, then 100 μL of 10 mM hexadecane in benzene was added to achieve the intended IS concentration of 1 mM. This diluted the VE concentration 20-fold to an estimated maximum of 5 mM (target analyte concentration for GC analysis).

CHAPTER 3 Autoxidation of Oleate

3.1 Introduction

Oleate is one of the most naturally abundant fatty acids in both plants and animals and is classified as the simplest monounsaturated omega-9 fatty acids, comprised 18 carbons with a cis-unsaturation at the 9 position. The study of the mechanism of methyl oleate autoxidation was initiated Sutton and Farmer in 1943 where they proposed that the product mixture would contain a combination of C_8 and C_{11} [60] [77]. The oleate autoxidation was further investigated by Farmer *et al.* who proposed a mechanism that presented an equal distribution of four products via a H-atom abstraction [59]. In 1984, Frankel *et al.* carried this research forward and applied contemporary analytical techniques (GC, MS, NMR) leading them to also report a symmetric distribution of products [78]. Dr. Ned Porter's research group disputed this finding in 1994 and instead proposed that the reversible addition of oxygen over the allylic radical followed by possible reversible bond rotation yielded the asymmetric distribution of six oleate autoxidation products (**Scheme 3.1**) [57].

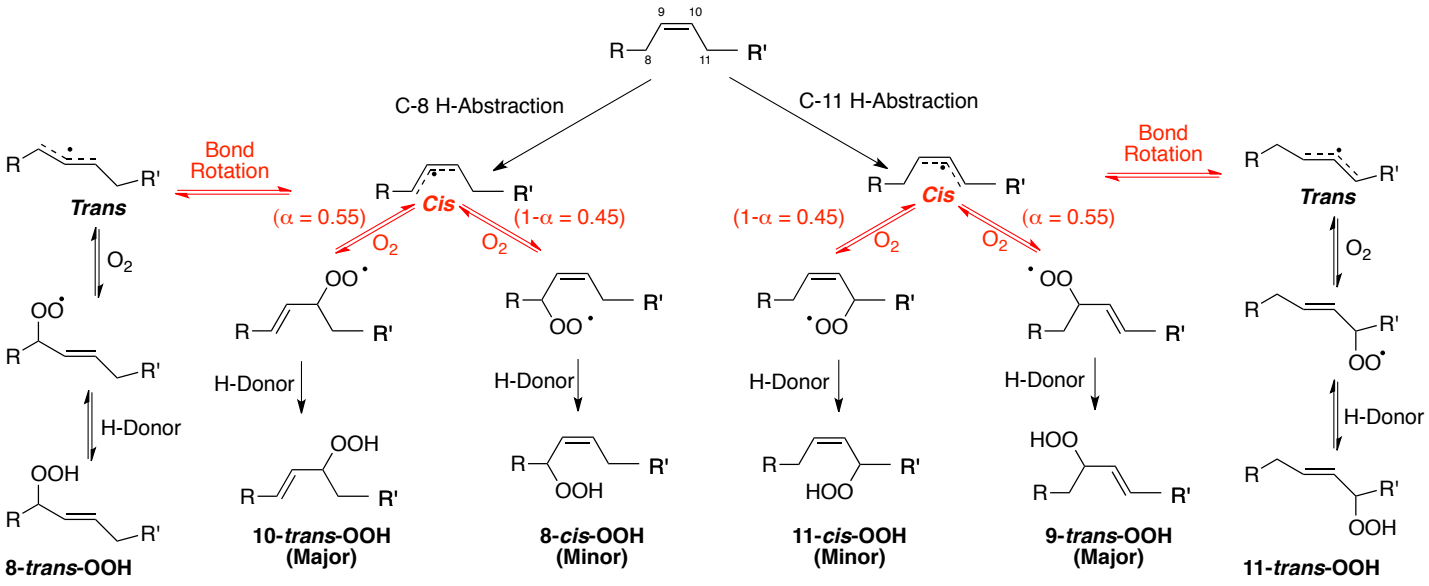

Scheme 3.1 Products of methyl oleate autoxidation as presented by Porter in 1994 [57].

The monounsaturated lipid, cholesterol, was reported to undergo both hydrogen atom transfer (HAT) and peroxyl radical addition (**Scheme 3.2**) but oleate, an analogous lipid, has only been reported to undergo HAT exclusively [4] [10]. Moreover, cholesterol epoxides were found to comprise 10-30 mol % of autoxidation product mixture [10]. Oleate epoxides have been reported as products of oxidation but an epoxidation mechanism has yet to be advanced [58] [79]. Recent reports of peroxyl radical addition to arachidonic acid unsaturations when autoxidized thereby generating *cis*- and *trans*-epoxyeicosatrienoic acids provide credence to our hypothesis that oleate can undergo peroxyl addition [80]. Based on the differences in reported product distributions from the autoxidation of seemingly similar substrates, one may propose that the presence of an H-atom donor may influence the favourability of either peroxyl radical addition or, H-atom abstraction pathways [10]. Additionally, the diminished steric hinderance in oleate compared to cholesterol may play a role in pathway selectivity.

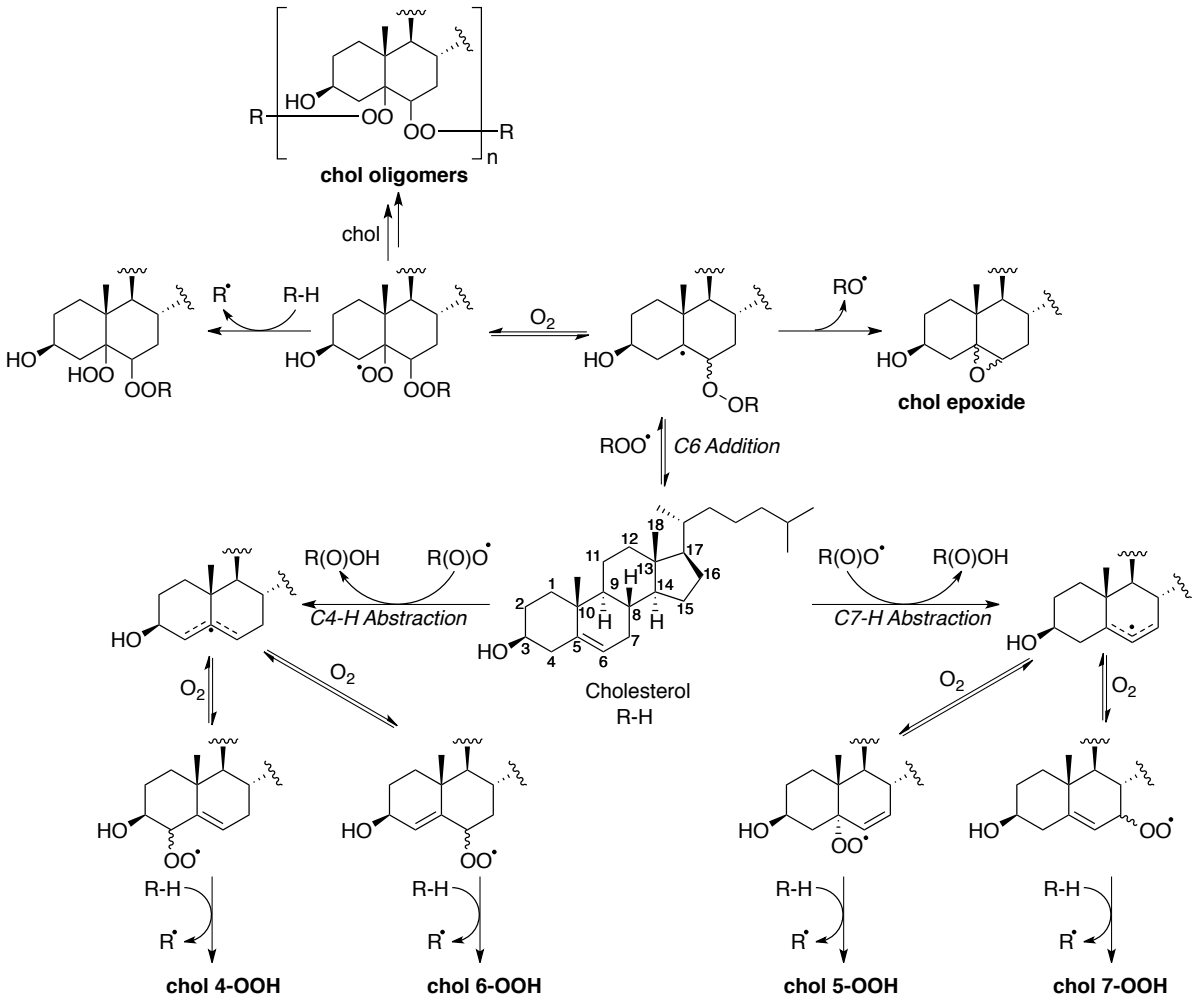

Scheme 3.2 Cholesterol autoxidation products (HAT and peroxyl radical addition) [10].

Dr. Zielinski performed the autoxidations with cholesterol and the deuterated analogue cholesterol-2,2,4,4,7,7-*d*$_6$. The inversion of product distributions was reported such that 25 % epoxide product and 75 % hydroperoxide product were formed in the autoxidation of cholesterol and 75 % epoxide product and 25 % hydroperoxide product were formed in the autoxidation of cholesterol-2,2,4,4,7,7-d$_6$ [10]. The KIE for the H-atom abstraction by peroxyl radicals in the autoxidation of cholesterol was 20 ± 1 with V70. When the autoxidation was performed with the deuterated analogue (cholesterol-2,2,4,4,7,7-d$_6$) the products distribution was reversed, where a 4-fold decrease in oxidation products but the

same epoxide product concentration was reported and this indicated that the rate of H-atom abstraction was influenced by deuteration while the rate of peroxyl addition was not affected [10]. The KIE values are greater than the classical limit for H-atom transfer from carbon to oxygen (~7), which implies quantum mechanical tunneling [10].

To establish if peroxyl radical addition, and to study the effect of selective deuteration of the allylic positions (C_7 and C_{10}), Dr. Zosia Zielinski synthesized the model substrate cis-hexadec-8-ene as it was symmetrical and greatly simplified the product distribution [58]. The model substrate was autoxidized under standard conditions established by Ned Porter *et al*. (V70; DTBN with and without ^{t}BuOOH) and epoxides were detected in all cases when analyzed using GC-FID [57]. The difference in detection methods used by Porter compared to Zielinski may account for the variation in autoxidation products.

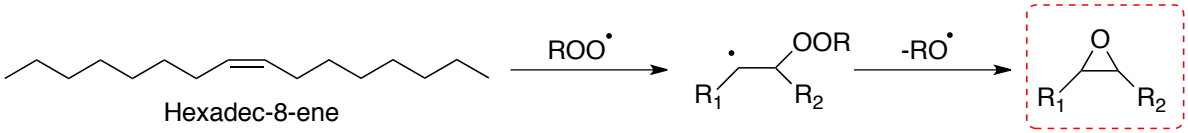

Scheme 3.3 Mechanism for epoxide formation in hexadec-8-ene [10].

It is unclear as to why epoxide products were reported in the cholesterol case but not for methyl oleate; we surmise that the issue was with Porter's mode of detection (UV-Vis) and the lack of chromophore in the epoxides. We revisited the autoxidation of the simple monounsaturated hydrocarbon with the aim to resolve these differences and consolidate the results to ascertain an accurate autoxidation mechanism. This was be done by demonstrating the formation of epoxide products through the peroxyl radical addition autoxidation pathway by applying contemporary analytical techniques for oleate epoxide detection. Methyl oleate, methyl oleate-8,8,11,11-d_4, and the epoxide standards (methyl oleate-9,10-*cis*-epoxide,

methyl oleate-9,10-*trans*-epoxide, and methyl oleate-9,10-*cis*-epoxide-8,8,11,11-d_4) were synthesized and autoxidized under reported autoxidation conditions [57].

3.2 Results

3.2.1 Synthesis of Methyl Oleate

Methyl oleate was synthesized from oleic acid via a standard Fischer esterification (**Scheme 3.4**).

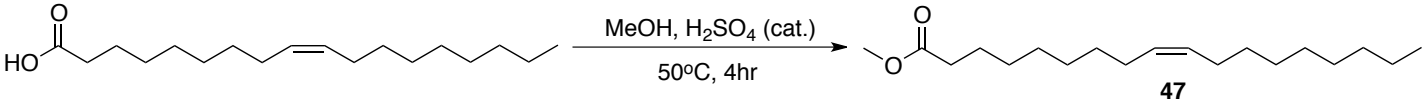

Scheme 3.4 Synthetic scheme illustrating the Fischer esterification of oleic acid to generate methyl oleate.

This first step was required to generate the methyl oleate stock that was used for d_4-methyl oleate, optimization of instrumental methods, and autoxidation conditions. The reaction proceeded to completion after approximately 4-hours of stirring at 50°C. After a basic workup and concentration, the clear colourless oil product was sufficiently pure to proceed to the next step without purification based on the NMR spectrum and consistent with reported characterization [57]. This was carried forward as is without further purification.

3.2.2 Synthesis of Methyl Oleate-8,8,11,11-d_4

The total synthesis of deuterated methyl oleate (**Scheme 3.5**) involved the fragmentation of methyl oleate via an ozonolysis, then selectively deuterating the individual fragments (nonanal and methyl-9-oxononanoate) and coupling to form the final product.

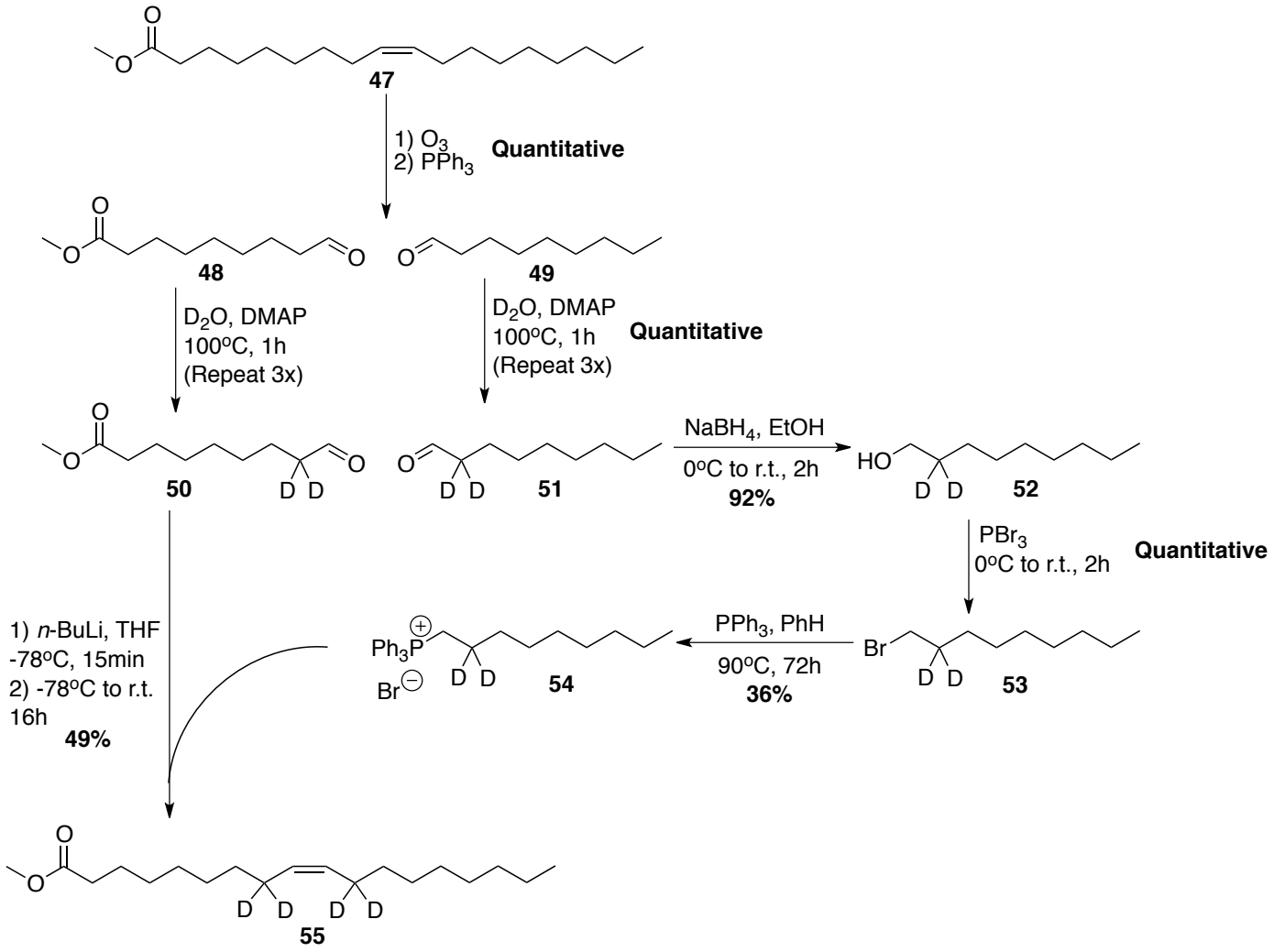

Scheme 3.5 Proposed synthesis of methyl oleate-8,8,11,11-d_4.

The first ozonolysis was performed under reported conditions using DCM as the solvent and triphenylphosphine to quench the ozonide intermediates (**Scheme 3.6**) [81].

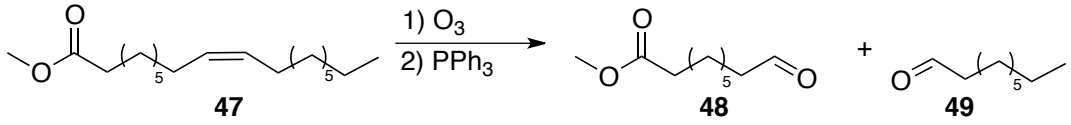

Figure 3.6 Ozonolysis of methyl oleate.

Following the ozonolysis, the reaction was left to stir for with PPh_3 to entirely reduce the primary and secondary ozonide intermediates since they were difficult to separate from the products of interest via column chromatography. The yellow crude oil that was obtained contained nonanal and methyl-9-oxononanoate and was purified using a silica gel column (gradient 20-50% EtOAc:Hexanes) which allowed for a quick purification and complete mass recovery of acceptably pure products [82] [83].

After separation of each of the methyl oleate fragments they were separately selectively deuterated at their α-position with respect to the aldehyde (**Scheme 3.7**). This was repeated 3 times to ensure complete suppression of the characteristic peak at 2.41ppm (^{1}H NMR in $CDCl_3$) corresponding to the C_α protons. The products obtained (methyl-9-oxononanoate-2,2-d_2 and 1-nonanal-2,2-d_2) were sufficiently pure and were not purified with column chromatography [84] [85].

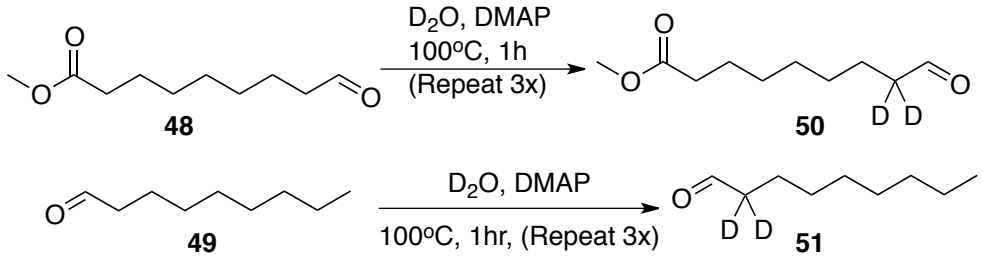

Scheme 3.7 Deuteration of α-protons to aldehyde in methyl-9-nonanoate (48) forming methyl-9-nonanoate-2,2-d_4 (50) and 1-nonanal (49) forming 1-nonanal-2,2-d_4 (51).

A sodium borohydride reduction was then carried out on 1-nonanal-d_2 to reduce it to 1-nonanol-d_2 (**Scheme 3.8**). This proceeded as described in literature [86]. The reaction progress was monitored with TLC (10% EtOAc:Hex) and after workup, it was carried forward crude as it was sufficiently pure [86].

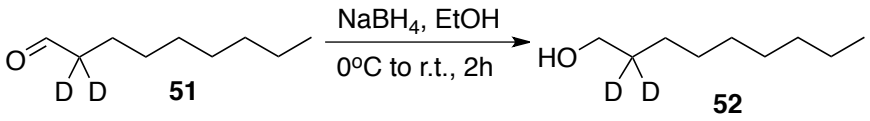

Scheme 3.8 Sodium borohydride reduction of 1-nonanal-2,2-*d*$_2$ (51) to 1-nonanol-2,2-*d*$_2$ (52).

Bromination of a primary alcohol was then performed neat on 1-nonanol-2,2-d_2, only requiring phosphorous tribromide (**Scheme 3.9**). The reaction was monitored using TLC, and after 2 hours it still contained a significant amount of unreacted SM present and was left to stir overnight at room temperature. The reaction may have been accelerated if new PBr_3 was acquired and used instead. This material was carried forward crude without additional purification [87].

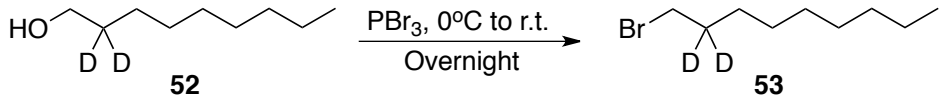

Scheme 3.9 Bromination of 1-nonanol-2,2-d_2 (52).

Synthesis of the nonyltriphenylphosphonium bromide-2,2-d_2 salt (**Scheme 3.10**) was the final reaction required to prepare the original 1-nonanal fragment prior to coupling with the methyl-9-oxononanoate-2,2-d_2 in the formation of methyl oleate-8,8,11,11-d_4. This reaction required harsh conditions (3-day reflux at 90ºC) to proceed to completion. The product was not highly soluble in any organic solvents, and as a result the side-products of this reaction (excess unreacted triphenylphosphine or SM) could be removed by solubilizing in an organic solvent allowing the product to precipitate and be isolated via filtration. This was a successful approach that yielded a sufficiently pure product that was used directly without further purification [82].

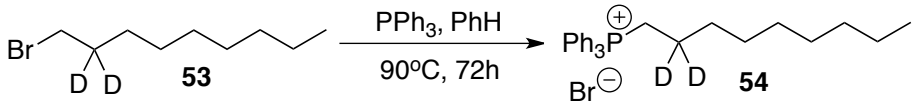

Scheme 3.10 Formation of nonyltriphenylphosphonium bromide-2,2-d_2 salt (54) [88].

Coupling of the two selectively deuterated methyl oleate intermediates (nonyltriphenylphosphonium bromide-2,2-d_2 salt and methyl-9-nonanoate-2,2-d_2 – **Scheme 3.11**) proceeded via a Wittig reaction [89]. The mixture was then left to stir overnight (16-hour reaction time) as it warmed to room temperature; the excess unreacted *n*-BuLi was quenched with water and the crude oil was purified via silica gel column chromatography. The target was synthetized with 49% yield; the TLC and NMR data affirmed the purity of methyl oleate-8,8,11,11- d_4 [87] [90].

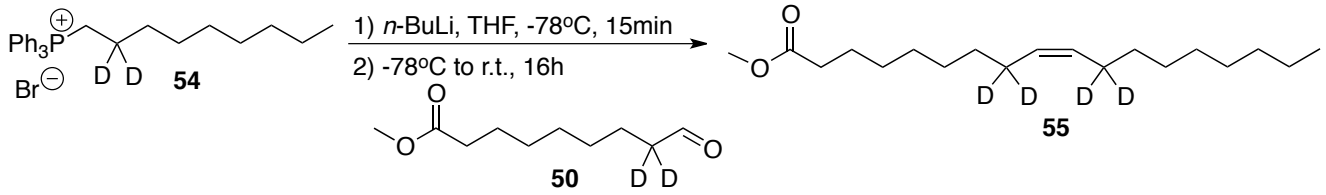

Scheme 3.11 Wittig reaction to produce methyl oleate-8,8,11,11-d_4 (55).

3.2.3 Synthesis of Methyl Oleate Epoxide Standards

The synthesis of the methyl oleate epoxide standards was necessary to accurately characterize the peaks in the chromatograms and establish if they were in fact formed as a by-product of autoxidation. The newly synthesized material was used to perform co-injections with the autoxidation mixture to confirm the identity and presence of the compounds corresponding to each peak based on the elution times.

The cis-epoxide of methyl oleate was synthesized using mCPBA from methyl oleate under experimental conditions have been reported previously [91]. This reaction (**Scheme**

3.12) proceeded to form the product quickly under mild reaction conditions (0 ^{o}C for 30 min). Once the reaction concluded, a 10 % $NaOH_{(aq.)}$ solution was used to quench unreacted mCPBA. The NMR analysis of the crude oil determined that the product of interest had formed along with benzoic acid which was removed via a short silica plug. After the second test reaction it was evident that the silica plug could be circumvented in favor of a more basic workup to ionize the benzoic acid to the aqueous phase. The isolated product was sufficiently pure. The aforementioned mCPBA epoxidation procedure was repeated with a very small quantity of the methyl oleate-8,8,11,11-d_4 to produce a deuterated methyl oleate-9,10-cis-epoxide standard for the LC methods. The target was generated and determined to be sufficiently pure for use.

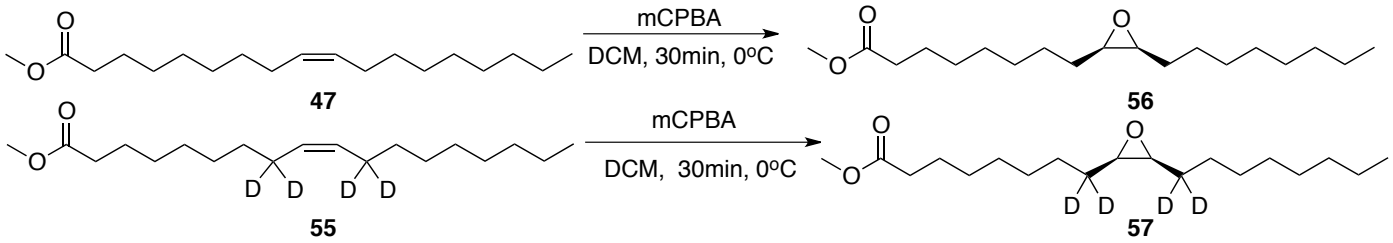

Scheme 3.12 mCPBA epoxidation of methyl oleate and methyl oleate-8,8,11,11-d_4 to produce the corresponding cis-epoxides.

The trans-epoxide of methyl oleate was synthesized using methyl elaidate (**Scheme 3.13**), following the experimental procedure described above. The first attempt failed due to unanticipated decomposition on the column. This was likely due to the more accessible trans-epoxide being less sterically hindered and therefore susceptible to nucleophilic attack resulting in ring opening and formation of a number of unwanted products. Once the more aggressive basic workup was applied the trans-epoxide of methyl oleate was isolated and deemed sufficiently clean for use as a standard.

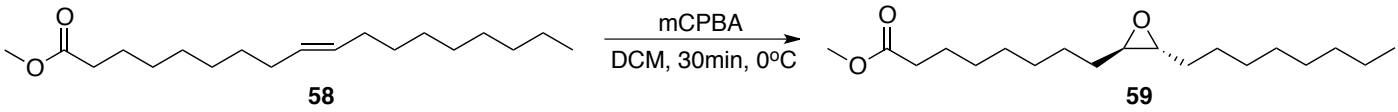

58 59

Scheme 3.13 mCPBA epoxidation of methyl elaidate (58) to generate a trans-epoxide (59).

3.2.4 Methyl Oleate Autoxidation

We sought to replicate the methyl oleate autoxidation reported by Porter *et al*. and apply contemporary analytical techniques for the detection of methyl oleate-9,10-epoxide formation [57]. Our approach involved the use of liquid chromatography coupled with tandem-MS (LC-MS/MS) to monitor the formation of the epoxides of interest. The synthesized methyl oleate *cis*- and *trans*-epoxide standards were preliminarily evaluated using an Ultra-Violet-Visible light spectrophotometry (UV-Vis) to affirm the appearance of the spectrum in order to determine which peak in the autoxidation chromatogram corresponded to the epoxides. The wavelength of maximal absorption was determined as being 195.55nm.

Direct injection of a 20 mM sample of methyl oleate-9,10-*cis*-epoxide in 0.6 % IPA:Hex on MS under APCI+ mode yielded the fragmentation spectrum shown in **Figure 3.1**.

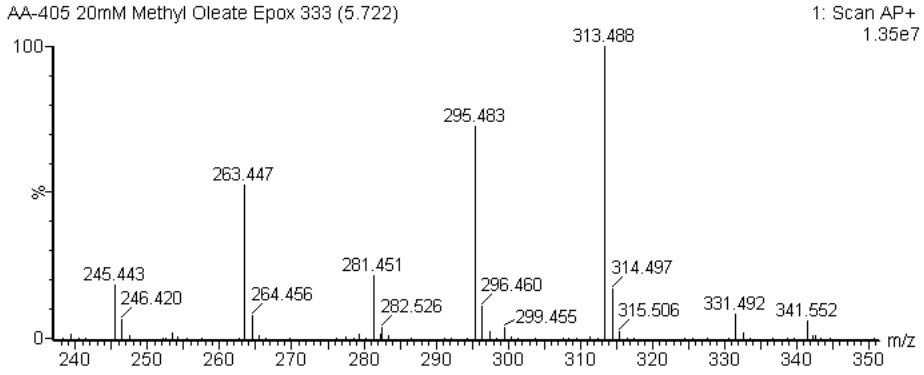

Figure 3.1 Chromatogram depicting the fragmentation pattern obtained via direct injection of 20 mM methyl oleate-9,10-*cis*-epoxide on MS in APCI+ mode.

The peak at m/z 313.488 corresponded to the molecular ion +1 mass unit (+ H^+), expected from the APCI source. The peak at m/z 295.483 corresponded to the vinylic cation resulting from loss of water from the protonated epoxide (+ H^+, -H_2O). The peak at m/z 281.451 corresponded to the protonated epoxide less methanol (+H^+, -CH_3OH). Finally, the peak at m/z 263.447 corresponded to the protonated epoxide less water and methanol (+H^+, -H_2O, -CH_3OH) (**Scheme 3.14**).

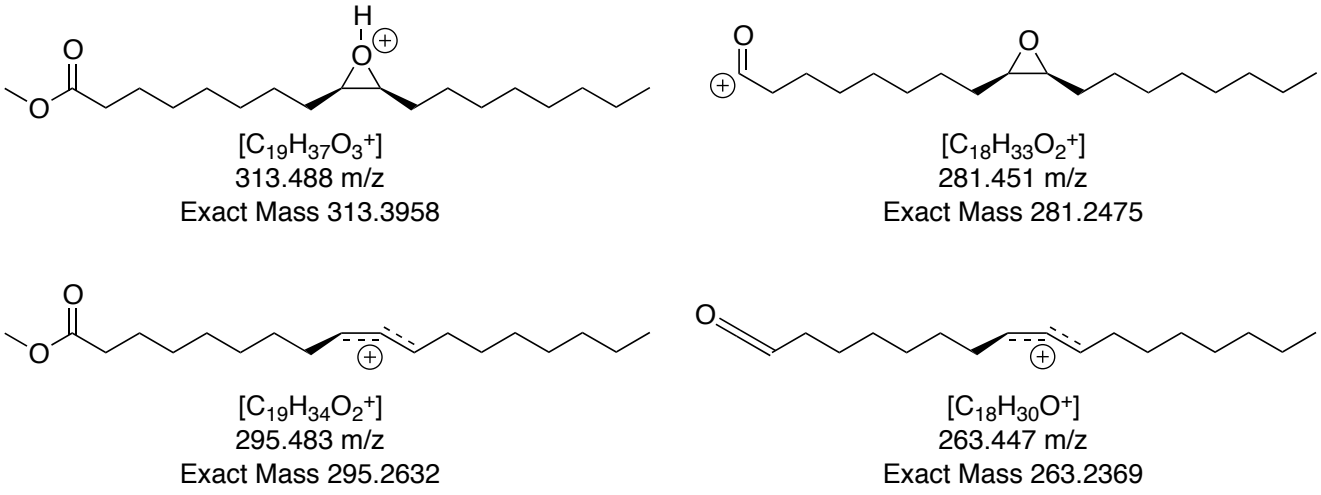

Scheme 3.14 Methyl oleate epoxide fragments.

The results obtained from the foundational MS fragmentation experiment were then used to develop a Selected Ion Recording (SIR) method since we were primarily interested in detection of the epoxide to establish if it was generated as a product of methyl oleate autoxidation. This was accomplished by direct injection and monitoring for a 313.3958 m/z ion. The resultant chromatogram was fairly low resolution as there was significant noise about the baseline, consequently an alternative and more precise method was required.

A multiple reaction monitoring (MRM) method was then developed to allow for greater ion selectivity and thus a higher signal-to-noise ratio. Two MS/MS transitions

selected were selected as they permitted for adequate sensitivity without sacrificing resolution. The first MS/MS transition was from the fragmentation of the 313.3958 m/z parent to the 263.2497 m/z daughter. The second MS/MS transition corresponded to the fragmentation of the 313.3958 m/z parent to the 281.2129 m/z daughter. The parameters of this selective detection protocol were fine-tuned to minimize noise and maximize signal response.

We sought to replicate Porter *et al.*'s chromatographic conditions in order to establish the elution time, and the lower limit of detection of the methyl oleate cis- and trans-epoxides [57]. The wavelength of maximal absorption and the enhanced MRM method were both used to affirm the identity of the methyl oleate epoxide corresponding to the peak of interest on the chromatogram. An array of methyl oleate cis- and trans-epoxide concentrations were tested until a lower limit of detection of 3 μM was established (**Figure 3.2**). We intended to use the methyl oleate-9,10-epoxide-8,8,11,11-d_4 as the internal standard for the methyl oleate autoxidation and the methyl oleate-9,10-epoxide as the internal standard for the methyl-8,8,11,11-d_4 autoxidation. Analysis of the *cis*-epoxide of methyl oleate LC-MS/MS results (**Figure 3.2**) indicated that the target eluted at 5.35 minutes while the *trans*-epoxide of methyl oleate eluted at 5.75 minutes. It is evident that there is a systemic increase in signal corresponding with the increased epoxide concentration, but it is still necessary to generate a standard curve which requires repeating in triplicates with more data points within this concentration range.

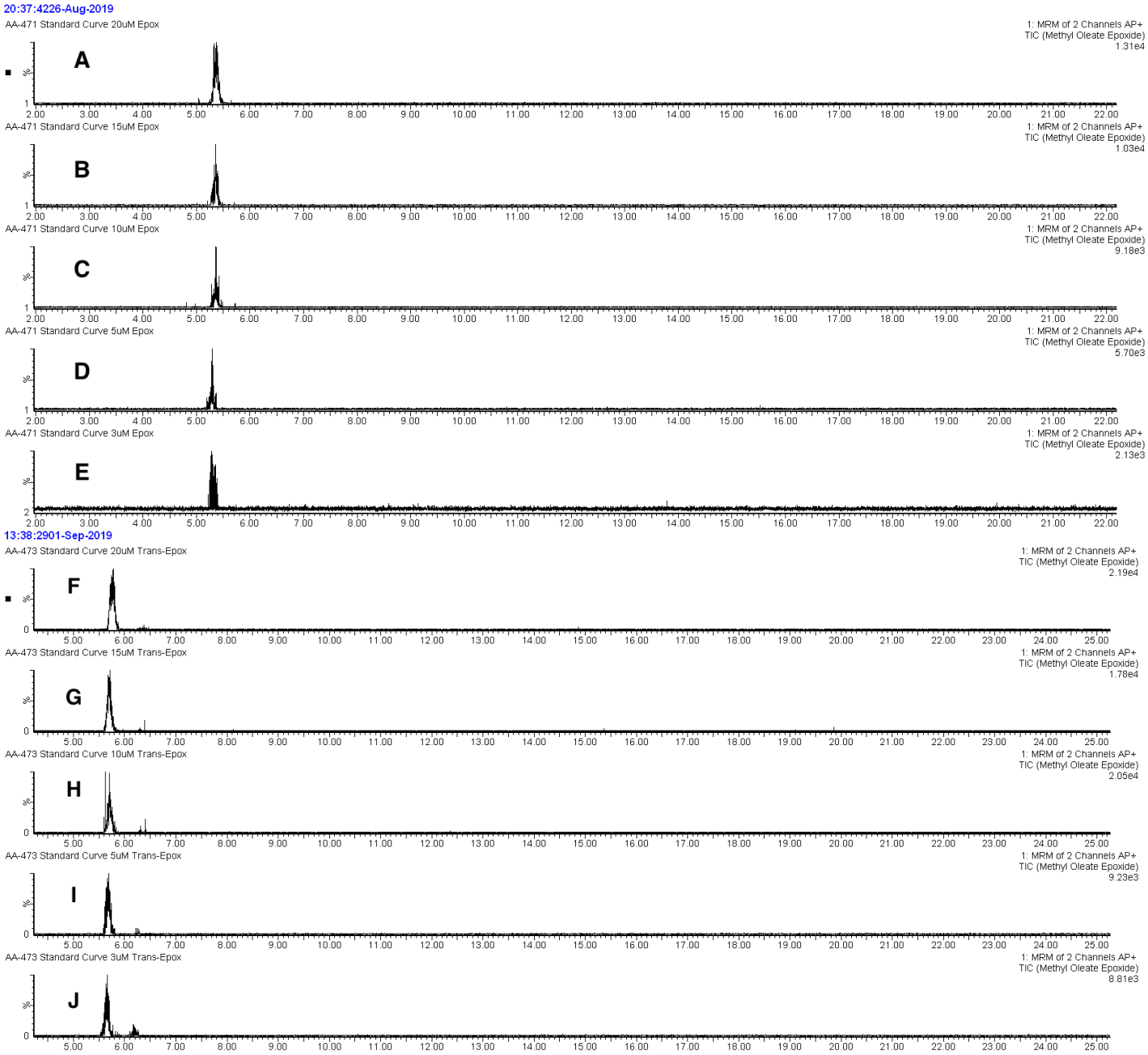

Figure 3.2 Chromatograms of methyl oleate-9,10-*cis*-epoxide (**A**: 20 µM, **B**: 15 µM, **C**: 10 µM, **D**: 5 µM, **E**: 3 µM) and methyl oleate-9,10-t**rans**-epoxide (**F**: 20 µM, **G**: 15 µM, **H**: 10 µM, **I**: 5 µM, **J**: 3 µM) in Hexanes obtained using NP-UPLC-MS/MS (m/z 313.3958 → m/z 281.2129 and m/z 313.3958 → m/z 263.2497) eluted with 0.6 % iPrOH:Hex @ 0.9 mL/min.

Once we were confident we could detect the epoxides - when they formed in an autoxidation - we carried out an autoxidation of methyl oleate as described by Porter *et al*. [57] (**Scheme 3.15**). The hydroperoxides were reduced to their corresponding alcohols in order to improve chromatographic separation between the products in accordance with reports by Porter [57]. Each aliquot was diluted 10-fold with hexanes prior to injection on the UPLC-UV.

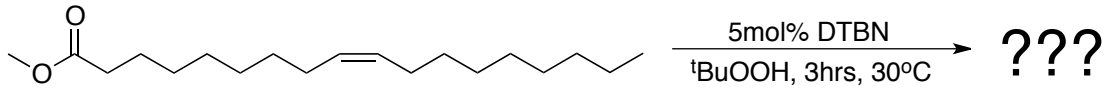

Scheme 3.15 Porter *et al*. **[57]** methyl oleate and ^{t}BuOOH coautoxidation conditions.

The coautoxidation was left to react for 24-hours to increase the concentration of the autoxidation products generated to a detectible level. Products were detected at 254 nm to enable direct comparison with the reported chromatograms [57]. The prolonged autoxidation time yielded the expected distribution of products based on the elution times of the peaks and their relative ratios, but there was poor separation between the chromatographic region of interest between 4 and 5 minutes (based on a series of epoxide standards run alongside the analysis of the autoxidation mixture). No epoxide related peaks present at 190-195 nm; additionally it was difficult to ascertain if the epoxide formed and had co-eluted with the 10-*trans* alcohols, or if the epoxide had not formed at all **(Figure 3.3**). This autoxidation was repeated with d_4-methyl oleate and yielded similar results with a slightly different peak distribution (**Appendix B – Figure 4.61**).

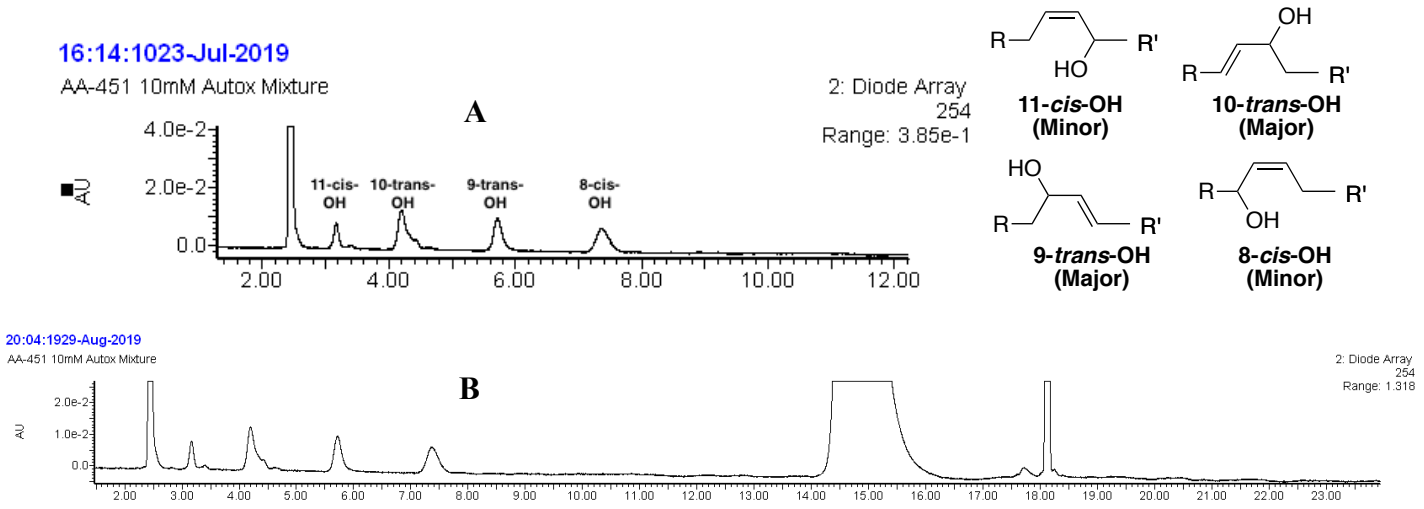

Figure 3.3 Chromatograms of methyl oleate co-autoxidation following Porter's method **[57]**. Conditions: 24-hour autoxidation run at 30 °C with methyl oleate (0.6mmol), with the radical initiator DTBN (5 mol% with respect to methyl oleate), and tert-butyl hydroperoxide (^{t}BuOOH; 0.73 mL – 6.67 Eq.); quenched with the radical inhibitor TTBP (1.0 Eq.) before concentrating to remove residual ^{t}BuOOH (bp_{20} = 35 °C) NP-UPLC-UV– 0.6 % IPA:Hex @ 0.9 mL/min. **A**: magnified view of the region of interest from chromatogram **B** corresponding products of the 10x diluted autoxidation mixture detected at 254 nm by PDA. The reduced hydroperoxide products are shown in the top right.

Once the autoxidation was confirmed to proceed as anticipated, the instrumental protocol was optimized for the separation and detection of the substrates of interest (methyl oleate and methyl oleate *cis*- and *trans*-epoxides) from the large solvent front. This included doubling the column length by connecting two normal phase columns in series (Sunfire and Wattman Columns), extending the elution time accordingly, from 30-minutes to 70-minutes. The detection of the methyl oleate epoxides was re-evaluated using the adjusted LC conditions in order to affirm the elution times of the methyl oleate epoxide standards, and the integrity of the methods, while ensuring they operate as required. The series of chromatograms (**Figure 3.4**) of methyl oleate-9,10-*cis*/*trans*-epoxides (40µM of each epoxide in 100% hexanes) co-injected on LC with the updated instrumental conditions established the elution times and validated detection of the two epoxides using each of the

different detection protocols that were developed (UV, SIR, and MRM [3 different transitions monitored]). The *cis*-epoxide of methyl oleate eluted first (9.1 minutes) while the *trans*-epoxide of methyl oleate eluted second (10.1 minutes). The inversion in elution order following the chromatographic modifications could not be explained.

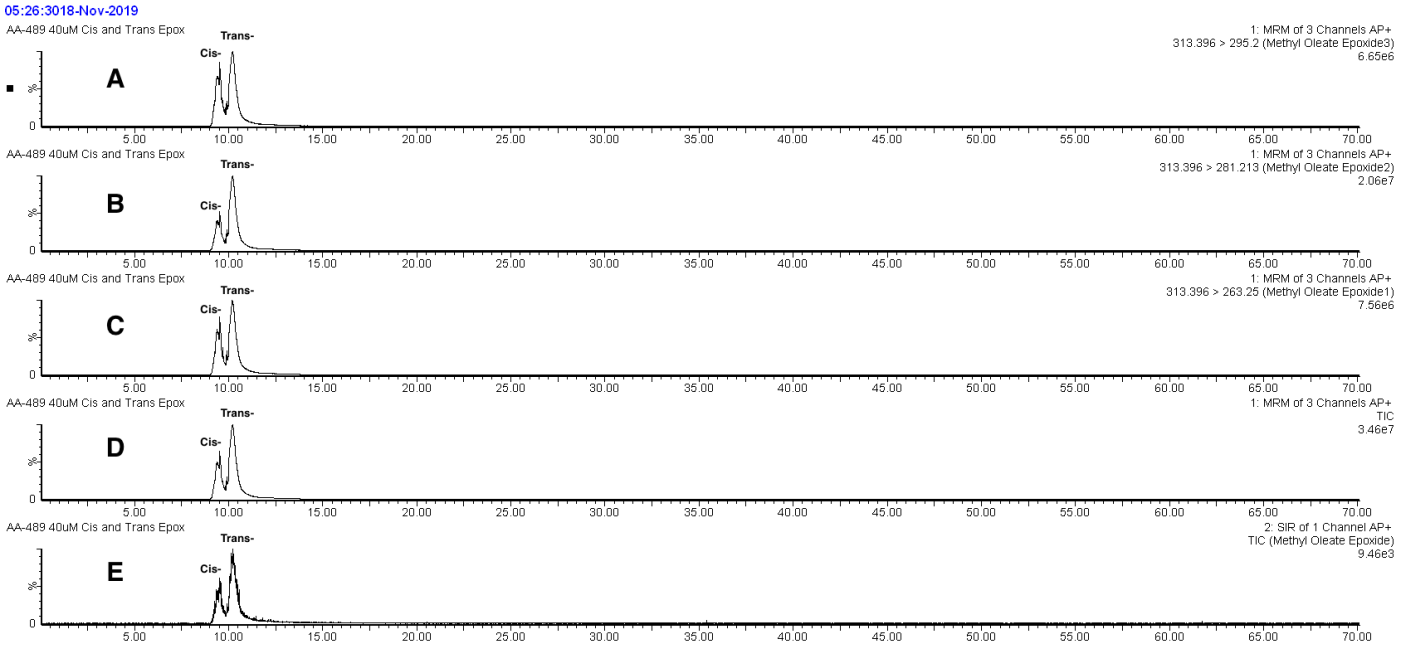

Figure 3.4 Chromatograms (SIR, MRM) of methyl oleate-9,10-*cis*-/*trans*-epoxides (40 μM of each epoxide in 100% hexanes) co-injected on LC with the updated instrumental conditions (doubling the column length and extending elution time to 70 min). NP-UPLC-MS/MS - 0.6 % IPA:Hex @ 0.9 mL/min. The *cis*-epoxide of methyl oleate eluted first (9.1 minutes) while the *trans*-epoxide of methyl oleate eluted second (10.1 minutes). **A**: MRM of the MS transition from *m/z* 313.3958 → *m/z* 295.2632. **B**: MRM of the MS transition from *m/z* 313.3958 → *m/z* 281.2129. **C**: MRM of the MS transition from *m/z* 313.3958 → *m/z* 263.2497. **D**: TIC of the 3 MRM channels. **E**: SIR results for the *m/z* 313.3958 ion.

The accumulated optimizations discovered throughout the course of this investigation were applied to the simultaneous execution of the autoxidation of methyl oleate and d_4-methyl oleate. Standards of each reagent were run alongside the autoxidation samples due to minor differences in retention time observed between the different runs. Additionally, co-

injections of the epoxide standards with the autoxidation solutions were run to affirm assignment of chromatographic peaks.

The coautoxidation of methyl oleate performed under the preestablished conditions was assessed using the updated instrumental method (**Figure 3.5**).

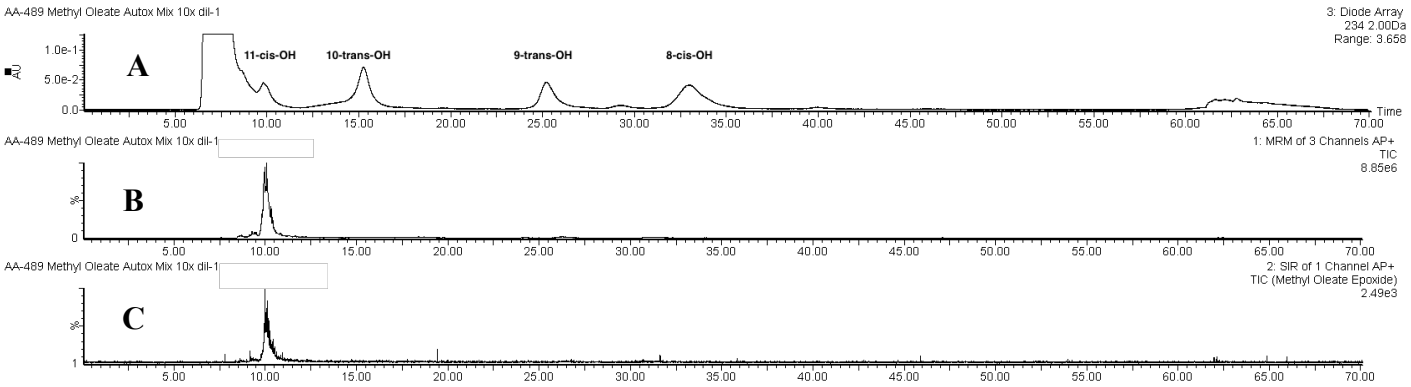

Figure 3.5 Chromatograms for the autoxidation of methyl oleate under established conditions **[57]**: 24-hour autoxidation run at 30°C with methyl oleate (0.6 mmol), with the radical initiator DTBN (5 mol% with respect to methyl oleate), and tert-butyl hydroperoxide (^{t}BuOOH; 0.73 mL – 6.67 Eq.); quenched with the radical inhibitor TTBP (1.0 Eq.) before concentrating to remove residual ^{t}BuOOH (bp_{20} = 35°C). NP-UPLC-UV– 0.6 % IPA:Hex @ 0.9 mL/min. **A**: PDA response at 234 nm and presents a typical product distribution. The bottom 2 chromatograms affirm the presence of the methyl oleate-9,10-*trans*-epoxide in the autoxidation mixture. **B**: MRM of the 3 channels for the MS transition from *m/z* 313.3958 → *m/z* 295.2632; *m/z* 313.3958 → *m/z* 281.2129; and *m/z* 313.3958 → *m/z* 263.2497. **C**: SIR results for the *m/z* 313.3958 ion.

The coautoxidation of methyl oleate-8,8,11,11-d_4 performed under established conditions was assessed using the updated instrumental method and yielded an improved separation that was consistent with Porter's reports [57] (**Figure 3.6**). The product distribution was not as expected since the 11-cis-OH and the 8-cis-OH appeared to be the major products in this autoxidation.

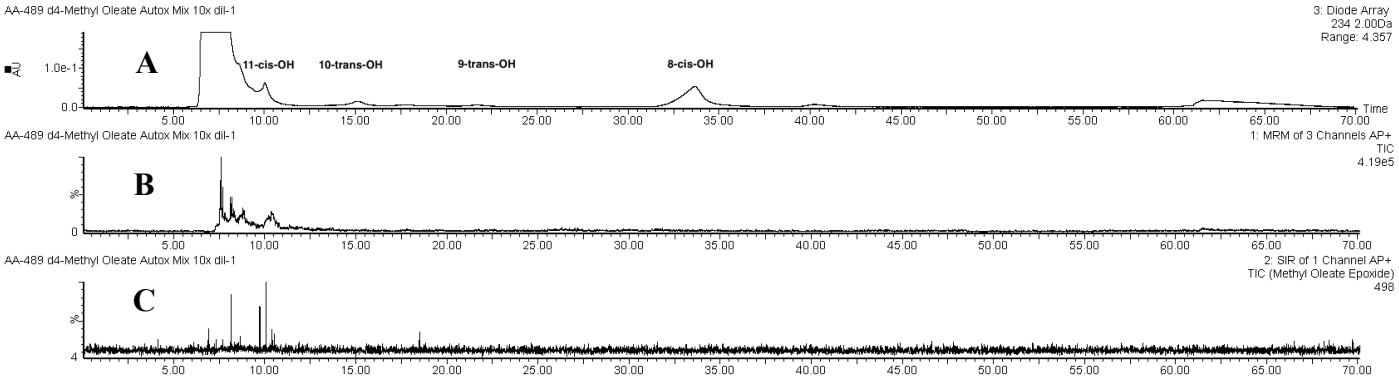

Figure 3.6 Chromatograms for the autoxidation of methyl oleate-8,8,11,11-d_4 under established conditions **[57]**: 24-hour autoxidation run at 30°C with methyl oleate (0.6 mmol), with the radical initiator DTBN (5 mol% with respect to methyl oleate), and tert-butyl hydroperoxide (^{t}BuOOH; 0.73 mL – 6.67 Eq.); quenched with the radical inhibitor TTBP (1.0 Eq.) before concentrating to remove residual tBuOOH (bp_{20} = 35°C). NP-UPLC-UV-MS/MS– 0.6 % IPA:Hex @ 0.9 mL/min. **A**: PDA response at 234 nm and presents a typical product distribution. The bottom 2 chromatograms demonstrate lack of methyl oleate-9,10-*cis*-/*trans*-epoxide formation. **B**: MRM of the 3 channels for the MS transition from *m/z* 313.3958 → *m/z* 295.2632; *m/z* 313.3958 → *m/z* 281.2129; and *m/z* 313.3958 → *m/z* 263.2497. **C**: SIR results for the *m/z* 313.3958 ion.

Both autoxidations (methyl oleate and methyl oleate-8,8,11,11-d_4) were repeated simultaneously again under the exact same conditions and injected along with the methyl oleate-9,10-*cis*-/*trans*-epoxide standards (**Figure 3.7**).

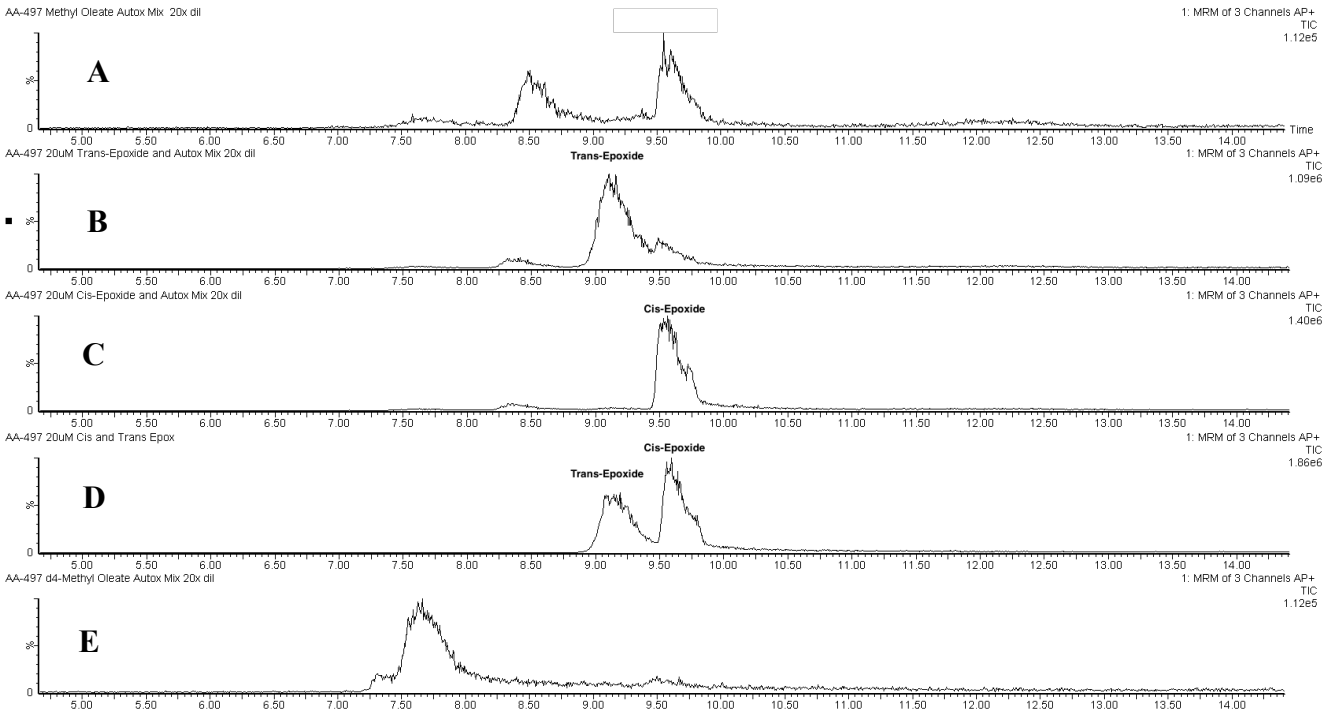

Figure 3.7 Combined chromatographic results (TICs of 3 MRM channels) of the autoxidations of methyl oleate and methyl oleate-8,8,11,11-d_4 along with co-injections with methyl oleate-9,10-*cis*-/*trans*-epoxide standards are also displayed comparison. The 24-hour autoxidation run at 30°C with methyl oleate (0.6 mmol) (or methyl oleate-8,8,11,11-d_4), with the radical initiator DTBN (5 mol% with respect to methyl oleate), and tert-butyl hydroperoxide (^{t}BuOOH; 0.73 mL – 6.67 Eq.); quenched with the radical inhibitor TTBP (1.0 Eq.) before concentrating to remove residual ^{t}BuOOH (bp_{20} = 35 °C). NP-UPLC-UV-MS/MS (*m/z* 313.3958 → *m/z* 295.2632; *m/z* 313.3958 → *m/z* 281.2129; *m/z* 313.3958 → *m/z* 263.2497) – 0.6 % IPA:Hex @ 0.9 mL/min. **A**: 20x diluted methyl oleate autoxidation mixture. **B**: co-injection of 20 μM *trans*-epoxide and 20x autoxidation mixture. **C**: co-injection of 20 μM *cis*-epoxide and 20x autoxidation mixture. **D**: co-injection of 20 μM *cis*-epoxide and 20 μM *trans*-epoxide. **E**: 20x diluted methyl oleate-8,8,11,11-d_4 autoxidation mixture. Note: Elution order inverted between the *cis*-/*trans*-epoxides.

3.3 Discussion

The main objective of this investigation was to establish if oleate epoxides were formed as products in an autoxidation. The key result of this investigation was that the mechanism of oleate autoxidation advanced by Porter in 1994 was incomplete since we have shown that epoxides were formed through peroxyl radical addition at the C9 and C10 positions. This reversible process can form both cis- and trans-oleate epoxides following the loss of the alkoxyl radical. This was not previously reported since the epoxide did not have an absorbance at the wavelengths monitored.

Epoxidation was reported to occur at higher rates in cholesterol than oleate due to the rigidity of cholesterol allowing the peroxyl addition to position it perfectly for the subsequent intramolecular homolytic substitution (S_Hi) reaction forming the epoxide immediately; compared with oleate where it adds then the S_Hi reaction forming the epoxide has to compete with the free rotation to a confirmation that is more stable and where epoxide formation cannot occur. S_Hi reactions have been reported to proceed at rates at around 10^5 s^{-1} in model systems [5] [80] [92] [93]. This free rotation is what gives rise to the *cis*- and *trans*-epoxide isomers, where the *cis*-epoxide formed through the addition and immediate subsequent addition where the peroxyl falls off reversibly, compared with the *trans*-epoxide which formed after a second isomerization following the initial peroxyl addition (**Scheme 3.16**). Although peroxyl radical addition products were demonstrated to form in oleate oxidations it still is not the prominent mechanism as evidenced by the reduced rates of the methyl oleate-8,8,11,11-d_4 consumption compared to oleate in the autoxidations.

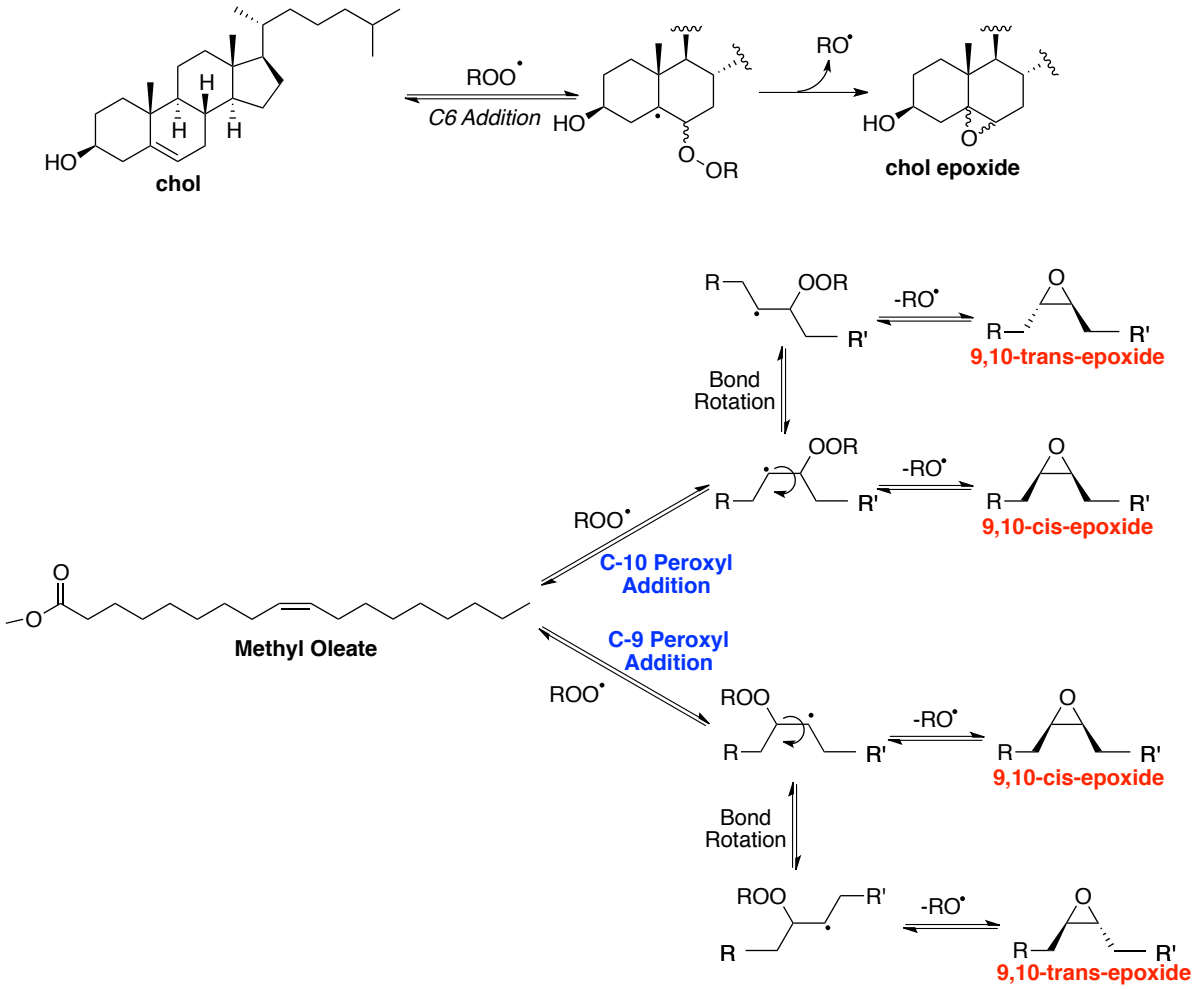

Scheme 3.16 Cholesterol and oleate S_Hi reactions forming epoxides.

The epoxide standards were evaluated with UV-Vis to determine the appearance of the spectrum; the wavelength of maximal absorbance was established as being 195.55 nm. Direct injection of the methyl oleate-9,10-*cis*-expoxide standard into the mass spectrometer yielded a fragmentation where the major daughter fragments were identified and used to attempt to develop an SIR method, but this did not generate chromatograms of acceptable resolution. An MRM method was then developed where tandem mass spectrometry was employed for the detection of methyl oleate-9,10-epoxide daughter fragments which were

used for the 3 different MS transitions (*m/z* 313.3958 → *m/z* 295.2632; *m/z* 313.3958 → *m/z* 281.2129; *m/z* 313.3958 → *m/z* 263.2497).

Once a robust methyl oleate-9,10-epoxide detection protocol was established, we turned our focus to the autoxidation conditions. Porter's co-autoxidation of methyl oleate with ^{t}BuOOH was reproduced and generated the same product distribution as reported through UPLC-UV (254 nm) spectral analysis [57]. The 11-*cis*-OH product appeared to co-elute with an epoxide based on the shared retention time. The column length was doubled, and elution time increased accordingly, to improve separation between the aforementioned peaks. The retention times of the *cis*- and *trans*-epoxide standards was measured again to account for the changes in protocol. The *cis*-epoxide of methyl oleate eluted first (9.1-minutes) while the *trans*-epoxide of methyl oleate eluted second (10.1-minutes). Perplexingly, we could not resolve the inversion of the product elution between the cis and trans epoxides following the lengthening of the column. The lower limit of detection was established at 3 μM and for both the *cis*- and *trans*-epoxide standards to demonstrate linearity in the concentration range of interest (**Figure 3.3**).

After Ned Porter's autoxidation results were reproduced using UV under the updated instrumental conditions, we applied our contemporary detection method using NP-UPLC-MS/MS. The autoxidations were conducted with methyl oleate and methyl oleate-8,8,11,11-d_4 under the same conditions. Analysis of the chromatograms from the autoxidation of methyl oleate under the reported conditions yielded the expected peak distribution with a greatly improved separation and resolution (PDA) between the 11-*cis*-OH and the 9,10-*trans*-epoxide. The tandem-MS chromatograms (SIR, and MRM of each of the 3 MS/MS transitions) confirmed the presence of a methyl oleate-9,10-*cis*-epoxide with potentially a

very small amount of methyl oleate-9,10-*trans*-epoxide as well. This experiment affirmed that the analytical method was selective for the epoxide since the other alcohol products that shared the same MS transitions did not obfuscate the signals generated in the SIR and MRM chromatograms. The methyl oleate epoxide products may not have been detected by Porter *et al.* due to the lower limit of detection of the UV detector. Analysis of the chromatograms generated from the autoxidation of methyl oleate-8,8,11,11-d_4 under the established standard conditions presented the reported peak distribution with a significant difference from the oleate autoxidation. The 8- and 11-*cis*-OH products were now the major products in lieu of the 9- and 10-*trans*-OH. This is evidence of a secondary kinetic isotope effect, since going from a sp^2 to sp^3 carbon hybridization upon O_2 addition is expected to give an inverse KIE. O_2 addition to the deuterated carbon should be faster than to the non-deuterated carbon, therefore the 9- and 10-*trans*-OH products should be suppressed compared to 8- and 11-*cis*-OH products. This is a surprising yet intriguing discovery that may also be influenced by β-secondary KIE since the CD_2 adjacent to the peroxyl in the 9- and 10-*trans* will offer less hyperconjugative stabilization than the CH_2 adjacent to the peroxyl in 8- and 11-*cis* [10].

The co-autoxidations were repeated a third time and the methyl oleate chromatograms from these autoxidations undoubtedly demonstrated methyl oleate epoxide formed in detectible concentrations and that the *cis*-epoxide was the predominant isomer. Conversely, the methyl oleate-8,8,11,11-d_4 chromatograms reflect the diminished rate of autoxidation and insignificant methyl oleate-8,8,11,11-d_4-epoxide production which is consistent with Dr. Zielinski's reports of hexadec-8-ene-7,7,10,10-d_4 autoxidation. Coincidentally, cholesterol autoxidation yielded 25% epoxide products and 75% hydroperoxides, while the cholesterol-2,2,4,4,7,7-d_6 autoxidation yielded 75% epoxide

products and 25% hydroperoxides [10].We proposed that the deuteration of the allylic positions would suppress the H-atom transfer pathway in favor of the alternative peroxyl radical addition pathway leading to epoxide formation, but this may not be the case. Upon review of the instrumental protocol it was noted that the oleate MS/MS method was applied directly (MS transitions: *m/z* 313.3958 → *m/z* 295.2632; *m/z* 313.3958 → *m/z* 281.2129; *m/z* 313.3958 → *m/z* 263.2497) instead of being modified to account for the increased mass imparted by the four deuterium atoms in the fragments sought (updated MS transitions: *m/z* 317.2988 → *m/z* 297.2883; *m/z* 317.2988 → *m/z* 285.2726; *m/z* 317.2988 → *m/z* 266.2777) (**Scheme 3.17**). The epoxide fragments could easily be differentiated by the presence of the 4-D, from the alcohols formed via HAT which only contain 3-D. As a result, the sensitivity would have been significantly reduced and the experiment requires replication with an updated method.

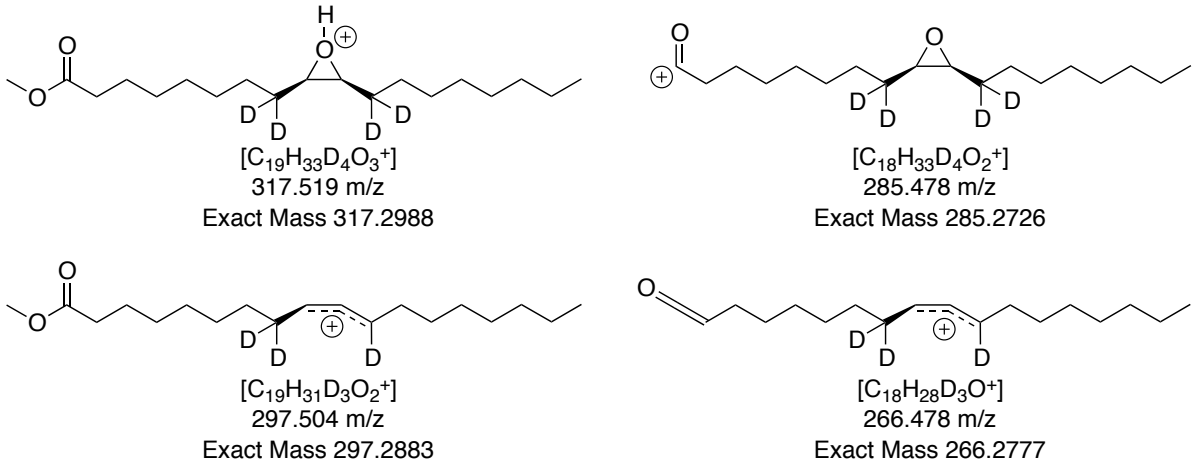

Scheme 3.17 Expected methyl oleate-8,8,11,11-d_4 epoxide fragments.

The combined LC-MS results revealed that epoxide products (cis-epoxide being the major product) were in fact formed through peroxyl radical addition in the autoxidation of methyl oleate which has previously never been reported (**Scheme 3.18**). The observation of

methyl oleate epoxide product was in accordance with Dr. Zielinski's report of hexadec-8-ene-epoxide product which, suggests that both HAT and peroxyl radical addition occur although H-atom abstraction predominates.

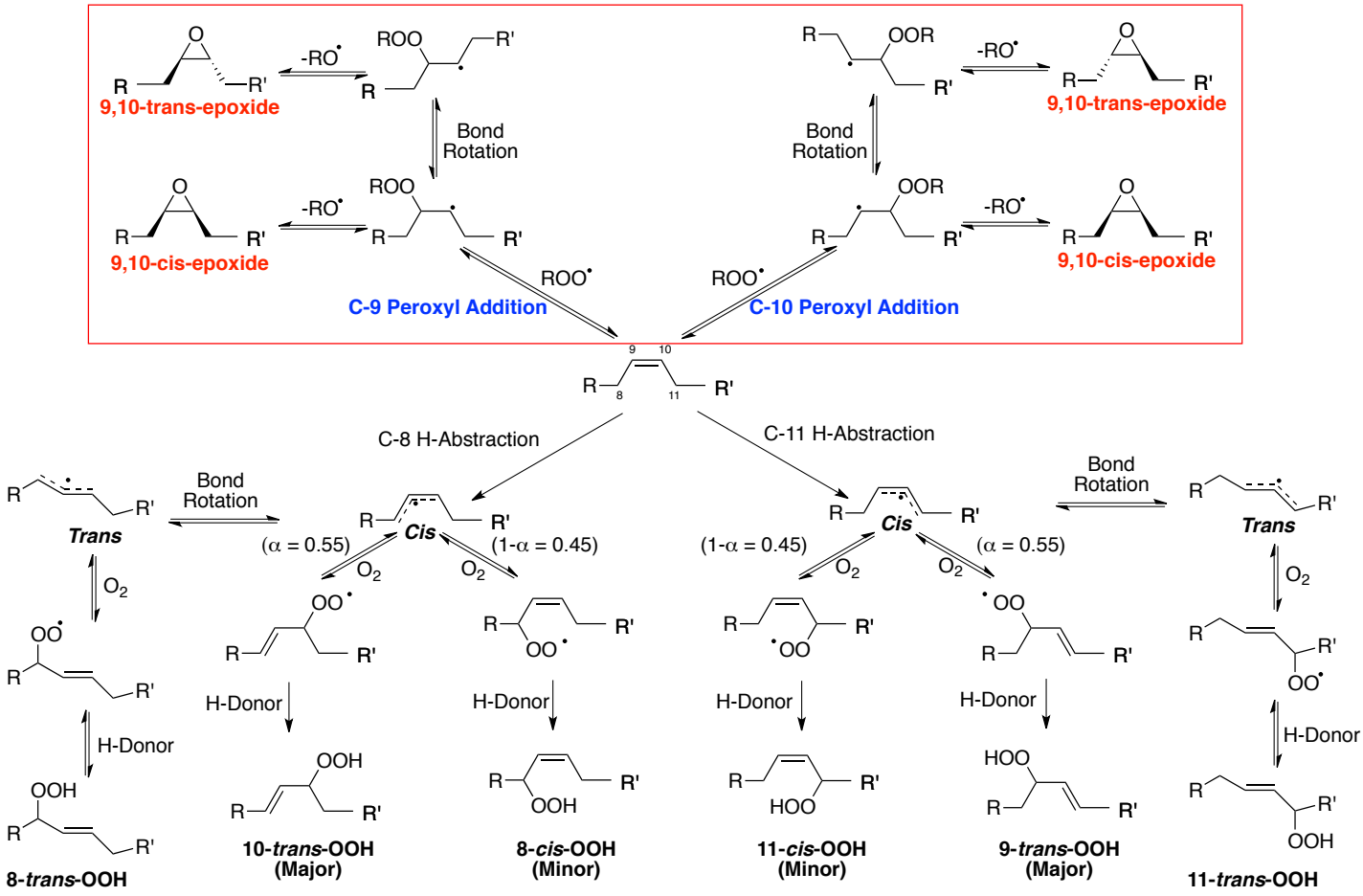

Scheme 3.18 Revised mechanism of methyl oleate oxidation.

3.4 Conclusion

We have reported the first evidence that epoxide products are formed through peroxyl radical addition to the monounsaturated lipid methyl oleate when co-autoxidized with ^{t}BuOOH using DTBN. The aggregated analytical results demonstrated that *cis*-epoxides were formed in detectible concentrations in the autoxidation of methyl oleate, but they were not formed in comparable concentrations (although still detectible) in the autoxidation with the deuterated analogue, methyl oleate-8,8,11,11-d_4. Hydroperoxides and epoxides were formed and detected in both cases. This was in accordance with reports of epoxide product formation hexadec-8-ene autoxidation and hexadec-8-ene-7,7,10,10-d_4; but this result contradicted the reported cholesterol autoxidation product distribution since a higher proportion of epoxide product was detected in the methyl oleate autoxidation mixture compared to the methyl oleate-8,8,11,11-d_4 autoxidation mixture.

Future work is necessary to understand the reactivity of monounsaturated lipids includes repeating the standard curves and applying the UPLC-MS/MS detection method to co-injections of the methyl oleate autoxidation mixture with isotopically labeled epoxide standard to accurately measure the concentration of epoxide formed over the course of the autoxidation. This should be repeated with methyl oleate-8,8,11,11-d_4 and the natural epoxide standards. The autoxidations necessary include use of V70 with and without ^{t}BuOOH, and DTBN with and without ^{t}BuOOH to allow for comparison with KIE values obtained by Dr. Zielinski for hexadec-8-ene.

3.5 Experimental

NMR Spectroscopy:

^{1}H NMR and ^{13}C NMR spectra obtained at 298K were recorded using a Bruker AVANCE 300 MHz, or Bruker AVANCE 400 MHz as indicated. Residual monoprotic solvent peaks were used as an internal reference for ^{1}H NMR ($CDCl_3$: δ = 7.26 ppm; C_6D_6: δ = 7.16 ppm) and ^{13}C NMR spectra ($CDCl_3$: δ = 77.2 ppm; C_6D_6: δ = 128.1 ppm). Coupling constants (*J*) are quoted to the nearest 0.1 Hz. The following abbreviations (or combinations thereof) were used to describe ^{1}H NMR multiplicities: s = singlet, d = doublet, t = triplet, q = quartet, m = multiplet. Residual solvent was present in the NMR spectra due to the volatility of the intermediates thereby limiting solvent removal under high vacuum.

Mass Spectrometry:

High-resolution ESI+ (m/z) spectra were measured on a Thermo-Fisher Scientific LTQ XL Orbitrap. High-resolution EI+ (m/z) spectra were measured on a Kratos Concept Magnetic Sector MS System. MassLynx 4.0 of Water-Micromass was used for data analysis.

Experimental Procedures, reagents and glassware:

All starting materials and reagents and solvents were purchased from commercial suppliers (Sigma-Aldrich, or Alfa) and used without further purification unless otherwise indicated. Reactions were performed under the positive pressure of anhydrous nitrogen gas in base-bath washed and oven-dried glassware. All reactions were monitored using silica gel TLC and visualized using potassium permanganate. Intermediates were stored at -80 ^{o}C to mitigate oxidative degradation. Column chromatography was carried out using flash silica gel (60 Å, 40-63 μ, 500 m^2/g).

Corresponding spectral raw data and characterization is provided in Appendix B

3.5.1 Synthetic Procedures

Fisher Esterification of Oleic Acid

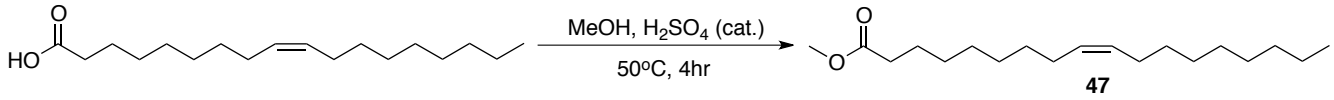

Methyl Oleate (47) To oleic acid (5.0 g, 17.7 mmol, 1.0 eq.) in a rbf charged with a stir bar was added methanol (15.6 g, 19.7 mL, 485.5 mmol, 27.5 eq.), and 18.4 M sulfuric acid (0.625 mL, 34 μmol, 0.002 eq.). The reaction mixture was refluxed at 50 °C for 4 hours until the SM has been consumed based on TLC analysis. The solvent was then evaporated until a viscous clear and colourless oil was obtained. The concentrated reaction mixture was worked up three times each with each of the following, diethyl ether, sodium carbonate, brine, and water. Magnesium sulfate was then added to the combined organic phase then the mixture was filtered and evaporated. The final product was a clear colourless oil obtained in quantitative yields (5.8 g). R_f = 0.3 (2 % DCM:Hex). ^{1}H NMR (400 MHz, Chloroform-*d*) δ 5.36 (p, 2H), 3.66 (s, 3H), 2.30 (t, *J* = 7.6 Hz, 2H), 2.00 (m, 4H), 1.61 (p, 2H), 1.28 (dt, *J* = 16.5, 5.1 Hz, 20H), 0.95 – 0.80 (m, 3H). ^{13}C NMR (400 MHz Chloroform-*d*)173.9, 130.2, 130.1, 51.4, 34.1, 32.1,29.9, 29.8, 29.7, 29.5, 29.3, 29.2, 27.3, 27.3, 25.1, 22.8, 14.2. Consistent with reported R_f and ^{1}H NMR shifts in literature [87].

Ozonolysis of Methyl Oleate

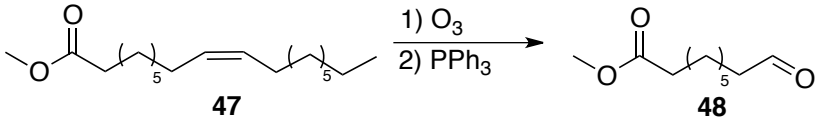

Methyl-9-Oxononanoate (48) A solution of methyl oleate (5.0 g, 16.9 mmol, 1.0 eq.) in anhydrous DCM (50 mL) was cooled to -78 °C using an acetone-dry ice bath. A stream of O_3 was bubbled through the reaction via a fritted glass ozonolysis probe. Once the reaction

appeared blue (1-1.5 hours), then nitrogen glass was flowed over the reaction and the reaction was quenched with a solution of triphenylphosphine (9.85 g, 37.6 mmol, 2.1 eq.) in DCM (50 mL). The reaction mixture was warmed to 23 ^{o}C and allowed to stir for at least 18 hours. The solvent was evaporated carefully to a minimum volume then the mixture was triturated with cold hexanes in order to precipitate triphenylphosphine oxide. This was filtered, and the precipitate was discarded; then the filtrate was concentrated carefully once more to yield a crude pale-yellow oil. The oil was purified via silica gel column chromatography using an increasing solvent polarity gradient ranging from 20 % to 50 % DCM:Hex to provide Methyl-9-Oxononanoate (3.14 g, quantitative yield) as a clear colourless oil. R_f = 0.2 (2 % Et_2O:Hexanes). ^{1}H NMR (400 MHz, Chloroform-*d*) δ 9.77 (t, *J* = 1.9 Hz, 1H), 3.67 (s, 3H), 2.42 (td, *J* = 7.4, 1.9 Hz, 2H), 2.31 (t, *J* = 7.5 Hz, 2H), 1.68 – 1.56 (m, 4H), 1.39 – 1.17 (m, 6H). ^{13}C NMR (400 MHz, Chloroform-*d*) δ 202.4, 173.8, 51.1 43.5, 33.7, 28.7, 28.6, 28.5,24.5, 21.7. Characterization is in accordance with reported ^{1}H NMR shifts in literature [82] [81] [83].

Selective Deuteration of α-C to Aldehyde

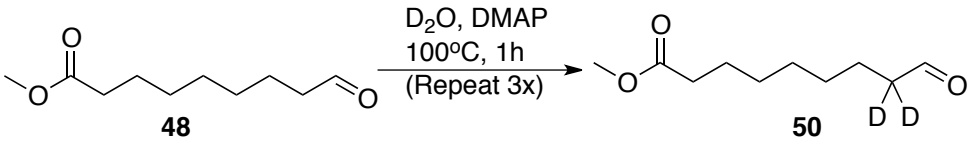

48 50

Methyl-9-Oxononanoate-d$_2$ (50) To Methyl-9-Oxononanoate (5.0 g, 26.9 mmol, 1.0 eq.) was added D_2O (13 mL; Excess) and DMAP (330 mg, 2.7 mmol, 0.1 eq.) in a flask and heated to 100^{o}C for 1 hour. DCM (150 mL) was added and the mixture was washed with 1M HCl (1x100 mL), $NaHCO_{3\ (aq.\ sat.)}$ (1x100 mL), and Brine (1x100 mL). The aggregated organic phase was then dried over magnesium sulfate, filtered, and concentrated. This was repeated (2-5 times) until the amount of deuteration was >99 % by NMR (multiplet at

2.41ppm disappears). The product was carried forward crude to the next synthetic step. Yield: 4.9 g; Quantitative yield and complete deuteration. R_f = 0.3 (2 % Et_2O:Hexanes). ^1H NMR (400 MHz, Chloroform-*d*) δ 9.74 (s, 1H), 3.64 (s, 4H), 2.28 (t, *J* = 7.5 Hz, 3H), 1.59 (d, *J* = 15.2 Hz, 5H), 1.39 – 1.19 (m, 8H). ^{13}C NMR (400 MHz, Chloroform-*d*) δ 202.6, 173.9, 51.4, 48.3, 34.0, 28.5, 28.3, 25.8, 25.8, 21.4. Characterization is in accordance with reported ^1H NMR shifts in literature [84].

Deuteration of α-C to Aldehyde

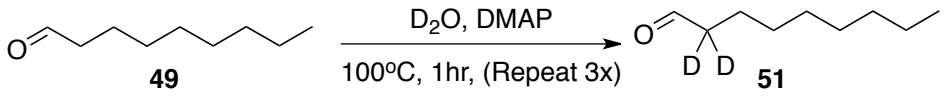

1-Nonanal-d_2 (51) To 1-Nonanal (8 mL, 6.6 g, 46.5 mmol, 1.0 eq.) was added D_2O (8 mL) and DMAP (570 mg, 4.7 mmol, 1.0 eq.) in a flask and heated to 100 ºC for 1 hour. DCM (150 mL) was added and the mixture was washed with 1M HCl (1x100 mL), $NaHCO_3$ (aq. sat.) (1x100 mL), and Brine (1x100 mL). The aggregated organic phase was then dried over magnesium sulfate, filtered, and concentrated. This was repeated (2-5 times) until the amount of deuteration was >99 % by NMR (multiplet at 2.41 ppm disappears). The product was carried forward crude to the next synthetic step. Yield: 5.0 g; Quantitative yield and complete deuteration. R_f = 0.2 (2% Et_2O:Hexanes). ^1H NMR (400 MHz, Chloroform-*d*) δ 9.77 (s, 1H), 1.28 (d, *J* = 11.3 Hz, 12H), 1.06 – 0.77 (t, 3H). ^{13}C NMR (400 MHz, Chloroform-*d*) δ 202.6, 48.3, 32.3, 29.6, 28.8, 23.2, 21.4, 14.1. Characterization is in accordance with reported ^1H NMR shifts in literature [85].

Reduction of Aldehyde to Corresponding Alcohol

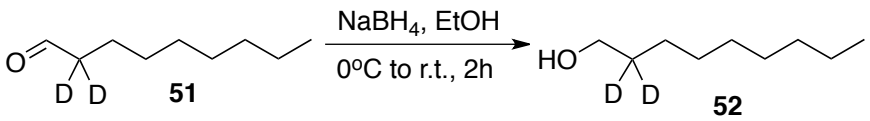

1-Nonanol-2,2-d_2 (52) To a solution of 1-nonanal-d_2 (13.2 g, 91.8 mmol, 1.0 eq.) in 99 % dry EtOH (470 mL) cooled to 0 ^oC was added $NaBH_4$ (3.8 g, 101.0 mmol, 1.1 eq.) in 4 portions to mitigate boil over. The mixture was allowed to stir while warming to room temperature over the course of 1 hour. Reaction progress was monitored via TLC (10 % EtOAc:Hexanes) Water was slowly added to quench the excess sodium borohydride present in the reaction mixture. Ethanol was carefully removed *in vacuo*, then DCM was added. The organic phase was extracted with water (1x100 mL), and Brine (2x100 mL). The aggregated organic extract was dried over $MgSO_4$, filtered, and concentrated. The product was carried forward crude to the next synthetic step as it was quite clean, and all SM had been converted to the target. Yield: 12.3 g; 91.7 %; clear colorless oil. R_f= 0.2 (10% EtOAc:Hexanes). ^1H NMR (400 MHz, Chloroform-*d*) δ 3.63 (s, 1H), 1.67 – 0.96 (m, 14H), 0.95 – 0.77 (m, 2H). ^{13}C NMR (400 MHz, Chloroform-*d*) δ 61.9, 39.4, 32.3, 29.6, 29.0, 26.3, 25.4, 23.2, 14.1. Characterization is in accordance with reported ^1H NMR shifts in literature [86].

Bromination of Primary Alcohol

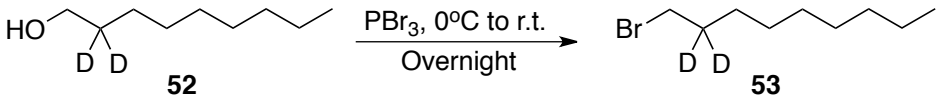

1-bromononane-2,2-d_2 (53) To a neat solution of nonanol-d_2 (12.3 g, 84.1 mmol, 1.0 eq.) cooled to 0^oC was slowly added PBr_3 (11.4 g, 4.0 mL, 42.1 mmol, 0.5 eq.). The reaction mixture was left to stir overnight at room temperature. The reaction mixture was taken up in ether, washed with water (2x250 mL), $NaHCO_{3\ (aq.\ sat.)}$ (1x250 mL), and Brine (1x250 mL). The combined organic layer was dried over $MgSO_4$, filtered, and concentrated. The target was difficult to characterize based on the crude NMR spectrum, but the TLC indicated that the product was clean and as such it was carried forward crude to the subsequent synthetic

step. TLC analysis (10 % EtOAc:Hexanes) was performed by UV, and by oxidizing the TLC plates with $KMnO_4$ stain to visualize. Yield: 10.1 g Clean; Quantitative yield. ^{1}H NMR (400 MHz, Chloroform-*d*) δ 3.39 (t, *J* = 1.0 Hz, 2H), 1.56 – 1.08 (m, 12H), 1.02 – 0.75 (t, 3H). ^{13}C NMR (400 MHz, Chloroform-*d*) δ 38.9, 32.3, 31.4, 29.6, 29.0, 27.5, 26.2, 23.2, 14.1. Characterization is in accordance with reported ^{1}H NMR shifts in literature [87].

Preparation of Triphenylphosphonium Bromide-d_2 Salt

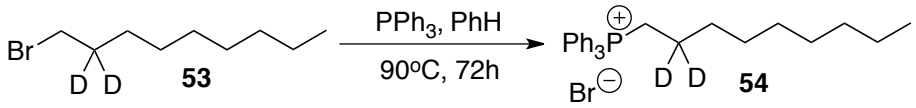

Nonyltriphenylphosphonium bromide-d_2 salt (54) A solution comprised of 1-bromononane-d_2 (10.1 g, 48.1 mmol, 1.0 eq.) and triphenylphosphine (13.9 g, 52.9 mmol, 1.1 eq.) in anhydrous benzene (77 ml dried over molecular sieves) was refluxed at 90^{o}C for 3 days under an inert nitrogen atmosphere. The reaction progress was monitored daily with TLC and NMR by assessing the increase in integration of the characteristic singlet peak at 3.79 ppm (^{1}H NMR in $CDCl_3$) corresponding to protons on the C_α with respect to the phosphonium bromide in the product. The solvent was removed under reduced pressure via rotary evaporation, and the resulting oil was triturated with dry ether until a solid product was generated. Ether forces the phosphonium bromide salt to crash out. The product was then isolated as a very viscous white solid following filtration. Yield: 8.1 g; 36%; White solid. ^{1}H NMR (400 MHz Chloroform-*d*) δ 7.86-7.80 (m, 6H), 7.78-7.76 (m, 3H), 7.70-7.66 (m, 6H), 3.79-3.78 (m, 2H), 1.60-1.59 (m, 4H), 1.24-1.17 (m, 10H), 0.83 (t, J = 7Hz, 3H). ^{13}C NMR (400MHz, Chloroform-*d*) δ 134.93, 134.91, 133.71, 133.64, 130.48, 130.38, 118.67, 118.08, 31.72, 30.42, 29.19, 29.11, 29.07, 22.63, 22.58, 22.54, 14.03. Characterization is in accordance with reported ^{1}H NMR shifts in literature [82].

Alkylation of Aldehyde with Nonyltriphenylphosphonium bromide-d_2 salt

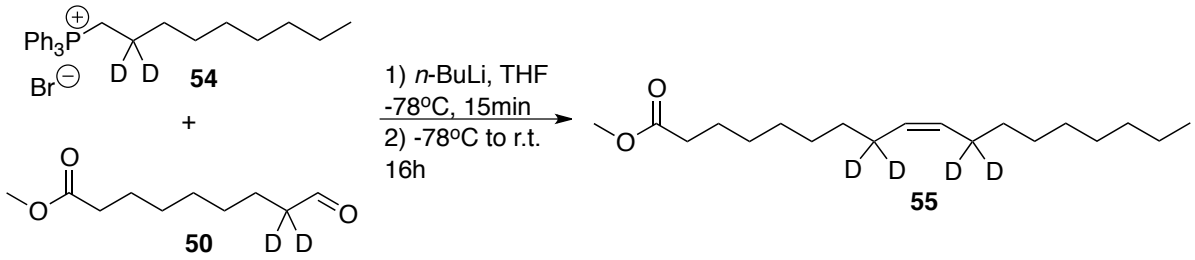

Methyl Oleate-8,8,11,11-*d_4* (55) Nonyltriphenylphosphonium bromide-d_2 salt **(54)** (5.9 g, 12.5 mmol, 1.0 eq.) was solubilized in dry THF (197 mL) then cooled to -78 ºC as the solution was stirred continuously to mitigate aggregation. *n*-BuLi (2.5 M in hexane; 5.0 mL, 12.5 mmol, 1.0 eq.) was then added dropwise at -78 ºC. The solution turned deep orange (similar to partially hydrolyzed PBr_3) as it was stirred for 15 minutes. A solution of octanal-d_2 **(50)** (2.4 g, 12.5 mmol, 1.0 eq.) in dry THF (19 mL) was prepared in a separate flask, then added dropwise to the reaction vessel at -78 ºC. The reaction was stirred as it warmed to r.t. overnight (~16 hours). TLC was used to monitor reaction progress (50 % DCM:Hex). The organic phase was extracted with DCM (3x 200mL), brine (1x200 mL), and water (1x200 mL). The combined organic phases were dried over magnesium sulfate, filtered and, concentrated. Yield: 1.9 g; 49%; clear colorless oil. R_f = 0.3; clear colorless oil. ^{1}H NMR (400 MHz Chloroform-*d*) δ 5.36 (p, 2H), 3.66 (s, 3H), 2.30 (t, *J* = 7.6 Hz, 2H), 1.61 (p, 2H), 1.28 (dt, *J* = 16.5, 5.1 Hz, 20H), 0.95 – 0.80 (m, 3H). ^{13}C NMR (400 MHz Chloroform-*d*) δ 173.9, 130.7, 130.6, 51.4, 35.4, 35.4, 35.0, 32.3, 29.6, 29.5, 29.4, 28.8, 28.6, 28.3, 25.9, 25.8, 25.6, 23.2, 14.1. HRMS (EI+) (M+) calculated 300.2966, found 300.2938. Characterization is consistent with reported ^{1}H NMR shifts and MS data in literature [90].

Epoxidation of Methyl Oleate

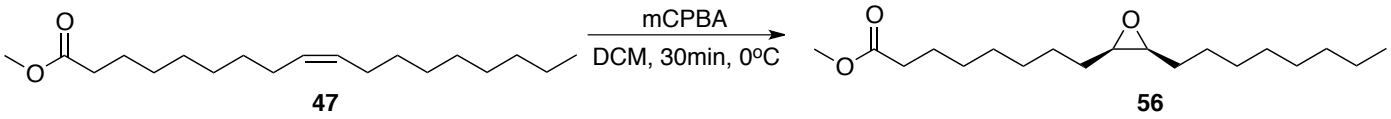

47 56

Methyl Oleate-9,10-*cis* Epoxide (56) To a cooled (0ºC) solution methyl oleate **(47)** (1.0 g, 3.5 mmol, 1.0 eq.) in DCM (12 mL) was slowly added mCPBA (77%; 893.8 mg, 3.9 mmol, 1.1 eq.). The reaction mixture was left to stir for 30minutes at r.t. before evaluating reaction progress with TLC (50% DCM:Hex). Once the SM has been consumed, the organic phase was extracted with Et_2O (3x100 mL), 10% $NaOH_{aq.\ sol.}$ (3x100 mL), brine (1x100 mL), and water (1x100 mL). The combined organic layers were dried over $MgSO_4$, filtered, and concentrated. The crude NMR indicated that the product formed fairly cleanly but still contained benzoic acid. a short silica gel plug was performed to remove the benzoic acid (50 % DCM:Hex). Yield: 1.11 g; Quantitative yield. R_f = 0.4 (50% DCM:Hex). ^{1}H NMR (400 MHz Chloroform-*d*) δ 3.67 (s, 3H), 2.90 (s, 2H), 2.30 (t, 2H), 1.62 (t, 2H), 1.39 (m, 22H), 0.88 (t, 3H). ^{13}C NMR (400 MHz Chloroform-*d*) δ 173.9, 56.3, 56.2, 51.4, 34.0, 31.9, 29.8, 29.5, 29.5, 29.2, 28.7, 28.7, 27.9, 25.8, 25.5, 22.7, 14.1. HRMS (EI+) (M+) calculated 312.2664, found 199.1300 [$C_{11}H_{19}O_3^+$]. Characterization is consistent with reported ^{1}H NMR shifts and MS data in literature [94].

Epoxidation of Methyl Oleate-8,8,11,11-d$_4$

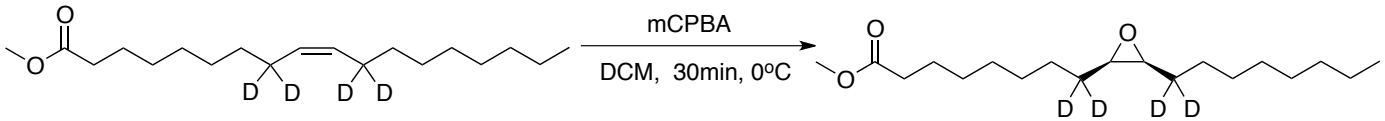

55 57

Methyl Oleate-9,10-cis-epoxide-8,8,11,11-d$_4$ (57) To a cooled (0ºC) solution of methyl oleate-8,8,11,11-*d*$_4$ **(55)** (150mg, 0.5mmol, 1.0eq.) in DCM (1.8mL) was slowly added mCPBA (77%; 116.5mg, 0.6mmol, 1.1eq.). The reaction mixture was left to stir for

30minutes at r.t. before evaluating reaction progress with TLC (50% DCM:Hex). Once the SM has been consumed, the organic phase was extracted with Et_2O (3x30mL), 10% $NaOH_{aq.\ sol.}$ (3x30 mL), brine (1x30 mL), and water (1x30 mL). The combined organic layers were dried over $MgSO_4$, filtered, and concentrated. Yield: 0.26 g; Quantitative yield. R_f = 0.3 (50 % DCM:Hex). ^{1}H NMR (400 MHz Chloroform-*d*) δ 3.67 (s, 3H), 2.89 (s, 2H), 2.30 (t, 2H), 1.63 (m, 2H), 1.47 (q, 2H), 1.32 (dtd, 18H), 0.88 (t, 3H). ^{13}C NMR (400 MHz Chloroform-*d*) δ 173.9, 55.8, 55.7, 51.4, 40.7, 40.6, 34.0, 32.3, 29.6, 29.2, 28.9, 28.2, 26.7, 25.8, 24.9, 24.8, 23.2, 14.0. Characterization is consistent with reported ^{1}H NMR shifts in literature [90].

Epoxidation of Methyl Elaidate

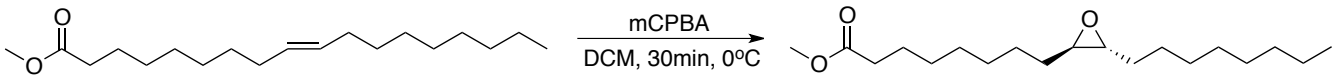

58 **59**

Methyl Elaidate-9,10-trans epoxide (59; Trans-9,10-Epoxide) To a cooled (0 °C) solution methyl elaidate **(58)** (500 mg, 1.7 mmol, 1.0 eq.) in DCM (6 mL) was slowly added mCPBA (68 %; 420 mg, 1.9 mmol, 1.1 eq.). The reaction mixture was left to stir for 30minutes at r.t. before evaluating reaction progress with TLC (50 % DCM:Hex). Once the SM has been consumed, the organic phase was extracted with Et_2O (3x60 mL), 10 % $NaOH_{aq.\ sol.}$ (3x60 mL), brine (1x60 mL), and water (1x60 mL). The combined organic layers were dried over $MgSO_4$, filtered, and concentrated. Crude was clean and used without further purification. Yield: 0.53 g; Quantitative yield. R_f = 0.4 (50% DCM:Hex). ^{1}H NMR (400 MHz Chloroform-*d*) δ 3.66 (s, 3H), 2.65 (s, 2H), 2.30 (t, 2H), 1.61 (d, 2H), 1.41 (m, 22H), 0.88 (t, 3H). ^{13}C NMR (400 MHz Chloroform-*d*) δ 173.9, 56.3, 56.2, 51.4, 34.0, 31.9, 29.8, 29.5, 29.5, 29.2, 28.7, 28.7, 27.9, 25.8, 25.5, 22.7, 14.1. HRMS (EI+) (M+) calculated 312.2664, found 281.2501 [$C_{18}H_{33}O_3^+$]. Characterization is consistent with reported^{1}H NMR shifts and MS data in literature [94].

3.5.2 Autoxidation Experimental Conditions

All LC based analysis was performed using a Waters Acquity UPLC-UV-MS/MS-APCI+ system. Samples were analyzed under NP-UPLC-UV at 0.6 % IPA:Hexanes (30 % of 2 % IPA:Hex + 70 % of 100 % Hex) with a flow rate of 0.9mL/min, and the 195, and 254 nm wavelengths (λ) were monitored. Samples were initially run in 100 % hexanes, but this was abandoned due to the extended elution times required and the expected poor separation when applied to the autoxidation mixture. This protocol was based on the basic instrumental conditions used by Porter *et al.* [57].

Standard autoxidation conditions were used following reported procedures by Ned Porter *et al.* [57]. A vial was charged with methyl oleate (0.178 g, 0.6 mmol), the radical initiator DTBN (5 mol% with respect to methyl oleate), and tert-butyl hydroperoxide (^{t}BuOOH; 0.73 mL – 6.67 Eq.) then heated at a constant 30 ^{o}C for 24-hours under an air atmosphere. The aliquots withdrawn at given time points throughout the autoxidation and quenched with TTBP (tri-tert-butylphenol) before concentrating to remove residual ^{t}BuOOH (bp_{20} = 35 ^{o}C). Each aliquot was diluted 10-fold with hexanes prior to injection on the UPLC-MS/MS. The methyl oleate hydroperoxide product distribution (11-cis:9-trans = 1:1.2) was consistent with literature reports by Porter *et al.* [57].Instrumental modifications were performed to reproduce Porter's chromatographic protocol. This included doubling the column length by connecting two normal phase columns in series (Sunfire and Wattman Columns) and extending the elution time to 70-minutes accordingly. Furthermore, there was incorporation of a solvent polarity ramp at the end of every run to remove residual compounds from the column, a polarity gradient during the wash cycle between every 3 samples to ensure consistency in results, and the samples were run in a random order.

References

[1] C. E. Frank, *Chemical Reviews,* vol. 46, no. 1, pp. 155-169, 1950.

[2] K. U. Ingold, *Accounts of Chemical Research,* vol. 2, p. 1, 1969.

[3] M. Conrad and D. A. Pratt, *Nature Chemical Biology,* vol. 15, p. 1137–1147, 2019.

[4] Z. A. M. Zielinski and D. A. Pratt, *The Journal of Organic Chemistry,* vol. 82, no. 6, pp. 2817-2825, 2017.

[5] H. Yin, L. Xu and N. A. Porter, *Chemical Reviews,* vol. 111, no. 10, pp. 5944-5972, 2011.

[6] S. Petruzzelli and C. A. Angeletti, *Chest,* vol. 98, no. 4, pp. 930-935, 1990.

[7] V. N. Bochkov, O. V. Oskolkova, K. G. Birukov, A. L. Levonen, C. J. Binder and J. Stöckl, *Antioxidants & Redox Signaling,* vol. 12, no. 8, pp. 1009-1059, 2010.

[8] Fenton, H. J. H.;, *Journal of the Chemical Society - Transactions,* vol. 65, pp. 899-910, 1894.

[9] A. U. Khan, *Biochemical and Biophysical Research Communications,* vol. 122, p. 668, 1984.

[10] Z. A. M. Zielinski and D. A. Pratt, *Journal of the American Chemical Society,* vol. 141, no. 7, pp. 3037-3051, 2019.

[11] J. A. Howard and K. U. Ingold, *Canadian Journal of Chemistry,* vol. 45, pp. 793-802, 1967.

[12] E. Niki, *Enzymology,* vol. 186, pp. 100-108, 1990.

[13] R. Shah, M. S. Shchepinov and D. A. Pratt, *ACS Central Science,* vol. 4, no. 3, pp. 387-396, 2018.

[14] L. J. Su, J. H. Zhang, H. Gomez, R. Murugan, X. Hong, D. Xu, F. Jiang and Z. Y. Peng, *Oxidative Medicine and Cellular Longevity,* vol. 5080843, 2019.

[15] R. O. Recknagel, *Pharmacological Review,* vol. 19, pp. 145-208, 1967.

[16] A. M. Firsov, M. A. Fomich, A. V. Bekish, O. L. Sharko, E. A. Kotova, H. J. Saal, D. Vidovic, V. V. Shmanai, D. A. Pratt, Y. N. Antonenko and M. S. Shchepinov, *The FEBS Journal,* vol. 286, no. 11, pp. 2099-2117, 2019.

[17] S. Hill, C. R. Lamberson, L. Xu, R. To, H. S. Tsui, V. V. Shamanai, A. V. Bekish, A. M. Awad, B. N. Marbois, C. R. Cantor, N. A. Porter, C. F. Clarke and M. S. Shchepinov, *Free Radical Biology and Medicine,* vol. 53, no. 4, pp. 893-906, 2012.

[18] M. S. Shchepinov, V. P. Chou, E. Pollock, J. W. Langston, C. R. Cantor, R. J. Molinari and A. B. Manning-Boğ, *Toxicological Letters,* no. 207, pp. 97-103, 2011.

[19] A. Broniec, R. Klonsinski, A. Pawlak, M. Wrona-Krol, D. H. Thompson and T. Sarna, *Free Radical Biology and Medicine,* vol. 50, pp. 892-898, 2011.

[20] N. Nagan and R. A. Zoeller, *Progress in Lipid Research,* vol. 40, no. 3, pp. 199-229, 2001.

[21] J. Van den Bossche, J. Shin and D. H. Thompson, *The Journal of Organic Chemistry,* vol. 72, no. 13, pp. 5005-5007, 2007.

[22] Y. Riu and D. H. Thompson, *The Journal of Organic Chemistry,* vol. 59, no. 19, pp. 5758-5762, 1994.

[23] R. Feulgen and K. Voit, *Pflüger's Archive ,* vol. 206, pp. 389-410, 1924.

[24] J. Shin, O. Gerasimov and D. H. Thompson, *The Journal of Organic Chemistry,* vol. 67, no. 18, pp. 6503-6508, 2002.

[25] M. M. Rapport, B. Lerner, N. Alonzo and R. E. Franzl, *The Journal of Biological Chemistry,* vol. 225, pp. 859-867, 1957.

[26] H. Debuch, *The Journal of Neurochemistry,* vol. 2, pp. 243-248, 1958.

[27] H. Debuch, P. Seng and F. Snyder, *Ether Lipids: Chemistry and Biology,* pp. 1-24, 1972.

[28] W. T. Norton, E. L. Gottfried and M. M. Rapport, *The Journal of Lipid Research,* vol. 3, no. 4, pp. 456-459, 1962.

[29] G. A. Thompson Jr., *Biochimica et Biophysica Acta (BBA) - Lipids and Lipid Metabolism,* vol. 152, no. 2, pp. 409-411, 1968.

[30] R. L. Wykle, M. L. Blank, B. Malone and F. Snyder, *Journal of Biological Chemistry,* vol. 247, p. 5442–5447, 1972.

[31] T. Harayama and H. Riezman, *Nature Reviews Molecular Cell Biology,* vol. 19, pp. 281-296, 1018.

[32] K. Watschinger and E. R. Werner, *Biochimie,* vol. 95, p. 59–65, 2013.

[33] W. Lorenzen, T. Ahrendt, K. A. Bozhüyük and H. B. Bode, *Nature Chemical Biology,* vol. 10, pp. 425-427, 2014.

[34] M. W. Ring, G. Schwär, V. Thiel, J. S. Dickschat, R. M. Kroppenstedt, S. Schulz and H. B. Bode, *Journal of Biological Chemistry,* vol. 281, p. 36691–36700, 2006.

[35] M. Elías-Arnanz, S. Padmanabhan and F. J. Murillo, *Current Opinion in Microbiology,* vol. 14, pp. 128-135, 2011.

[36] A. Gallego-García, A. J. Monera-Girona, E. Pajares-Martínez, E. Bastida-Martínez, R. Pérez-Castaño and A. A. Iniesta, *Science,* vol. 366, no. 6461, p. 128, 2019.

[37] H. Esterbauer, J. Gebicki, H. Pauhl and G. Jurgens, *Free Radical Biology and Medicine,* vol. 13, p. 341, 1992.

[38] J. A. Berliner and J. W. Heinecke, *Free Radical Biology and Medicine,* vol. 20, p. 707, 1996.

[39] A. Antczak, D. Nowak, B. Shariati, M. Krol, G. Piasecka and Z. Kurmanowska, *European Respiratory Journal,* vol. 10, p. 1235, 1997.

[40] P. Montuschi, M. Corradi, G. Ciabattoni, J. Nightingale, S. A. Kharitonov and P. J. Barnes, *American Journal of Respiratory and Critical Care Medicine,* vol. 160, p. 216, 1999.

[41] Penonmenome Discoveries Inc..WO Patent 071418, 23 May 2013.

[42] N. A. Simonian and J. T. Coyle, *Annual Review of Pharmacology and Toxicology,* vol. 36, pp. 83-110, 1996.

[43] L. M. Sayre, D. A. Zelasko, P. L. R. Harris, G. Perry, R. G. Salomon and M. A. Smith, *Journal of Neurochemistry,* vol. 68, p. 2092, 1997.

[44] A. O. Oyewole and M. A. Birch-Machin, *FASEB Journal ,* vol. 29, no. 12, pp. 4766-4771, 2015.

[45] A. Puri, *Pharmaceutics,* vol. 6, no. 1, pp. 1-25, 2014.

[46] G. Spiteller, *Free Radical Biology and Medicine,* vol. 41, no. 3, pp. 362-387, 2006.

[47] A. Broniec, A. Żądło, A. Pawlak, B. Fuchs, R. Kłosiński, T. Sarna and D. H. Thompson, *Free Radical Biology and Medicine,* vol. 106, pp. 368-378, 2017.

[48] S. Stadelmann-Ingrand, R. Pontcharraud and B. Fauconneau, *Chemistry and Physics of Lipids,* vol. 131, no. 1, pp. 93-105, 2004.

[49] A. Noel, S. Ingrand and L. Barrier, *Biochimie,* vol. 137, pp. 158-164, 2017.

[50] M. E. Greenberg, X. M. Li, B. G. Gugiu, X. Gu, J. Qin, R. G. Salomon and S. L. Hazen, *Journal of Biological Chemistry,* vol. 283, p. 2385, 2008.

[51] J. Wong-Ekkabut, Z. Xu, W. Triampo, I. M. Tang, D. P. Tieleman and L. Monticelli, *Journal of Biophysics,* vol. 93, p. 4225, 2007.

[52] C. R. Stewart, L. M. Wilson, Q. Zhang, C. L. L. Pham, L. J. Waddington, M. K. Staples, D. Stapleton, J. W. Kelly and G. Howlett, *Journal of Biochemistry,* vol. 46, p. 5552, 2007.

[53] R. C. Murphy, *Chemical Research in Toxicology,* vol. 14, pp. 463-472, 2001.

[54] L. A. Hammad, G. Wu, M. M. Saleh, I. Klouckova, L. E. Dobrolecki, R. J. Hickey, L. Schnaper, M. V. Novotny and Y. Mechref, *Rapid Communications in Mass Spectrometry,* vol. 23, pp. 863-876, 2010.

[55] C. L. Rector, J. G. Gillmore, D. A. Pratt, C. Punta and N. Porter, *The Journal of Organic Chemistry,* vol. 71, no. 9, pp. 3527-3532, 2006.

[56] E. A. Haidasz, A. T. M. Van Kessel and D. A. Pratt, *The Journal of Organic Chemistry,* vol. 81, no. 3, pp. 737-744, 2016.

[57] N. A. Porter, K. A. Mills and R. L. Carter, *Journal of the American Chemical Society,* vol. 116, p. 6690, 1994.

[58] A. Köckritz, M. Blumenstein and A. Martin, *European Journal of Lipid Science and Technology,* vol. 110, no. 6, pp. 581-586, 2008.

[59] E. H. Farmer, H. P. Koch and D. A. Sutton, *Journal of the Chemical Society,* p. 541, 1949.

[60] E. H. Farmer and D. A. Sutton, *Journal of the Chemical Society,* p. 119, 1943.

[61] E. N. Frankel, W. E. Neff and W. K. Rohwedder, *Lipids,* p. 901, 1977.

[62] N. A. Porter and C. Vigo-Pelfrey, *Membrane Lipid Oxidation,* pp. 33-62, 1990.

[63] J. Shin, O. Gerasimov and D. H. Thompson, *The Journal of Organic Chemistry,* vol. 68, no. 17, pp. 6760-6766, 2003.

[64] V. C. Anderson and D. H. Thompson, *Macromolecular Assemblies in Polymeric Systems,* pp. 154-170, 1992.

[65] O. V. Gerasimov, A. Schwan and D. H. Thompson, *Biochimica et Biophysica Acta (BBA) – Biomembranes,* vol. 1324, no. 2, pp. 200-214, 1997.

[66] D. H. Thompson, H. D. Inerowicz, J. Grove and T. Sarna, *Photochemistry and Photobiology,* vol. 78, no. 4, pp. 323-330, 2003.

[67] A. Loidl-Stahlhofen, K. Hanneman, R. Felde and G. Spiteller, *Biochemical Journal,* vol. 309, no. 3, pp. 807-812, 1995.

[68] B. Neises and W. Steglich, *Angewandte Chemie International Edition,* vol. 17, pp. 522-524, 1978.

[69] S. R. Park, C. Kim, D. Kim, N. Thrimurtulu, H. S. Yeom, J. Jun, S. Shin and Y. H. Rhee, *Organic Letters,* vol. 15, no. 6, pp. 1166-1169, 2013.

[70] Y. Kon, T. Fujitani, T. Nakashima, T. Murayama and W. Ueda, *Catalysis Science and Technology,* vol. 8, pp. 4618-4625, 2018.

[71] S. Lluis, C. Jaume, A. Moyano, M. A. Pericás and A. Riera, *Tetrahedron Letters,* vol. 33, no. 20, pp. 2863-2866, 1992.

[72] T. Tsuchimoto, H. Matsubayashi, M. Kaneko, Y. Nagase, T. Miyamura and E. Shirakawa, *Journal of the American Chemical Society,* vol. 130, no. 47, pp. 15823-15835, 2008.

[73] M. Azzedine, I. Satoshi and R. Yamauchi, *Bioscience, Biotechnology, and Biochemistry,* vol. 74, no. 5, pp. 1013-1017, 2010.

[74] N. Noguchi, H. Yamashita, N. Gotoh, Y. Yamamoto, R. Numano and E. Niki, *Free Radical Biology & Medicine,* vol. 24, no. 2, pp. 259-268, 1998.

[75] Z. A. M. Zielinski and D. A. Pratt, *Journal of the American Chemical Society,* vol. 138, no. 22, pp. 6932-6935, 2016.

[76] J. Exner, S. Eusterwiemann, O. Janka, C. Doerenkamp, A. Massolle, O. Niehaus, C. G. Daniliuc, R. Pöttgen, J. Neugebauer, A. Struder and H. Eckert, *Physical Chemistry Chemical Physics,* vol. 20, pp. 28979-28983, 2018.

[77] J. Ross, A. I. Gebhart and J. F. Gerecht, *Journal of the Americal Chemical Society,* vol. 71, no. 1, pp. 282-286, 1049.

[78] E. N. Frankel, R. F. Garwood, B. P. Khambay, G. P. Moss and B. C. Weedon, *Journal of the Chemical Society Perkin Transcript I,* pp. 2233-2240, 1984.

[79] L. Vanoye, Z. E. Hamami, J. Wang, C. de Bellefon, P. Fongarland and A. Favre-Réguillon, *European Journal of Lipid Science and Technology,* vol. 119, no. 5, p. 1600281, 2016.

[80] T. Aliwarga, B. S. Raccor, R. N. Lemaitre, N. Sotoodehnia, S. A. Gharib, L. Xu and R. A. Totah, *Free Radical Biology & Medicine,* no. 112, pp. 131-140, 2017.

[81] J. F. R. Benitez.Canada Patent CA2006117197Al, 2006.

[82] W. J. Dejarlais and E. A. Emken, *Lipids,* no. 11, p. 594, 1976.

[83] E. Dunny and P. Evans, *Journal of the Chemical Society,* vol. 75, no. 15, pp. 5334-5336, 2010.

[84] L. Crombie and S. J. Holloway, *Journal of the Chemical Society,* vol. 1, pp. 2425-2434, 1985.

[85] X. Ariza, G. Asins, J. Garcia, F. G. Hergardt, K. Makowski, D. Serra and J. Velasco, *Journal of Labelled Compounds and Radiopharmaceuticals,* vol. 53, no. 8, pp. 556-558, 2010.

[86] P. W. Westerman, J. M. Pope, N. Phonphok, J. W. Doane and D. W. Dubro, *Biochimica Et Biophysica Acta (BBA) – Biomembranes,* vol. 939, no. 1, pp. 64-78, 1988.

[87] B. Behrouzian, C. K. Savile, B. Dawson, P. H. Buist and J. Shanklin, *Journal of the American Chemical Society,* vol. 124, no. 13, pp. 3277-3283, 2002.

[88] R. J. Vandenberg, S. N. Mostyn, J. E. Carland, S. Shimmon, R. M. Ryan and T. Rawling, *ACS Chemical Neuroscience,* vol. 8, pp. 1949-1959, 2017.

[89] G. Wittig, R. Mangold and G. Felletschen, *Justus Liebigs Annalen der Chemie,* vol. 560, no. 1, pp. 116-127, 1948.

[90] P. H. Buist and D. B. Maclean, *Canadian Journal of Chemistry,* vol. 59, pp. 828-838, 1981.

[91] F. Fringuelli, R. Germani, F. Pizzo and G. Savelli, *Tetrahedron Letters,* vol. 30, no. 11, pp. 1427-1428, 1989.

[92] N. A. Porter and J. R. Nixon, *Journal of the American Chemical Society,* vol. 100, no. 22, pp. 7116-7117, 1978.

[93] C. Chatgilialoglu, K. U. Ingold and J. C. Scaiano, *Journal of the American Chemical Society,* vol. 103, no. 26, pp. 7739-7742, 1981.

[94] S. P. Bunker and R. P. Wool, *Journal of Polymer Science A Polymer Chemistry,* vol. 40, pp. 451-458, 2002.

[95] S. C. Schou, *Journal of Labelled Compounds and Radiopharmaceuticals,* vol. 53, no. 1, p. 556, 2010.

[96] Z. Liu, Q. Ma, Y. Liu and Q. Wang, *Organic Letters,* vol. 16, no. 1, pp. 236-239, 2014.

[97] J. P. Marino and N. H. Nguyen, *The Journal of Organic Chemistry,* vol. 67, no. 18, pp. 6291-6296, 2002.

[98] M. Galbis-Martínez, S. Padmanabhan, F. J. Murillo and M. Elías-Arnanz, *Journal of Bacteriology,* vol. 194, pp. 1427-1436, 2012.

[99] M. Galbis-Martínez, F. J. Murillo, L. Galbis-Martínez and M. Fontes, *Microbiology,* vol. 154, pp. 895-904, 2008.

[100] F. J. Murillo, L. Galbis-Martínez and M. Fontes, *Molecular Microbiology,* vol. 47, pp. 561-571, 2003.

[101] G. V. Marinetti and J. Erbland, *Biochimica et Biophysica Acta (BBA) - Lipids and Lipid Metabolism,* vol. 26, no. 2, pp. 429-430, 1957.

[102] B. Li, J. R. Harjani, N. S. Cormier, H. Madarati, J. Atkinson, G. Cosa and D. A. Pratt, *Journal of the American Chemical Society,* vol. 135, no. 4, pp. 1394-1405, 2013.

[103] F. Haber and J. Weiss, *Proceedings of the Royal Society (London A) Math Physics and Engineering Sciences,* vol. 147, no. 861, pp. 332-351, 1934.

[104] J. P. Sindelar, Z. Guan, G. Dallner and L. Ernster, *Free Radical Biology and Medicine,* vol. 26, no. 3-4, pp. 318-324, 1999.

[105] S. Bennett and Canadian Institutes of Health Research.Canada Patent 364730, 2016.

[106] C. Kiryu, M. Makiuchi, J. Miyazaki, T. Fujinaga and K. Kakinuma, *FEBS Letters,* vol. 443, p. 154, 1999.

[107] M. Prein and W. Adam, *Angewandte Chemie,* vol. 35, p. 477, 1996.

[108] D. A. Pratt, J. H. Mills and N. A. Porter, *Journal of the American Chemical Society,* vol. 125, p. 5801, 2003.

[109] D. Hardeman and H. Van den Bosch, *Biochimica et Biophysica Acta (BBA) - Lipids and Lipid Metabolism,* vol. 1006, no. 1, pp. 1-8, 1989.

[110] S. J. Leung and M. Romanowski, *Theranostics,* vol. 2, no. 10, pp. 1020-1036, 2012.

[111] X. Chen and R. W. Gross, *Biochemistry,* vol. 34, no. 22, pp. 7356-7364, 1995.

[112] R. P. Wu, T. Hayashi, H. B. Cottam, G. Jin, S. Yao, C. C. N. Wu, M. D. Rosenbach, M. Corr, R. B. Schwab and D. A. Carson, *Proceedings of the National Academy of Sciences of the U.S.A.,* vol. 107, no. 16, pp. 7479-7484, 2010.

[113] R. L. Silverstein and M. Febbraio, *Science Signaling,* vol. 2, no. 72, p. re3, 2009.

[114] D. A. Pratt, K. A. Tallman and N. A. Porter, *Accounts of Chemical Research,* vol. 44, no. 6, pp. 458-467, 2011.

Appendix A – Spectral Data

Plasmalogen:

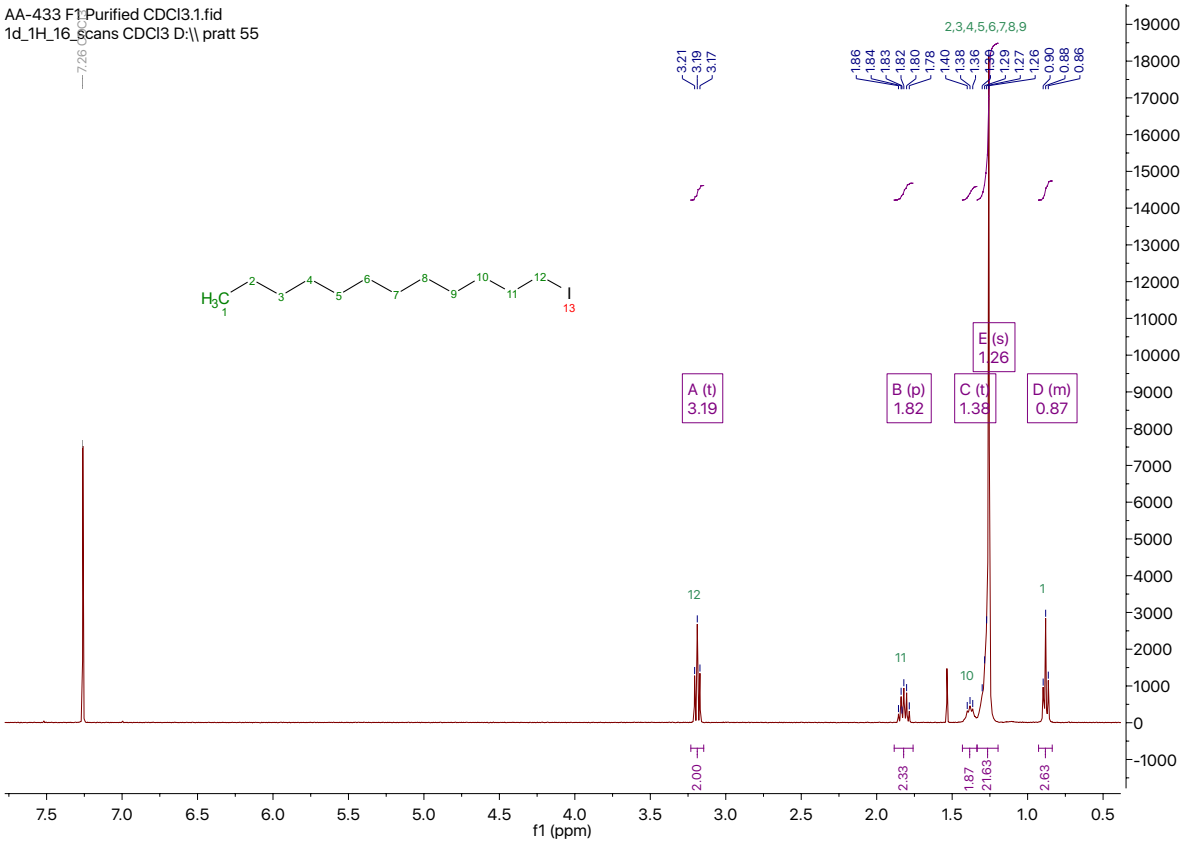

Figure 4.1 ^{1}H NMR ($CDCl_3$, 400 MHz) spectra of 1-iodododecane (24).

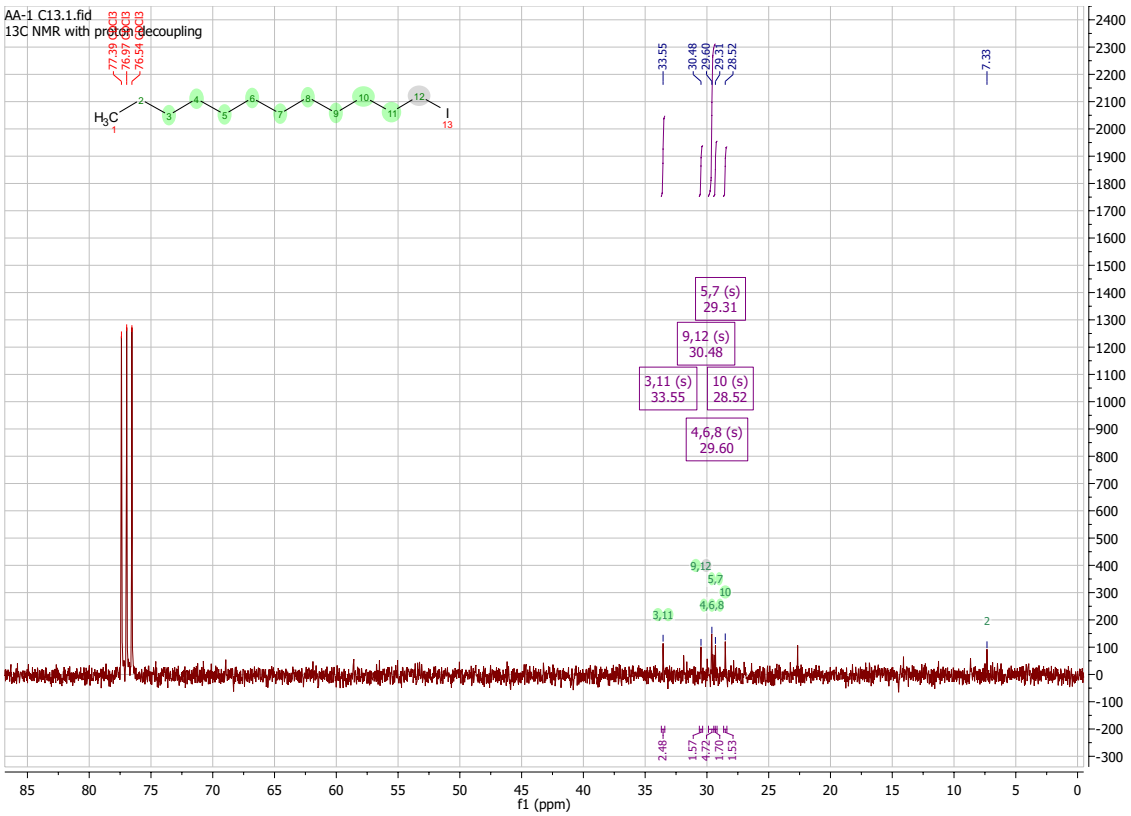

Figure 4.2 ^{13}C NMR ($CDCl_3$, 400 MHz) spectra of 1-iododododecane (24).

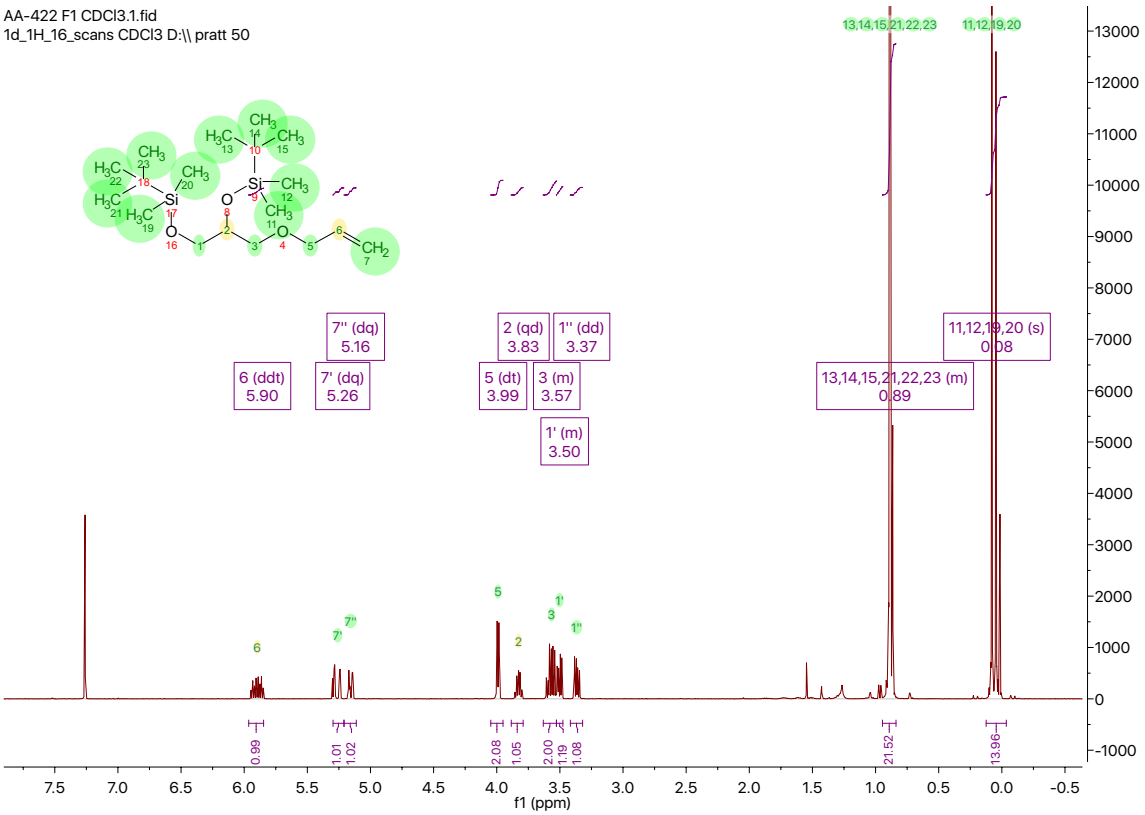

Figure 4.3 ^{1}H NMR ($CDCl_3$, 400 MHz) spectra of 5-((allyloxy)methyl)-2,2,3,3,8,8,9,9-octamethyl-4,7-dioxa-3,8-disiladecane (2).

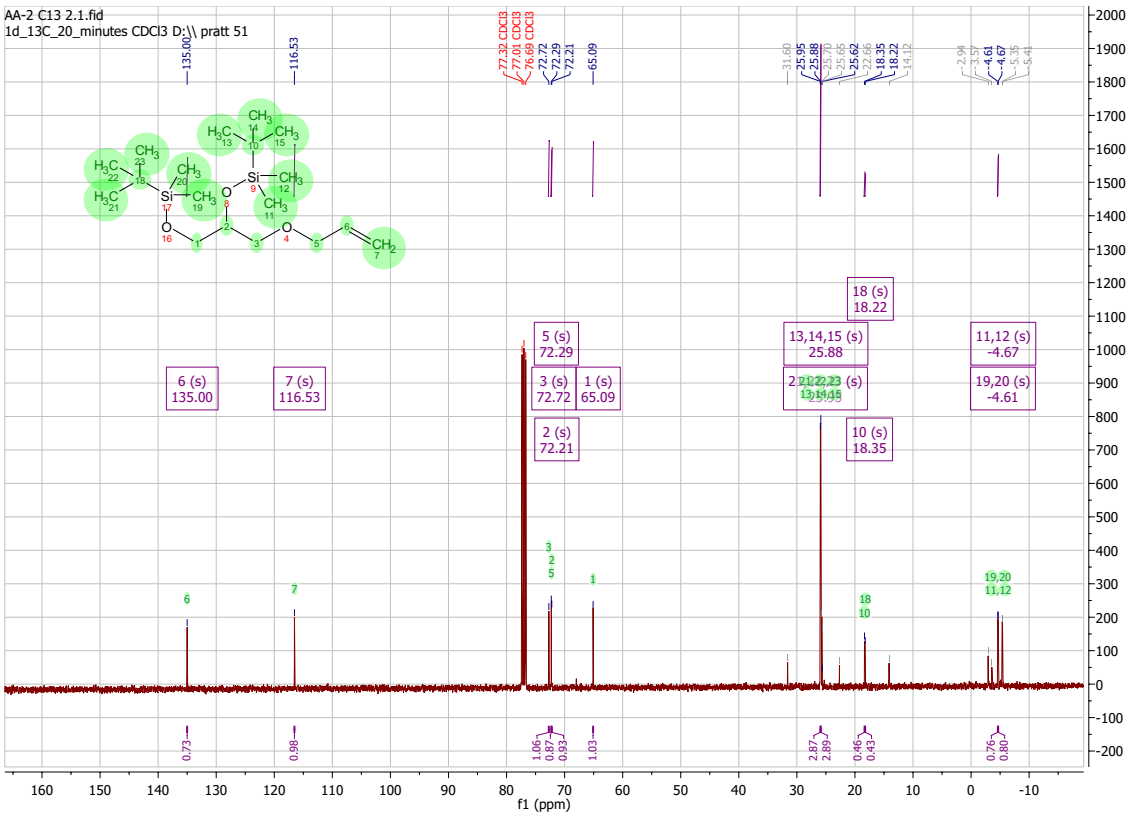

Figure 4.4 ^{13}C NMR ($CDCl_3$, 400 MHz) spectra of 5-((allyloxy)methyl)-2,2,3,3,8,8,9,9-octamethyl-4,7-dioxa-3,8-disiladecane (2).

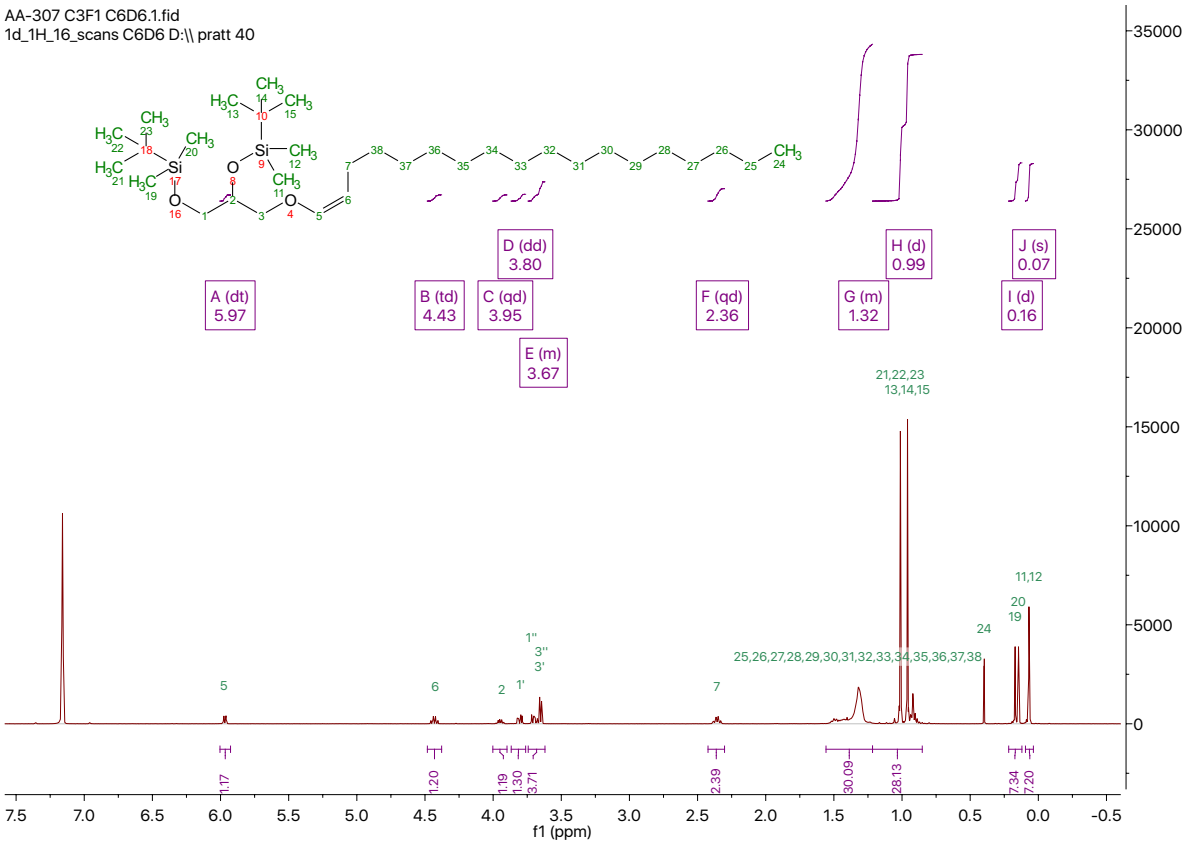

Figure 4.5 ^{1}H NMR (C_6D_6, 400 MHz) spectra of (Z)-2,2,3,3,8,8,9,9-octamethyl-5-((pentadec-1-en-1-yloxy)methyl)-4,7-dioxa-3,8-disiladecane (25).

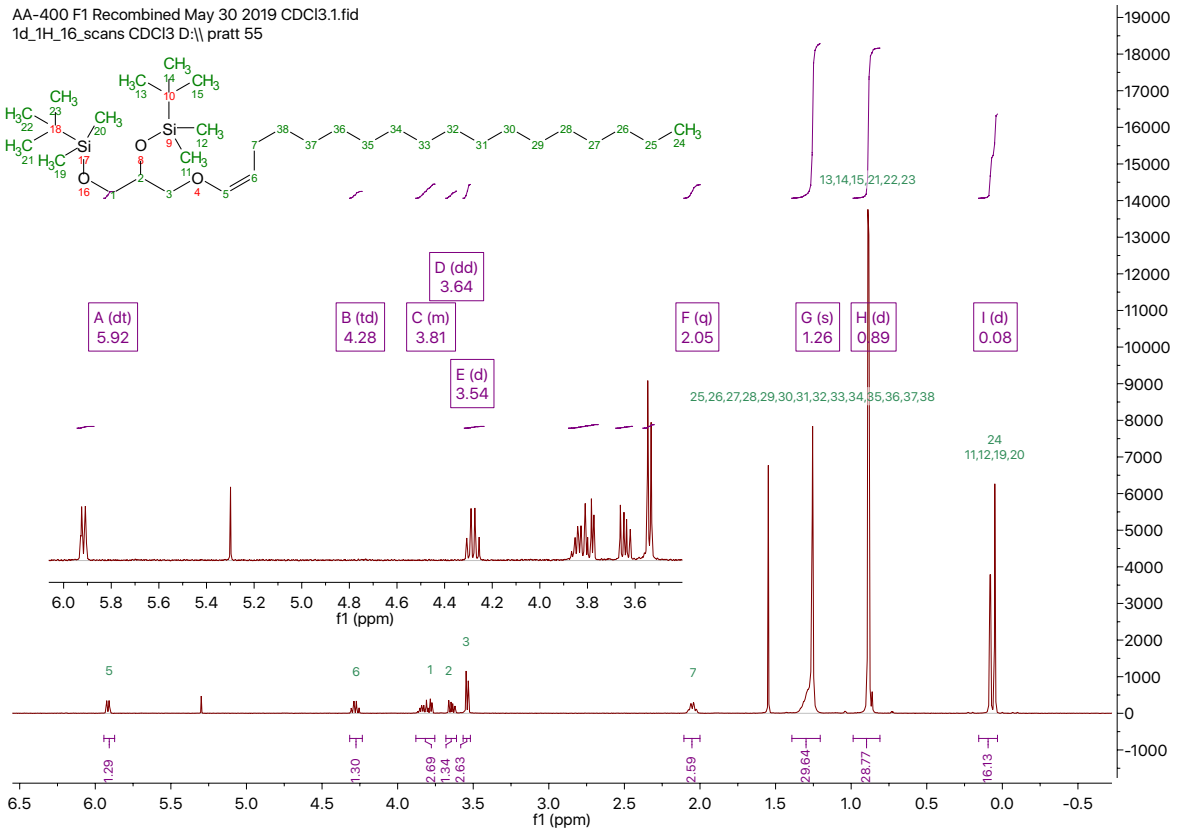

Figure 4.6 ^{1}H NMR ($CDCl_3$, 400 MHz) spectra of (Z)-2,2,3,3,8,8,9,9-octamethyl-5-((pentadec-1-en-1-yloxy)methyl)-4,7-dioxa-3,8-disiladecane (25).

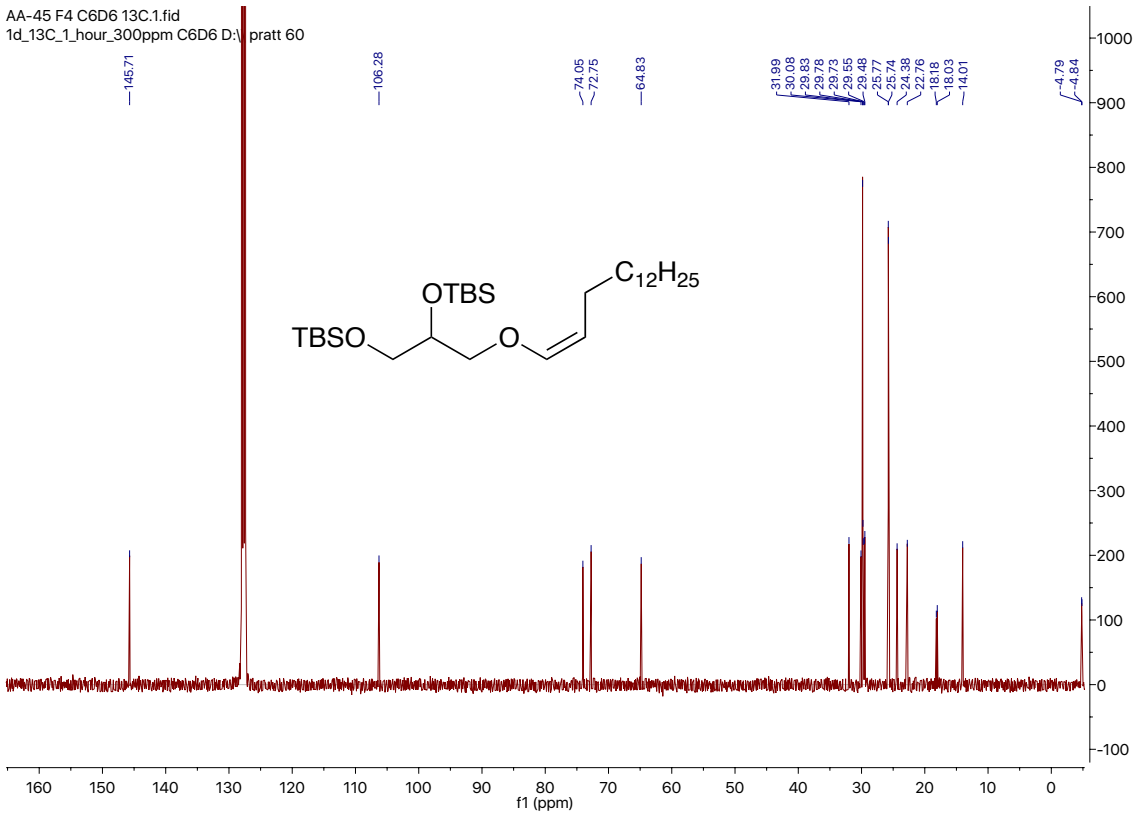

Figure 4.7 ^{13}C NMR (C_6D_6, 400 MHz) spectra of (Z)-2,2,3,3,8,8,9,9-octamethyl-5-((pentadec-1-en-1-yloxy)methyl)-4,7-dioxa-3,8-disiladecane (25).

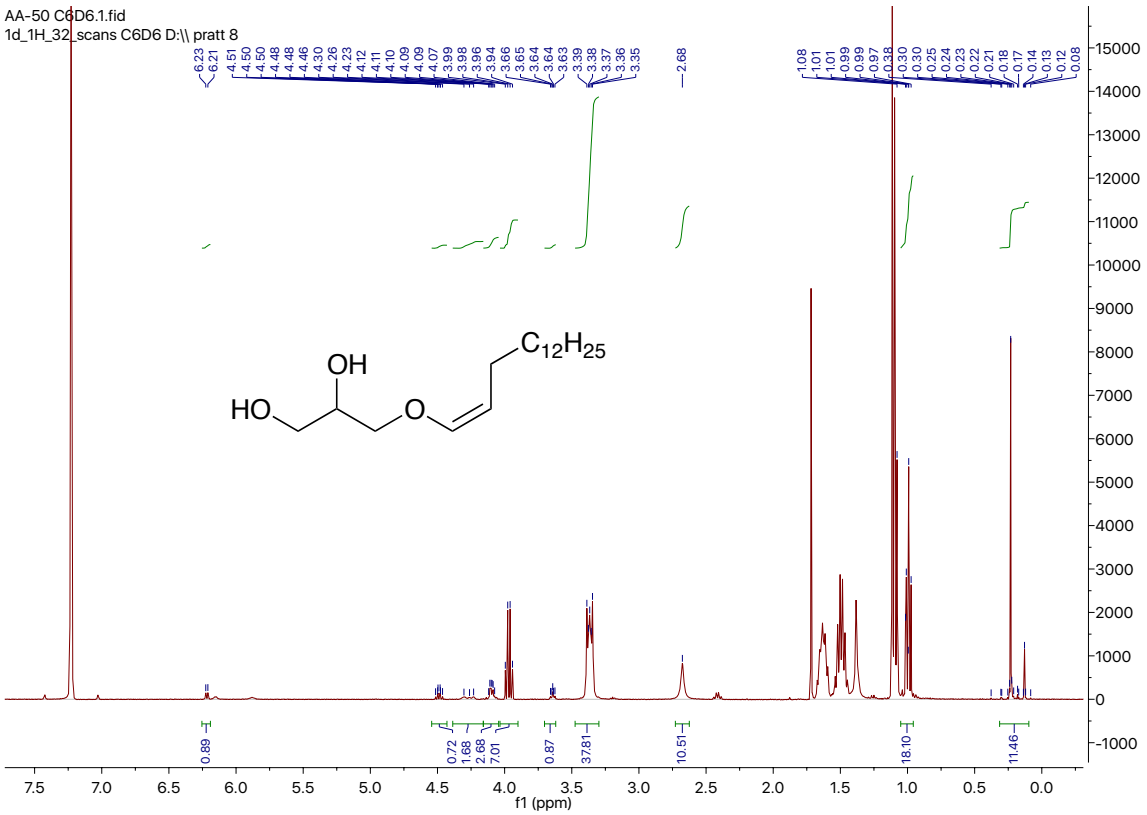

Figure 4.8 ^{1}H NMR (C_6D_6, 400 MHz) spectra of (Z)-3-(pentadec-1-en-1-yloxy)propane-1,2-diol (26).

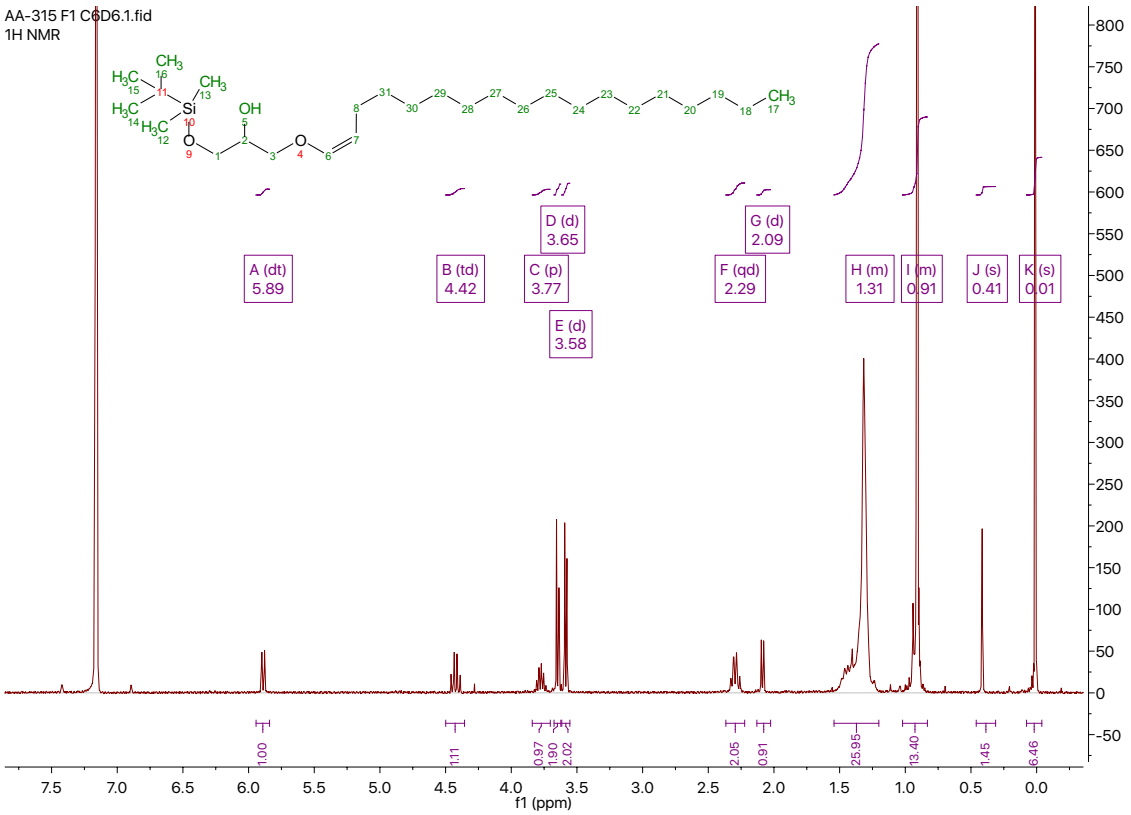

Figure 4.9 ^{1}H NMR (C_6D_6, 400 MHz) spectra of (Z)-1-((tert-butyldimethylsilyl)oxy)-3-(pentadec-1-en-1-yloxy)propan-2-ol (27).

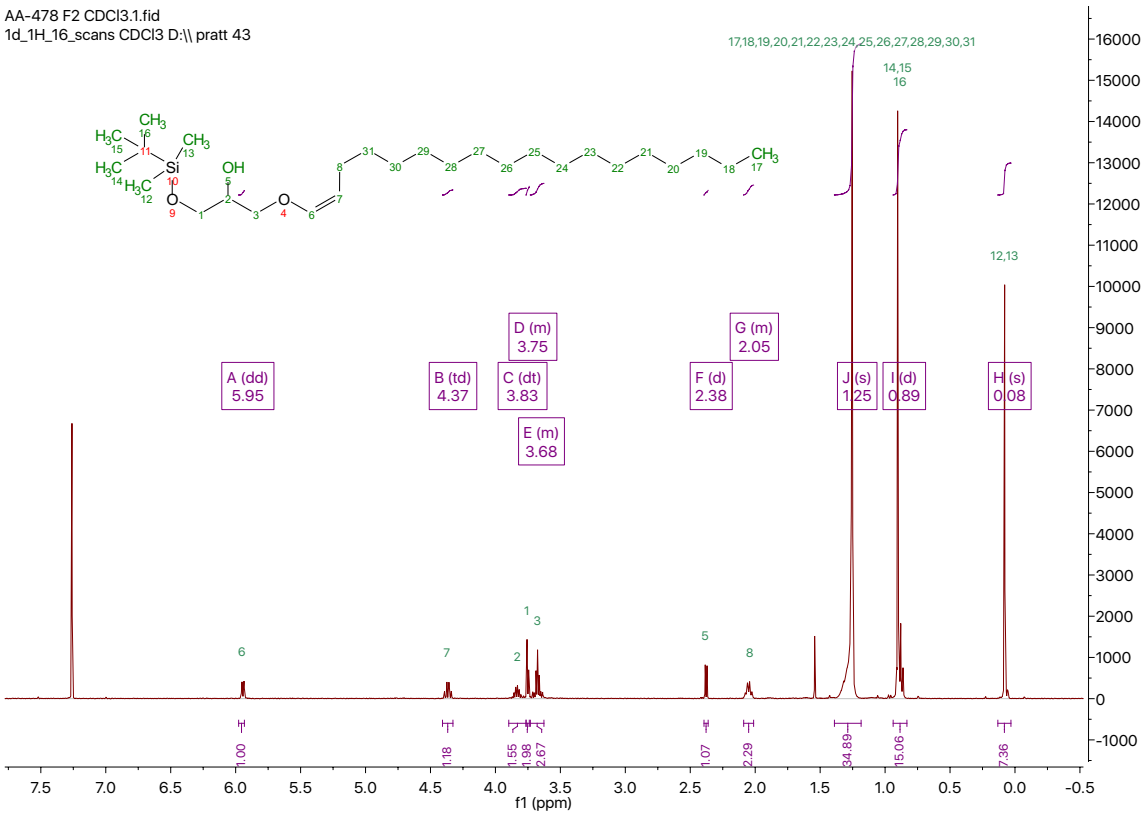

Figure 4.10 ^{1}H NMR ($CDCl_3$, 400 MHz) spectra of (Z)-1-((tert-butyldimethylsilyl)oxy)-3-(pentadec-1-en-1-yloxy)propan-2-ol (27).

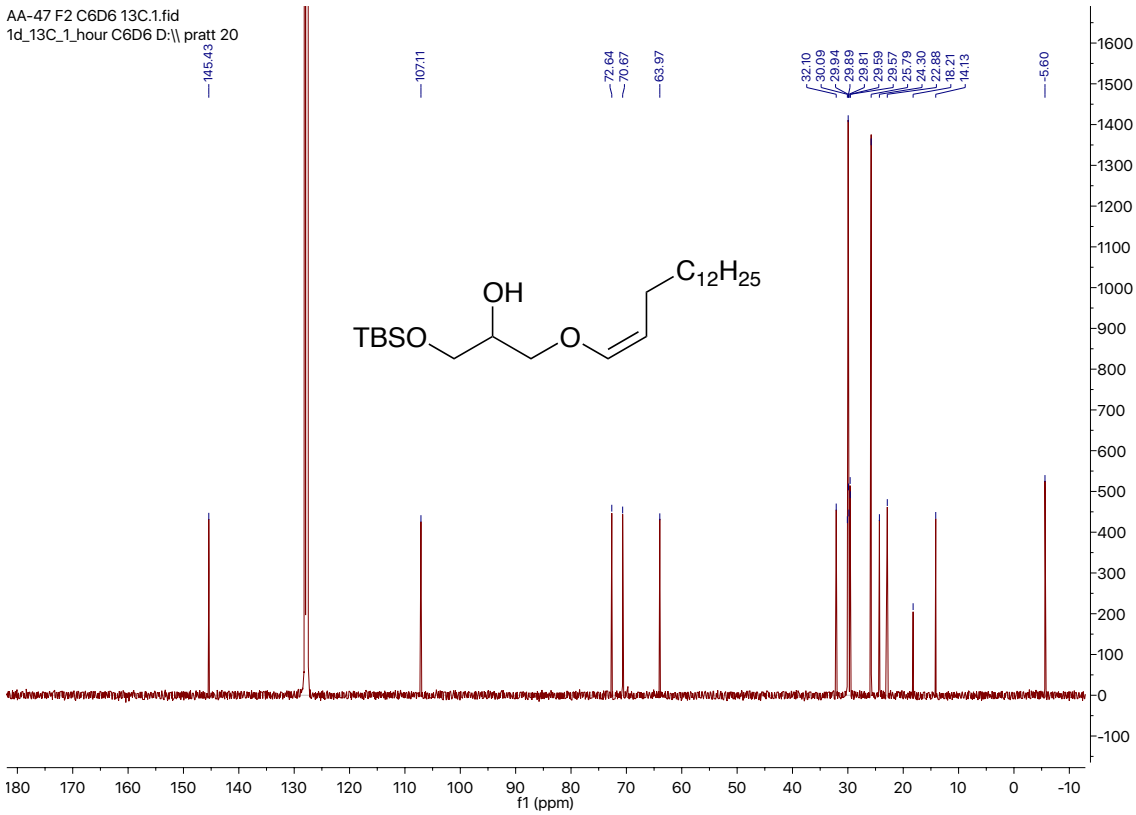

Figure 4.11 ^{13}C NMR (C_6D_6, 400 MHz) predicted spectra of (Z)-1-((tert-butyldimethylsilyl)oxy)-3-(pentadec-1-en-1-yloxy)propan-2-ol (27).

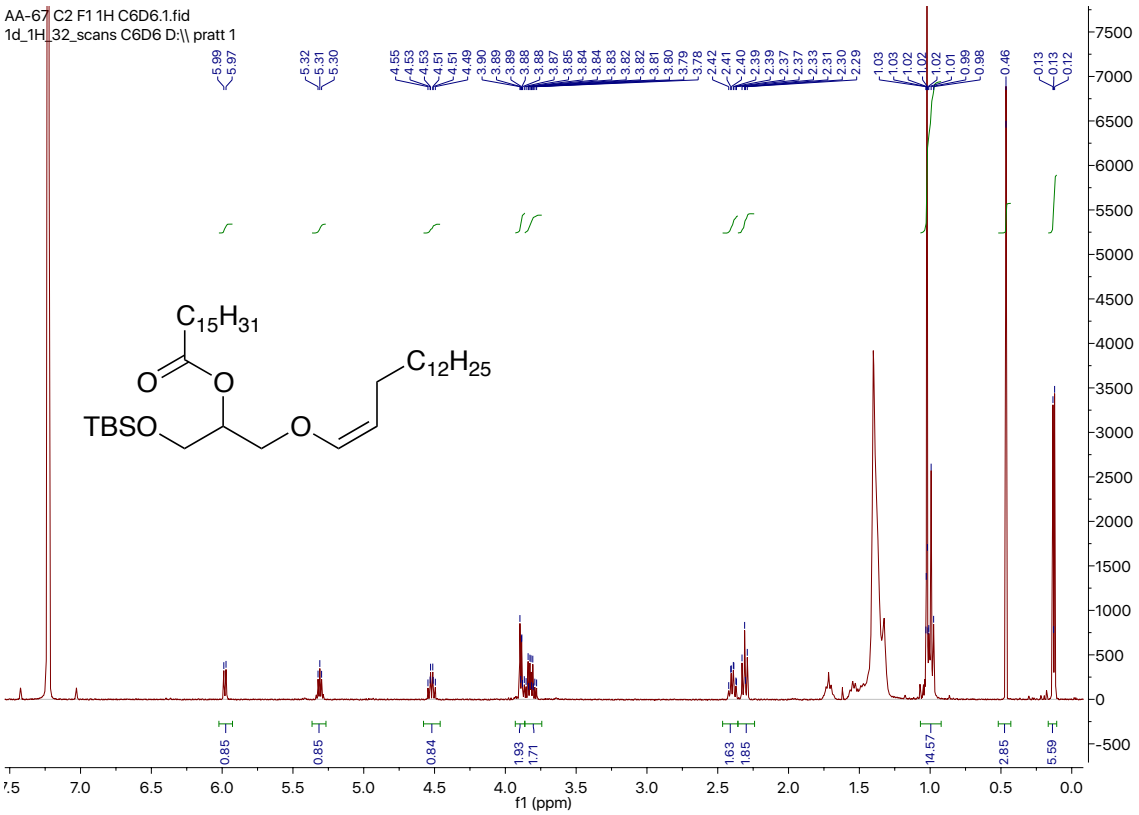

Figure 4.12 ^{1}H NMR (C_6D_6, 400 MHz) spectra of (Z)-1-((tert-butyldimethylsilyl)oxy)-3-(pentadec-1-en-1-yloxy)propan-2-yl palmitate (28).

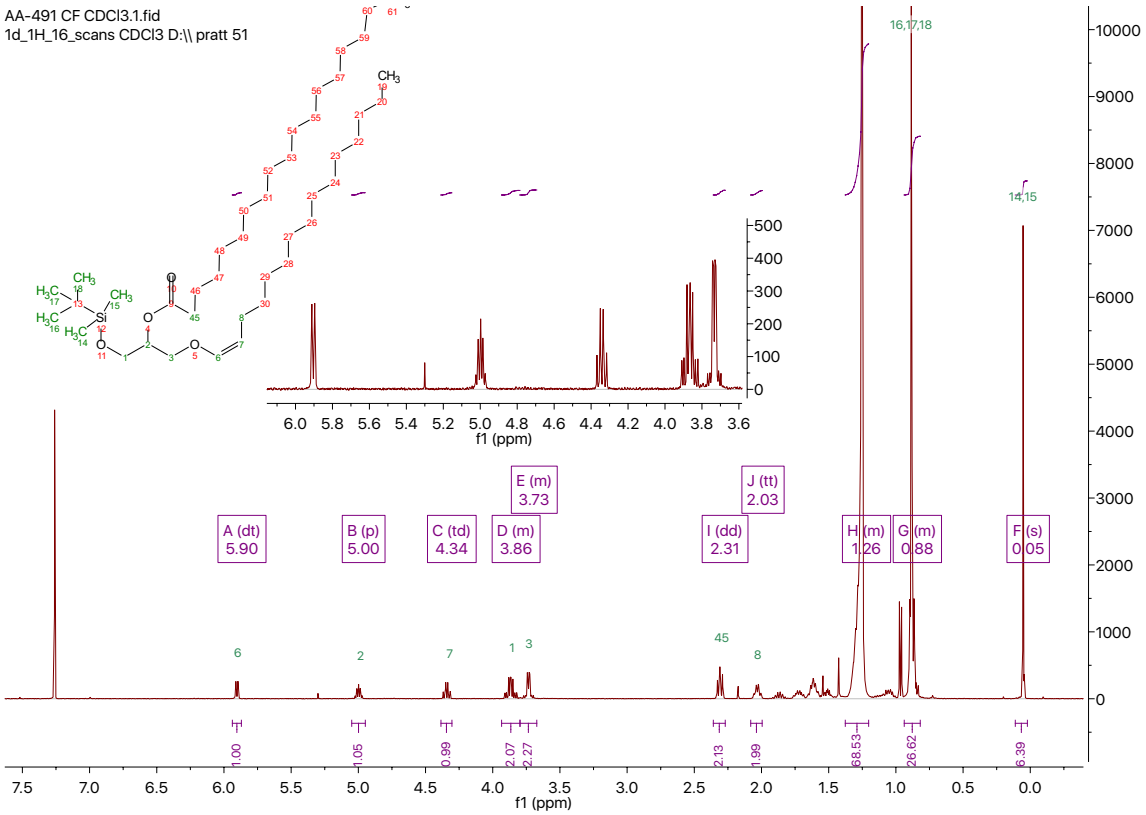

Figure 4.13 ^{1}H NMR ($CDCl_3$, 400 MHz) spectra of (Z)-1-((tert-butyldimethylsilyl)oxy)-3-(pentadec-1-en-1-yloxy)propan-2-yl palmitate (28).

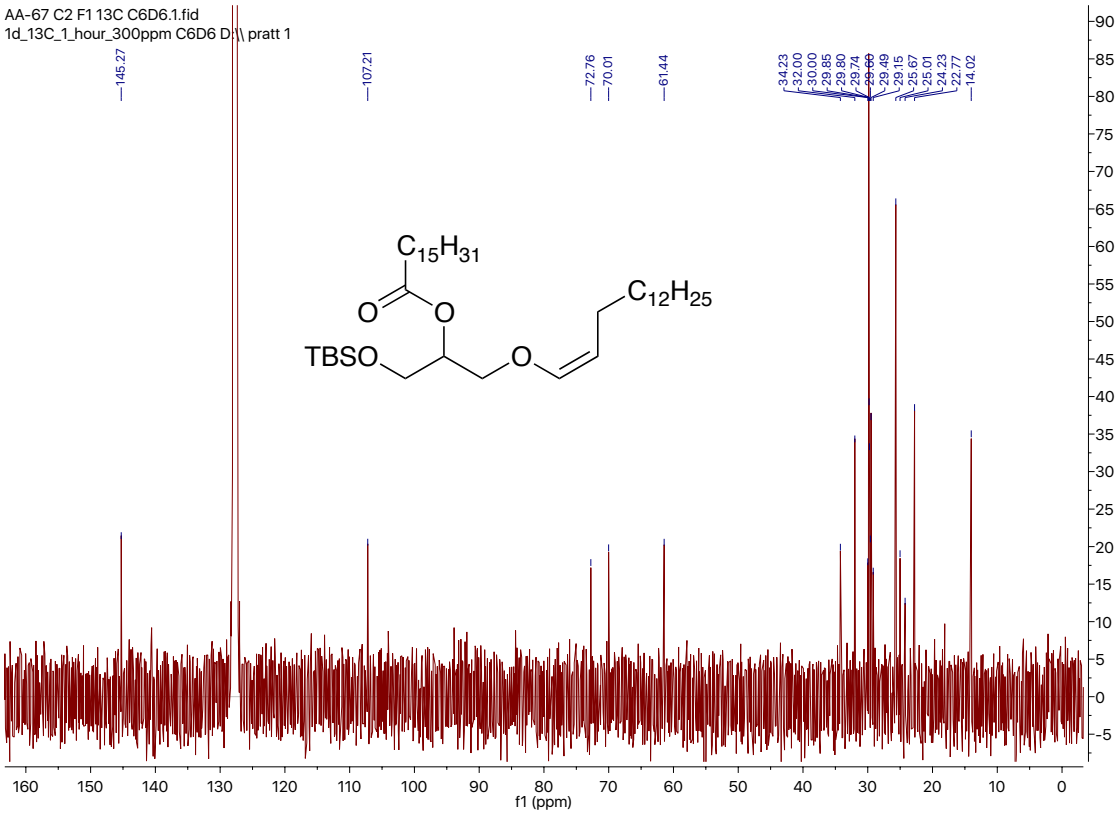

Figure 4.14 ^{13}C NMR (C_6D_6, 400 MHz) spectra of (Z)-1-((tert-butyldimethylsilyl)oxy)-3-(pentadec-1-en-1-yloxy)propan-2-yl palmitate (28).

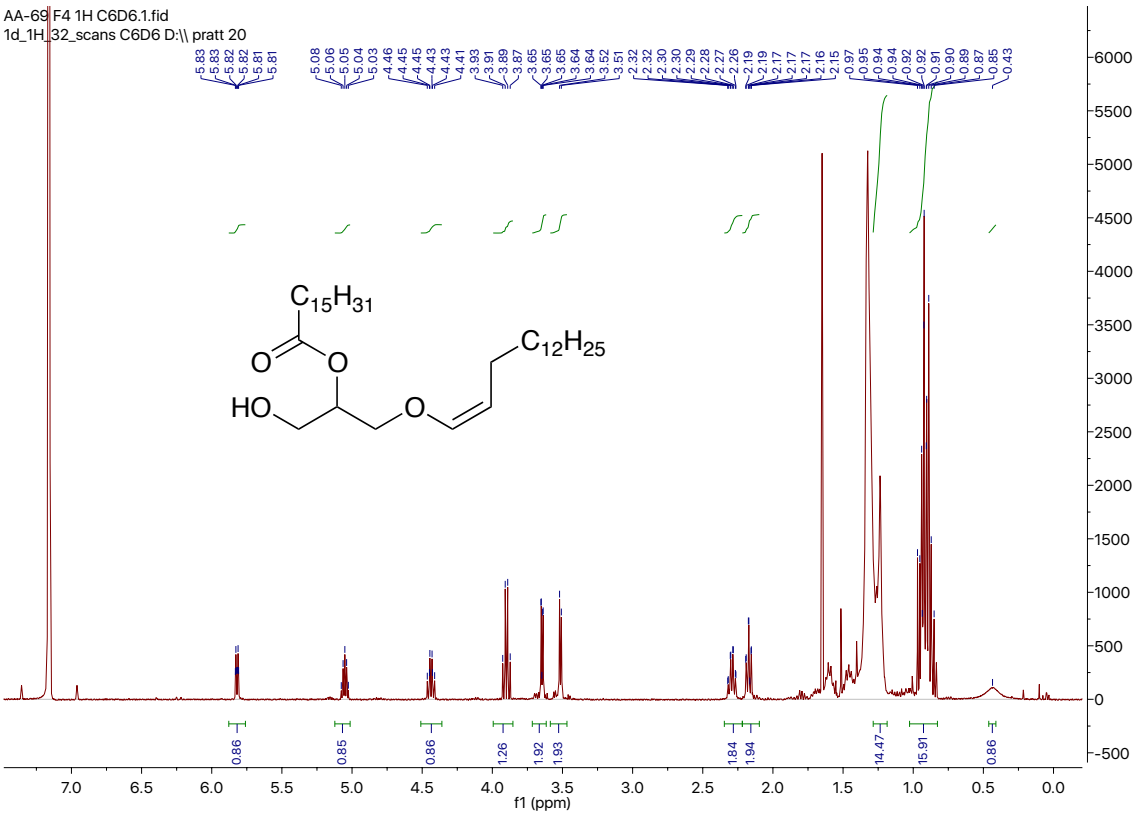

Figure 4.15 ^{1}H NMR (C_6D_6, 400 MHz) spectra of (Z)-1-hydroxy-3-(pentadec-1-en-1-yloxy)propan-2-yl palmitate (29).

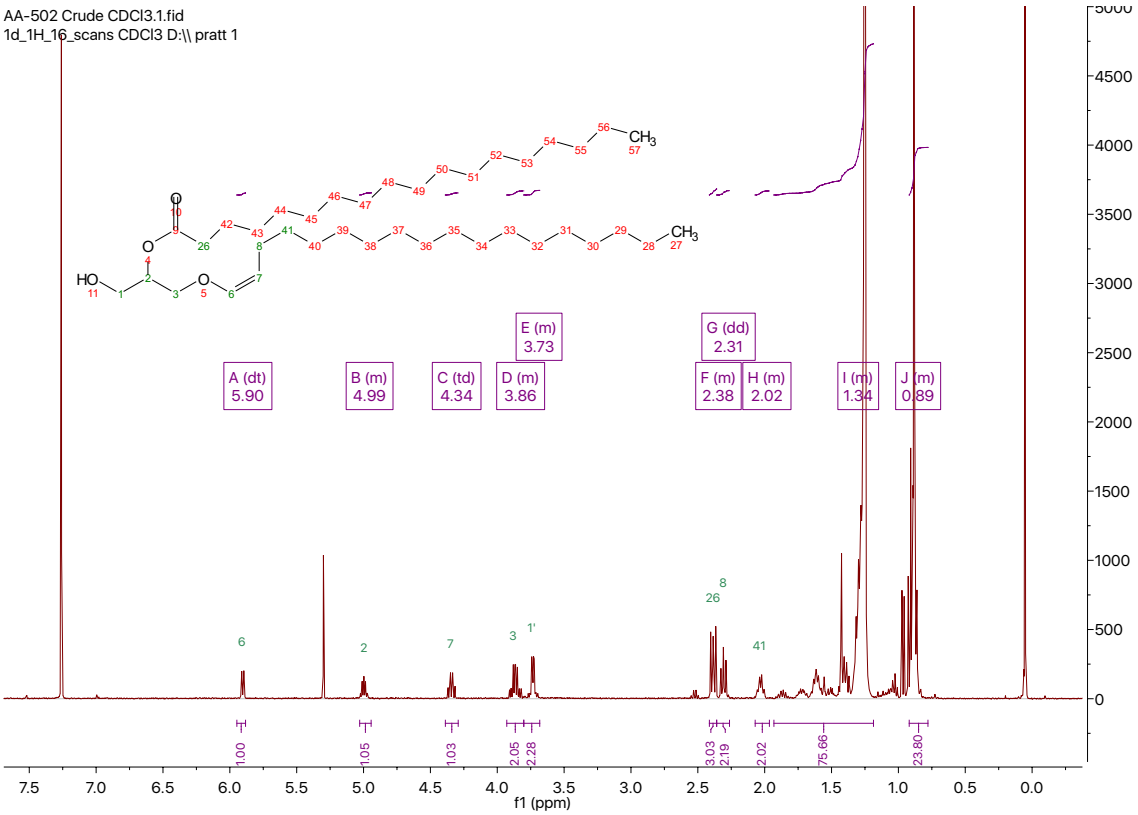

Figure 4.16 ^{1}H NMR ($CDCl_3$, 400 MHz) spectra of (Z)-1-hydroxy-3-(pentadec-1-en-1-yloxy)propan-2-yl palmitate (29).

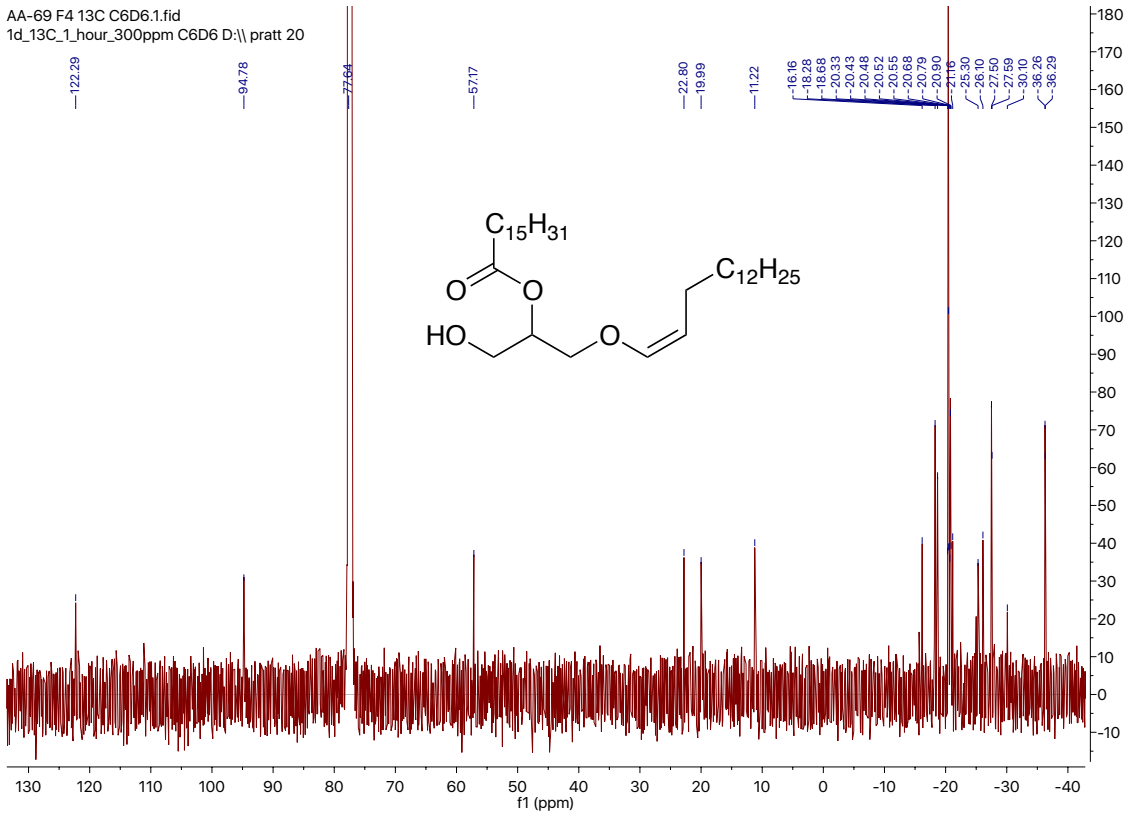

Figure 4.17 ^{13}C NMR (C_6D_6, 400 MHz) spectra of (Z)-1-hydroxy-3-(pentadec-1-en-1-yloxy)propan-2-yl palmitate (29).

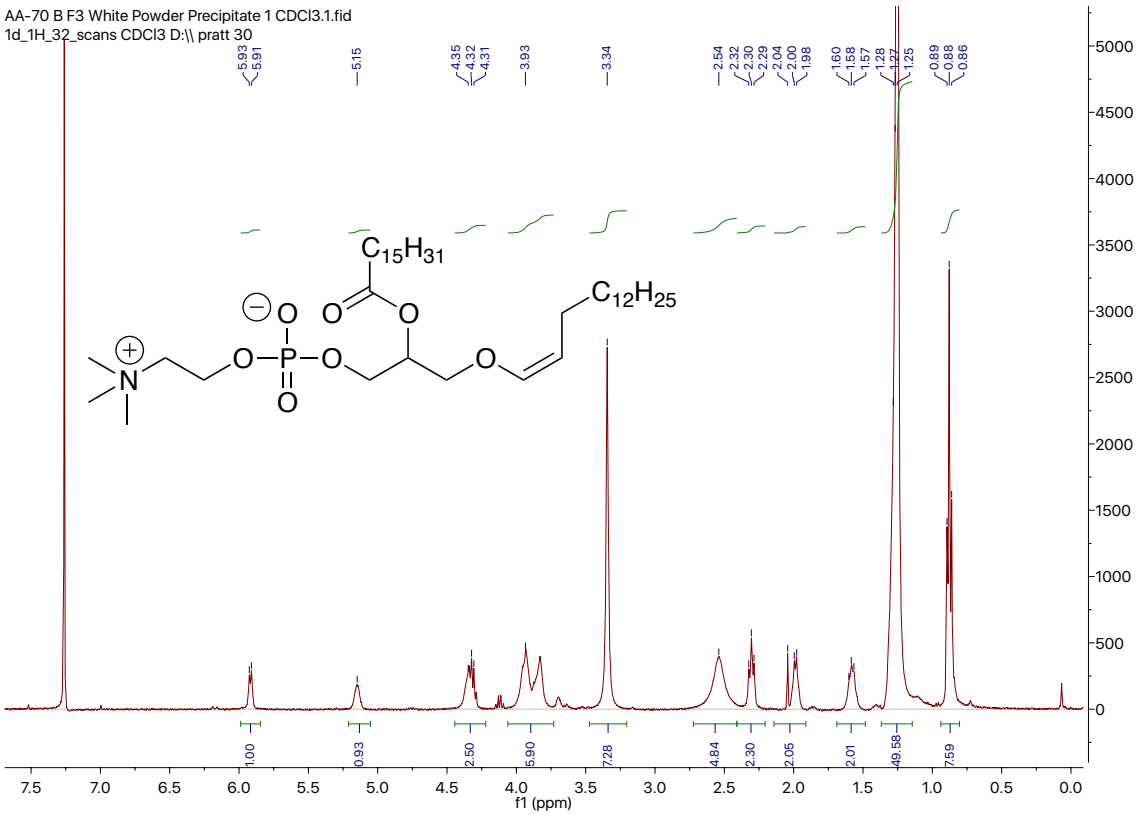

Figure 4.18 ^{1}H NMR ($CDCl_3$, 400 MHz) spectra of Plasmenylcholine (30). Result of first attempt at synthesis.

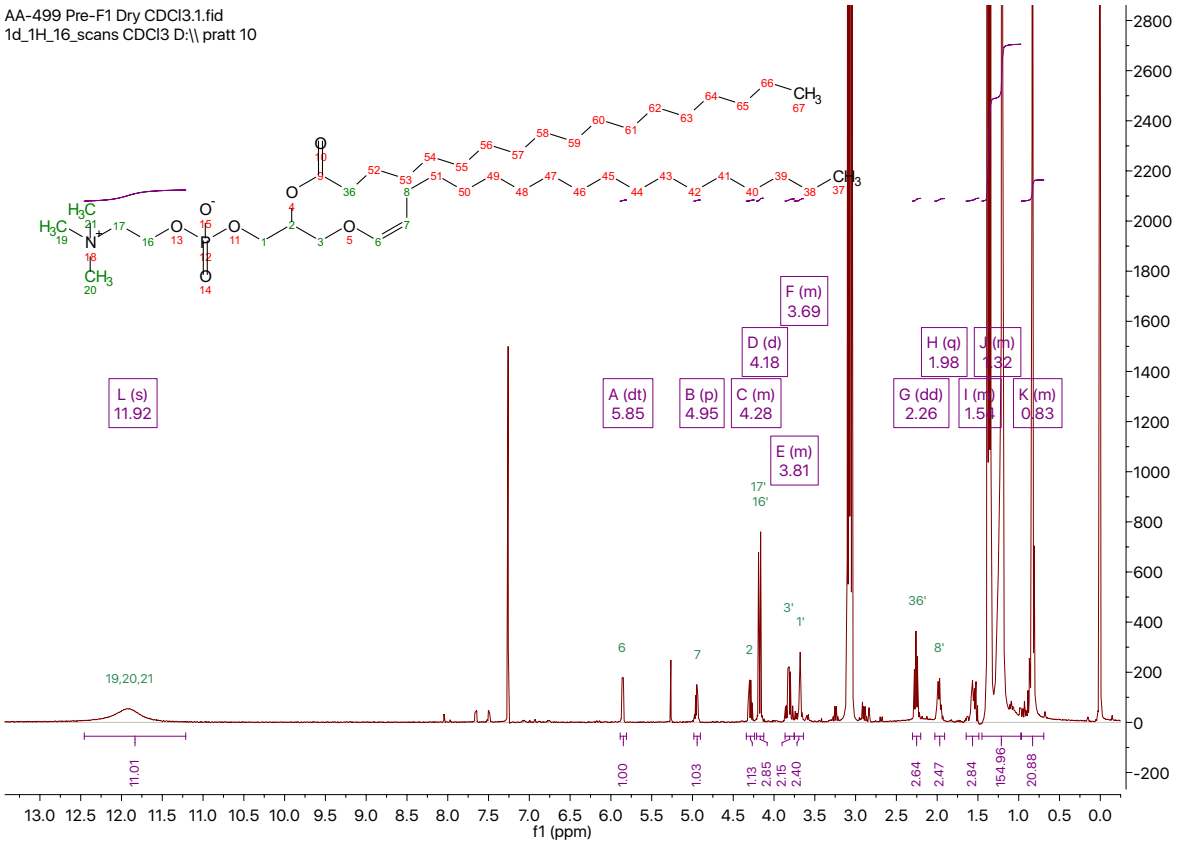

Figure 4.19 ^{1}H NMR ($CDCl_3$, 400 MHz) spectra of Plasmenylcholine (30).

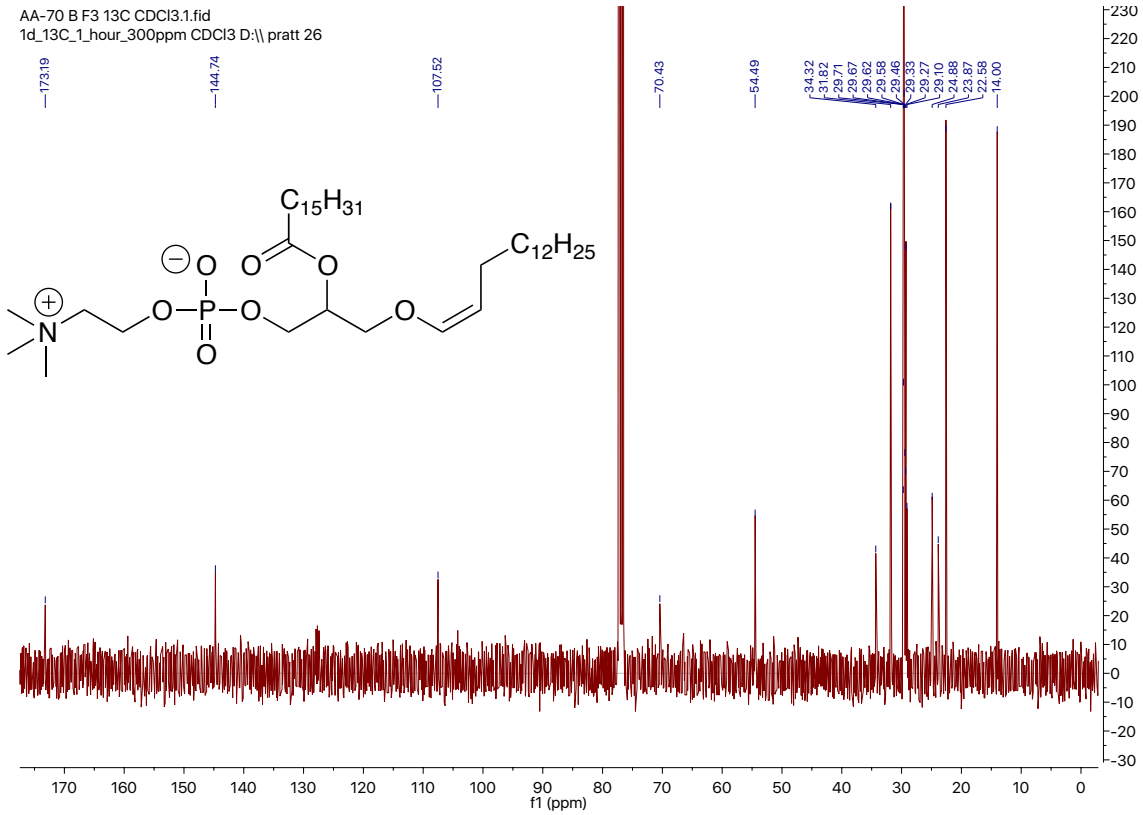

Figure 4.20 ^{13}C NMR ($CDCl_3$, 400 MHz) spectra of Plasmenylcholine (30).

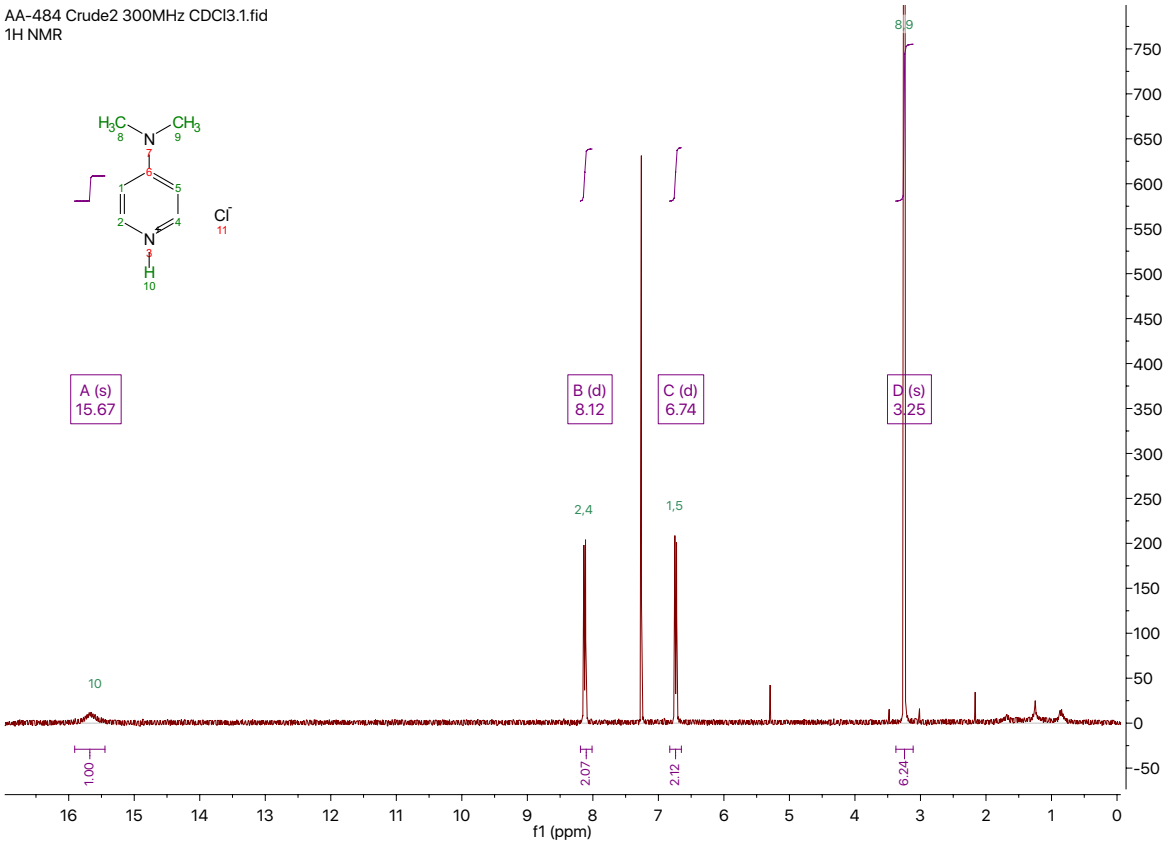

Figure 4.21 ^{1}H NMR ($CDCl_3$, 300 MHz) spectra of DMAP-HCl salt.

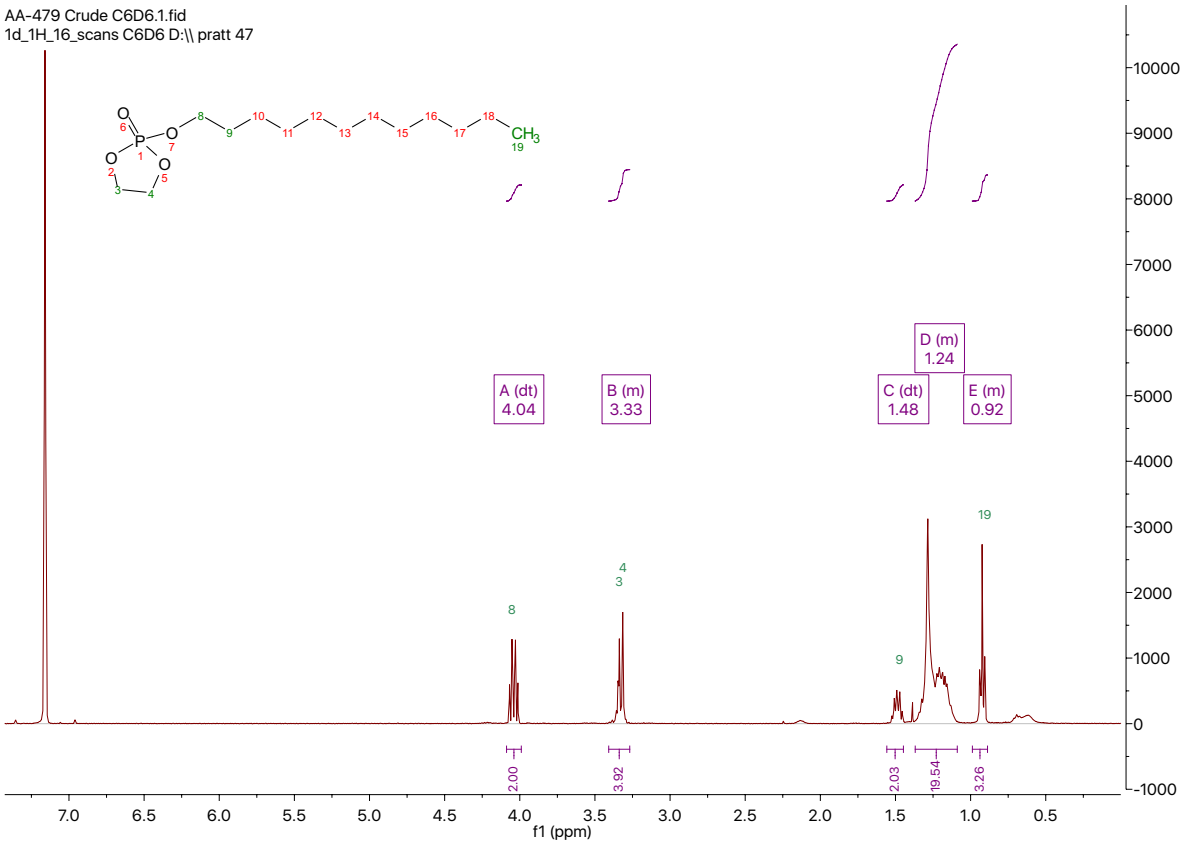

Figure 4.22 ^{1}H NMR (C_6D_6, 400 MHz) spectra of product of ethylene chlorophosphate addition to a primary alcohol (choline head addition test reaction).

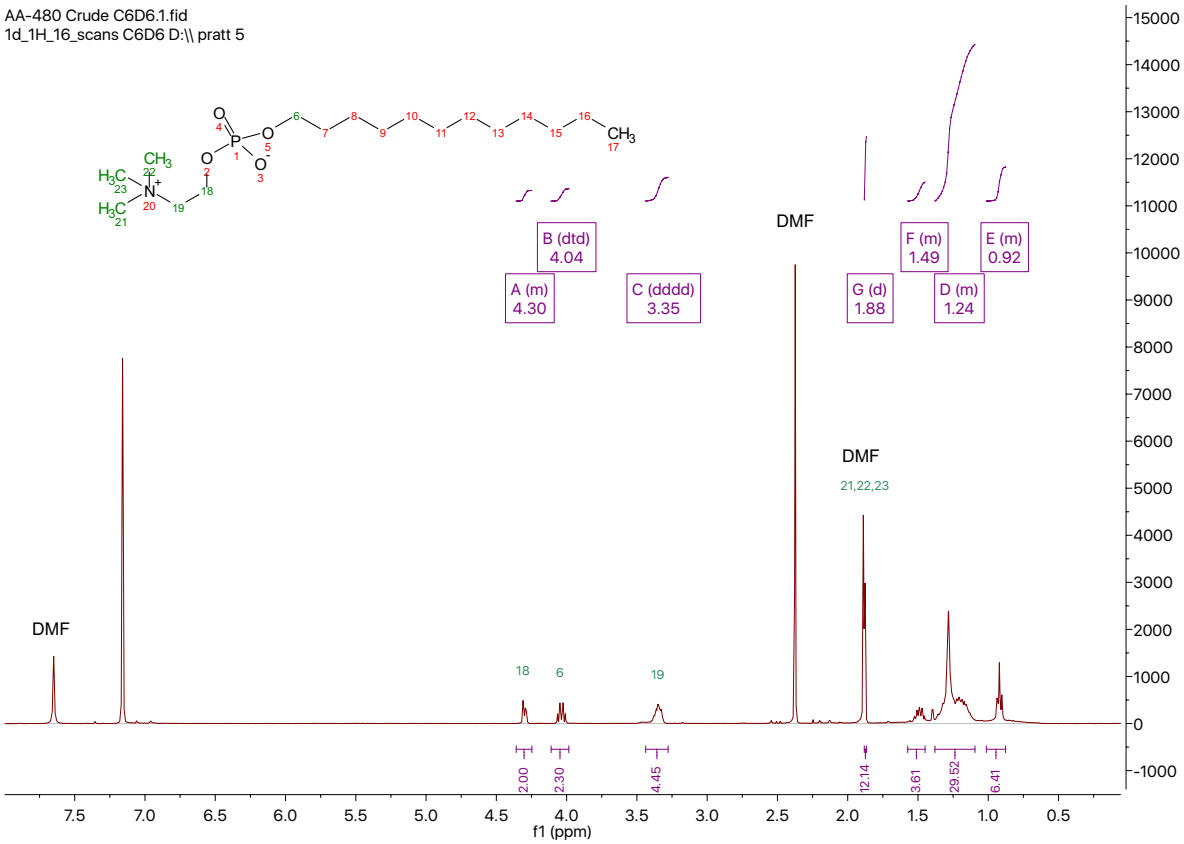

Figure 4.23 ^{1}H NMR (C_6D_6, 400 MHz) spectra of product of phosphate ring opening via trimethylamine.

Model Substrate:

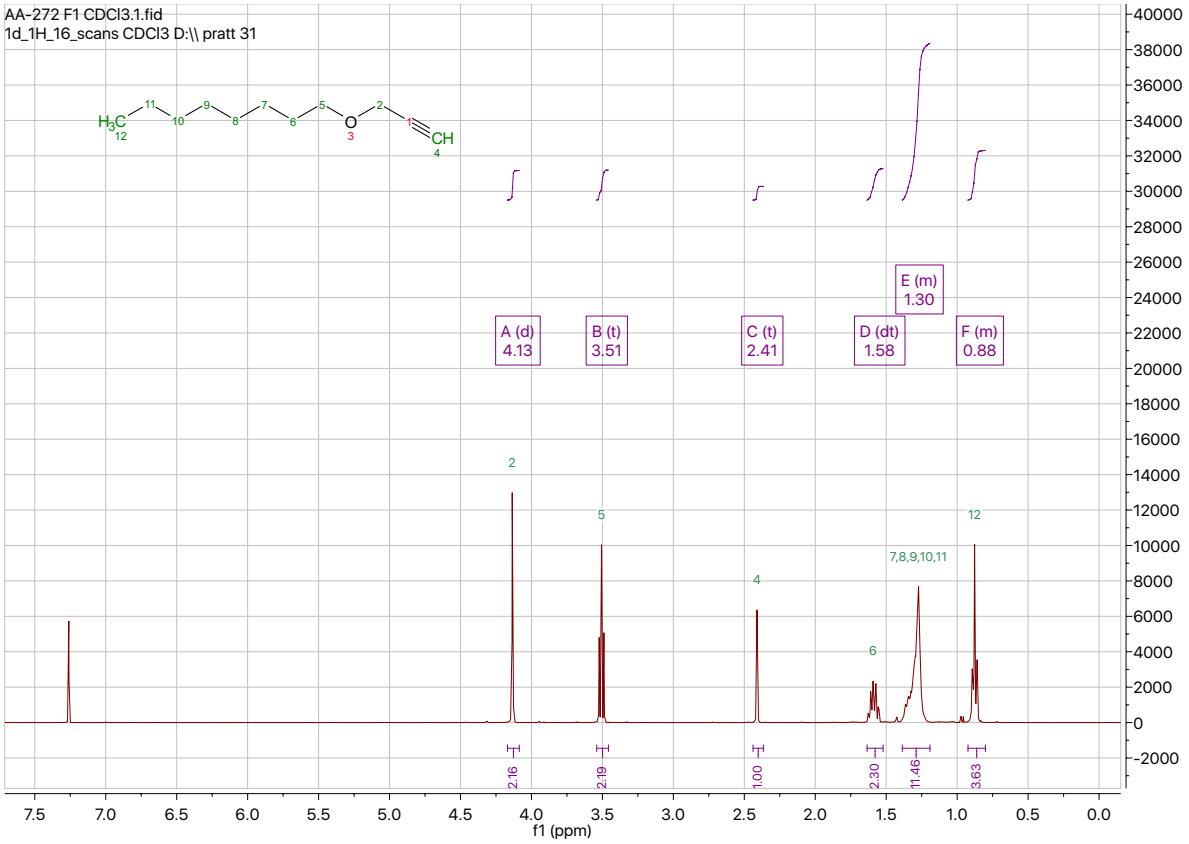

Figure 4.24 ^{1}H NMR ($CDCl_3$, 400 MHz) spectra of 1-(prop-2-yn-1-yloxy)hexane (31).

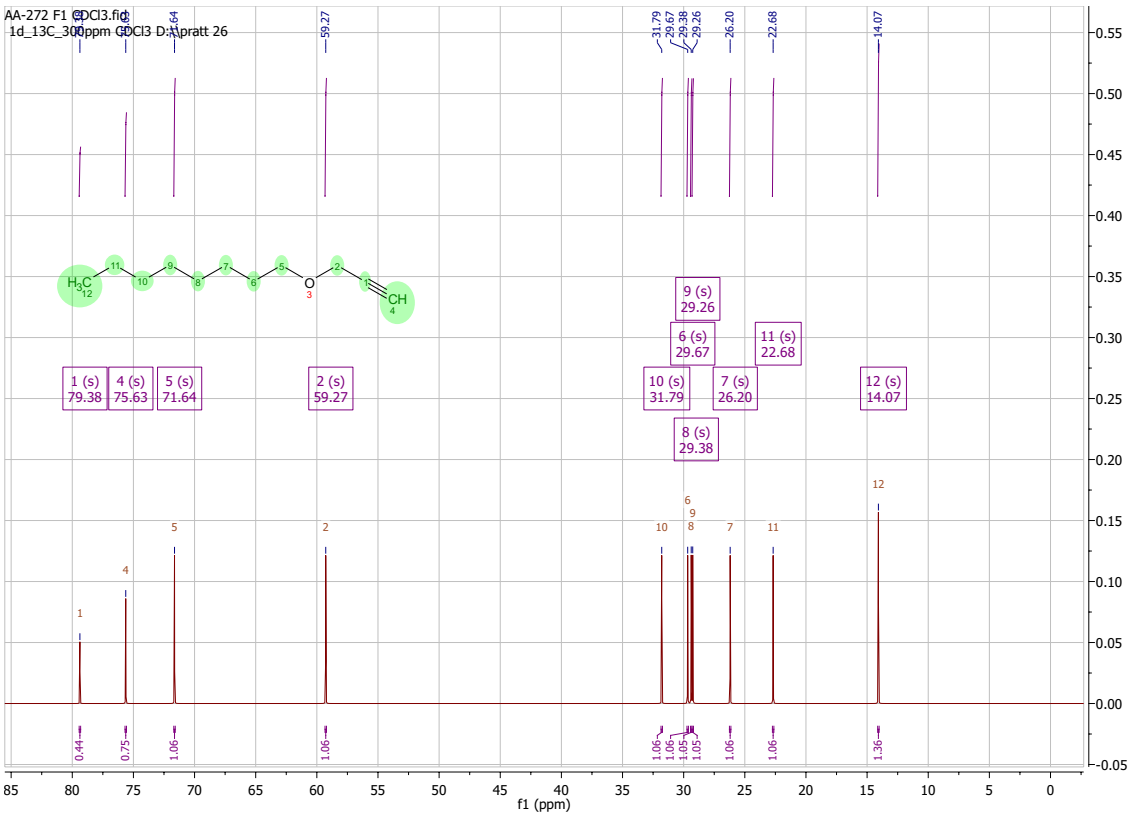

Figure 4.25 ^{13}C NMR ($CDCl_3$, 400 MHz) predicted spectra of 1-(prop-2-yn-1-yloxy)hexane (31).

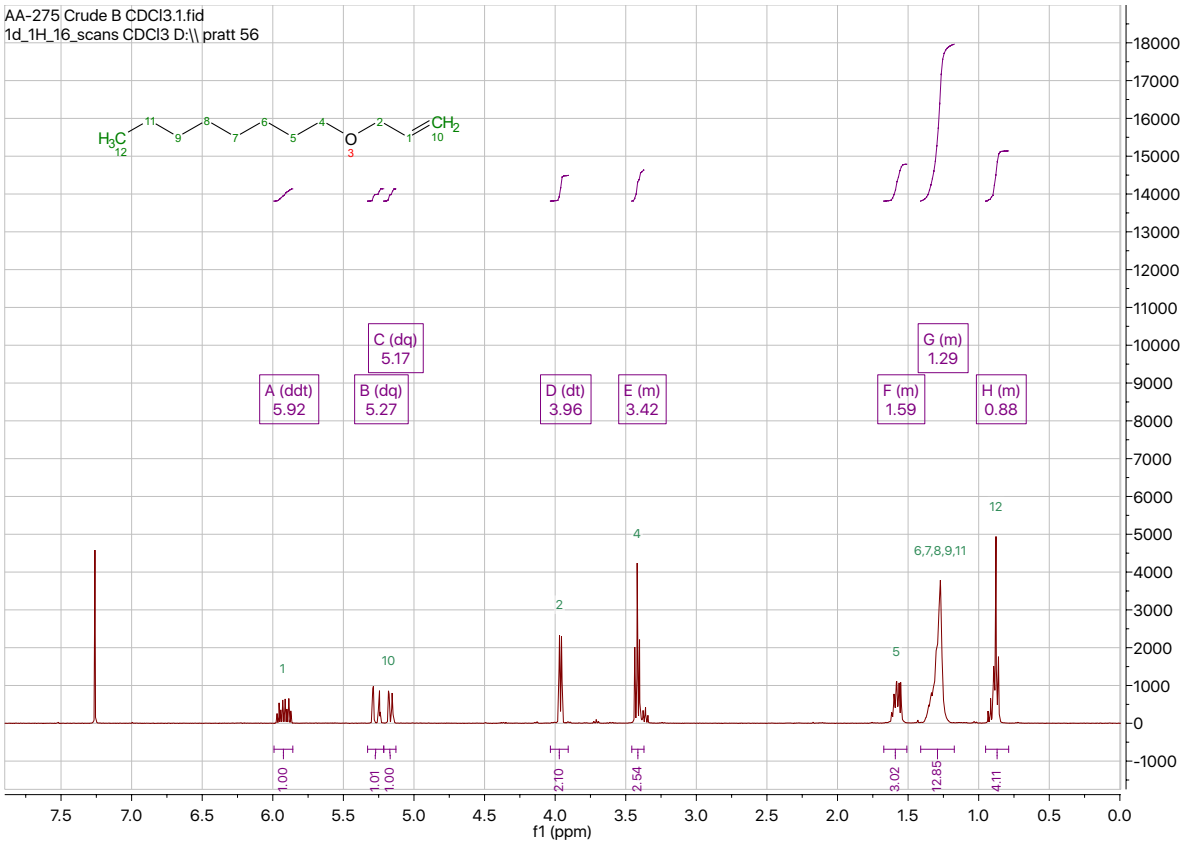

Figure 4.26 ^{1}H NMR ($CDCl_3$, 400 MHz) spectra of 1-(allyloxy)hexane (32).

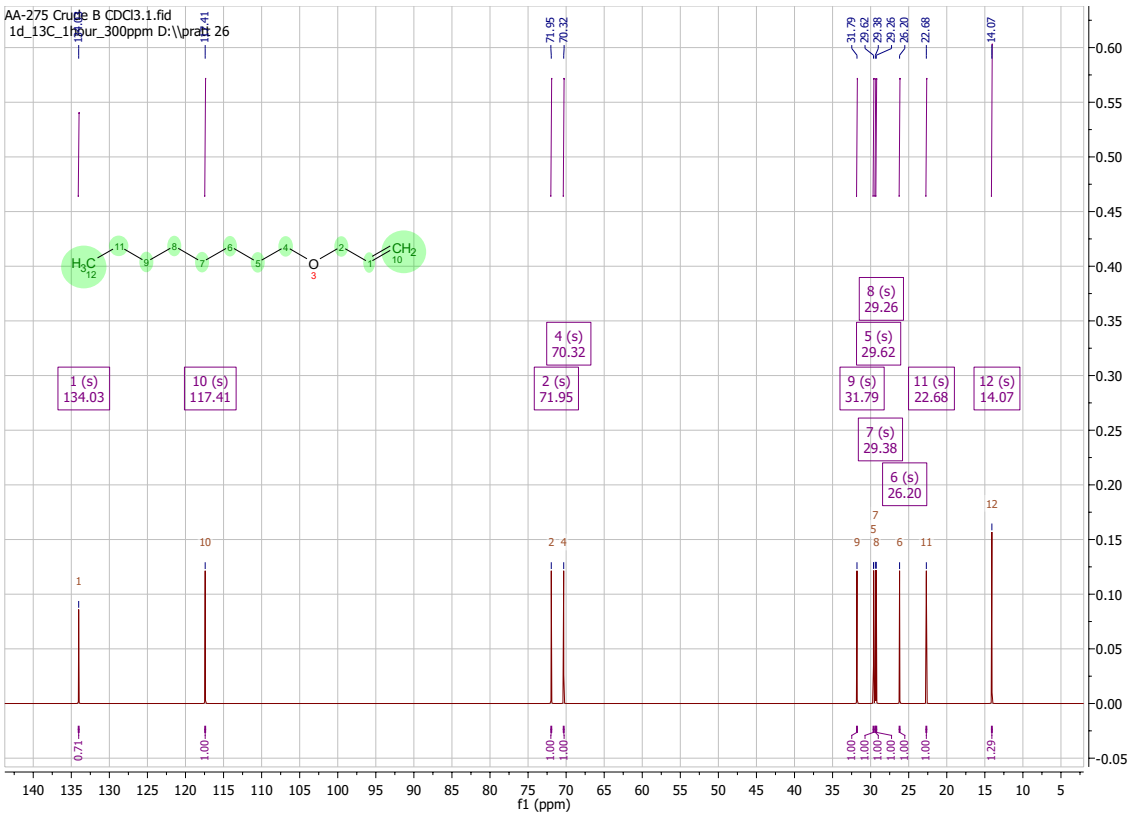

Figure 4.27 ^{1}H NMR ($CDCl_3$, 400 MHz) predicted spectra of 1-(allyloxy)hexane (32).

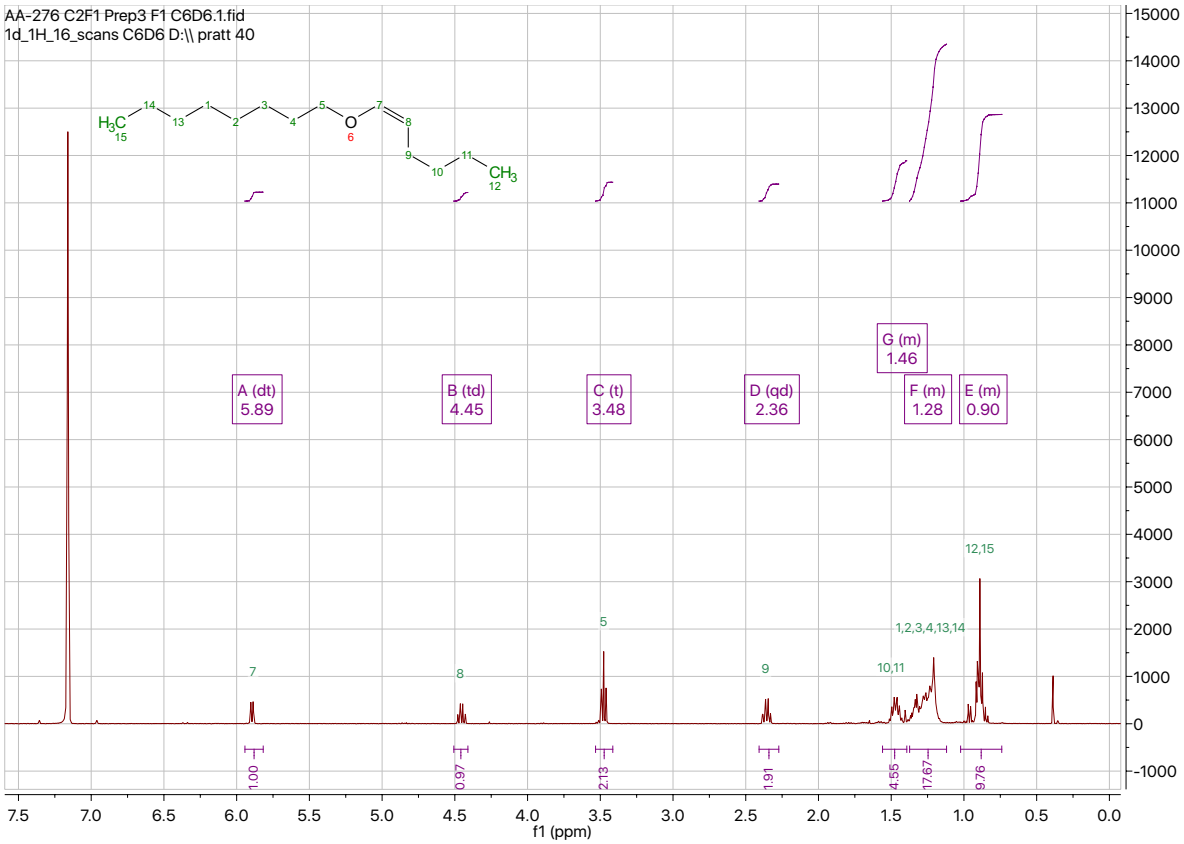

Figure 4.28 ^{1}H NMR (C_6D_6, 400 MHz) spectra of (*Z*)-1-(heptyloxy)hept-1-ene (33).

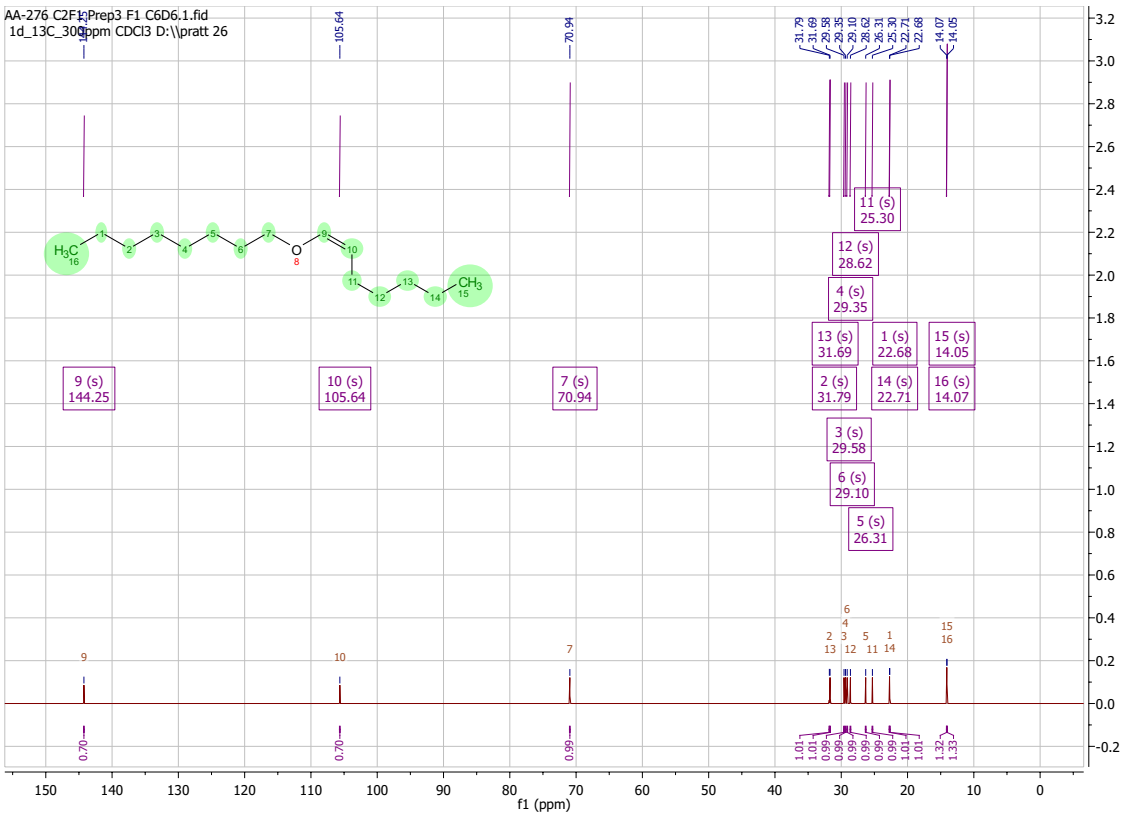

Figure 4.29 ^{13}C NMR (C_6D_6, 400 MHz) predicted spectra of (*Z*)-1-(heptyloxy)hept-1-ene (33).

Deuterated Model Substrate:

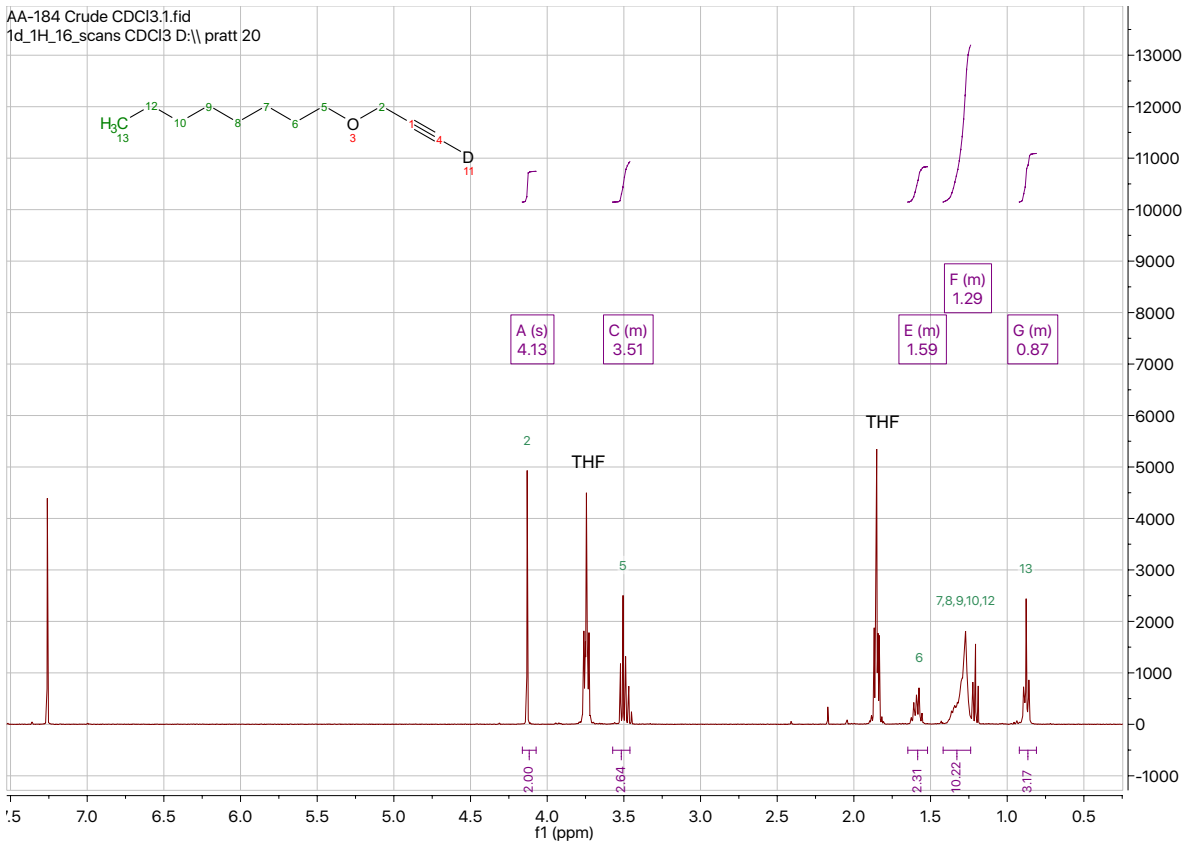

Figure 4.30 ^{1}H NMR ($CDCl_3$, 400 MHz) spectra of 1-(prop-2-yn-1-yloxy)hexane-d_1 (34).

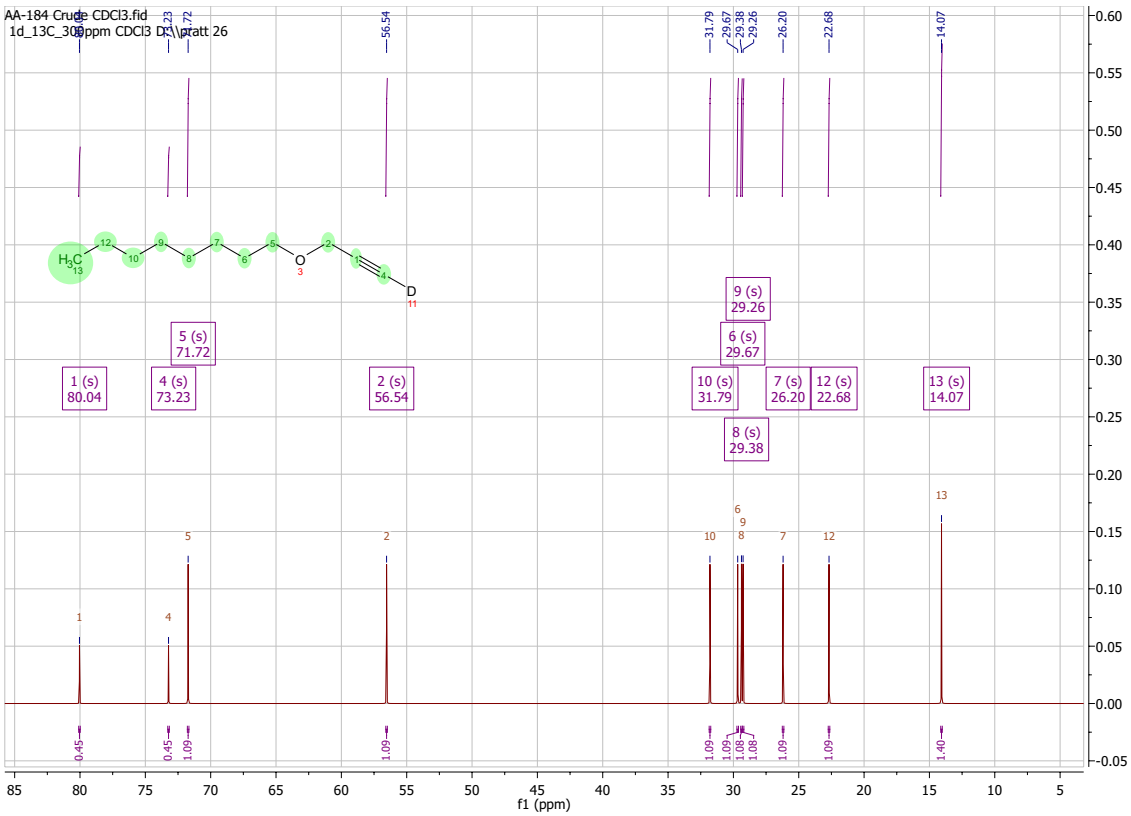

Figure 4.31 ^{13}C NMR ($CDCl_3$, 400 MHz) predicted spectra of 1-(prop-2-yn-1-yloxy)hexane-d_1 (34).

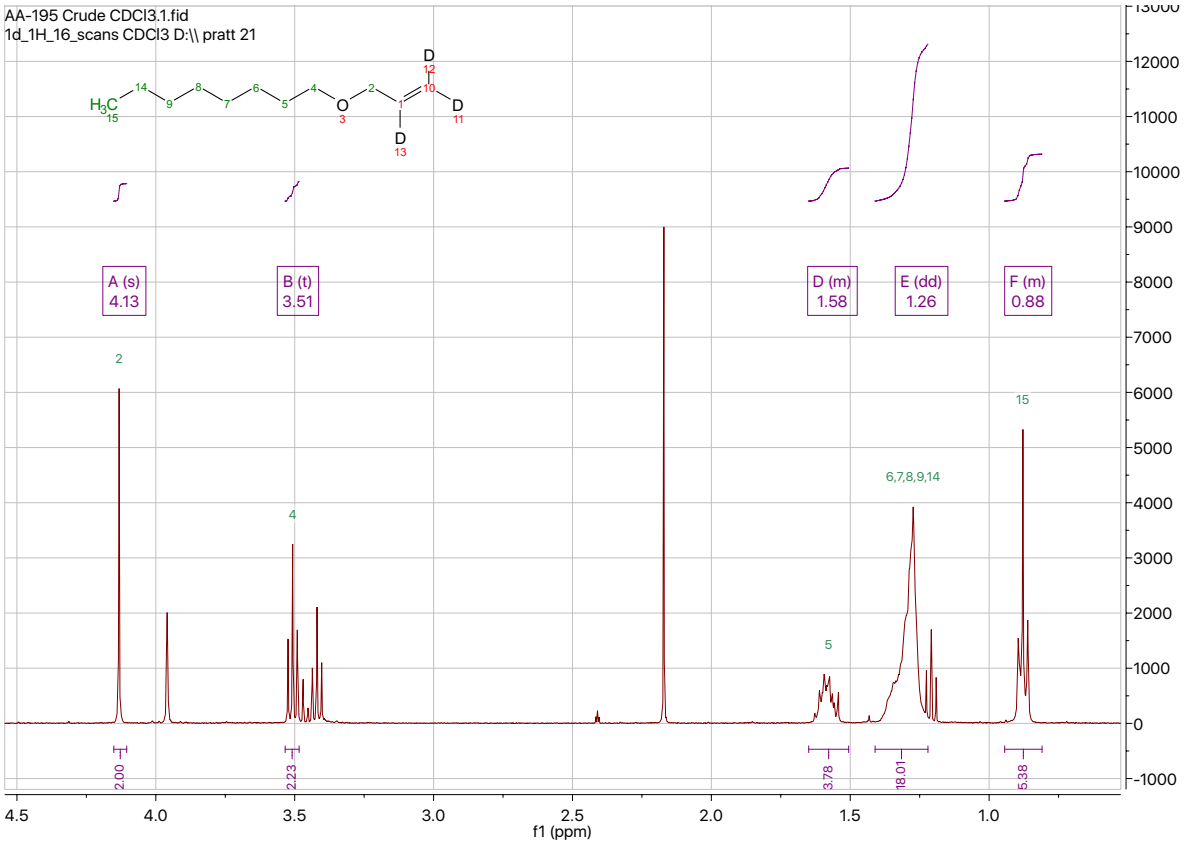

Figure 4.32 ^{1}H NMR ($CDCl_3$, 400 MHz) spectra of 1-(allyloxy)hexane-d_3 (35).

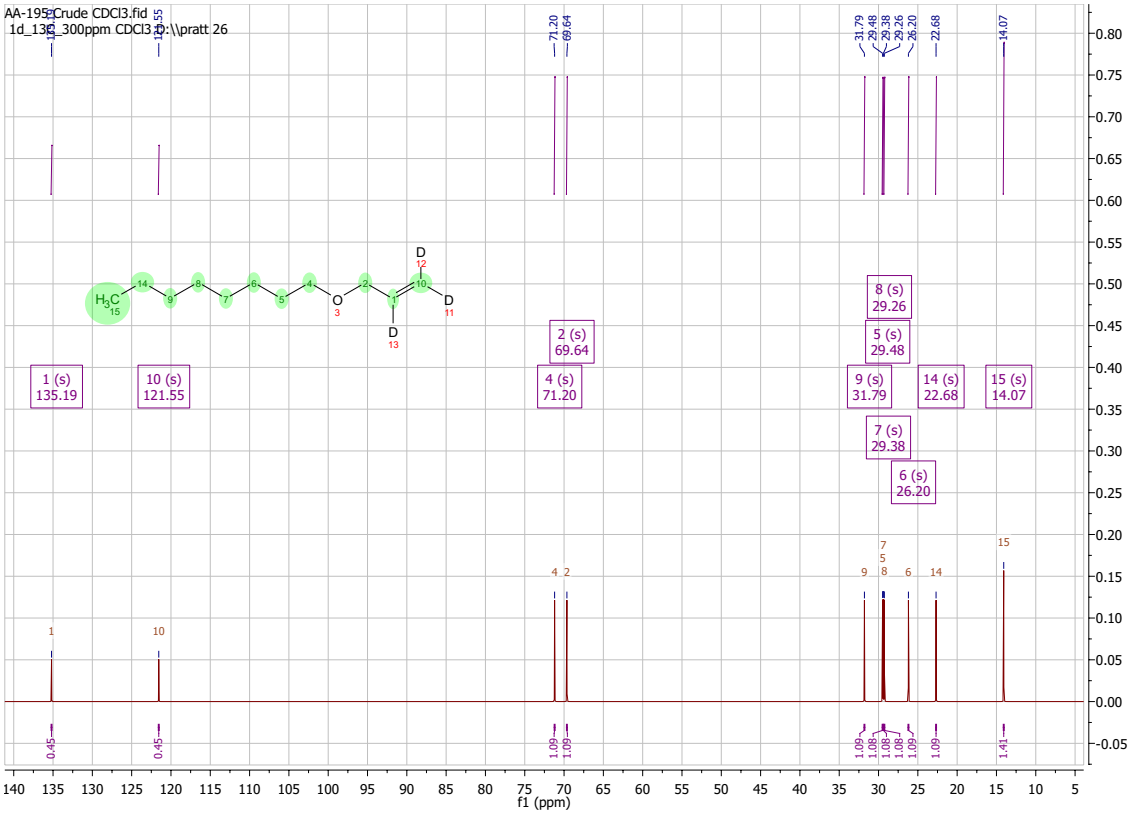

Figure 4.33 ^{13}C NMR ($CDCl_3$, 400 MHz) predicted spectra of 1-(allyloxy)hexane-d_3 (35).

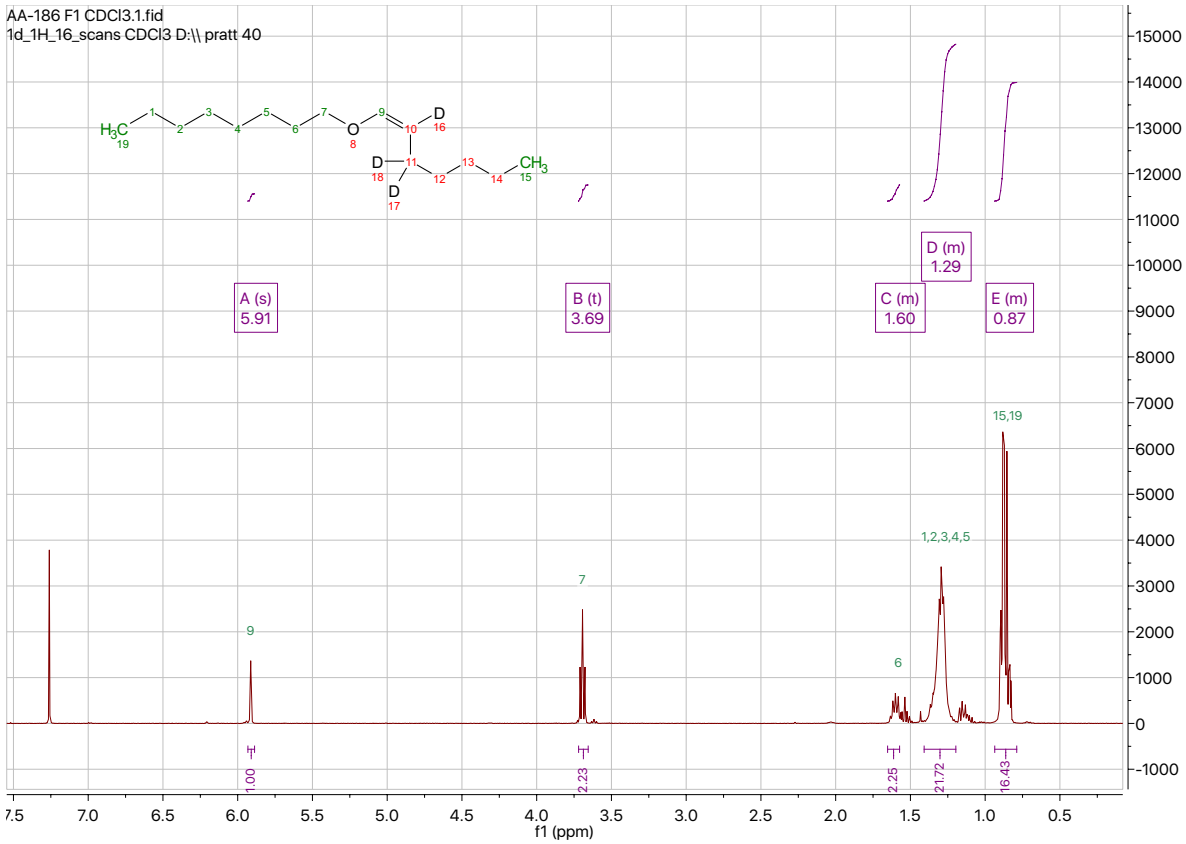

Figure 4.34 ^{1}H NMR ($CDCl_3$, 400 MHz) spectra of d_3-(*Z*)-1-(heptyloxy)hept-1-ene (36).

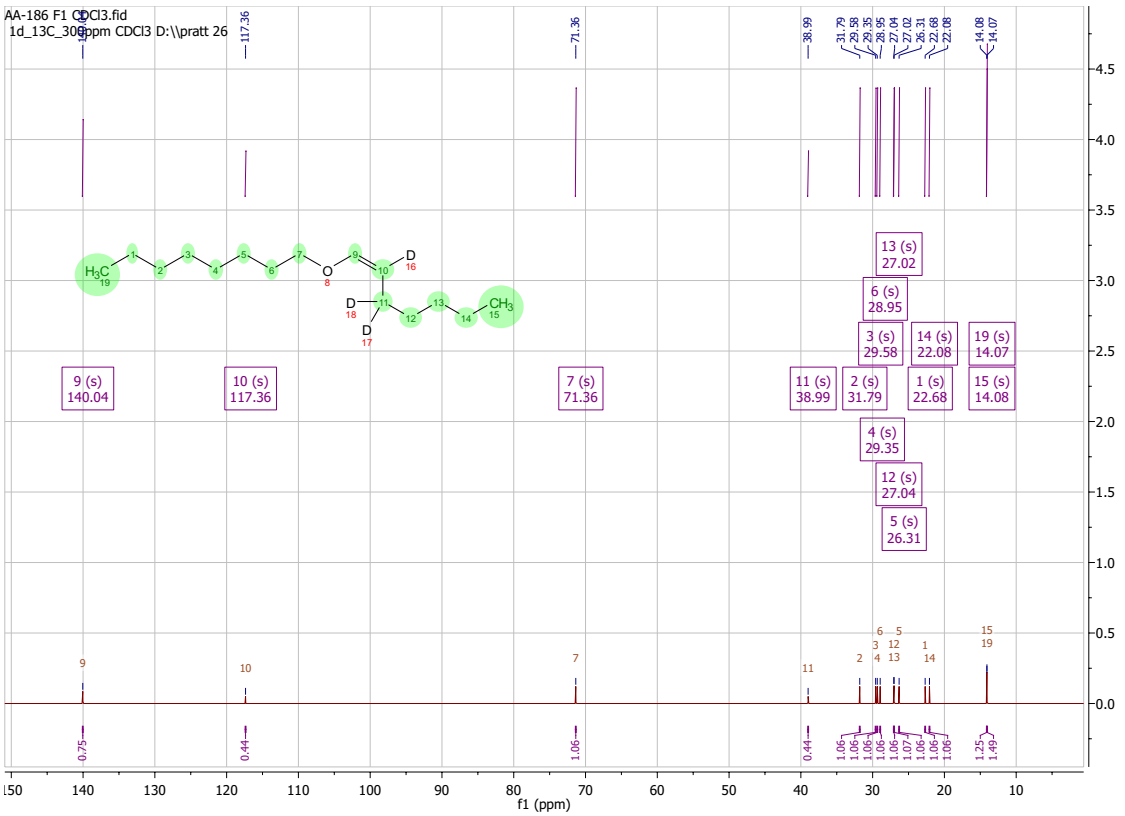

Figure 4.35 ^{13}C NMR ($CDCl_3$, 400 MHz) spectra of d_3-(*Z*)-1-(heptyloxy)hept-1-ene (36).

Appendix B – Spectral Data

Methyl Oleate:

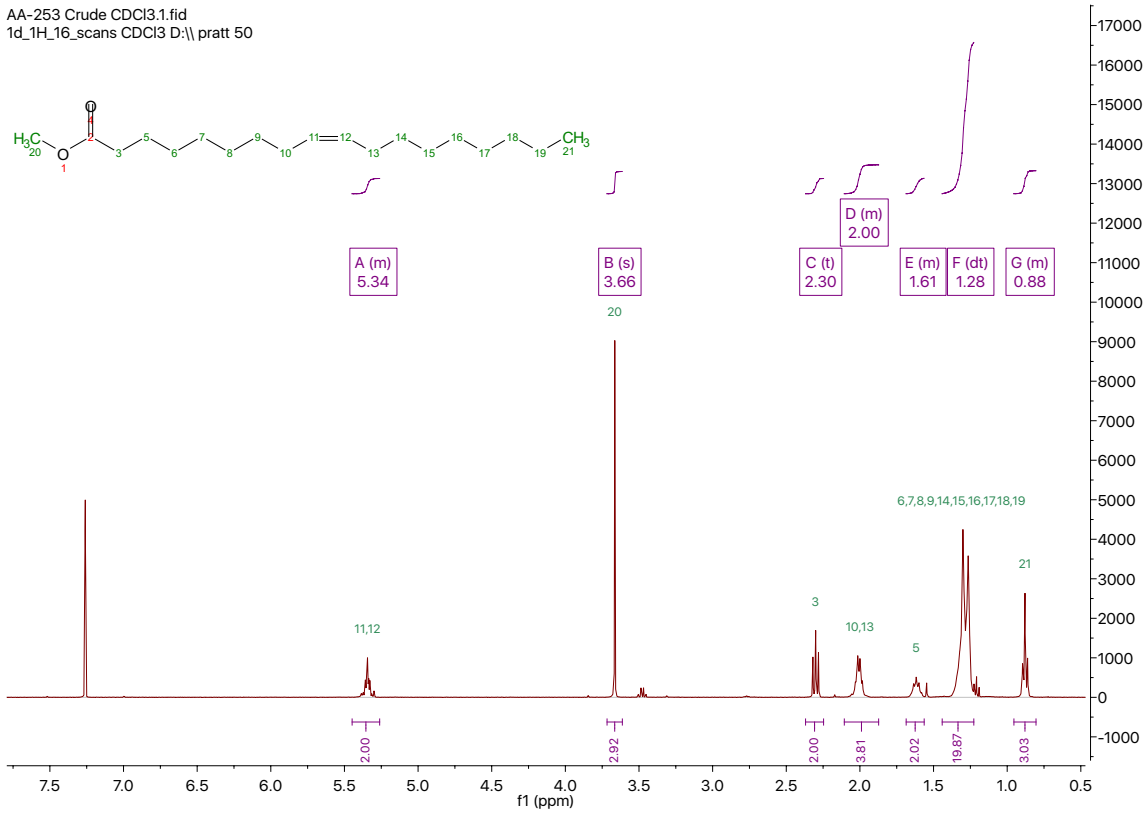

Figure 4.36 ^{1}H NMR ($CDCl_3$, 400 MHz) spectra of Methyl Oleate (47).

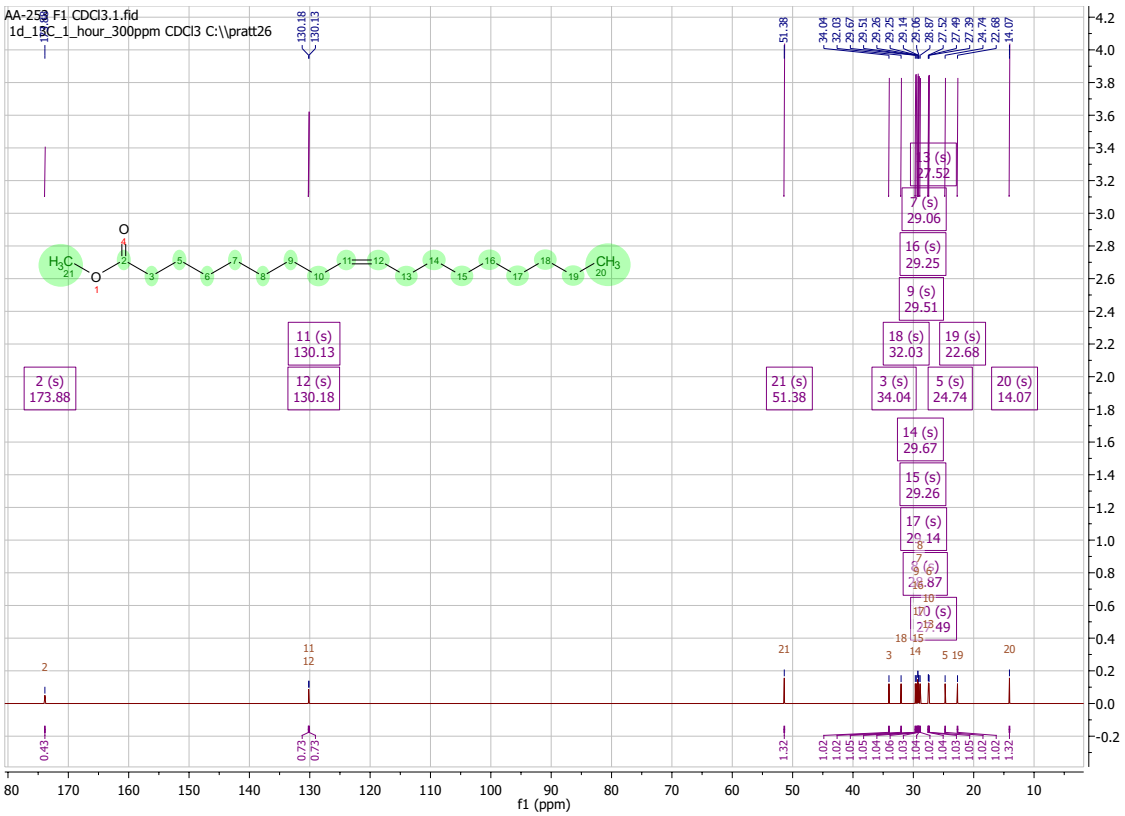

Figure 4.37 ^{13}C NMR ($CDCl_3$, 400MHz) predicted spectra of Methyl Oleate (47).

d_4-Methyl Oleate:

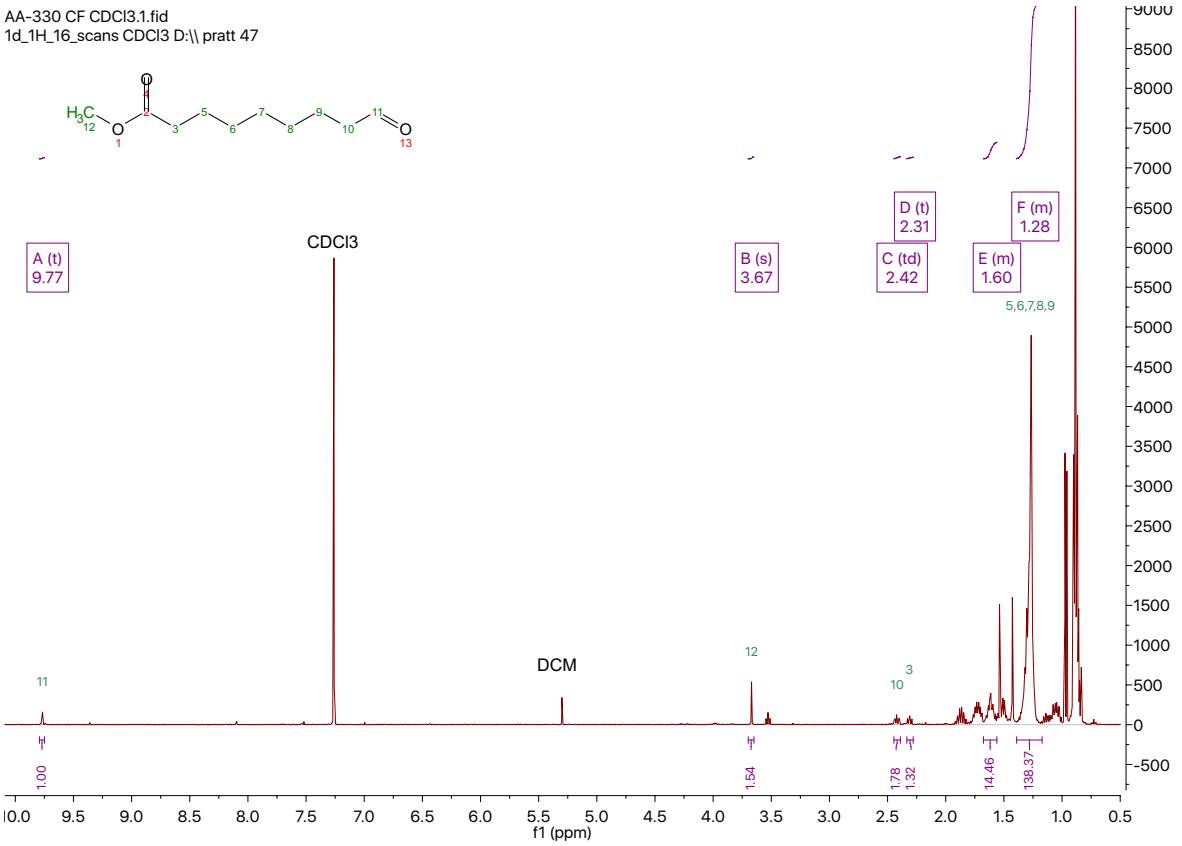

Figure 4.38 ^{1}H NMR ($CDCl_3$, 400 MHz) spectra of Methyl-9-oxononanoate (48).

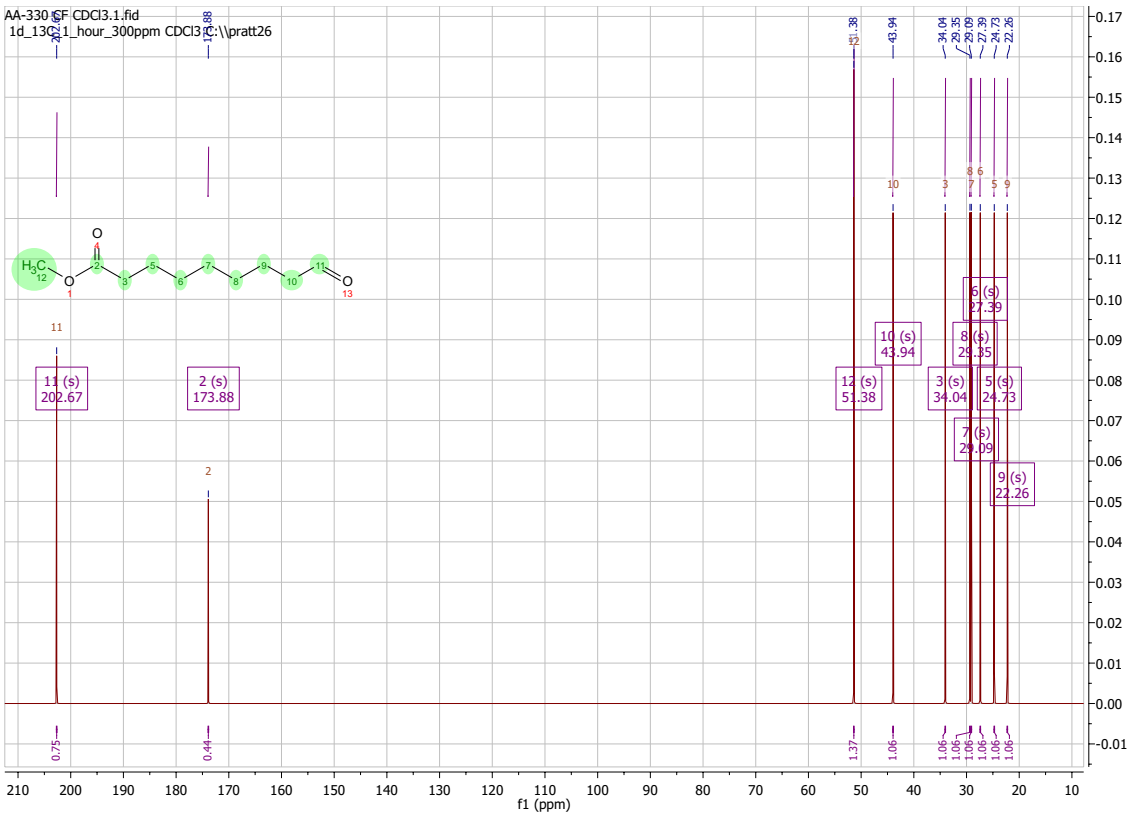

Figure 4.39 ^{13}C NMR ($CDCl_3$, 400MHz) predicted spectra of Methyl-9-oxononanoate (48).

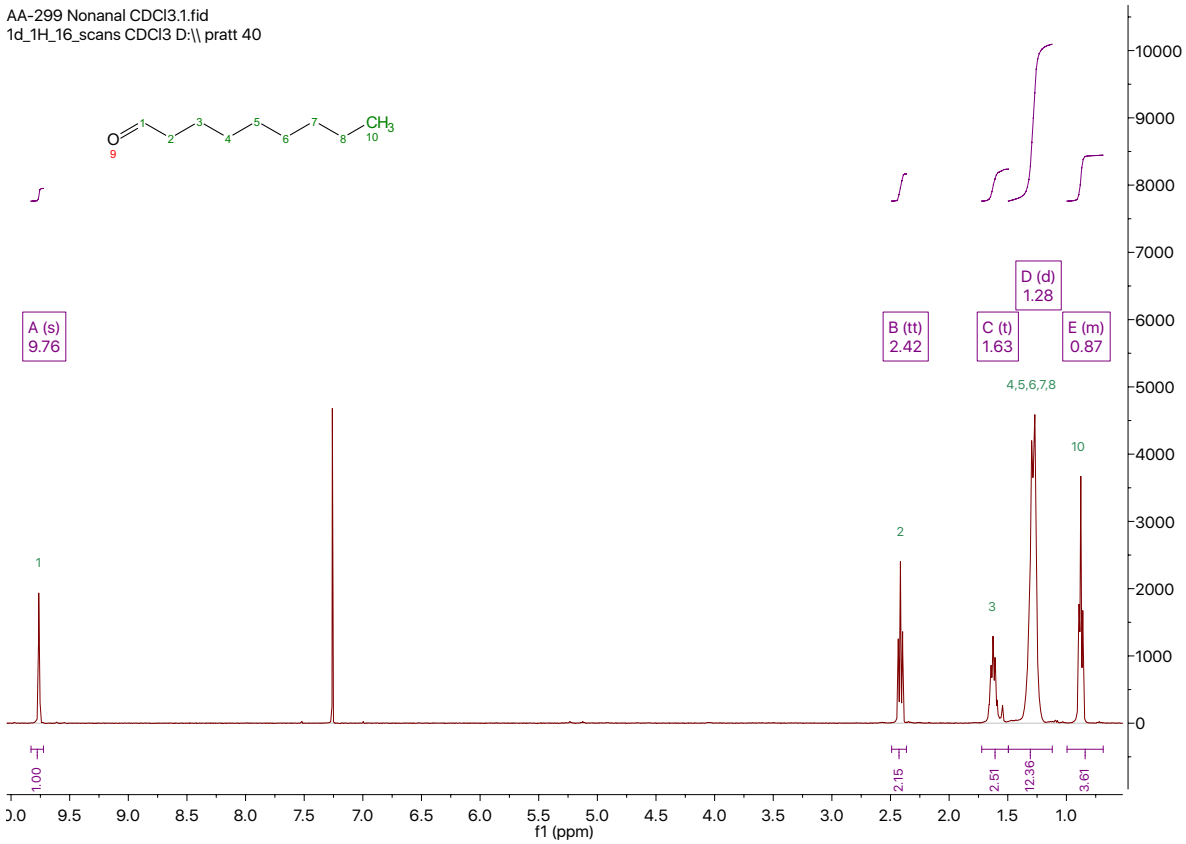

Figure 4.40 ^{1}H NMR ($CDCl_3$, 400MHz) spectra of 1-Nonanal (49).

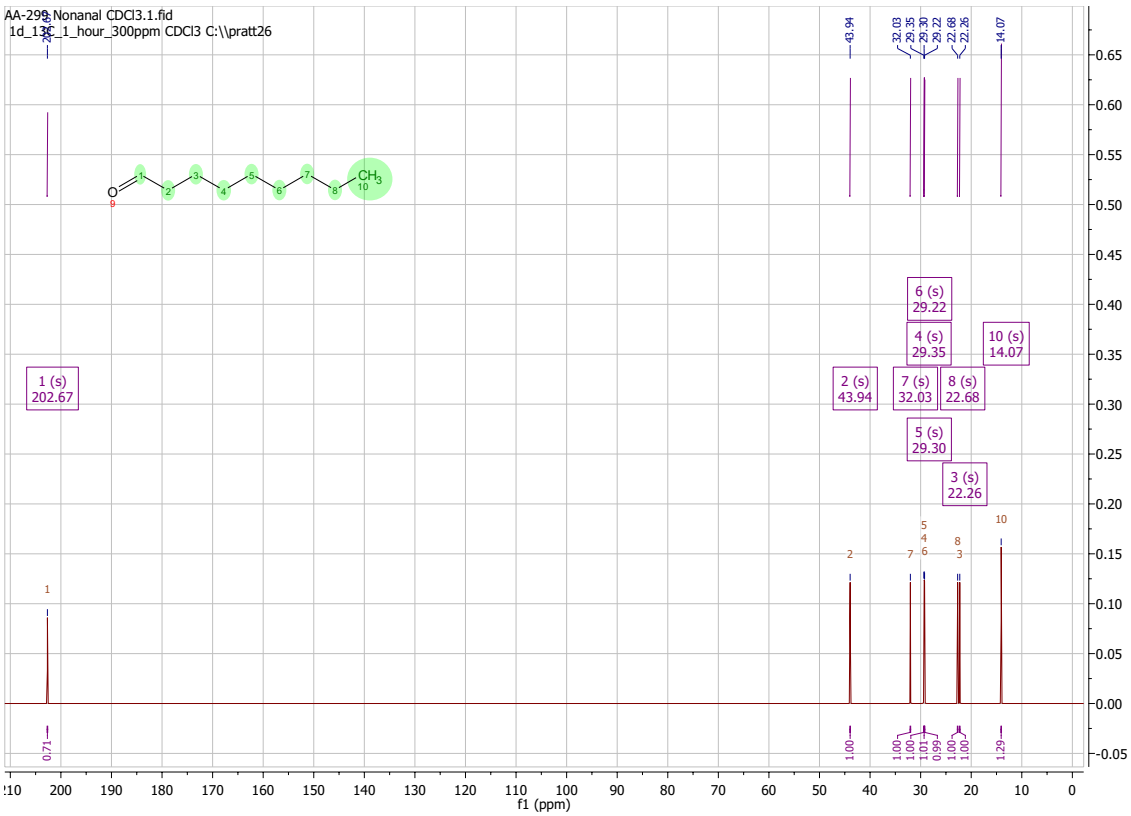

Figure 4.41 ^{13}C NMR ($CDCl_3$, 400 MHz) predicted spectra of 1-Nonanal (49).

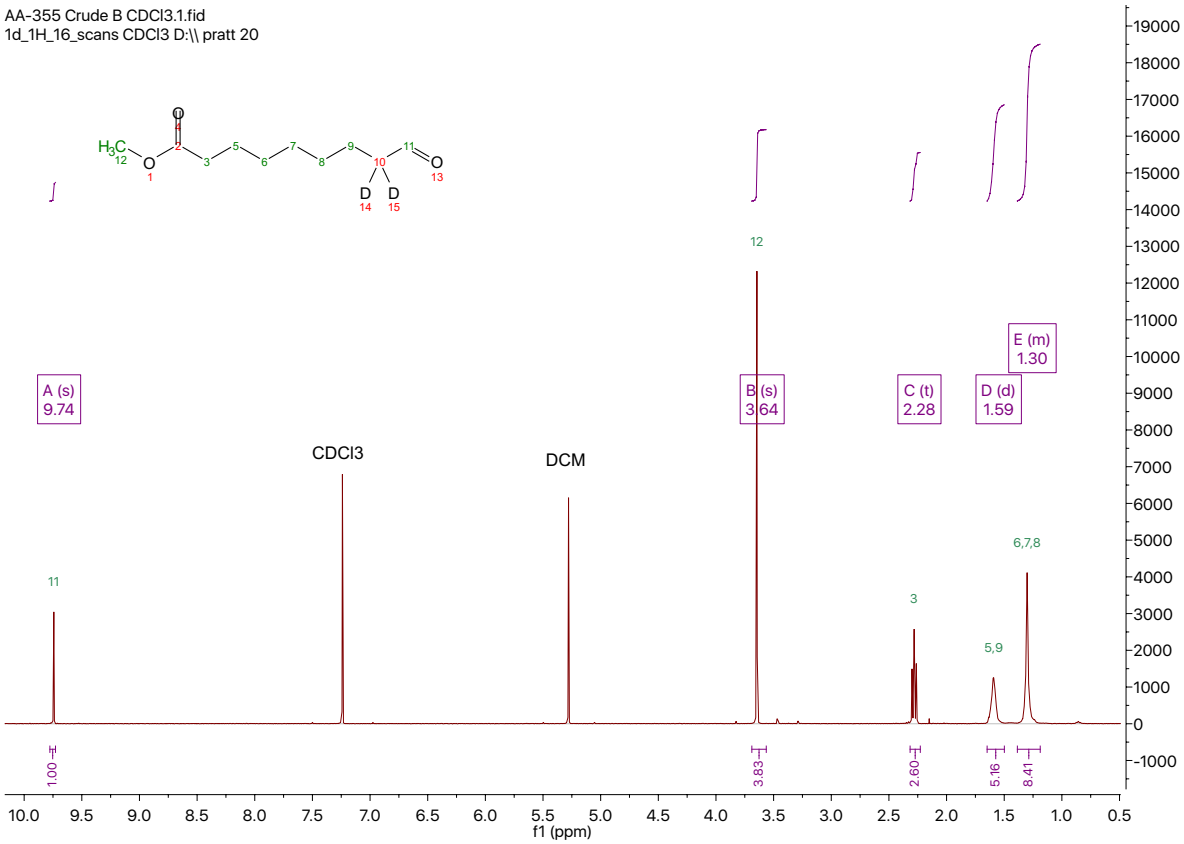

Figure 4.42 ^{1}H NMR ($CDCl_3$, 400 MHz) spectra of Methyl-9-oxononanoate-d_2 (50).

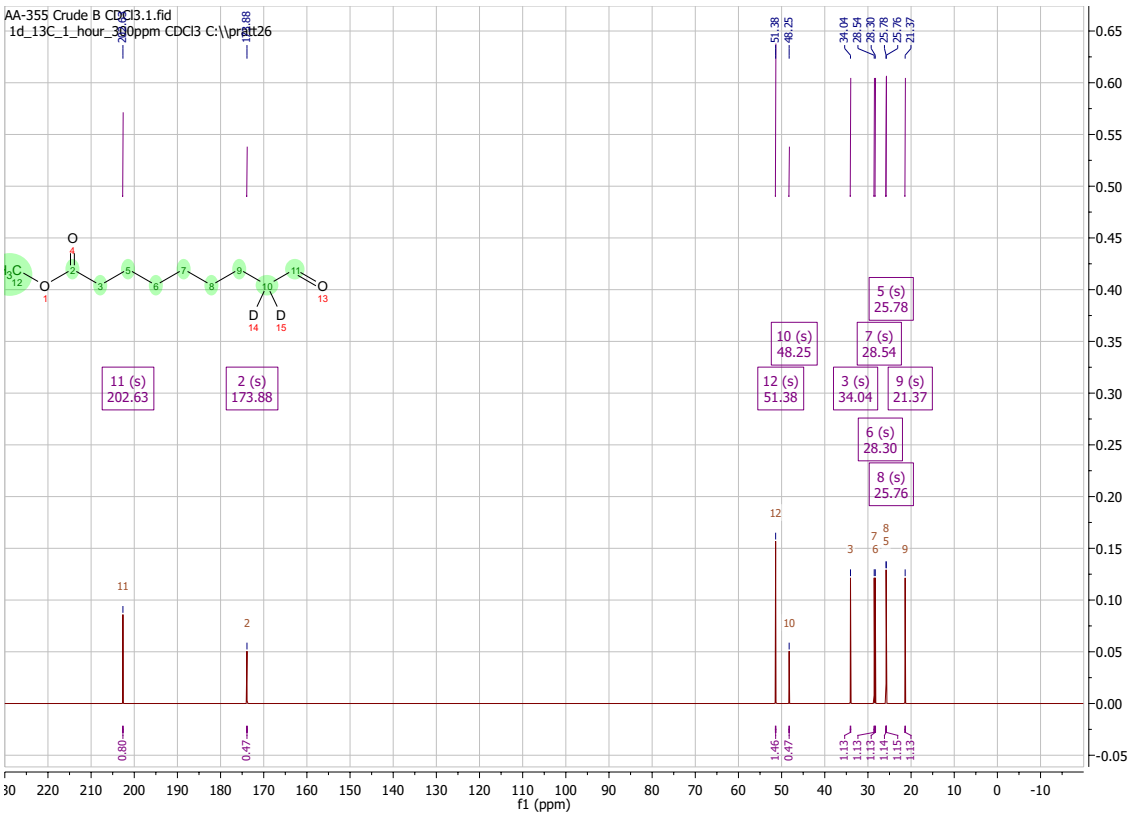

Figure 4.43 ^{13}C NMR ($CDCl_3$, 400 MHz) predicted spectra of Methyl-9-oxononanoate-d_2 (50).

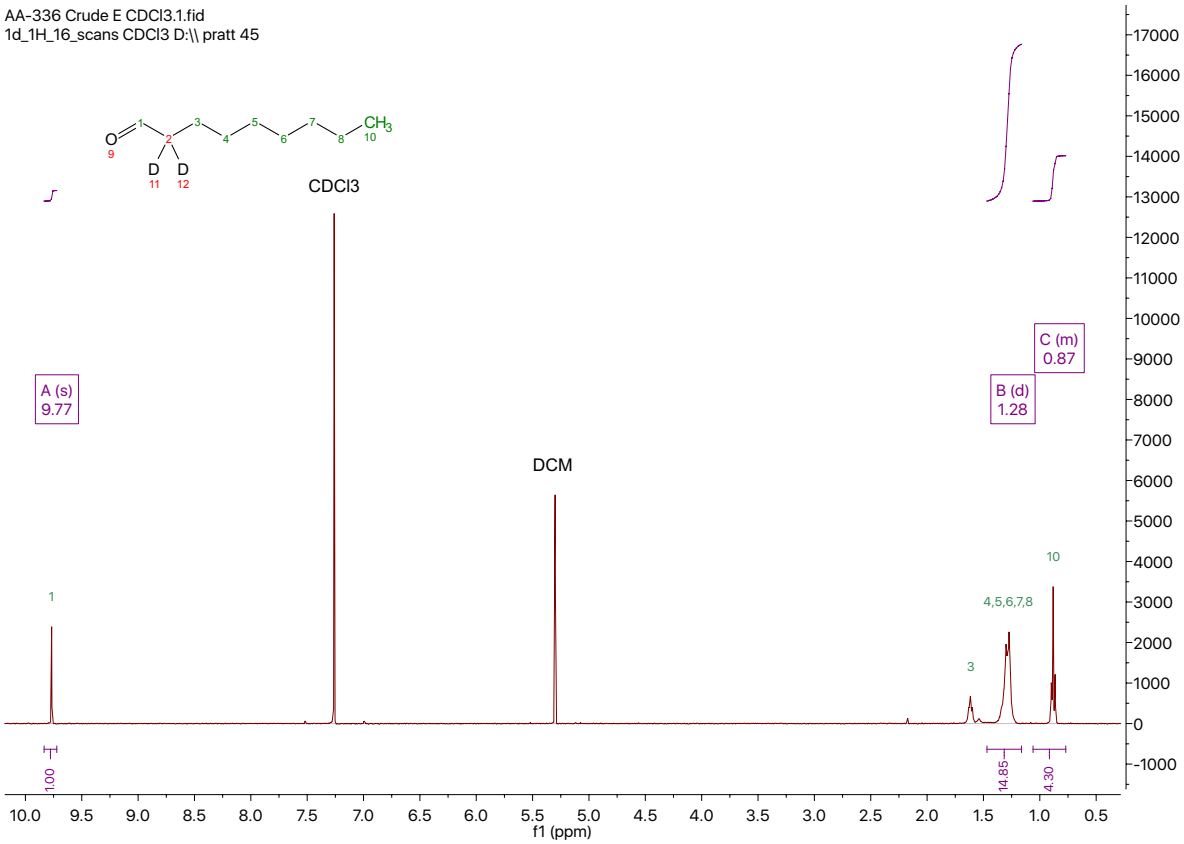

Figure 4.44 ^{1}H NMR ($CDCl_3$, 400 MHz) spectra of 1-Nonanal-d_2 (51).

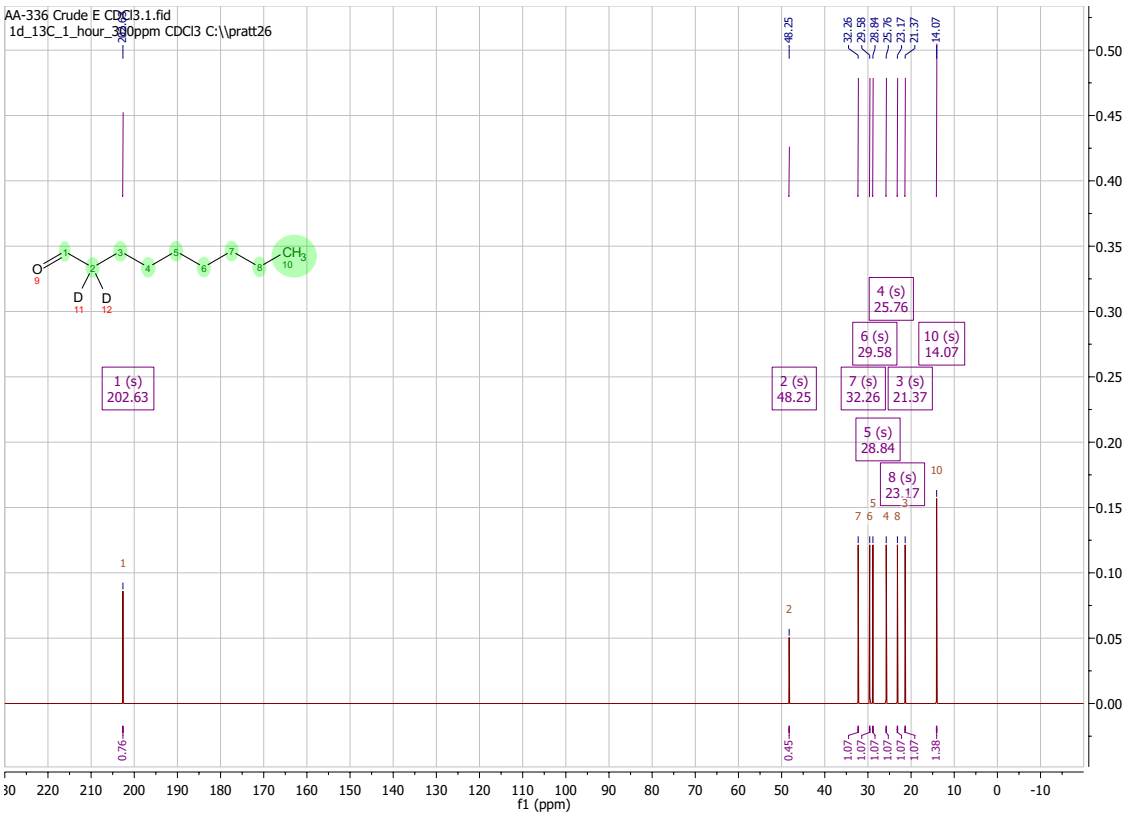

Figure 4.45 ^{13}C NMR ($CDCl_3$, 400 MHz) predicted spectra of 1-Nonanal-d_2 (51).

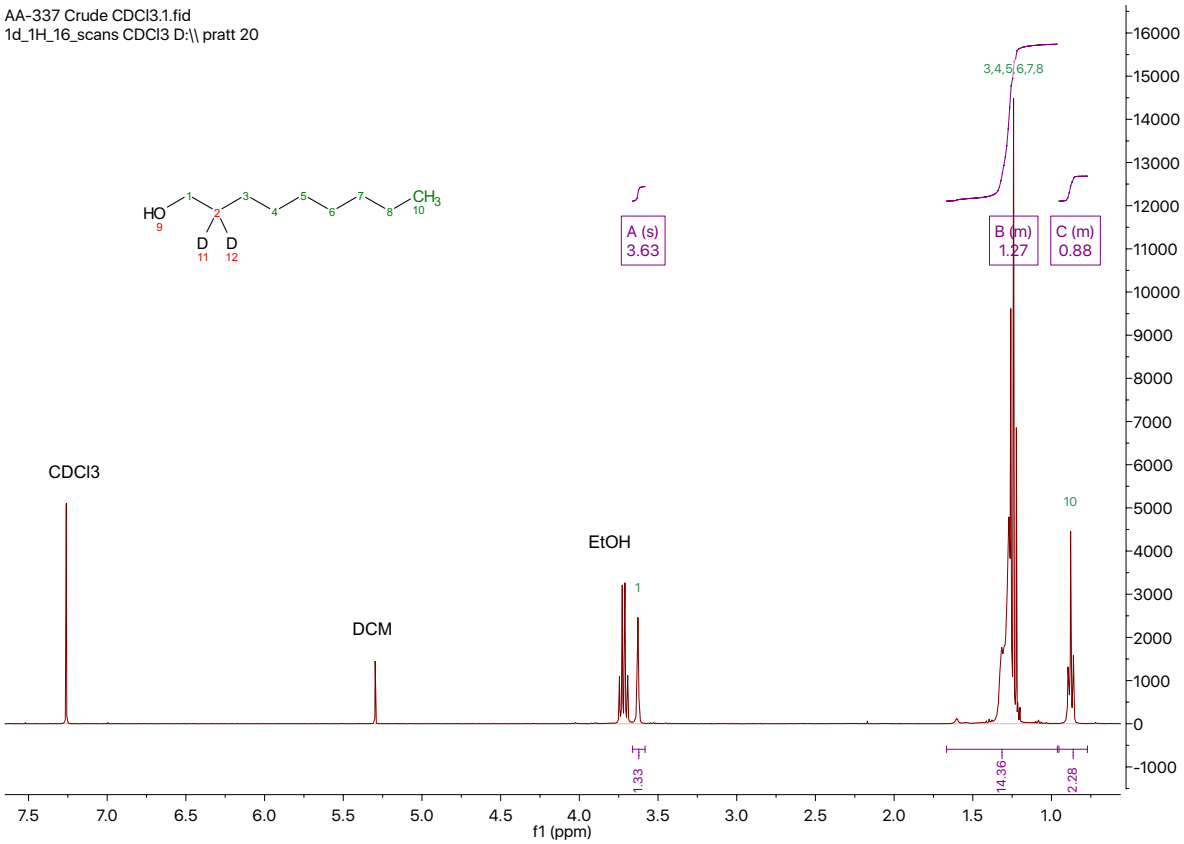

Figure 4.46 ^{1}H NMR ($CDCl_3$, 400 MHz) spectra of 1-Nonanol-d_2 (52).

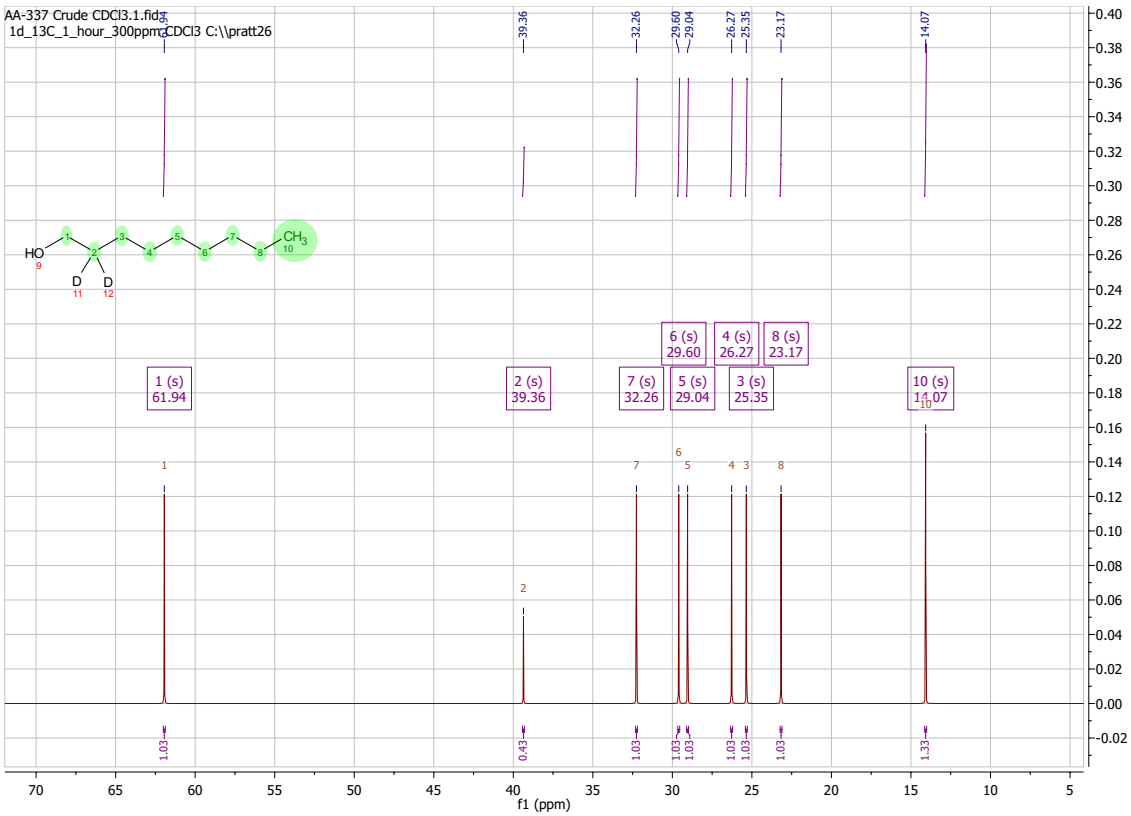

Figure 4.47 ^{13}C NMR ($CDCl_3$, 400 MHz) predicted spectra of 1-Nonanol-d_2 (52).

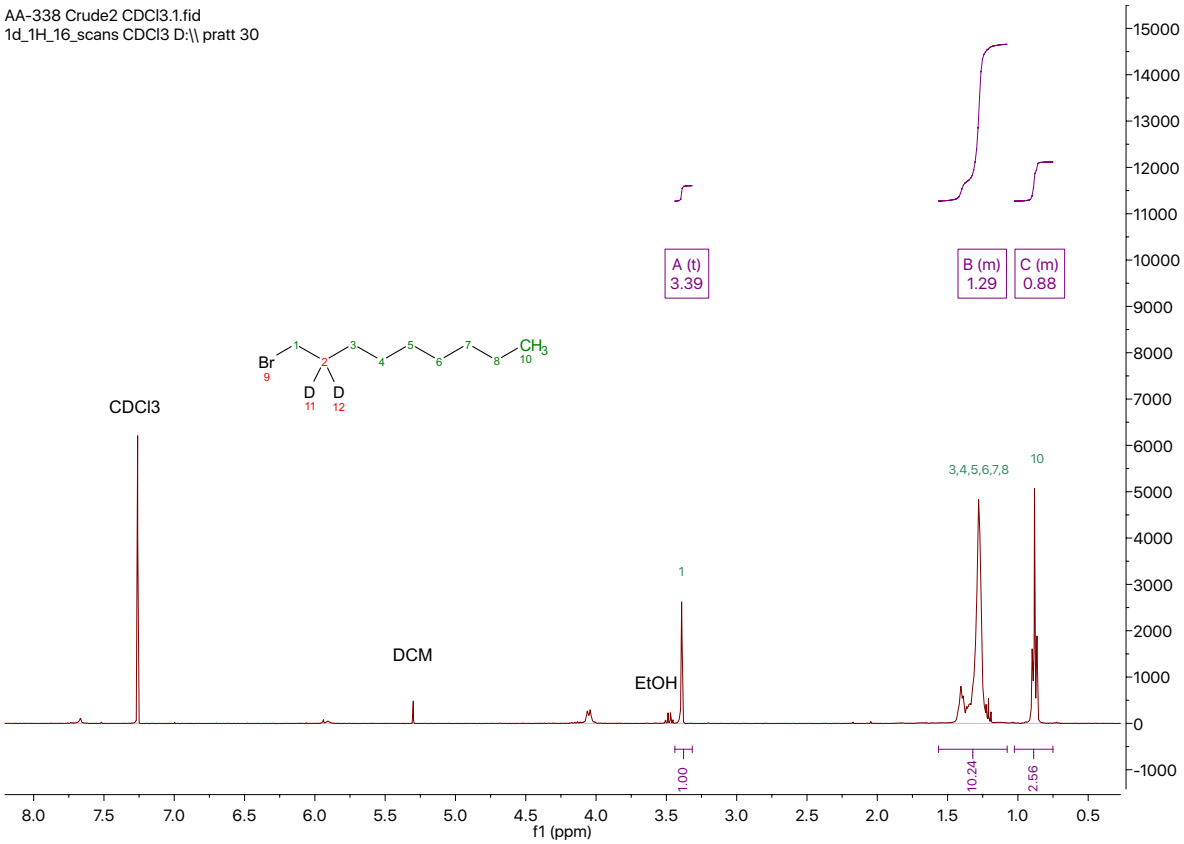

Figure 4.48 ^{1}H NMR ($CDCl_3$, 400 MHz) spectra of 1-Bromononane-d_2 (53).

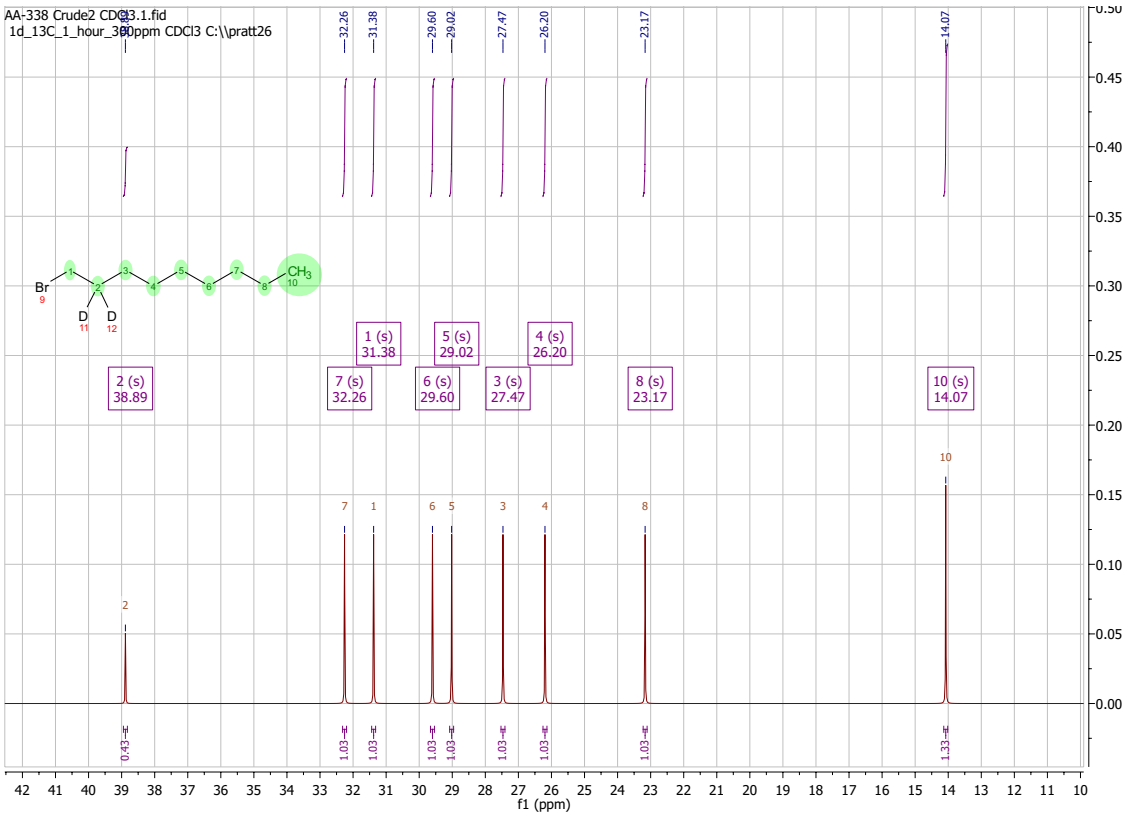

Figure 4.49 ^{13}C NMR ($CDCl_3$, 400 MHz) predicted spectra of 1-Bromononane-d_2 (53).

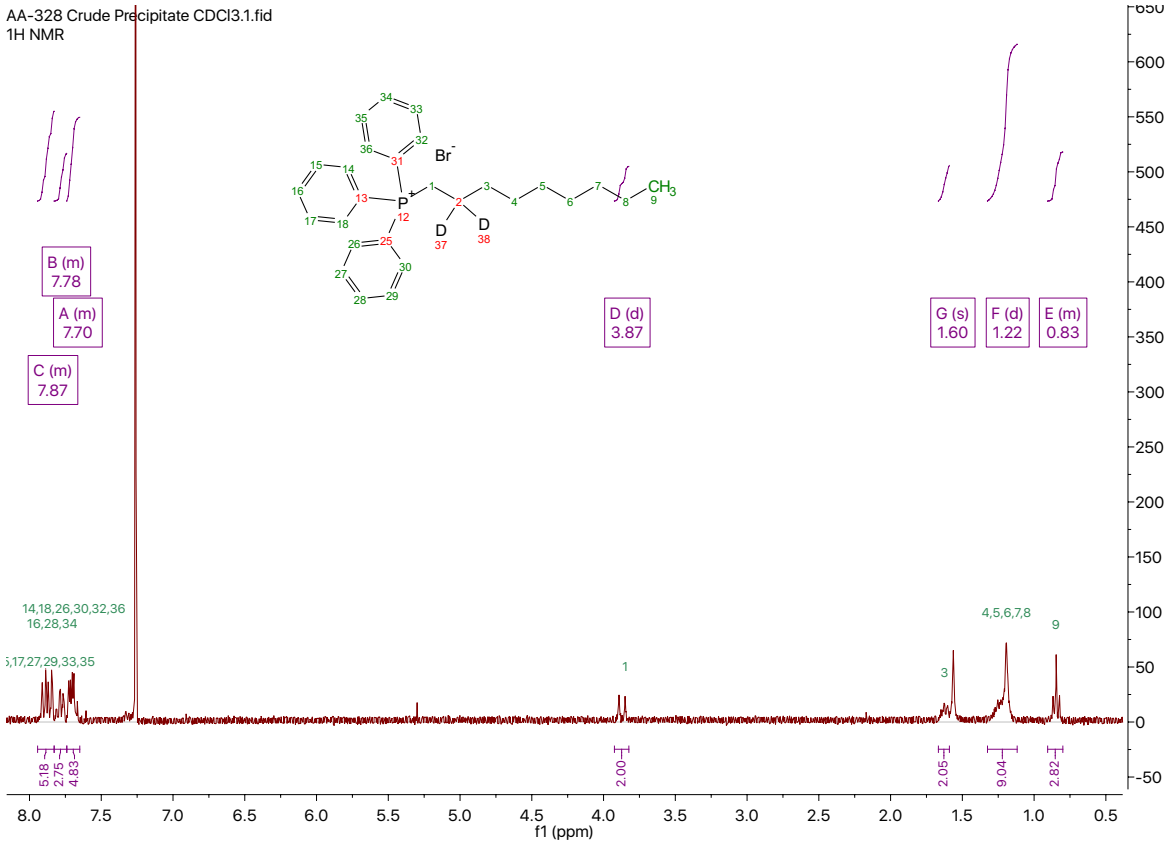

Figure 4.50 ^{1}H NMR ($CDCl_3$, 400 MHz) spectra of nonyltriphenylphosphonium bromide-d_2 salt (54).

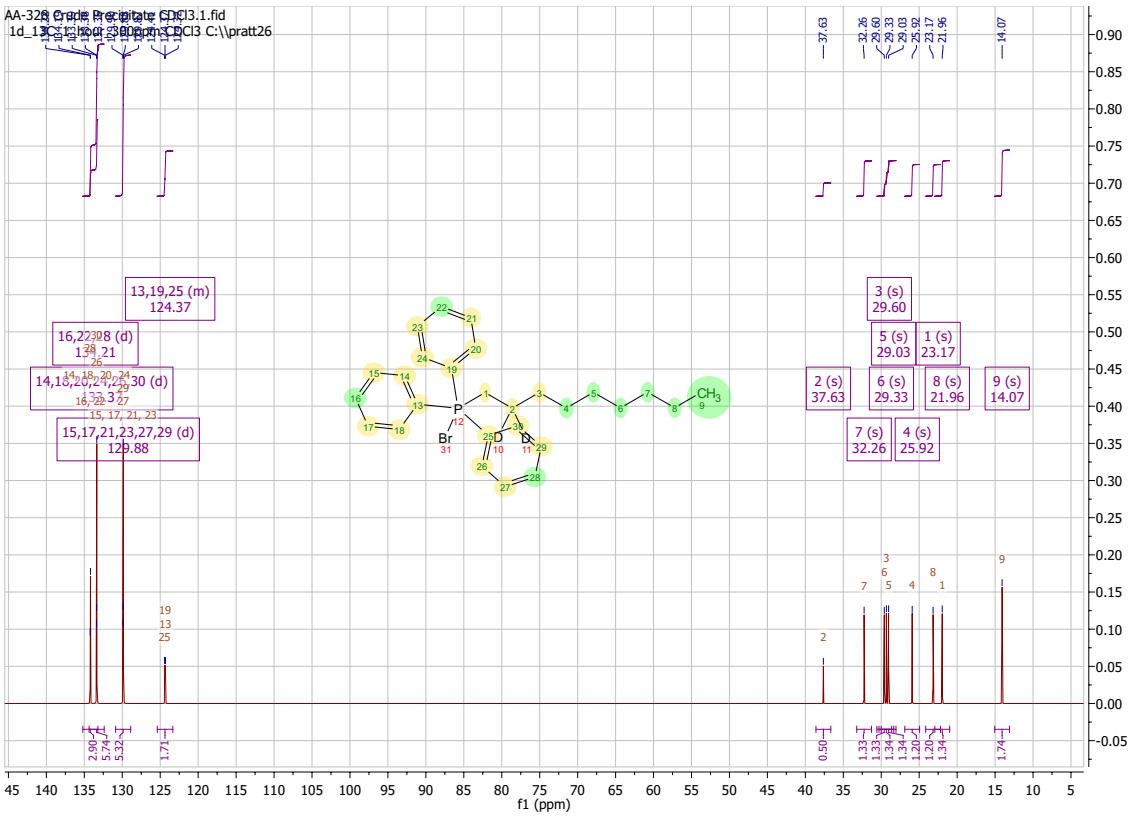

Figure 4.51 ^{13}C NMR ($CDCl_3$, 400 MHz) predicted spectra of nonyltriphenylphosphonium bromide-d_2 salt (54).

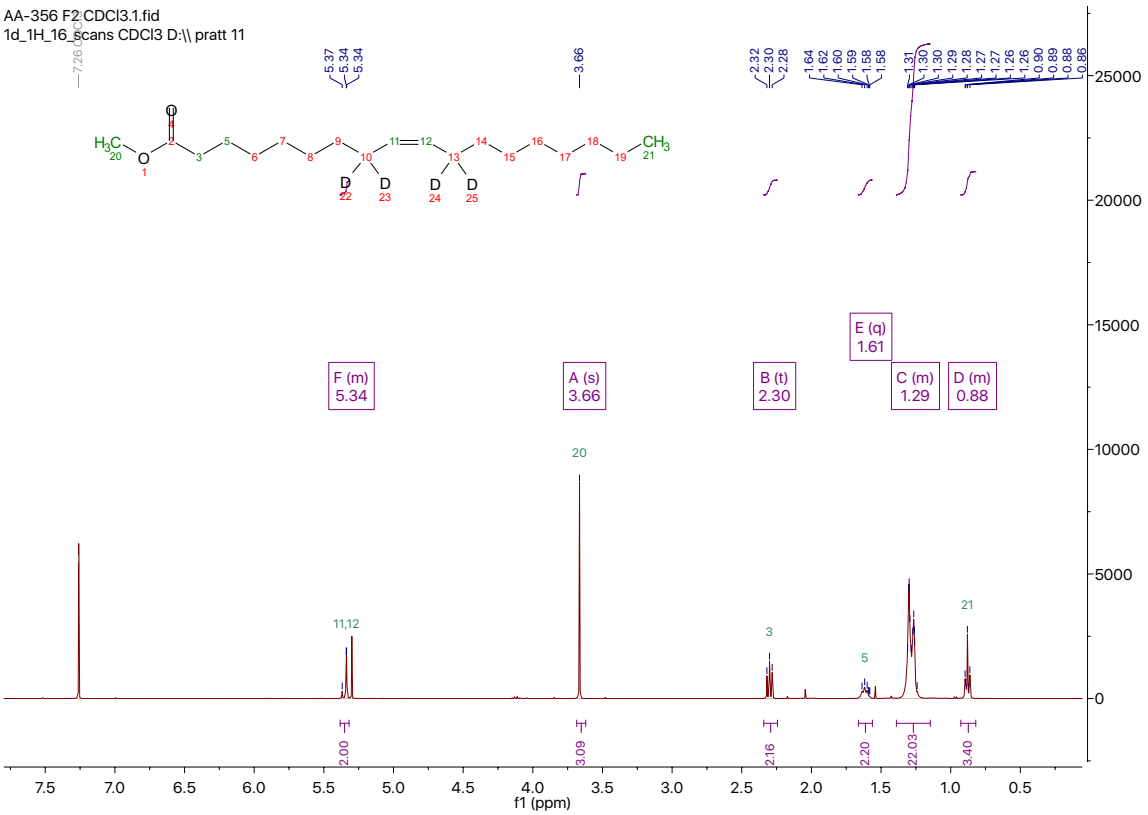

Figure 4.52 ^{1}H NMR ($CDCl_3$, 400 MHz) spectra of Methyl Oleate-d_4 (55).

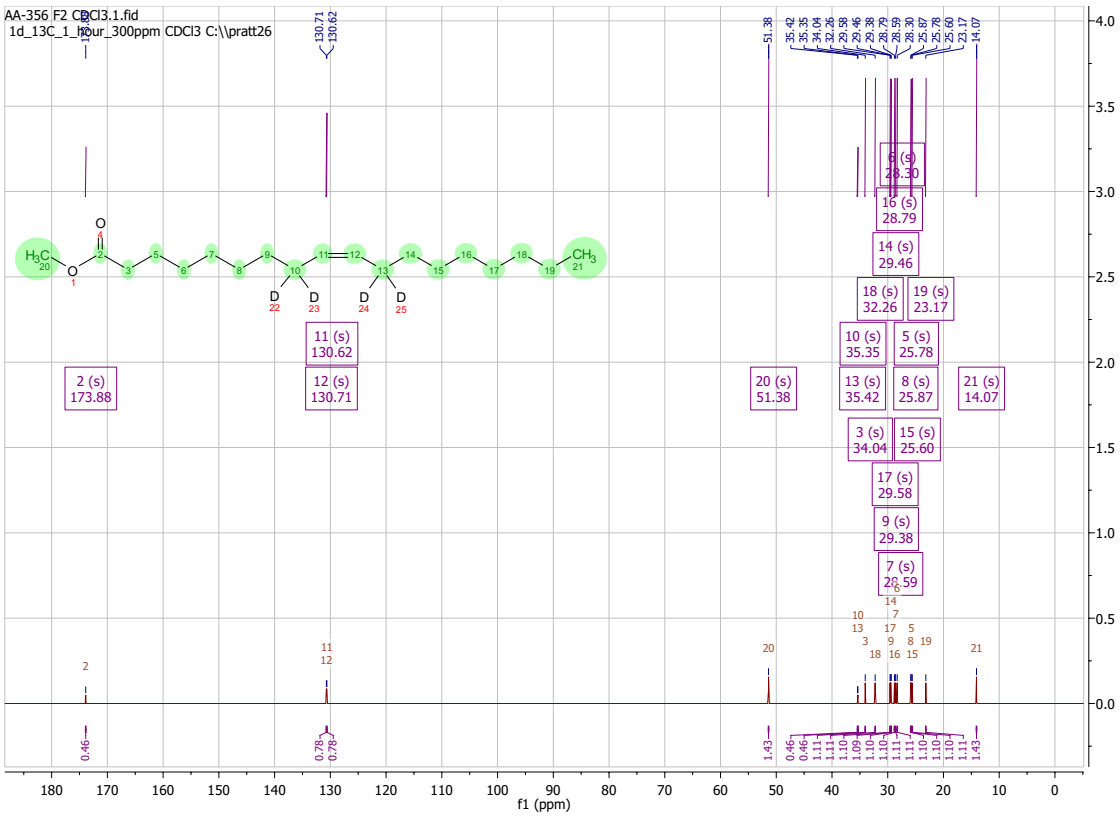

Figure 4.53 ^{13}C NMR ($CDCl_3$, 400 MHz) predicted spectra of Methyl Oleate-d_4 (55).

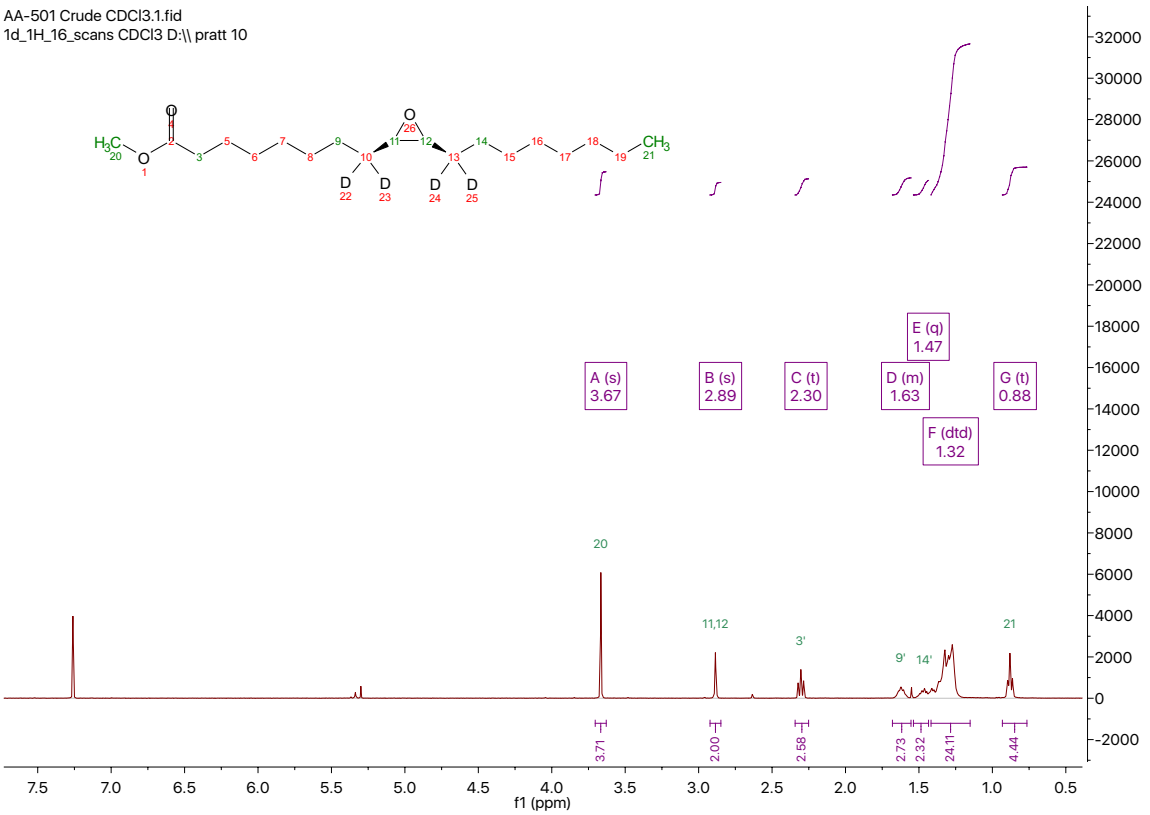

Figure 4.54 ^{1}H NMR ($CDCl_3$, 400 MHz) spectra of 9,10-cis-epoxide of methyl oleate-8,8,11,11-d_4 (57).

Figure 4.55 ^{13}C NMR ($CDCl_3$, 400 MHz) predicted spectra of 9,10-cis-epoxide of methyl oleate-8,8,11,11-d_4 (57).

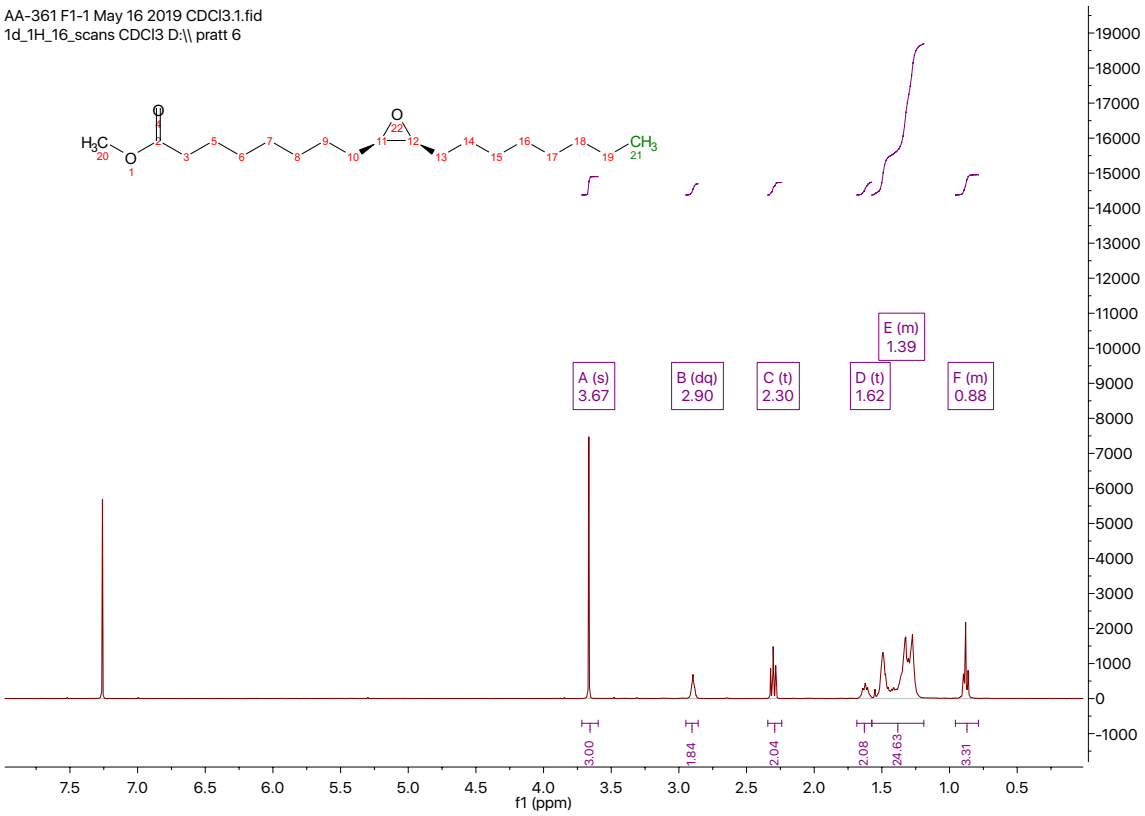

Figure 4.56 ^{1}H NMR ($CDCl_3$, 400MHz) spectra of the 9,10-cis-epoxide of methyl oleate (56).

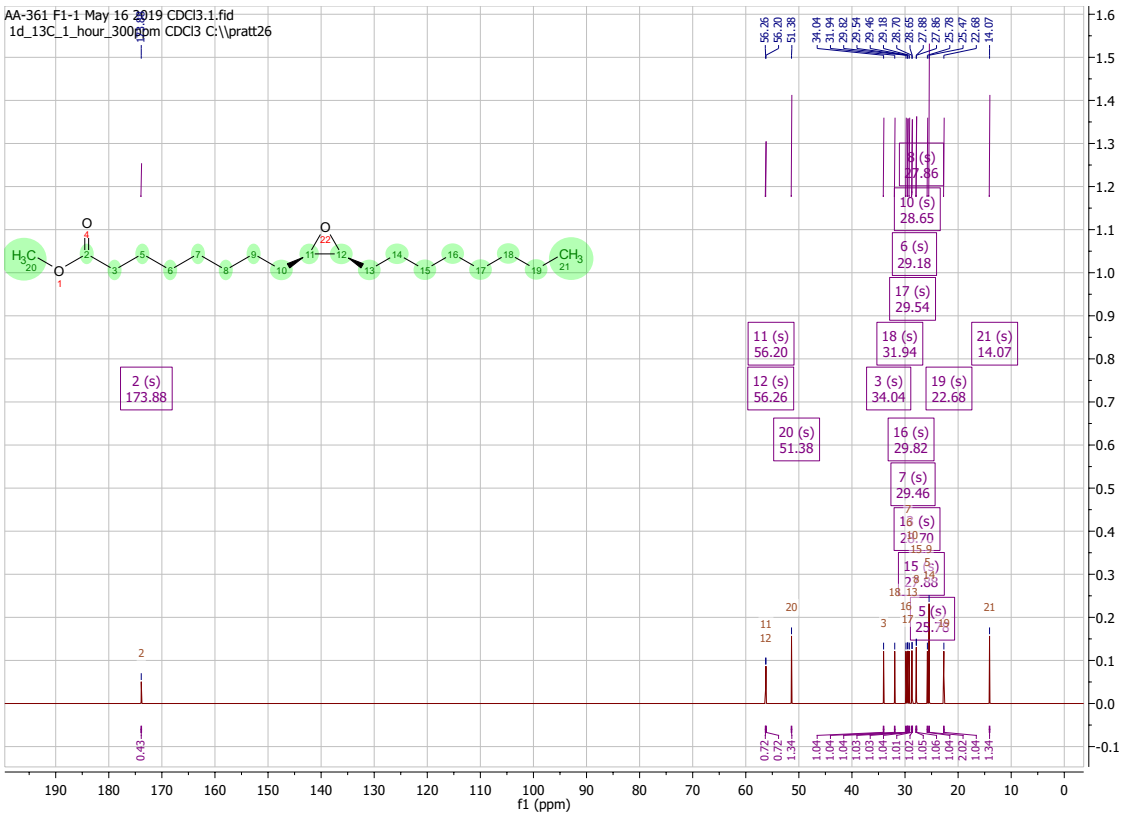

Figure 4.57 ^{13}C NMR ($CDCl_3$, 400 MHz) predicted spectra of the cis-epoxide of methyl oleate (56).

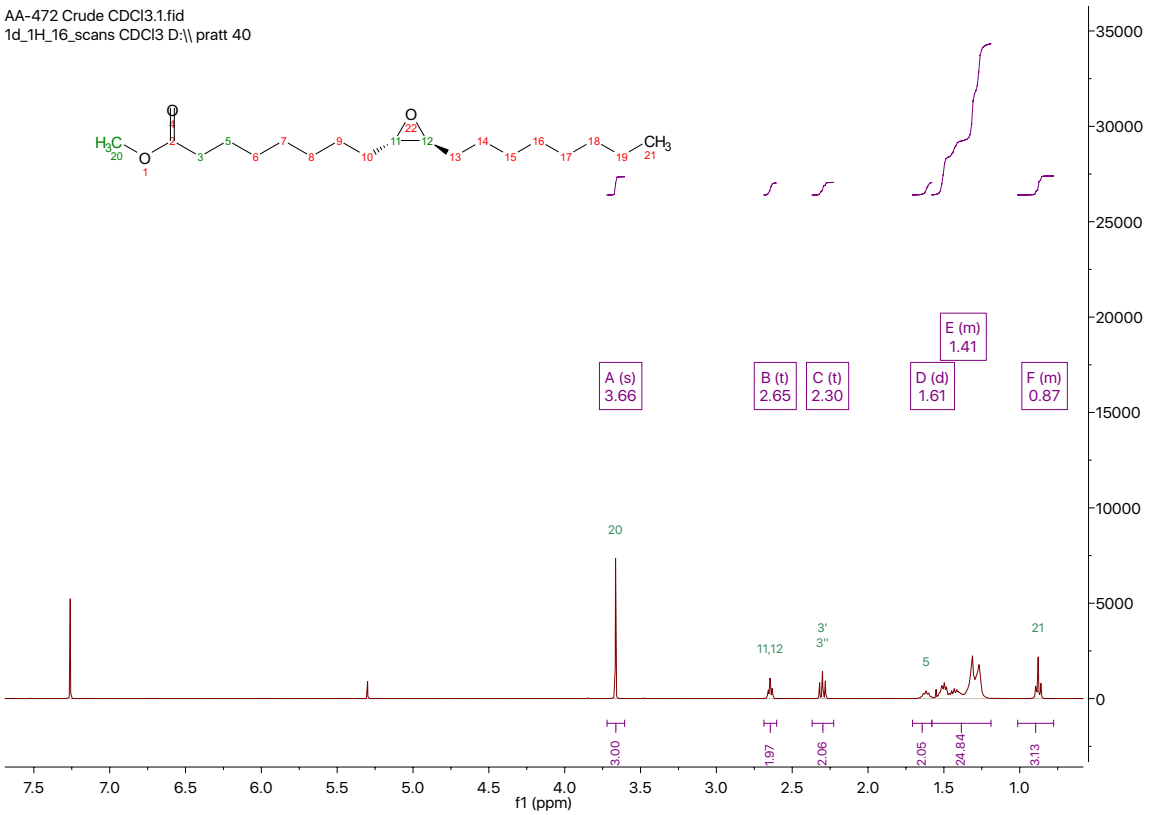

Figure 4.58 ^{1}H NMR ($CDCl_3$, 400 MHz) spectra of spectra of 9,10-trans-epoxide of methyl oleate (59).

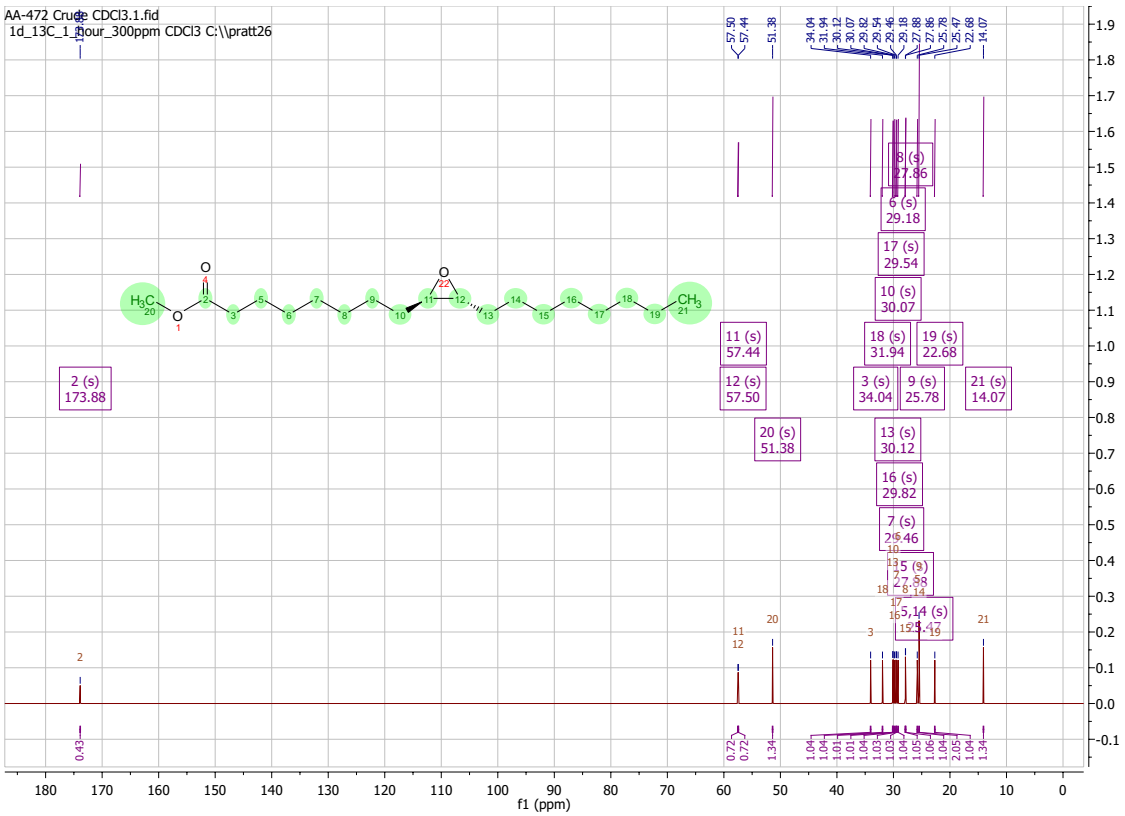

Figure 4.59 ^{13}C NMR ($CDCl_3$, 400MHz) predicted spectra of 9,10-trans-epoxide of methyl oleate (59).

Chromatograms:

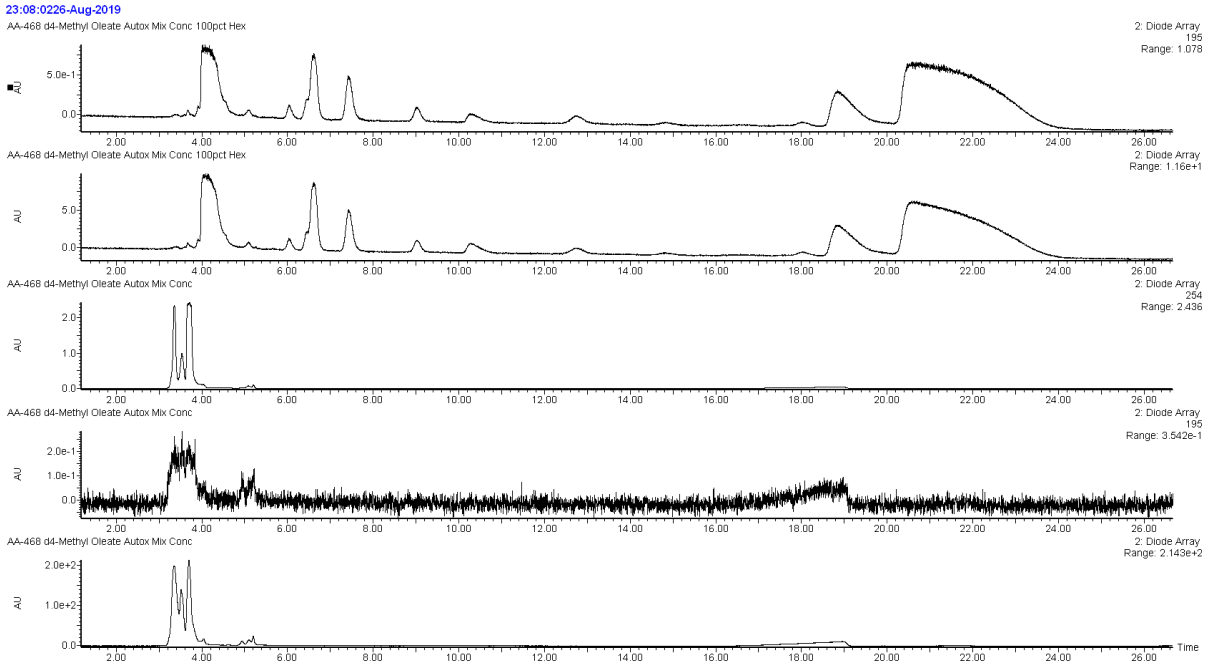

Figure 4.60 Chromatograms of methyl oleate-8,8,11,11-d_4 (55) co-autoxidation following Ned Porters method **[57]**. Conditions: 3-hour autoxidation run at 30ºC with methyl oleate (0.6 mmol), with the radical initiator DTBN (5mol% with respect to methyl oleate), and tert-butyl hydroperoxide (**t**BuOOH; 0.73mL – excess equivalence); quenched with TTBP. UPLC-UV/MS-MS – 0.6% IPA:Hexanes @ 0.9 mL/min.

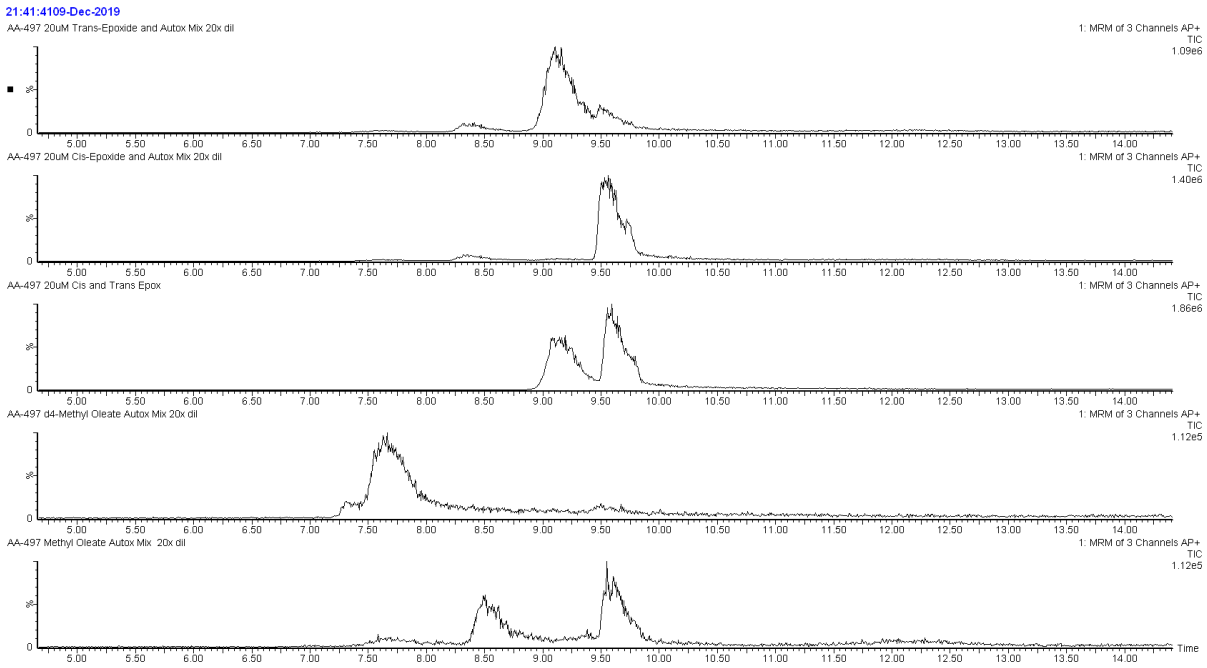

Figure 4.61 Expanded view of the chromatograms presented in Figure 3.23.